IRON HOMEOSTASIS IS HIERARCHICALLY REGULATED BY MULTIPLE INPUTS: EVIDENCE FOR THE ROLE OF REACTIVE OXYGEN SPECIES AND IRON-ZINC CROSS TALK

A Dissertation

Presented to

The Faculty of the Graduate School

at the University of Columbia - Missouri

In partial fulfillment

of the Requirements for the Degree

Doctor of Philosophy

By

SAMUEL ALONZO MCINTURF

Dr. Mendoza-Cózatl, Dr. Gassmann, Dr. Hunt, Dr. Kazic, Dr. Mitchum

Dissertation Supervisors

December 2018

The undersigned, appointed by the dean of the Graduate School, have examined the thesis entitled

IRON HOMEOSTASIS IS HEIRARCHICALLY REGULATED BY MULTIPLE INPUTS:

EVIDENCE FOR THE ROLE OF REACTIVE OXYGEN SPECIES AND IRON-ZINC CROSS TALK

Presented by Samuel Alonzo McInturf

a candidate for the Degree of Doctor of Philosophy,

and herby certify that, in their opinion, is worthy of acceptance.

_____

Professor David Mendoza-Cózatl

_____

Professor Walter Gassmann

_____

Professor Heather Hunt

_____

Professor Toni Kazic

_____

Professor Melissa Mitchum

William Alonzo McInturf

For my father who has always demonstrated a dedication to hard, honest work.

Lanelle Jane McInturf

For my mother, who has been continually supportive, through all of my phases.

Dr. Molly Alona McCarthy

For my sister, who has shown me what it means to persevere and flourish in face of attrition and hardship.

To these people I owe my circumstance which has allowed me to come so far.

ACKNOWLEDGEMENTS

I would like to thank Dr. Mendoza-Cózatl for the years of support, for the challenges brought, and met, and those lost as well. His insights and guidance have led me to grow both as a scientist and as a person, more than I thought I ever would. For this trial, for this burden, for this growth, and for this joy, I am deeply grateful.

I would like to thank Dr. Kazic for first showing me, and then reminding me why computational biology is beautiful and for helping me through the hardships.

I would like to thank Dr. Mitchum and Dr. Gassmann for overseeing my growth and for the advice and lessons they passed down.

I would like to thank Dr. Hunt showing me how to manage groups, for her advice, but most importantly for reminding me where my feet stand, and that the sky resides above that point.

For the Doctors' Dowd, for their years of friendship, without which I dare not consider.

My lab mates, Dr. Mather Khan who brought me half way around the world. For Dr. Nga Ngyuen, for the comradery of the journey. For Dr. Norma Castro-Guerrero for reminding me that, we just don't think about "The Spaghetti Incident?".

For my friends with whom I counted the small hours, and for those with whom I have spun my most favored yarns.

Ph'nglui mglw'nafh Cthulhu R'lyeh wgah'nagl fhtagn!

TABLE OF CONTENTS

Chapter 3
bZIP23 as a putative link between zinc and iron homeostasis

Chapter 4
SPIP: A Small Plant Imaging Platform

Chapter 5
Insights into the transcriptional and translational regulation of companion cells during Fe deficiency

SUPPLEMENTAL DATA

Chapter 2
Cadmium interference with iron sensing reveals transcriptional programs sensitive and insensitive to reactive oxygen species

Chapter 3
bZIP23 as a putative link between zinc and iron homeostasis

Chapter 4
SPIP: A Small Plant Imaging Platform

TABLE OF FIGURES

Chapter 1
Iron Homeostasis

Chapter 2
Cadmium interference with iron sensing reveals transcriptional programs sensitive and insensitive to reactive oxygen species

Chapter 3
bZIP23 as a putative link between zinc and iron homeostasis

Chapter 4
SPIP: A Small Plant Imaging Platform

Chapter 5
Insights into the transcriptional and translational regulation of companion cells during Fe deficiency

TABLE OF SUPPLEMENTAL FIGURES

Chapter 2
Cadmium interference with iron sensing reveals transcriptional programs sensitive and insensitive to reactive oxygen species

Chapter 3
bZIP23 as a putative link between zinc and iron homeostasis

Chapter 4
SPIP: A Small Plant Imaging Platform

ABSTRACT

Iron (Fe) is a heavy metal micronutrient vital for all forms of life. In plants, Fe deficiency results in chlorosis and reduced growth, while Fe excess results in lipid peroxidation through the generation of reactive oxygen species. Hence, Fe homeostasis must be tightly regulated. Plants have been shown to use multiple sensing mechanisms to regulate whole plant Fe demand (systemically) and at through protein level changes at the root epidermis (locally). The companion cell of the phloem has recently been strongly implicated as the site of systemic Fe sensing. In this work I demonstrate that leaves and roots are subject to multiple regulatory inputs which modulate Fe dependent gene expression in a hierarchical fashion, and was able to separate these responses into reactive oxygen species (ROS) dependent and independent groups. Excess heavy metal has been shown to generate ROS, hence plants must also balance relative abundances of each heavy metal to prevent deficiency/toxicity. We identified bZIP23, which was previously described as an inducer of Zn uptake, as a likely candidate to mediate the mediate Fe-Zn crosstalk through the characterization of the double mutant *bzip23-1/opt3-2* which suppresses *opt3* dependent induction of Fe deficiency responses, likely by directly regulating the Fe uptake machinery. To facilitate the identification of time dependent changes in root growth phenotypes, such as under heavy metal stress, I designed and constructed a Small Plant Imaging Platform (SPIP) which able to capture high quality images for automated time course analysis which we aim to distribute throughout the plant science community. Finally, I have performed the two complementary experiments to first identify Fe dependent changes in gene translation in companion cells which is paired with the identification of transcription factor which directly regulate OPT3. Initial results indicate a novel mechanism of Fe release from the cell wall in the leaf vasculature during Fe deficiency, and implicate transcription factors known to mediate Fe deficiency responses as being responsible for the rapid induction of OPT3 upon Fe deficiency

Chapter 1
Iron (Fe) homeostasis

1 Introduction

Iron (Fe) is an essential mineral nutrient for all forms of life, as it serves as an electron carrier in the electron transport chains of the chloroplast and mitochondria, as well as serving as a metal cofactor in proteins involved in a large variety of biological processes including redox reactions. In humans, Fe deficiency (-Fe), also called anemia, manifests as chronic fatigue, dizziness, weakness, and irregular heart beat as red blood cells lack the Fe-rich hemoglobin that delivers oxygen to the body to aerobic metabolism. Anemia affects roughly 30% of the worlds' population (WHO and UNICEF, 2001), and disproportionately effects pregnant women and young children due to their increased Fe demand (Zimmermann and Hurrell, 2007). Anemia is not restrained to developing countries where caloric intake is limiting, and also affects people in developed countries with nutritionally poor diets (White, 2005).

Plants, like humans, also suffer from Fe deficiency. Fe deficiency reduces carbon assimilation, biomass and yield, mainly by limiting chlorophyll biosynthesis, thus reducing the overall photosynthetic capacity. For these reasons, finding ways to improve Fe availability or enhance the ability of plants to grow on Fe limiting soils is an important agronomic trait sought after around the globe. However, and due to its high reactivity, Fe uptake must be tightly regulated and in some cases limited; the highly reactive nature of free Fe produces reactive oxygen species (ROS), which are damaging for cells. Fe is able to generate H_2O_2 (one kind of ROS) through the spontaneous transfer of one electron to H_2O, or by reacting with H_2O_2 to produce the super oxide anion through the Fenton reaction (Winterbourn, 1995; Strlič *et al.*, 2003). ROS are also very

reactive molecules that can damages membrane lipids and other biomolecules by peroxidation reactions; hence the need for a tight regulation of Fe uptake to balance deficiency and toxicity.

In plants, Fe homeostasis is maintained at the transcriptional level by several interconnected transcription factor networks which typically induce their targets to uptake or sequester Fe in subcellular compartments. Alternatively, Fe homeostasis can be regulated locally through post translational mechanisms; phosphorylation, ubiquitin mediated degradation, and cycling between internal membranes and the plasma membrane being the most prevalent. While local regulation typically acts to repress Fe uptake to prevent toxicity, the transcriptional Fe deficiency responses are signaled systemically from leaves to roots to activate or repress the Fe uptake machinery (see below).

Presented here is a description of the current understanding of Fe homeostasis in Arabidopsis thaliana. We follow Fe as it travels from the soil to shoots, describing the regulation of what is known as "the FIT network", which controls Fe uptake pathway and the synthesis of Fe chelating organic acids. Next, how the PYE network regulates some FIT network members is described to maintain intracellular Fe homeostasis, Fe translocation from root to shoot, and finally describe our current understand of systemic Fe signaling in the companion cell of the phloem.

2 The Fe uptake pathway

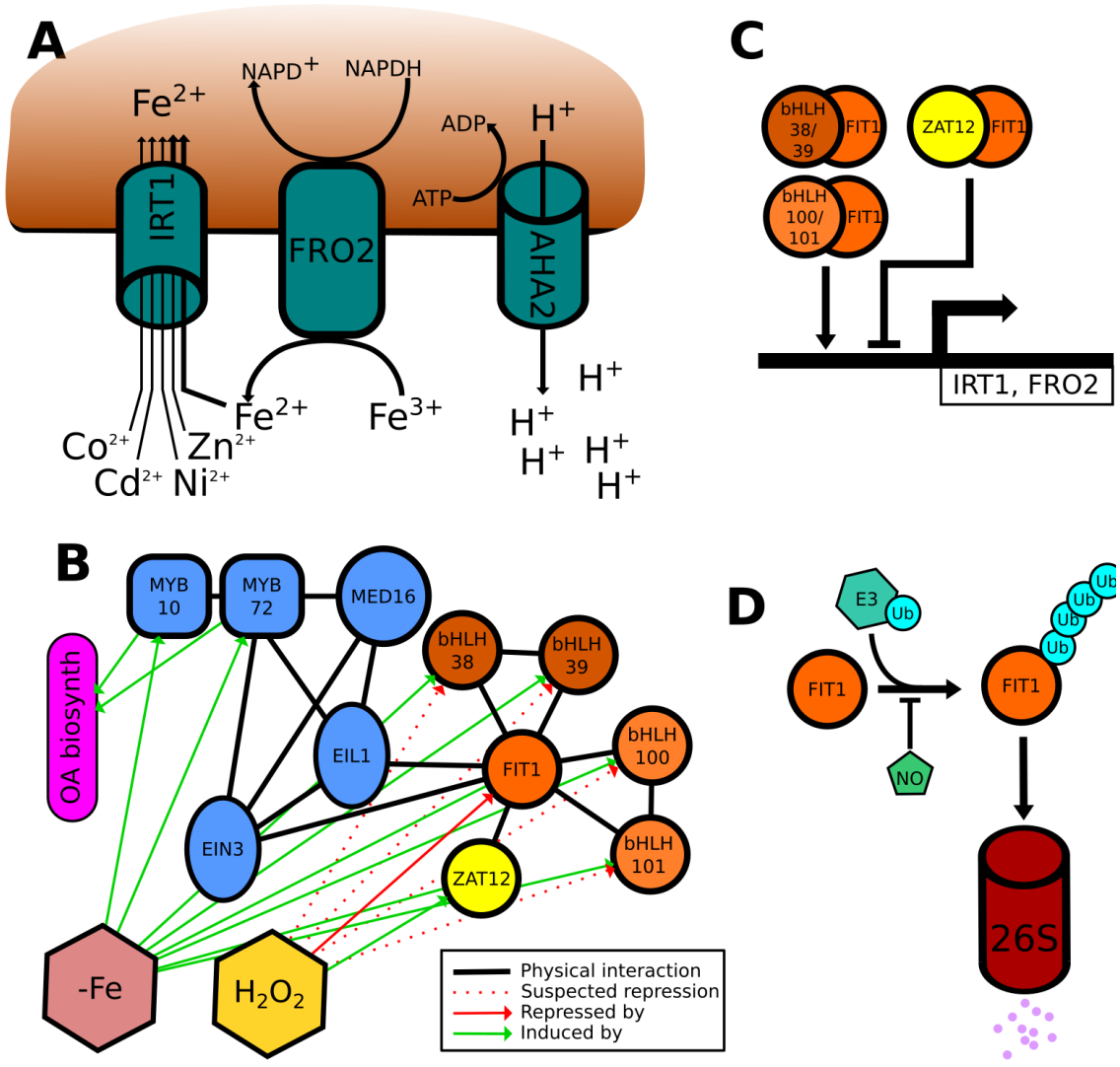

Figure 1 Schematic representation of the operations of the FIT network to uptake Fe from the rhizosphere. (A) FIT interacts with a cohort of Ib bHLHs, ZAT12, and EIN3/EIL1 to control Fe uptake. EIN3/EIL1 associate with the Mediator complex along with MYB10 and MYB72, linking organic acid biosynthesis and ethylene signaling with FIT1 activity. H_2O_2 induces ZAT12, which inhibits FIT1 activity and likely inhibits the other Ib bHLHS. (B) IRT1, FRO2, and other unknown targets are induced by the dimerization of FIT1 with one of the other Ib bHLHs to coordinate Fe uptake from multiple inputs. (C) FIT1 is regulated post translationally via the 26S proteasome after polyubiquitination by an unknown E3 ligase. This polyubiquitination activity is repressed by the presence of NO. (D) The final output of FIT network signaling is the induction of the proton pump AHA2 to release Fe^{3+} from the soil, FRO2 to reduce Fe^{3+} to Fe^{2+}, and finally transport across the plasma membrane by IRT1. In addition to high affinity Fe transport, IRT1 is able to transport other divalent cations with lesser affinities.

Despite being one of the most prevalent heavy metals in the earths' crust, Fe is biologically unavailable in many soil types (White and Broadley, 2009; Stein, 2010). This is because Fe in the soil is most often found as Fe^{3+} which, unlike Fe^{2+}, is insoluble in water. Hence plants have evolved multiple strategies to extract Fe from the soil by chelating the Fe^{3+} in a soluble complex, or by directly reducing Fe^{3+} to Fe^{2+} ; these two strategies are appropriately named *the chelation strategy* and *the reduction strategy* (or strategy II and strategy I, respectively) (Hindt and Guerinot, 2012).

2.1 The reduction strategy for Fe^{2+} uptake

The reduction strategy directly addresses the problem solubility by directly reducing Fe^{3+} at the plasma membrane prior to transport into root cells. Iron reduction and uptake occurs at and near the root tip, but not along the maturation zone. Upregulation of this process begins when root epidermal cells receive a still unknown iron deficiency signal from leaves, which in turn induces a cohort of bHLH transcription factors (TFs) referred to as the FIT network (discussed in detail below). These TFs go on to induce the transcription of genes directly responsible for Fe acquisition, resulting in a three-step extraction of Fe (**Figure 1A**). First, the transmembrane P-type ATPase AHA2 hydrolyzes ATP at the cytosolic face to pump H^+ into the rhizosphere (Santi and Schmidt, 2009). Acidification of the rhizosphere inhibits the interaction of Fe^{3+} with the negatively charged cell wall or soil particles, allowing them to reach the plasma membrane. Next, a second transmembrane protein Ferric Reduction Oxidase (FRO2) hydrolyzes NADPH to reduce Fe^{3+} to Fe^{2+} (Robinson *et al.*, 1999). Finally, the now soluble Fe^{2+} is transported across the plasma membrane by the high affinity Fe^{2+} transporter Iron Regulated Transporter 1 (IRT1) (Eide *et al.*, 1996; Korshunova *et al.*, 1999). Once inside the root epidermis, free Fe^{2+} must be chelated or compartmentalized to prevent oxidative damage. Fe is likely stored in the vacuole, or other vesicles, by the low affinity transporter Iron Regulated Transporter 2 (IRT2). IRT2 is implicated in

this role for several reasons: IRT2 expression is highly correlated with IRT1 and FRO2, GFP fusion proteins localizes to intracellular vesicles in roots, and the *irt2* mutant shows no chlorosis or phenotypes on -Fe media (Vert *et al.*, 2009), which suggests a role for Fe storage, but not uptake. Excess Fe may also be stored in the vacuole by Vacuolar Iron Transporter 1 (VIT1) (Kim *et al.*, 2006; Roschzttardtz *et al.*, 2009), although VIT1 expression has not been shown to be correlated with IRT1, indicating a more general role in storage of excess Fe. This array of molecular machines must be tightly regulated to balance deficiency and toxicity, which is accomplished though the coordinated action of the *FIT network*.

2.2 Regulation of reduction strategy uptake by the FIT network

The *FIT network* is composed of five bHLH Ib transcription factors: bHLH29 (FIT), bHLH38, bHLH39, bHLH100, and bHLH101 (**Figure 1B**). Several of the initial studies of Fe deficiency were performed in the chlorotic tomato mutant *fer*, whose phenotype were attributed to the loss of a bHLH TF *LeFER* (Ling *et al.*, 2002). The direct homolog of LeFER in *Arabidopsis* was named Fe-deficiency Induced Transcription Factor 1 (Colangelo, 2004), and like *fer*, *fit* mutants are unable to induce Fe uptake upon Fe deficiency. FIT1 was later found to dimerize with bHLHs within the Ib subfamily bHLH38, bHLH39, bHLH100, and bHLH101 to induce IRT1 and FRO2 (Wang *et al.*, 2013). Attempts to induce IRT1 through the overexpression of FIT1 demonstrate that a coincident overexpression of one of the other Ib bHLHs is needed to induce Fe uptake (Wang *et al.*, 2013). While these Ib bHLHs are able to dimerize with FIT1 to control Fe uptake, they are expressed throughout the plant, indicating that they have additionally regulatory roles independent of FIT (Yuan *et al.*, 2008). While bHLH38/39/100/101 single mutants have no known phenotypes, the double mutants *bhlh38/39* and *bhlh100/101* are chlorotic and stunted on -Fe media, only bHLH38/39 has been shown to directly regulate IRT1 and FRO2 as a FIT heterodimer (Yuan *et al.*, 2008), while

bHLH100/101 are believed to induce IRT1 via both FIT1 dependent and FIT1 independent pathways (Sivitz *et al.*, 2012)(**Figure 1B**).

While these mechanisms all serve to acquire Fe during deficiency, toxic levels of free Fe can readily occur. Hence, Fe homeostasis is responsive to other biological inputs outside of Fe deficiency, as is demonstrated through Zinc finger of Arabidopsis Thaliana 12 (ZAT12). ZAT12 is induced by H_2O_2 and prolonged Fe deficiency. In contrast to the Ib bHLHs dimerization of ZAT12 with FIT1 inhibits FIT1 function (Le *et al.*, 2016). This mechanism is thought to be in response to general oxidative stress, as ZAT12 is not induced until 10 days after -Fe exposure and is induced after H_2O_2 exposure (Le *et al.*, 2016), well after FIT1 and IRT1 reach their maximum expression (Vert *et al.*, 2003).

In addition to induction by the unknown Fe deficiency signal, and repression by H_2O_2 exposure, FIT1 is also known to be induced by the plant stress hormone ethylene. FIT1 forms heterodimers with the transcription factors Ethylene INsensitive 3 (EIN3) and its homolog EIN3-like 1 (EIL1) (Lingam *et al.*, 2011). EIN3 and EIL1 coordinate ethylene dependent responses during both biotic and abiotic stresses by inducing ethylene dependent transcripts (Chao *et al.*, 1997; Solano *et al.*, 1998; Yanagisawa *et al.*, 2003; Potuschank *et al.*, 2013). EIN3 and EIL1 interact with the Mediator complex (Yang *et al.*, 2014) to further promote Fe deficiency responses through activation of MYB10 and MYB72, discussed in Section 2.3.

In summary, the reduction strategy of Fe uptake is regulated primarily by the FIT network. The FIT network is induced by ethylene signaling and by a shoot-borne yet unknown Fe deficiency signal, while repression of the network occurs by H_2O_2, which is mediated by the induction of ZAT12 to block FIT1 activity. After induction of this pathway FIT/Ib heterodimers induce IRT1, FRO2, and AHA2 to extract Fe from the surrounding rhizosphere.

2.3 Fe mobilization from the rhizosphere

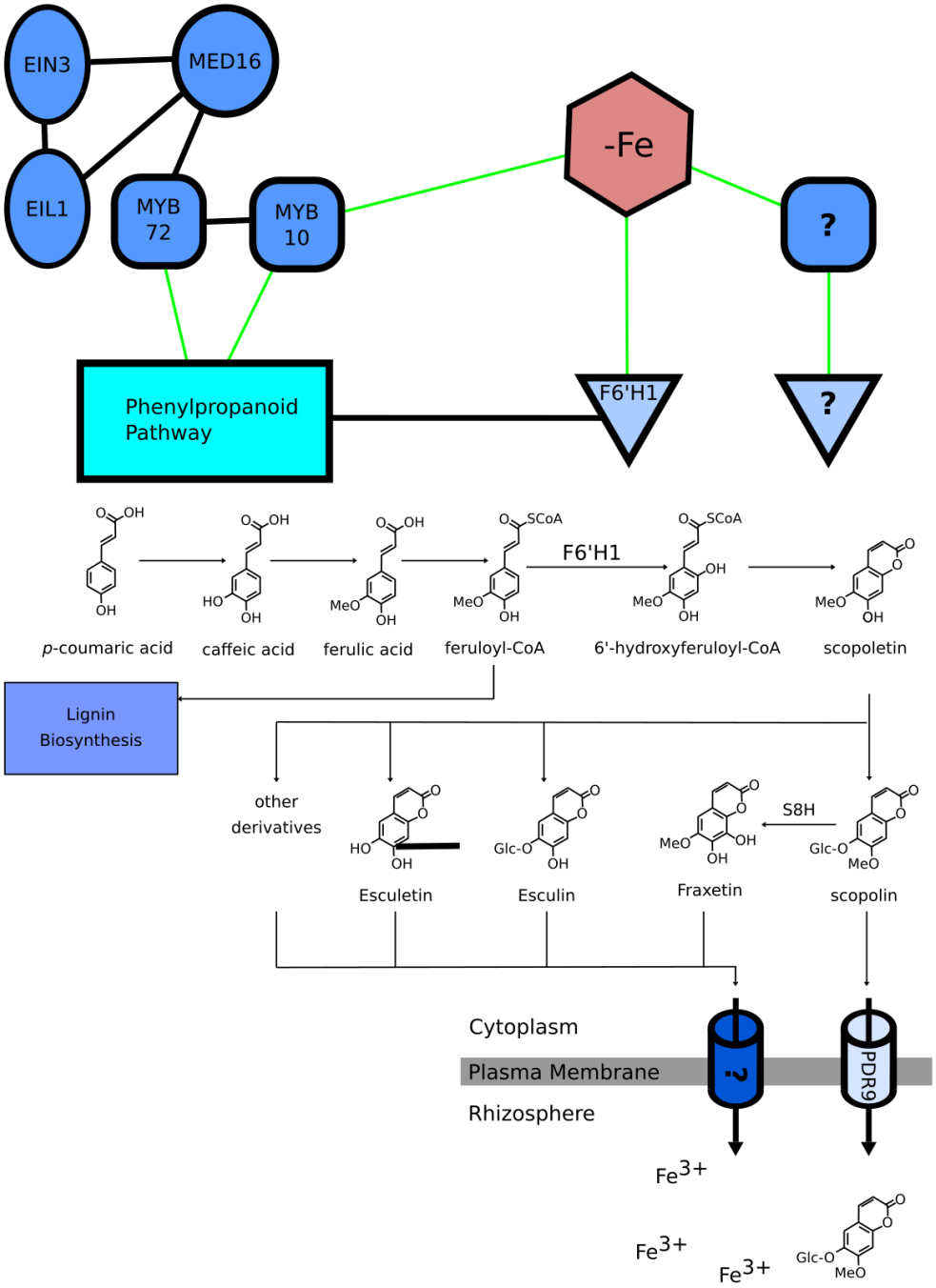

Figure 2 Schematic representation of Fe mobilization from the rhizosphere. The synthesis of organic acids for Fe mobilization is initiated in the phenylpropanoid pathway with the production of *p*-coumaric acid, which is regulated by the Fe deficiency responsive transcription factors MYB10 and MYB72. *p*-coumaric undergoes a multistep reaction to feruloyl-CoA. The conversion of feruloyl-CoA to 6'-hydroferuloyl-CoA by F6'H1 is the first dedicated step from the phenylpropanoid pathway to the synthesis of the organic acids. 6'-hydroxyferuyolyl-CoA is converted to scopoletin which is converted to scopolin and transported to the rhizosphere by PDR9, or further derivatized and transported to the rhizosphere by an unknown mechanism. Once in the rhizosphere these acids are able to chelate Fe, presumably to serve as a substrate for FRO2.

As previously discussed, AHA2 acidifies the rhizosphere to release Fe^{3+} from the soil and apoplast. While this does release Fe^{3+}, it does not allow Fe^{3+} to interact with FRO2 for reduction to Fe^{2+}. Recently a class of organic acids derived from *p*-coumarin have been implicated in this role, and is hence a side branch of the reduction strategy. These organic acids are polycyclic compounds derived from the phenylpropanoid pathway, diverging from lignin biosynthesis via an *ortho*-hydroxylation of feruloyl-CoA's central ring (Schmidt *et al.*, 2014; Clemens and Weber, 2016). The committed step between the synthesis of these chelators and the lignin pathway occurs through the action of a 2-oxoglutarate and Fe^{2+} dependent oxygenase family protein, F6'H1, which provides the needed *ortho*-hydroxylation of feruloyl-CoA to ultimately produce scopoletin (Sun *et al.*, 2015; Kai *et al.*, 2008). Scopoletin derivatives are then processed by a host of unknown proteins to generate scopolin, fraxetin, fraxin, isofraxinol, esculetin, and esculin (Clemens and Weber, 2016; Tsai *et al.*, 2018). These organic acids are capable of chelating Fe^{3+} in the rhizosphere, but the mechanism of export is unknown, except in the case of scopolin which is exported via the transporter pleotropic drug resistance 9 (PDR9) (Fourcroy *et al.*, 2014). Once in the rhizosphere these organic acids are expected to chelate and maintain solubilize Fe^{3+} soluble allowing FRO2 to reduce Fe^{3+} to Fe^{2+} and subsequent uptake by IRT1.

Only two transcription factors have been identified as regulators this system, MYB10 and MYB72 (Palmer *et al.*, 2013). *myb10/72* mutants display a chlorotic phenotype and decreased Fe in leaves, but are able to properly induce IRT1 (Palmer *et al.*, 2013). The regulation of this pathway was demonstrated by the *myb10/72* mutant, which is unable to induce the phenylpropanoid pathway and subsequent production of scopoletin derivatives (Stringlis *et al.*, 2018). MYB10 and MYB72 dependent induction of the phenylpropanoid pathway is coordinated with the induction of the FIT network, which is presumed to occur through the Mediator 16 (MED16) complex and

EIN3/EIL1 (**Figure 2**). Both, MYB10 and MYB72 have been shown to interact with the MED16 EIN3/EIL1 complex (Lingam *et al.*, 2011; Palmer *et al.*, 2013). Interestingly, MYB72 has also been implicated in roles outside of direct Fe homeostasis, having been shown to mediate rhizobacteria-induced systemic resistance (Zamioudis *et al.*, 2014).

Taken together the biosynthesis of coumarin derived organic acids has been shown to be important for the remobilization of Fe from the root apoplast and cell wall in conjunction with the primary reduction strategy proteins FRO2 and IRT1.

3 The Chelation strategy of Fe uptake (Strategy II)

The reduction strategy describes the Fe uptake in plants such as *Arabidopsis*, but a second pathway exists in grasses such as *Zea maize* and *Oryza sativa*. This pathway is reminiscent of the organic acid branch of the reduction strategy, using organic acids to chelate Fe in the rhizosphere, with the distinction of using a specific Fe chelators called phytosiderophores and directly transporting the Fe-phytosiderophore complex into the cell, rather than reducing it at the plasma membrane (Hindt and Guerinot, 2012).

Phytosiderophores (PS), utilized in the chelation strategy are synthesized from the condensation of S-adenosyl methionine (SAM). The best described chelator is deoxymutagenic acid (DMA), which is synthesized from the condensation of three molecules of SAM to form nicotianamine, which itself is an important Fe chelator for Fe remobilization within the plant body. Nicotianamine is then activated to form DMA and released from the root at daybreak through exocytosis at the root plasma membrane (Sakaguchi *et al.*, 1999; Negishi *et al.*, 2002; Schenkeveld *et al.*, 2014). Interestingly, excreted DMA is degraded by soil microbes (Takagi *et al.*, 1988), and populations

which solely rely on DMA as a carbon source have been isolated (Shi *et al.*, 1988). This draws another parallel between the organic acids of the reduction strategy and the chelation strategy, as the excretion of each family of chelators controls microbial populations.

In *Maize*, DMA:Fe is imported by the yellow stripe 1 (YS1) transporter (Wirén *et al.*, 1994; Curie *et al.*, 2001). While YS1 is unique to *Maize,* it became the founding member of the yellow stripe-like (YSL) family of transporters found across the plant kingdom, and direct homologs of YS1 have been found in barley and rice (Conte and Walker, 2011).

In summary, chelation strategy Fe uptake is utilized by grasses to directly import Fe^{3+}-DMA from the soil by YS family transporters. The chelation strategy likely evolved after the reduction strategy, as it is monophyletic in the plant kingdom, functional IRT1 homologs which directly uptake Fe^{2+} have been identified in grasses such as rice, suggesting multiple losses of the reduction strategy proteins in the grass lineage. Finally the metal chelator nicotianamine is found in all land plants, but only in grasses is it converted to DMA. No matter the route which Fe enters the cell, it is vital for plants to maintain their intercellular homeostasis to prevent oxidative damage.

4 The PYE network regulates intracellular Fe homeostasis in leaves and roots

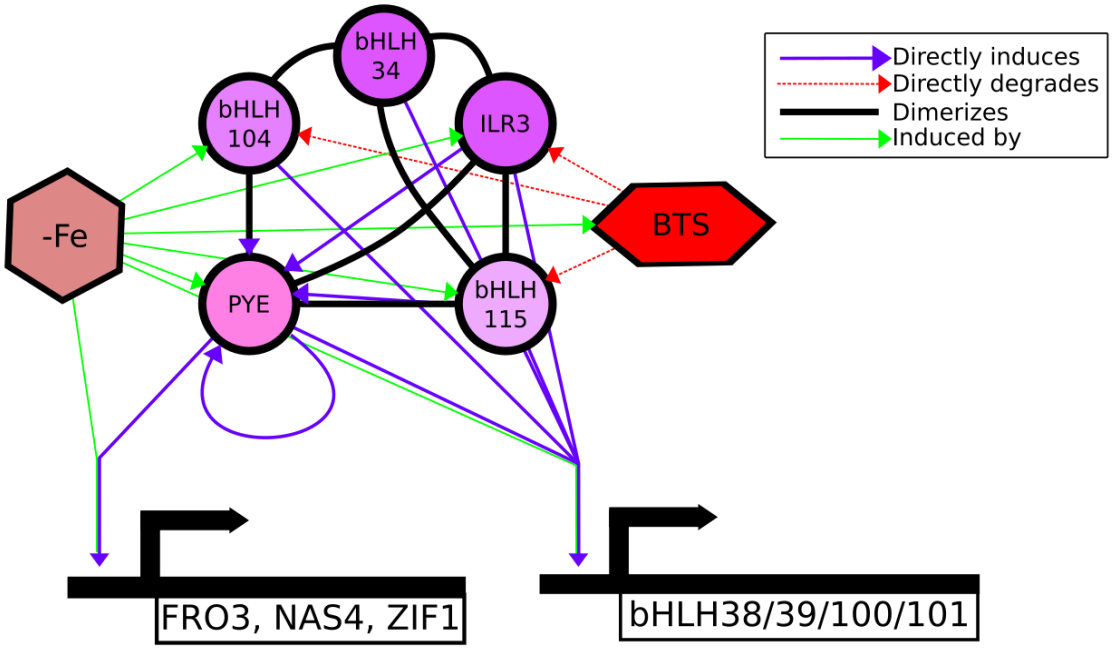

Figure 3 Schematic representation of the PYE network. The IVc bHLHs are able to physically interact with one another, and individually are able to bind the promoters of several key Fe homeostasis genes, as well as the Ib bHLHs. BTS initiates the ubiquitin mediated degradation of the PYE network, excluding PYE itself.

In leaves and roots intracellular Fe homeostasis is maintained by a second cohort of bHLH transcription factors, referred to as the *PYE network* (**Figure 3**). Like the FIT network, the PYE network was named for its founding member, POPEYE (PYE). PYE was found as a -Fe responsive gene in a time-course study of Fe deficient roots, and has largely been described by Long *et al.*, 2010. PYE is a subgroup IVc bHLH TF whose expression is highly localized to the root pericycle and is responsible for mediating intracellular Fe homeostasis by inducing members of the ZIP-family metal transporters that regulate cellular Fe concentrations. *pye* mutants are chlorotic and grow poorly on Fe deficient media, which is attributed to an insufficient induction the FIT network. ChIP-on-chip experiments demonstrate that PYE directly regulates the Fe homeostasis markers (Zinc Induced Facilitator 1 (ZIF1), Ferric Reduction Oxidase 3 (FRO3), and nicotianamine synthase

4 (NAS4)) which are responsible for intracellular Fe homeostasis (Long *et al.*, 2010). Further PYE directly regulates the Ib bHLHs from the FIT network. Finally, PYE acts as a transcriptional hub in roots, as it not only interacts with most of the PYE network, but is also directly regulated other members of the PYE network, as well as undergoing transcriptional autoregulation.

Four bHLH proteins make up the remainder of the PYE network; bHLH104, IAA-Resistant 3 (ILR3, bHLH105), bHLH115, and bHLH34. These proteins are all able to bind the promoters of Ib bHLHs, and dimerize with each other (Rampey *et al.*, 2006; Long *et al.*, 2010; Zhang *et al.*, 2015; Li *et al.*, 2016; Liang *et al.*, 2017). An exception exists between bHLH104 and bHLH34, which have not been shown to dimerize with bHLH115 (Zhang *et al.*, 2015).

Unlike the other bHLH IVc family members, ILR3 contains a basic leucine zipper motif in addition to the bHLH domain, and was described well before the discovery of PYE (Rampey *et al.*, 2006). ILR3 was found while screening mutagenized seeds for insensitivity towards the plant hormone auxin (IAA), and showed enhanced root growth in the presence of exogenous IAA. IAA, like other plant hormones, is stored as bioinactive amino acid conjugates which can be rapidly hydrolyzed to produce active IAA through the action of IAA hydrolases, which utilize heavy metal cofactors such as Mn and Co (Bartel and Fink, 1995; Davies, 1999; LeClere *et al.*, 2002). Interestingly, over expression of ILR3 in the presence toxic concentrations of Mn^{2+} rescued the short root phenotype typically associated with Mn toxicity. Gene expression analysis suggest that ILR3 regulates the vacuolar heavy metal transporters Vacuolar Iron Transporter-like 1 (VILT1), VITL3, and VITL5 (Rampey *et al.*, 2006), which were later characterized as vacuole Fe loading proteins (Kim *et al.*, 2006). This leads to a concise model where ILR3 regulates concentration of unconjugated IAA by modulating the activity of IAA hydrolases through the availability of their metal cofactors.

bHLH115 appears to regulate Fe uptake through the Ib bHLHs by directly binding the Ib bHLH promoters (Liang *et al.*, 2017). As expected, overexpression of bHLH115 results in the induction of FRO2, IRT1, and the FIT network during both Fe replete and Fe deficient conditions, although PYE and BTS (discussed below) are only induced during deficient conditions. As expected from the bHLH115 promoter binding, Ib bHLHs are repressed in *bhlh115*, as well as FRO2 and IRT1, but not PYE or BTS. This suggests that bHLH115 activity is restrained within the context of the PYE network, but within the FIT network, bHLH115 is a key regulator.

bHLH104 and bHLH34 are similar to one another as they do not dimerize with bHLH115, but are similar to the rest of the clade in that their regulation of the Ib bHLHs and induction/repression of the FIT network and Fe uptake pathway in overexpression/mutant lines. While expected of the rest of the clade, bHLH104, bHLH34, and ILR3 were shown to be expressed in the root tip in Li *et al.*, 2016.

The PYE network is simply summarized as a non-redundant family of bHLH proteins which control Fe homeostasis through the induction of bHLH38/39/100/101 and metal transporters, or by altering active hormone pools. In contrast, one prominent negative regulator controls the protein abundance of the *PYE network*. BRUTUS (BTS) is an ubiquitin E3 ligase with six haemerythrin (HEE) domains, a Fe/Zn binding motif (Kobayashi *et al.*, 2013), which is expressed throughout the plant body (Selote *et al.*, 2015). BTS is able to interact with all of the PYE network members, excluding PYE itself, and presumably targets each of them for 26S proteasome degradation (Selote *et al.*, 2015). It should be noted that *pye* mutants have deformed emergent lateral roots, with a bulging mass of epidermal/cortical cells near primary-lateral root boundary which resembles the biceps of a certain fictional sailor. While BRUTUS degrades TFs associated with POPEYE, but is unable to degrade POPEYE itself. BTS is a curious protein as it is induced by Fe deficiency and increased Fe supply increases ubiquitination activity *in vitro*, yet BTS degrades TFs responsible for inducing Fe

deficiency responses (Long *et al.*, 2010; Selote *et al.*, 2015; Hindt *et al.*, 2017). The model put forth suggests that BTS protein accumulates, presumably in an inactive form, until conditions are met to begin PYEL protein degradation, a process which is then regulated by free Fe pools, thereby preventing Fe toxicity.

In summary, the PYE network is composed of PYE, bHLH104, bHLH115, ILR3, bHLH34, and BTS. These TFs serve to induce Fe deficiency responses through induction of their targets, which include the Ib bHLHs 38/39/100/101, throughout the root and leaves (excluding PYE). These proteins are degraded by BTS which is induced under -Fe but serves to degrade PYEL proteins upon Fe sufficiency, thereby preventing Fe toxicity.

4.1 Fe-citrate complexes are translocated from roots to leaves via the xylem

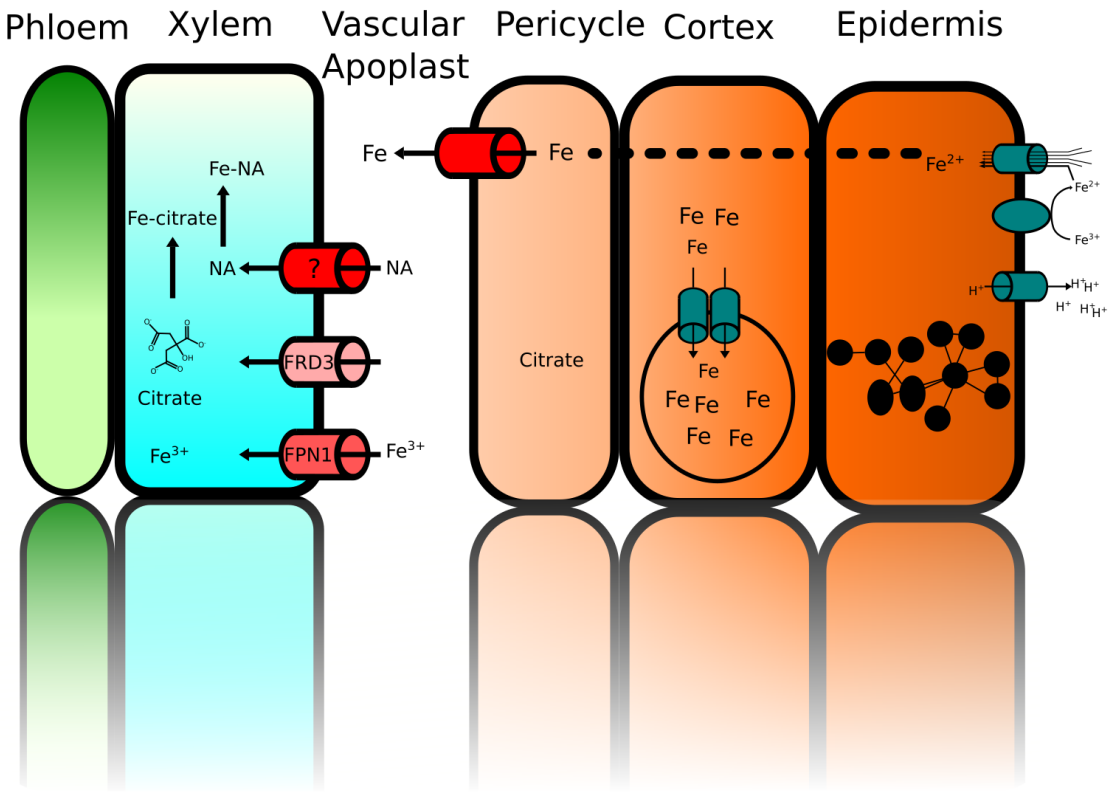

Figure 4 Schematic representation of Fe transport from the epidermis to the xylem. Fe taken up by the FIT network at the epidermis and is transported symplastically through the cortex. While excess Fe can be stored in the root vacuole, Fe that reaches the vascular apoplast is loaded to the xylem through FPN1 where it is chelated by citrate or NA, where it is translocated to the shoot through transevaporational forces.

The first step in root-to-shoot Fe translocation from the site of uptake occurs symplastically through the root cortex (**Figure 4**). Once in the root stele, Fe is carried from root to shoots via the xylem where it is found to be chelated by citrate (Rellán-Álvarez *et al.*, 2010). Citrate is loaded into xylem by the MATE family transporter ferric reductase defective 3 (FRD3) (Durrett *et al.*, 2007), while Fe is loaded into the xylem via Iron Regulated 1 (IREG1) (Morrissey *et al.*, 2009). Although Fe-citrate complexes are important for proper Fe homeostasis, other complexes have been detected and their importance cannot not be ruled out, such as Fe-nicotianamine complexes (Waters *et al.*, 2006; Kumar *et al.*, 2017). *frd3* mutants are of particular interest because they

provide the first insights into the current Fe sensing system. The adult *frd3* mutants are chlorotic despite having high root Fe concentrations, but similar leaf Fe concentrations to wild type. Perl's staining of *frd3* leaves shows Fe being concentrated along the vasculature, while isolation of protoplasts, which are primarily non-vascular cells, show low Fe concentrations (Green, 2004). Further, this chlorotic phenotype of *frd3* can be rescued by foliar application of Fe-EDTA (Green, 2004). The low concentration of Fe in mesophyll cells, high concentrations of Fe in roots, and rescue of the chlorotic phenotype by exogenous foliar Fe suggests a role for Fe citrate in the symplastic loading of Fe in leaves. Perhaps the most significant phenotype of *frd3* is a constitutive induction of Fe deficiency in roots (Rodgers and Guerinot, 2002), which is clearly related to the chlorotic leaves, but suggest that the leaves, and not the roots, are responsible for sensing the Fe status of the plant to activate or repress the Fe uptake machinery (discussed in Section 6.2).

5 Local regulation of Fe deficiency

The response to Fe deficiency in roots is not singular, just as root growth is plastic based on the local environment, individual roots are able to respond to Fe deficiency based on their local Fe supply. This was most clearly demonstrated through split root experiments by Vert *et al.*, 2003. Here, the root system of individual plants was divided into two media regimes, +Fe/+Fe or +Fe/-Fe. The root system exposed to Fe deficiency did not accumulate IRT1 protein, while its' opposing half in replete media showed an increased IRT1 and FRO2 protein accumulation relative to the split root systems with no Fe deficiency. This indicates the total plant Fe status is relayed to the root system where the realization of Fe uptake is resolved based on the local Fe supply.

Fe uptake is not only controlled at the level of protein abundance, but is additionally regulated by post translational modifications. Plants overexpressing FRO2 accumulate both *FRO2* transcript and protein but do not show increased ferric reductase activity, unless exposed to Fe deficient

media. AHA2, the proton pump which releases Fe^{3+} from the soil, shows a similar behavior, as it is only active after phosphorylation initiated by Fe deficiency (Fuglsang *et al.*, 2007; Haruta *et al.*, 2010).

In addition to the tissue-wise regulation of IRT1 abundance, three other mechanisms of IRT1 regulation have been described. IRT1 is found predominately found in the early endosome, where it can be trafficked to the plasma membrane during Fe deficiency. IRT1 stability at the plasma membrane is dependent on the ubiquitination of two residues within a cytoplasmic facing loop by IRT1 Dedradation Factor 1 (IDF1) (Barberon *et al.*, 2011). Upon Fe sufficiency, IRT1 is transported from the plasma membrane back to the early endosome by Sorting Nexin 1 (SNX) (Ivanov *et al.*, 2014) where it can later be returned to the plasma membrane during Fe deficiency. The broad substrate range of IRT1 allows for concomitant influx of divalent cations during Fe deficiency. IRT1 is able to sense the cytoplasmic concentrations of non-iron metals, as they bind to a histidine rich region of the along the cytoplasmic face, inducing the phosphorylation of IRT1 by CIPK23 and subsequent ubiquitination by IDF1 (at a different site than leads to IRT1 stability), leading to vacuolar degradation (Guillaume *et al.*, 2018).

Taken together these results show that Fe uptake is locally controlled, but largely at the post translational level. This system allows for a systemic Fe deficiency signal to be sent to each root, which is resolved only after local conditions are met. Importantly, removal of all Fe from the rhizosphere and root apoplast using the strong Fe chelator bipyridyl prevents Fe deficiency responses, indicating that some free Fe must be present in the apoplast to induce a Fe deficiency response. (Vert *et al.*, 2003). This produces an efficient uptake mechanism which does not waste resources attempting to retrieve Fe from root zones which are devoid of Fe.

6 The systemic Fe deficiency signal and the role of companion cells in leaves

While roots are the site of Fe acquisition, and maintain several complex regulatory networks to maintain homeostasis, leaves present the largest demand for Fe in the plant. Although it has long been speculated that leaves are the site of an Fe sensing system (Vert *et al.*, 2003), only recently have major advancements in the identification of the molecular mechanism of Fe sensing been made. Before discussing the role of leaves in Fe sensing, we will establish one mechanism of Fe homeostasis within photosynthetically active leaves referred to as the chloroplast/vacuole shuttle (CVS), which provides a closed loop for Fe trafficking once in the cell. No efflux of Fe from the mesophyll has been described in the context of a Fe deficiency response, suggesting that Fe status sensing occurs elsewhere. Next, evidence for the role of companion cells in directly sensing the Fe deficiency response is described through observations of *frd3* and *opt3* mutants.

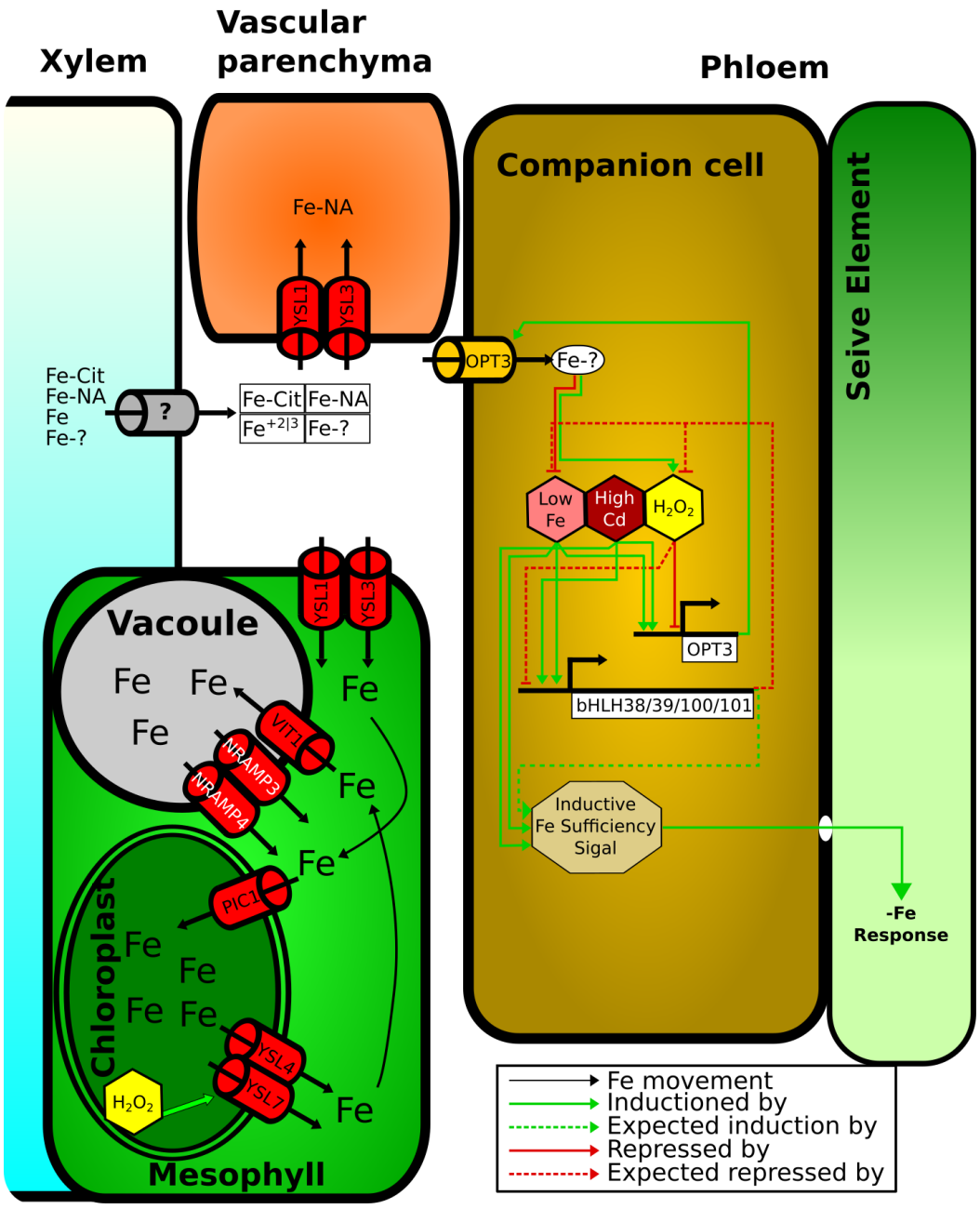

Figure 5 Schematic representation of the vacuole/chloroplast shuttle and Fe sensing in the companion cell. Fe which reaches the vascular apoplast is loaded into photosynthetically active cells by YSL1 and YSL3. Once in the cell Fe is transported to the chloroplast by PIC1. When chloroplastic Fe levels begin producing H2O2, excess Fe is exported from the chloroplast to the cytosol by YSL4 and YSL7. Cytosolic Fe can then be transported into the vacuole for long term storage by VIT1. During Fe deficiency vacuolar Fe is released to the cytoplasm by NRAMP3 and NRAMP4, where it can again be loaded into the chloroplast by PIC1. Fe which is not loaded into the photosynthetically active cells can be transported into the companion cell by OPT3. The companion cell likely contains a yet undescribed Fe sensor. Hence, Fe loaded into the companion cell by OPT3 serve to repress Fe deficiency responses, such as Ib bHLHs and OPT3. Cd is able to induce Fe deficiency responses, presumably by acting as a Fe mimic which does not transduce a Fe sufficiency signal. Meanwhile H2O2, generated by free Fe or another mechanism is able to suppress Fe deficiency responses. The net output of these mechanisms is a leaf to root signal which represses Fe deficiency responses in roots.

6.1 Fe homeostasis in photosynthetically active cells is maintained by the chloroplast-vacuole shuttle

Fe is utilized in a variety of biochemical processes, all of which can be hampered by Fe deficiency as enzymes compete for available Fe. In the particular case of photosynthetically active chloroplasts, Fe is critical as it mediates many steps in photosynthesis (Hindt and Guerinot, 2012; Ivanov *et al.*, 2012; Rout and Sahoo, 2015). Within the chloroplast Fe is stored as an inorganic crystal within the central cavity of ferritin protein complexes, with individual complexes holding up to 4,500 Fe ions (Harrison and Arosio, 1996; Arosio *et al.*, 2009). Despite the capacity of the chloroplast to hold large quantities of Fe, the vacuole remains the largest storage compartment of Fe in plant cells (Lanquar *et al.*, 2005; Roschzttardtz *et al.*, 2009). Hence, ferritins do not serve as long term storage of excess Fe, but rather serve as a buffer against Fe deficiency and excess as demand fluctuate at the thylakoid membrane. During Fe excess, Fe can generate reactive oxygen species by the spontaneous decay of Fe^{3+} to $Fe^{2+} + e^-$ (Arosio *et al.*, 2009), or by the Fenton reaction in where Fe reacts with H_2O_2 to generate the potent free radical superoxide (Winterbourn, 1995).

Consequently plants have evolved mechanisms to remove Fe from the chloroplast via the transporters Yellow-Stripe like 4 (YSL4) and YSL6 (Divol *et al.*, 2013)(**Figure 5**), which presumably respond to increased ROS levels as the ferritins reach their holding capacity. Upon export to the cytosol, Fe is imported into the vacuole by VIT1, and possibly other VITL proteins (Kim *et al.*, 2006; Gollhofer *et al.*, 2014). During increased Fe demand or Fe deficiency, vacuolar Fe can be remobilized from the vacuole to the cytosol by the Natural Resistance-Associated Macrophage Protein 3 (NRAMP3) and NRAMP4 (Mary *et al.*, 2015; Molins *et al.*, 2013). Cytosolic Fe can again be mobilized to the chloroplast by Permease In Chloroplasts 1 (PIC1) (Duy *et al.*, 2011), completing

the shuttle from chloroplast to vacuole and back again under alternating Fe excess and Fe demand.

While the CVS describes the intracellular trafficking of Fe through photosynthetically active cells, no mechanism of remobilization of Fe back to the apoplast has been described in the context of Fe deficiency. It is unlikely that such a mechanism exists as it pertains to Fe deficiency, as it has long been observed that chlorosis induced by Fe deficiency affects developing tissues, while mature leaves show no signs of Fe stress, suggesting that Fe is not remobilized. While this does not rule out a non-iron signaling molecule being transmitted from the photosynthetically active tissue to the roots, studies of several mutants thoroughly demonstrate that companion cells within the vasculature are the likely site responsible for signaling the Fe status of the plant to the roots.

6.2 The systemic Fe sensor

The plant's vasculature is divided into three major tissues: xylem, vascular parenchyma, and phloem. While the xylem is composed of the highly lignified remains of a cell with no nuclei or organelles and transports water from the root to shoot via transevaporational forces, the phloem is a living cell whose cytoplasm flows along a sucrose gradient from source to sink, often from leaf to roots or leaf to seed.

The phloem is composed of two cell types: the sieve element and companion cells. The sieve element is a metabolically active, living cell with chloroplasts and mitochondria, but has no nucleus nor free ribosomes (Evert, 2006; Tetyuk *et al.*, 2013). Homeostasis of the sieve element is maintained by one or more companion cells, which are typically derived from the same mother cell as the sieve element. Indeed the death of the sieve element or companion cell results in the

death of the other, emphasizing the importance of the relationship between the two cells (van Bel and Knoblauch, 2000). In contrast to the sieve element, the cytoplasm of the companion cell is extremely dense, containing rough endoplasmic reticulum, chloroplasts which rarely have starch granules, mitochondria, and few vacuoles, suggesting that the companion cell metabolically maintains the sieve element (Evert, 2006). These two cells are interconnected through highly branched plasmadesmata, which are enervated by the endoplasmic reticulum and display no active transport between cells; that is, molecules as large as GFP (27kDa) are able to diffuse from companion cells into sieve elements for long-distance transport (Kempers and Van Bel, 1997). While transport from the companion cell to the sieve element is nonrestrictive, transport from the apoplast into the companion cell is highly regulated, at least in plant such as Arabidopsis which are described as *apoplastic* loaders. That is, the companion cell is cytoplasmically isolated from the surrounding vascular parenchyma in most species, allowing the companion cell to control the influx of metabolites to the sieve element (Gamalei, 1989; Braun and Slewinski, 2009).

OPT3 is one such companion cell loading transporters, believed to load Fe or an Fe complex into companion cells (Zhai *et al.*, 2014; Mendoza-Cózatl *et al.*, 2014). OPT3 expression is highly correlated with the Fe status of the plant as was demonstrated through expression of a luciferase reporter gene under control of the OPT3 promoter. When transferred to -Fe media luciferase activity increased dramatically, which was quickly abolished upon Fe resupply (Khan *et al.*, 2018). Although this demonstrates the importance of OPT3 in Fe homeostasis, the phenotypes of OPT3 mutants provide the most significant evidence that companion cells play a key role in Fe sensing in leaves.

While *opt3-1* knock-out mutants are embryo lethal (Stacey *et al.*, 2002), the knock-down mutants *opt3-2* and *opt3-3 (opt3*) exhibit two important phenotypes: first, roots of *opt3* exhibit a

constitutive induction of the Fe uptake pathway (Stacey *et al.*, 2008; Mendoza-Cózatl *et al.*, 2014), which is caused by an induction of the FIT network (Khan *et al.*, 2018). The induction of Fe deficiency genes in *opt3-2* is not limited to the FIT network and its targets, as the transcriptome of *opt3-2* roots appears to be under constant Fe deficiency. The constitutive induction of IRT1 results in the over-accumulation of heavy metals such as Fe, Zn, and Mn in both leaves and roots, suggesting that *opt3* roots are unable to sense their own Fe status. Second, *opt3* leaves show a transcriptional profile in line with an Fe overload. This is in agreement with over accumulation of Fe found in *opt3* leaves, and suggests that unlike roots, *opt3* leaves are able to properly sense their Fe status. While both, the whole leaf and leaf vasculature are Fe rich, the phloem sap and companion cell of *opt3* contains ~50% less Fe than wild type plants (Zhai *et al.*, 2014). This reduction supports the role of OPT3 as an Fe transporter; however, whether OPT3 transports free Fe, and Fe complex or a molecule required for Fe mobilization is not known (Zhai *et al.*, 2014). Furthermore, despite the Fe deficient conditions in companion cells, the Fe deficiency responses are not induced in *opt3* companion cells, as no differential expression of bHLH38/39/100/101 is observed in *opt3-2* leaves (Khan *et al.*, 2018). This suggests that OPT3 function is not strictly that of a Fe importer. Expression of OPT3 expression in green tissues, including the companion cell, complements the *opt3-2* mutant, indicating that defects in *opt3-2* originate in leaves (Mendoza-Cózatl *et al.*, 2014). Taken together this indicates the Fe status signal is a function of the concentration of Fe in the companion cell mediated by OPT3, and the Fe concentration in the companion cell controls the root Fe deficiency response.

Although studies in *opt3* are unable to rule out the possibility of a root to leaf signal, as *opt3* phenotypes could result from the translocation of a root borne Fe signal which is not realized due to the absence of OPT3. *frd3* demonstrates that this root borne signal does not exist. *frd3*, like *opt3*, induces Fe deficiency responses in the root and accumulates Fe along the leaf vasculature.

Unlike *opt3,* the *frd3* phenotype can be rescued by the foliar application of Fe-EDTA, indicating that *opt3* is able to receive Fe from the root, but is unable to process it into a systemic shoot-to-root signal.

As previously established, it is unlikely that photosynthetically active mesophyll cells are responsible for reloading the apoplast during Fe excess as a means to communicate their Fe status. This is further supported by the observation that the companion cells are able to mount a Fe deficiency response before the mesophyll (Khan *et al.*, 2018). Indeed, the companion cell induces Fe responsive genes more quickly than roots, with OPT3 being induced in as little as 2 hours, relative to the full induction of FIT1 after 8 hours (Khan *et al.*, 2018). Additionally bHLH38/39/100/101 are preferentially expressed in companion cells (Mustroph *et al.*, 2009b) and bHLH100 was shown to rapidly respond to -Fe along similar time scales as OPT3 (Khan *et al.*, 2018). Further, Fe deficiency responses seem to occur in companion cells hours ahead of the mesophyll response (Khan *et al.*, 2018).

Besides hormones like IAA and ethylene, other molecules have been known to impair Fe homeostasis, one of them being the non-essential element cadmium (Cd). Cd exposure is able to induce a Fe deficiency-like response in leaves and roots. In Chapter 2 we will describe how Cd is able to induce an iron deficiency response in the companion cell despite the presence of large quantities of Fe present in the vasculature, suggesting that the Fe sensor in companion cells is impaired by Cd. Cd and Fe share similar atomic features as they both exist as +2 cations and have similar electron cloud radii, owing to the overlapping valence shells found in transition metals, although Cd does not share the same redox potential as Fe. Hence, we hypothesize that Cd is able to bind and disrupt the Fe sensor mechanism thereby inducing an Fe deficiency response. This work will be discussed in detail in Chapter 2.

In summary, we present a model (**Figure 5**) where the Fe concentration in the vascular apoplast is reduced by either an increase in Fe absorption to the mesophyll (increased Fe demand), or by the reduction in Fe translocation from root to shoot (decreased Fe supply), both resulting in a decreased concentration of Fe in the vasculature, including companion cells. This in turns triggers a transcriptional cascade involving bHLH38/39/100/101 within the companion cell which results in an activation of an Fe deficiency response. In addition, and during Fe deprivation, a shoot-borne Fe-related repressive signal is lost thus signaling the roots the lack of available Fe and allowing the upregulation of the root Fe deficiency response that includes the Fe reduction and uptake machinery.

7 Conclusion

Fe is a vital nutrient for all forms of life due to its roles through primary and secondary metabolism, but must be carefully regulated to balance deficiency and toxicity. During Fe deficiency, Fe levels in companion cell decrease, resulting in the transmission of a Fe deficiency signal to roots. This unknown systemic signal induces the FIT network to initiate the uptake of Fe from the rhizosphere via the reduction strategy of Fe uptake. Once taken into the root Fe is stored in vacuoles or transported in the xylem to distal tissues, including leaves. The translocated Fe is then able to restore Fe levels in companion cell and repress the Fe deficiency signal (or restore the Fe sufficiency/repressing signal). During prolonged Fe deficiency, the broad substrate range of IRT1 allows for non-iron metals to accumulate in excess and induce oxidative damage. This damage is prevented by local Fe regulation of IRT1, which take the form of post translational modifications which result in the degradation or loss of activity.

In sum, Fe homeostasis is a robust system with multiple levels of feedforward and feedback regulation loops which allows for the efficient sensing and mobilization of Fe from the soil to all plant organs and tissues.

8 Bibliography

Arosio, P., Ingrassia, R. and Cavadini, P. (2009) Ferritins: A family of molecules for iron storage, antioxidation and more. *Biochim. Biophys. Acta - Gen. Subj.*, **1790**, 589–599.

Barberon, M., Zelazny, E., Robert, S., Conéjéro, G., Curie, C., Friml, J. and Vert, G. (2011) Monoubiquitin-dependent endocytosis of the iron-regulated transporter 1 (IRT1) transporter controls iron uptake in plants. *Proc. Natl. Acad. Sci.*, **108**, E450--E458.

Bartel, B. and Fink, G.R. (1995) ILR1, an amidohydrolase that releases active indole-3-acetic acid from conjugates. *Science (80-.).*, **268**, 1745–1748.

Bel, A.J.E. van and Knoblauch, M. (2000) Sieve element and companion cell: the story of the comatose patient and the hyperactive nurse. *Funct. Plant Biol.*, **27**, 477–487.

Braun, D.M. and Slewinski, T.L. (2009) Genetic control of carbon partitioning in grasses: roles of sucrose transporters and tie-dyed loci in phloem loading. *Plant Physiol.*, **149**, 71–81.

Chao, Q., Rothenberg, M., Solano, R., Roman, G., Terzaghi, W. and Ecker, J.R. (1997) Activation of the ethylene gas response pathway in arabidopsis by the nuclear protein ETHYLENE-INSENSITIVE3 and related proteins. *Cell*, **89**, 1133–1144.

Clemens, S. and Weber, M. (2016) The essential role of coumarin secretion for Fe acquisition from alkaline soil. *Plant Signal. Behav.*, **11**, 1–6.

Colangelo, E.P. (2004) The Essential Basic Helix-Loop-Helix Protein FIT1 Is Required for the Iron Deficiency Response. *Plant Cell Online*, **16**, 3400–3412.

Conte, S.S. and Walker, E.L. (2011) Transporters Contributing to Iron Trafficking in Plants. *Mol. Plant*, **4**, 464–476.

Curie, C., Panaviene, Z., Loulergue, C., Dellaporta, S.L., Briat, J.-F. and Walker, E.L. (2001) Maize yellow stripe1 encodes a membrane protein directly involved in Fe(III) uptake. *Nature*, **409**, 346.

Davies, R.T. (1999) IAR3 Encodes an Auxin Conjugate Hydrolase from Arabidopsis. *Plant Cell Online*, **11**, 365–376.

Divol, F., Couch, D., Conejero, G., Roschzttardtz, H., Mari, S. and Curie, C. (2013) The Arabidopsis YELLOW STRIPE LIKE4 and 6 Transporters Control Iron Release from the Chloroplast. *Plant Cell*, **25**, 1040–1055.

Durrett, T.P., Gassmann, W. and Rogers, E.E. (2007) The FRD3-Mediated Efflux of Citrate into the Root Vasculature Is Necessary for Efficient Iron Translocation. *Plant Physiol.*, **144**, 197–205.

Duy, D., Stübe, R., Wanner, G. and Philippar, K. (2011) The chloroplast permease PIC1 regulates plant growth and development by directing homeostasis and transport of iron. *Plant Physiol.*, pp--110.

Eide, D., Broderius, M., Fett, J. and Guerinot, M. Lou (1996) A novel iron-regulated metal transporter from plants identified by functional expression in yeast. *Proc. Natl. Acad. Sci.*, **93**, 5624–5628.

Evert, R.F. (2006) *Esau's plant anatomy: meristems, cells, and tissues of the plant body: their*

structure, function, and development, John Wiley & Sons.

Fourcroy, P., Sisó-Terraza, P., Sudre, D., et al. (2014) Involvement of the ABCG37 transporter in secretion of scopoletin and derivatives by Arabidopsis roots in response to iron deficiency. *New Phytol.*, **201**, 155–167.

Fuglsang, A.T., Guo, Y., Cuin, T.A., et al. (2007) Arabidopsis Protein Kinase PKS5 Inhibits the Plasma Membrane H+-ATPase by Preventing Interaction with 14-3-3 Protein. *Plant Cell Online*, **19**, 1617–1634.

Gamalei, Y. (1989) Structure and function of leaf minor veins in trees and herbs. *Trees*, **3**, 96–110.

Gollhofer, J., Timofeev, R., Lan, P., Schmidt, W. and Buckhout, T.J. (2014) Vacuolar-iron-transporter1-like proteins mediate iron homeostasis in Arabidopsis. *PLoS One*, **9**, e110468.

Green, L.S. (2004) FRD3 Controls Iron Localization in Arabidopsis. *Plant Physiol.*, **136**, 2523–2531.

Guillaume, D., Neveu, J., Enric, Z. and Vert, G. (2018) Metal Sensing by the IRT1 Transporter-Receptor Orchestrates Its Own Degradation and Plant Metal Nutrition. *Mol. Cell*, **69**, 953–964.

Harrison, P.M. and Arosio, P. (1996) The ferritins: Molecular properties, iron storage function and cellular regulation. *Biochim. Biophys. Acta - Bioenerg.*, **1275**, 161–203.

Haruta, M., Burch, H.L., Nelson, R.B., Barrett-Wilt, G., Kline, K.G., Mohsin, S.B., Young, J.C., Otegui, M.S. and Sussman, M.R. (2010) Molecular characterization of mutant Arabidopsis plants with reduced plasma membrane proton pump activity. *J. Biol. Chem.*, **285**, 17918–17929.

Hindt, M.N., Akmakjian, G.Z., Pivarski, K.L., Punshon, T., Baxter, I., Salt, D.E. and Guerinot, M. Lou (2017) BRUTUS and its paralogs, BTS LIKE1 and BTS LIKE2, encode important negative regulators of the iron deficiency response in Arabidopsis thaliana. *Metallomics*, **9**, 876–890.

Hindt, M.N. and Guerinot, M. Lou (2012) Getting a sense for signals: regulation of the plant iron deficiency response. *Biochim Biophys Acta*, **1823**, 1521–1530.

Ivanov, R., Brumbarova, T. and Bauer, P. (2012) Fitting into the harsh reality: Regulation of iron-deficiency responses in dicotyledonous plants. *Mol. Plant*, **5**, 27–42.

Ivanov, R., Brumbarova, T., Blum, A., Jantke, A.-M., Fink-Straube, C. and Bauer, P. (2014) SORTING NEXIN1 Is Required for Modulating the Trafficking and Stability of the Arabidopsis IRON-REGULATED TRANSPORTER1. *Plant Cell*, **26**, 1294–1307.

Kai, K., Mizutani, M., Kawamura, N., Yamamoto, R., Tamai, M., Yamaguchi, H., Sakata, K. and Shimizu, B.I. (2008) Scopoletin is biosynthesized via ortho-hydroxylation of feruloyl CoA by a 2-oxoglutarate-dependent dioxygenase in Arabidopsis thaliana. *Plant J.*, **55**, 989–999.

Kempers, R. and Bel, A.J.E. Van (1997) Symplasmic connections between sieve element and companion cell in the stem phloem of Vicia faba L. have a molecular exclusion limit of at least 10 kDa. *Planta*, **201**, 195–201.

Khan, M.A., Castro-Guerrero, N.A., McInturf, S.A., et al. (2018) Changes in iron availability in Arabidopsis are rapidly sensed in the leaf vasculature and impaired sensing leads to opposite transcriptional programs in leaves and roots. *Plant. Cell Environ.*, 1–14.

Kim, S.A., Punshon, T., Lanzirotti, A., Li, A., Alonso, J.M., Ecker, J.R., Kaplan, J. and Guerinot, M. Lou (2006) Localization of iron in Arabidopsis seed requires the vacuolar membrane transporter VIT1. *Science (80-.).*, **314**, 1295–1298.

Kobayashi, T., Nagasaka, S., Senoura, T., Itai, R.N., Nakanishi, H. and Nishizawa, N.K. (2013) Iron-binding haemerythrin RING ubiquitin ligases regulate plant iron responses and accumulation. *Nat. Commun.*, **4**, 1–12.

Korshunova, Y.O., Eide, D., Clark, W.G., Guerinot, M. Lou and Pakrasi, H.B. (1999) The IRT1 protein from Arabidopsis thaliana is a metal transporter with a broad substrate range. *Plant Mol. Biol.*, **40**, 37–44.

Kumar, R.K., Chu, H.-H., Abundis, C., Vasques, K., Chan-Rodriguez, D., Chia, J.-C., Huang, R., Vatamaniuk, O.K. and Walker, E.L. (2017) Iron-Nicotianamine Transporters are Required for Proper Long Distance Iron Signaling. *Plant Physiol.*, **175**, pp.00821.2017.

Lanquar, V., Lelièvre, F., Bolte, S., et al. (2005) Mobilization of vacuolar iron by AtNRAMP3 and AtNRAMP4 is essential for seed germination on low iron. *EMBO J.*, **24**, 4041–4051.

Le, C.T.T., Brumbarova, T., Ivanov, R., Stoof, C., Weber, E., Mohrbacher, J., Fink-Straube, C. and Bauer, P. (2016) ZINC FINGER OF ARABIDOPSIS THALIANA12 (ZAT12) Interacts with FER-LIKE IRON DEFICIENCY-INDUCED TRANSCRIPTION FACTOR (FIT) Linking Iron Deficiency and Oxidative Stress Responses. *Plant Physiol.*, **170**, 540–557.

LeClere, S., Tellez, R., Rampey, R.A., Matsuda, S.P.T. and Bartel, B. (2002) Characterization of a family of IAA-amino acid conjugate hydrolases from Arabidopsis. *J. Biol. Chem.*, **277**, 20446–20452.

Li, X., Zhang, H., Ai, Q., Liang, G. and Yu, D. (2016) Two bHLH Transcription Factors, bHLH34 and bHLH104, Regulate Iron Homeostasis in *Arabidopsis thaliana*. *Plant Physiol.*, **170**, 2478–2493.

Liang, G., Zhang, H., Li, X., Ai, Q. and Yu, D. (2017) BHLH transcription factor bHLH115 regulates iron homeostasis in Arabidopsis thaliana. *J. Exp. Bot.*, **68**, 1743–1755.

Ling, H.-Q., Bauer, P., Bereczky, Z., Keller, B. and Ganal, M. (2002) The tomato fer gene encoding a bHLH protein controls iron-uptake responses in roots. *Proc. Natl. Acad. Sci.*, **99**, 13938–13943.

Lingam, S., Mohrbacher, J., Brumbarova, T., Potuschak, T., Fink-Straube, C., Blondet, E., Genschik, P. and Bauer, P. (2011) Interaction between the bHLH Transcription Factor FIT and ETHYLENE INSENSITIVE3/ETHYLENE INSENSITIVE3-LIKE1 Reveals Molecular Linkage between the Regulation of Iron Acquisition and Ethylene Signaling in *Arabidopsis*. *Plant Cell*, **23**, 1815–1829.

Long, T.A., Tsukagoshi, H., Busch, W., Lahner, B., Salt, D.E. and Benfey, P.N. (2010) The bHLH transcription factor POPEYE regulates response to iron deficiency in Arabidopsis roots. *Plant Cell*, **22**, 2219–2236.

Mary, V., Ramos, M.S., Gillet, C., et al. (2015) Bypassing iron storage in endodermal vacuoles rescues the iron mobilization defect in the nramp3nramp4 double mutant. *Plant Physiol.*, pp--00380.

Mendoza-Cózatl, D.G., Xie, Q., Akmakjian, G.Z., et al. (2014) OPT3 is a component of the iron-signaling network between leaves and roots and misregulation of OPT3 leads to an over-accumulation of cadmium in seeds. *Mol. Plant*, **7**, 1455–1469.

Molins, H., Michelet, L., Lanquar, V., Agorio, A., Giraudat, J., Roach, T., Krieger-Liszkay, A. and Thomine, S. (2013) Mutants impaired in vacuolar metal mobilization identify chloroplasts as a target for cadmium hypersensitivity in Arabidopsis thaliana. *Plant, Cell Environ.*, **36**, 804–817.

Morrissey, J., Baxter, I.R., Lee, J., Li, L., Lahner, B., Grotz, N., Kaplan, J., Salt, D.E. and Guerinot, M.L. (2009) The Ferroportin Metal Efflux Proteins Function in Iron and Cobalt Homeostasis in Arabidopsis. *Plant Cell*, **21**, 3326–3338.

Mustroph, A., Zanetti, M.E., Jang, C.J.H., Holtan, H.E., Repetti, P.P., Galbraith, D.W., Girke, T. and Bailey-Serres, J. (2009) Profiling translatomes of discrete cell populations resolves altered cellular priorities during hypoxia in Arabidopsis. *Proc. Natl. Acad. Sci.*, **106**, 18843–18848.

Negishi, T., Nakanishi, H., Yazaki, J., Kishimoto, N., Fujii, F. and Shimbo, K. (2002) cDNA microarray analysis of gene expression during Fe-deficiency stress in barley suggests that polar transport of vesicles is implicated in phytosiderophore secretion in Fe-deficient barley roots. , **30**.

Palmer, C.M., Hindt, M.N., Schmidt, H., Clemens, S. and Guerinot, M. Lou (2013) MYB10 and MYB72 are required for growth under iron-limiting conditions. *PLoS Genet*, **9**, e1003953.

Potuschank, T., Lechner, E., Parmentier, Y., Yanagisawa, S., Grava, S., Koncz, C. and Genschik, P. (2013) EIN3-Dependent Regulation of Plant Ethylene Hormone Signaling by Two Arabidopsis F Box Proteins: EBF1 and EBG2. *Cell*, **115**, 32.

Rampey, R.A., Woodward, A.W., Hobbs, B.N., Tierney, M.P., Lahner, B., Salt, D.E. and Bartel, B. (2006) An arabidopsis basic helix-loop-helix leucine zipper protein modulates metal homeostasis and auxin conjugate responsiveness. *Genetics*, **174**, 1841–1857.

Rellán-Álvarez, R., Giner-Martínez-Sierra, J., Orduna, J., Orera, I., Rodríguez-Castrilln, J.Á., García-Alonso, J.I., Abadía, J. and Álvarez-Fernández, A. (2010) Identification of a Tri-Iron(III), Tri-Citrate Complex in the Xylem Sap of Iron-Deficient Tomato Resupplied with Iron: New Insights into Plant Iron Long-Distance Transport. *Plant Cell Physiol.*, **51**, 91–102.

Robinson, N.J., Procter, C.M., Connolly, E.L. and Guerinot, M. Lou (1999) A ferric-chelate reductase for iron uptake from soils. *Nature*, **397**, 694.

Rodgers, E.E. and Guerinot, M. Lou (2002) FRD3, a Member of the Multidrug and Toxin Efflux Family, Controls Iron Deficiency Responses in Arabidopsis. *Plant Cell*, **14**, 1787–1799.

Roschzttardtz, H., Conejero, G., Curie, C. and Mari, S. (2009) Identification of the Endodermal Vacuole as the Iron Storage Compartment in the Arabidopsis Embryo. *Plant Physiol.*, **151**, 1329–1338.

Rout, G.R. and Sahoo, S. (2015) Role of Iron in Plant Growth and Metabolism. *Rev. Agric. Sci.*, **3**, 1–24.

Sakaguchi, T., Nishizawa, N.K., Nakanishi, H., Yoshimura, E. and Mori, S. (1999) The role of

potassium in the secretion of mugineic acids family phytosiderophores from iron-deficient barley roots. , 221–227.

Santi, S. and Schmidt, W. (2009) Dissecting iron deficiency-induced proton extrusion in Arabidopsis roots. *New Phytol.*, **183**, 1072–1084.

Schenkeveld, W.D.C., Schindlegger, Y., Oburger, E., Puschenreiter, M., Hann, S. and Kraemer, S.M. (2014) Geochemical processes constraining iron uptake in strategy II fe acquisition. *Environ. Sci. Technol.*, **48**, 12662–12670.

Schmidt, H., Günther, C., Weber, M., Spörlein, C., Loscher, S., Böttcher, C., Schobert, R. and Clemens, S. (2014) Metabolome analysis of Arabidopsis thaliana roots identifies a key metabolic pathway for iron acquisition. *PLoS One*, **9**.

Selote, D., Samira, R., Matthiadis, A., Gillikin, J.W. and Long, T.A. (2015) Iron-Binding E3 Ligase Mediates Iron Response in Plants by Targeting Basic Helix-Loop-Helix Transcription Factors. *Plant Physiol.*, **167**, 273–286.

Shi, W.M., Chino, M., Youssef, R.A., Mori, S. and Takagi, S. (1988) The occurrence of mugineic acid in the rhizosphere soil of barley plant. *Soil Sci. Plant Nutr.*, **34**, 585–592.

Sivitz, A.B., Hermand, V., Curie, C. and Vert, G. (2012) Arabidopsis bHLH100 and bHLH101 control iron homeostasis via a FIT-independent pathway. *PLoS One*, **7**, e44843.

Solano, R., Stepanova, A., Chao, Q. and Ecker, J.R. (1998) Nuclear events in ethylene signaling: A transcriptional cascade mediated by ETHYLENE-INSENSITIVE3 and ETHYLENE-RESPONSE-FACTOR1. *Genes Dev.*, **12**, 3703–3714.

Stacey, M.G., Koh, S., Becker, J. and Stacey, G. (2002) AtOPT3, a member of the oligopeptide transporter family, is essential for embryo development in Arabidopsis. *Plant Cell*, **14**, 2799–2811.

Stacey, M.G., Patel, A., McClain, W.E., Mathieu, M., Remley, M., Rogers, E.E., Gassmann, W., Blevins, D.G. and Stacey, G. (2008) The Arabidopsis AtOPT3 protein functions in metal homeostasis and movement of iron to developing seeds. *Plant Physiol.*, **146**, 589–601.

Stein, A.J. (2010) Global impacts of human mineral malnutrition. *Plant Soil*, **335**, 133–154.

Stringlis, I.A., Yu, K., Feussner, K., et al. (2018) MYB72-dependent coumarin exudation shapes root microbiome assembly to promote plant health. *Proc. Natl. Acad. Sci.*, **115**, E5213–E5222.

Strlič, M., Kolar, J., Šelih, V.S., Kočar, D. and Pihlar, B. (2003) A comparative study of several transition metals in fenton-like reaction systems at circum-neutral pH. *Acta Chim. Slov.*, **50**, 619–632.

Sun, X., Zhou, D., Kandavelu, P., Zhang, H., Yuan, Q., Wang, B.C., Rose, J. and Yan, Y. (2015) Structural insights into substrate specificity of feruloyl-CoA 6'-hydroxylase from Arabidopsis thaliana. *Sci. Rep.*, **5**, 1–10.

Takagi, S., Kamei, S. and Yu, M. (1988) Efficiency of iron extraction from soil by mugineic acid family phytosiderophores. *J. Plant Nutr.*, **11**, 643–651.

Tetyuk, O., Benning, U.F. and Hoffmann-Benning, S. (2013) Collection and Analysis of Arabidopsis

Phloem Exudates Using the EDTA-facilitated Method. *J. Vis. Exp.*, 1–11.

Tsai, H.-H., Rodriguez-Celma, J., Lan, P., Wu, Y.-C., Vélez-Bermúdez, I.C. and Schmidt, W. (2018) Scopoletin 8-Hydroxylase-Mediated Fraxetin Production is Crucial for Iron Mobilization. *Plant Physiol.*, **177**, pp.00178.2018.

Vert, G. a, Briat, J.-F. and Curie, C. (2003) Dual regulation of the Arabidopsis high-affinity root iron uptake system by local and long-distance signals. *Plant Physiol.*, **132**, 796–804.

Vert, G., Barberon, M., Zelazny, E., Séguéla, M., Briat, J.-F. and Curie, C. (2009) Arabidopsis IRT2 cooperates with the high-affinity iron uptake system to maintain iron homeostasis in root epidermal cells. *Planta*, **229**, 1171–1179.

Wang, N., Cui, Y., Liu, Y., Fan, H., Du, J., Huang, Z., Yuan, Y., Wu, H. and Ling, H.-Q. (2013) Requirement and functional redundancy of Ib subgroup bHLH proteins for iron deficiency responses and uptake in Arabidopsis thaliana. *Mol. Plant*, **6**, 503–513.

Waters, B.M., Chu, H.-H., Didonato, R.J., Roberts, L.A., Eisley, R.B., Lahner, B., Salt, D.E. and Walker, E.L. (2006) Mutations in Arabidopsis yellow stripe-like1 and yellow stripe-like3 reveal their roles in metal ion homeostasis and loading of metal ions in seeds. *Plant Physiol.*, **141**, 1446–1458.

White, K.C. (2005) Anemia is a poor predictor of iron deficiency among toddlers in the United States: for heme the bell tolls. *Pediatrics*, **115**, 315–320.

White, P.J. and Broadley, M.R. (2009) Biofortification of crops with seven mineral elements often lacking in human diets - iron, zinc, copper, calcium, magnesium, selenium, and iodine. , **182**, 49–84.

WHO and UNICEF (2001) UNU. *Iron Defic. anaemia assessment, Prev. Control. a Guid. Program. Manag. Geneva World Heal. Organ.*

Winterbourn, C.C. (1995) Toxicity of iron and hydrogen peroxide: the Fenton reaction. *Toxicol. Lett.*, **82**–**83**, 969–974.

Wirén, N. Von, Mori, S., Marschner, H., Romheld, V., Hohenheim, U. and Germany, N.W. (1994) Iron Inefficiency in Maize Mutant ysl (Zea mays 1 Yellow-Stripe) I s Caused by a Defect in Uptake of iron Phytosiderophores ’. , 71–77.

Yanagisawa, S., Yoo, S.-D. and Sheen, J. (2003) Differential regulation of EIN3 stability by glucose and ethylene signalling in plants. *Nature*, **425**, 521.

Yang, Y., Ou, B., Zhang, J., Si, W., Gu, H., Qin, G. and Qu, L.J. (2014) The Arabidopsis Mediator subunit MED16 regulates iron homeostasis by associating with EIN3/EIL1 through subunit MED25. *Plant J.*, **77**, 838–851.

Yuan, Y., Wu, H., Wang, N., Li, J., Zhao, W., Du, J., Wang, D. and Ling, H.-Q. (2008) FIT interacts with AtbHLH38 and AtbHLH39 in regulating iron uptake gene expression for iron homeostasis in Arabidopsis. *Cell Res.*, **18**, 385–397.

Zamioudis, C., Hanson, J. and Pieterse, C.M.J. (2014) ß-Glucosidase BGLU42 is a MYB72-dependent key regulator of rhizobacteria-induced systemic resistance and modulates iron deficiency responses in Arabidopsis roots. *New Phytol.*, **204**, 368–379.

Zhai, Z., Gayomba, S.R., Jung, H., et al. (2014) OPT3 Is a Phloem-Specific Iron Transporter That Is Essential for Systemic Iron Signaling and Redistribution of Iron and Cadmium in Arabidopsis. , 1–17.

Zhang, J., Liu, B., Li, M., et al. (2015) The bHLH Transcription Factor bHLH104 Interacts with IAA-LEUCINE RESISTANT3 and Modulates Iron Homeostasis in Arabidopsis. *Plant Cell*, **27**, 787–805.

Zimmermann, M.B. and Hurrell, R.F. (2007) Nutritional iron deficiency. *Lancet*, **370**, 511–520.

Cadmium interference with iron sensing reveals transcriptional programs sensitive and insensitive to reactive oxygen species.

1 Abstract

Iron (Fe) is an essential nutrient for all forms of life, but excess Fe is capable of damaging biomolecules through peroxidation by reactive oxygen species (ROS). Cadmium (Cd) is a toxic non-essential element which is also capable of inducing ROS and also has been found to induce an Fe deficiency-like response, presumably by inhibiting Fe uptake. Here, we used Cd to probe the extent on Fe deficiency responses in wildtype plants Col and in an Fe over accumulating mutant (*opt3-2*). Our results demonstrate that Cd induces a conserved set of Fe deficiency responsive genes in leaves. This include regulators of Fe deficiency in companion cells which in turn transduce a Fe deficiency signal to roots. Interestingly, some of these Fe deficiency genes failed to be induced by Cd in *opt3-2,* presumably due to the presence of excess Fe. Moreover, we found that the combination of Fe excess and Cd substantially elevates ROS levels. ROS thus triggering additional changes in the leaf and root transcriptional programs. Despites this increase in ROS, a select cluster of Fe deficiency markers in leaves was found to remain induced by Cd, independently of the presence of excess Fe or high ROS, suggesting that in this case Cd interferes directly with Fe sensing. We further implicate the chloroplast as one site of the generation of these ROS, as determined by a dramatic decrease in photosynthetic efficiency in *opt3-2* after Cd exposure. Altogether, our data points to a hierarchical regulation of Fe deficiency responses based on multiple inputs, including the perceived global Fe status, the levels of ROS within tissues, and a sensing core unique to leaves, which is particularly labile in the presence of cadmium.

2 Introduction

Iron (Fe) is a vital component of all biological systems. Fe is used as a metal cofactor in proteins such as Fe super oxide dismutase, and is also found as Fe-Sulfur (FeS) clusters in ferredoxins, and proteins within the electron transport chains in the mitochondria and chloroplasts (Rout and Sahoo, 2015). These and other roles in a plethora of biological processes make Fe a vital nutrient, without which life cannot flourish. On the other hand, due to its chemical reactivity, Fe excess is also detrimental to any living system due to the production of free radicals. For this reason, Fe homeostasis (i.e. uptake, storage and allocation) is tightly regulated to prevent either deficiency or toxicity.

While Fe is extremely abundant in most soils, it is typically found as insoluble Fe^{3+} and is unavailable for uptake into root cells (Römheld and Marschner, 1986). In turn, land plants have evolved two strategies to overcome the challenge of solubilizing and importing Fe into roots from the rhizosphere. The first is a chelation strategy, strategy II, which is mediated by the release phytosiderophores such as deoxymugineic acid into the rhizosphere where they produce a soluble Fe^{3+} complex which can be imported into the root body by transporters of the Yellow Stripe family (Curie *et al.*, 2001; Curie *et al.*, 2009; Lee *et al.*, 2009; Inoue *et al.*, 2009). The reduction strategy, or strategy I, is carried out at the plasma membrane where membrane bound reductases directly reduce Fe^{3+} to Fe^{2+} prior to transport across the membrane by transporters of the ZIP family (Hindt and Guerinot, 2012).

Of the two strategies, the reduction strategy in dicot plants such as Arabidopsis forms the core of our understanding of the regulation of Fe uptake. Under this strategy, Fe^{3+} is released from negatively charged soil particles by acidifying the rhizosphere. This is mediated by the P-type ATPase AHA2, which hydrolyzes ATP to export H^+ into the rhizosphere (Santi and Schmidt, 2009). Once released from the soil, Fe^{3+} can be reduced to Fe^{2+} by Ferric Reduction Oxidase (FRO2), a membrane bound enzyme which oxidizes NADPH on the cytosolic face while reducing Fe^{3+} on the apoplastic face. Fe^{2+} uptake is then mediated by the Iron Regulated Transporter 1 (IRT1). While IRT1 has high affinity towards Fe^{2+} , it is able to transport a broad range of divalent metals, such as zinc, manganese, and cadmium (Cd) (Korshunova *et al.*, 1999).

The transcriptional regulation of this Fe uptake pathway is mediated by several transcriptional regulatory networks (Long *et al.*, 2010; Cui *et al.*, 2018; Hindt and Guerinot, 2012; Ivanov *et al.*, 2012). The best characterized network is the FIT network, named after the founding member FER-like regulator of iron uptake (FIT1) (Jakoby *et al.*, 2004). The FIT network coordinates five subgroup Ib bHLH transcription factors (TFs): FIT1, bHLH38, bHLH39, bHLH100, and bHLH101. These genes are under independent regulatory schemes but are they believed to function as dimers, allowing for multiple input signals to regulate Fe root uptake by IRT1 (Sivitz *et al.*, 2012; Yuan *et al.*, 2008; Wang *et al.*, 2013). Additionally, it has been demonstrated that FIT1 undergoes post translational regulation, undergoing ubiquitination and subsequent 26S proteasome-mediated turnover for proper function (Sivitz *et al.*, 2011). Interestingly, nitric oxide (NO) was shown to enhance Fe uptake by inhibiting the 26S mediated degradation of FIT1,

resulting in increased levels of FIT1 protein (Meiser *et al.*, 2011), suggesting a role for an ethylene/NO signaling cascade to locally regulate Fe uptake (Yang *et al.*, 2014).

While the FIT network coordinates the direct uptake of Fe in roots, a second clade of bHLH proteins regulate intracellular Fe homeostasis through the PYE network. The founding member of this clade, POPEYE (PYE), is a bHLH transcription factor whose induction under Fe deficiency in roots was first observed by time course Fe deficiency mRNA profiling (Long *et al.*, 2010). Like the FIT network PYE is a bHLH protein which dimerizes with a cohort of PYE-like proteins to mediate intracellular Fe homeostasis in roots (Long *et al.*, 2010). PYE-like bHLHs, but not PYE itself, are subject to ubiquitin mediated 26S proteasome degradation by the E3 ligase BRUTUS (BTS) (Hindt *et al.*, 2017; Liang *et al.*, 2017).

While the mechanisms of Fe uptake have been known for some time, how the Fe status is sensed and signaled at the whole plant level is an ongoing active area of research. *Arabidopsis* is known to have at least two distinct Fe sensing systems, a local sensing system in roots, and a systemic sensing system in leaves (Vert *et al.*, 2003). The systemic sensing system allows the leaves to dictate the amount of Fe to be acquired by roots, while the local sensing system allows individual roots to regulate their response in accordance with their local environment, which appears to be post-translational in nature (Sivitz *et al.*, 2011; Guillaume *et al.*, 2018; Barberon *et al.*, 2011).

Recent insights into the mechanism of shoot-to-root communication have largely come from studying mutants of the Oligopeptide Transporter 3 (OPT3). OPT3 is mainly

expressed in leaf companion cells (CCs) (Mendoza-Cózatl *et al.*, 2014; Zhai *et al.*, 2014; Khan *et al.*, 2018) and is rapidly induced within 2 hr after plants have been transferred from replete hydroponic solution to Fe deficient media (Khan *et al.*, 2018). Complete knockout of OPT3 is embryo lethal (Stacey *et al.*, 2002), while the knock down mutants *opt3-2* and *opt3-3* (*opt3*) are viable despite showing a significant reduction (~6% of wild type in leaves) of the *OPT3* transcript. An unexpected consequence of this reduced *OPT3* expression, is that *opt3* plants show an induction of a broad range of Fe deficiency markers in roots including IRT1, FRO2, as well as the *FIT network*. A consequence of this is a constitutive induction of *IRT1,* which leads to an over accumulation of Fe, Mn, and Zn in both roots and shoots (Stacey *et al.*, 2008). In contrast to the root phenotype of *opt3*, leaves exhibit a transcriptional profile consistent with a Fe excess (Khan *et al.*, 2018).

Cadmium is a non-essential toxic element capable of entering root cells using the Fe uptake machinery. Cadmium has also been shown to induce genes such as *IRT1* and *OPT3,* which are usually induced under Fe limiting conditions; however, whether this Fe deficiency-like response is only due to reduced Fe uptake in the presence of Cd or whether Cd directly impairs the Fe sensing mechanism is currently not known. Recently, there has been significant advances at defining Fe responsive gene networks in a tissue-specific manner (i.e. roots and shoots). In addition, *Arabidopsis* mutants that constitutively over accumulate Fe in leaves and roots are also available (*opt3-2 and opt3-3*). Therefore, in this work, and similar to a chemical genetics approach, we used low levels of Cd to test whether this non-essential element directly impairs Fe sensing in wild type plants and mutants that over accumulates Fe in leaves and roots (*opt3-2*). Our results show that in

wild type plants Cd does induce a Fe deficiency response in leaves and roots. However, many of these genes were not induced by Cd in plants that over accumulate Fe (*opt3-2*). Notably, despite the presence of high levels of Fe in *opt3* leaves, Cd consistently induces a specific core of genes associated with Fe deficiency responses, including genes known to be localized in the leaf vasculature. Further analyses demonstrate that genes originally induced by Cd in wild type plants but not in *opt3-2* (Fe excess conditions) belong to gene clusters associated with pathogen response and oxidative stress. Taken together, our results suggest that when plants experience opposite cues (Fe deficiency and high ROS), there is a hierarchical regulation of Fe homeostasis where ROS overrides the induction of a subset of genes that otherwise would have been induced by Fe deficiency.

3 Results

3.1 Mild Cd exposure induces a partial Fe deficiency response in roots and leaves.

Plants respond to cadmium exposure in a concentration dependent manner, we therefore began this work by identifying a cadmium concentration where the visual damage to leaves (i.e. chlorosis) was minimal. Since a key part of this project was to test the Cd-induced Fe deficiency-like responses in a plant that constitutively over accumulates Fe in leaves (*opt3*), both Col-0 and *opt3-2* plants were grown in replete hydroponic solution to bolting stage (approx. 4 weeks) and then exposed to several concentrations of $CdCl_2$ for 72hr. While high concentrations of Cd (> 50 μM) induced leaf yellowing and necrotic

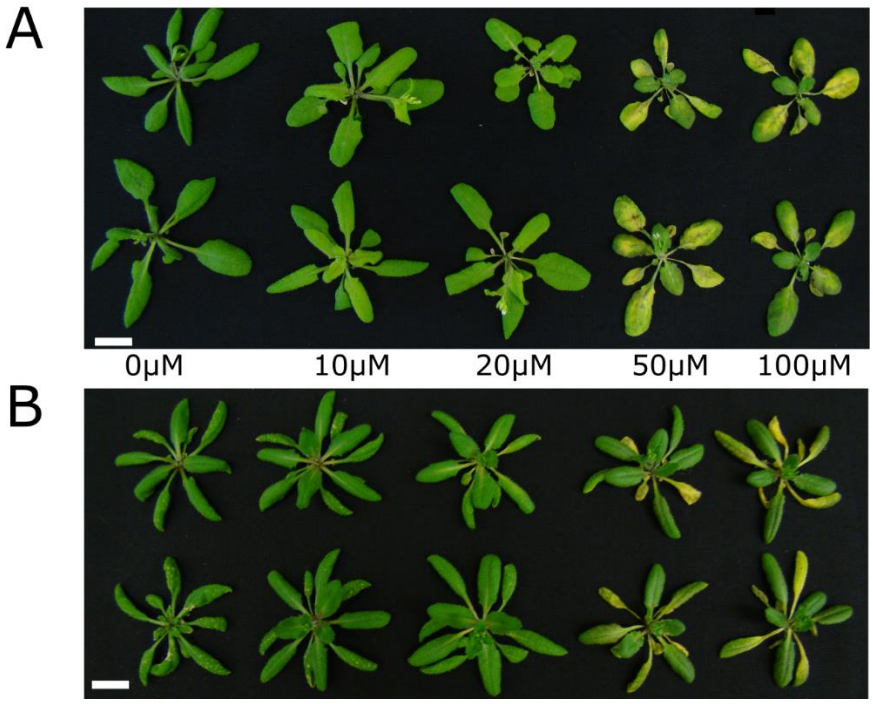

Figure 6 A mild Cd exposure of 10-20μM CdCl2 does not induce severe visual symptoms of oxidative damage. (A) Col-0. (B) opt3-2

lesions, 10 and 20μM $CdCl_2$ had minimal impact on plant morphology in both genotypes, Col and *opt3-2* (**Figure 6**); therefore, we selected 20μM $CdCl_2$ for further analyses.

To begin dissecting Col and *opt3-2* responses to Cd exposure, we conducted whole-genome transcriptome analyses of leaves and roots separately. Three biological replicates of each tissue type were used for Illumina sequencing, rendering a total of 754 million reads, of which 95% were uniquely mapped to the *Arabidopsis* TAIR10 genome and after removal of low confidence base pairs and short reads, 716 million reads were used for calling differential expression under the overdispersed binomial model implemented in edgeR (Robinson *et al.*, 2009). To minimize unreliable fold changes, only genes with at least 50 reads in any condition and fold changes with absolute $\log_2$ fold changes ≥ 0.5 were considered for statistical analyses.

In wild type plants, Cd induced changes in 3,292 genes in leaves (46% induced) and 4,256 genes in roots (49% induced). A similar number of genes (3,735; 46% induced) were differentially regulated in *opt3-2* leaves; however, Cd induced a substantial deregulation of transcripts in *opt3-2* roots, totaling 6,527 differentially expressed genes, of which 42% were induced (Supp. Figure 1). To determine the extent of the Fe deficiency response induced by Cd, we compared the identity of Cd deregulated genes against datasets specific to leaves and roots containing genes deregulated under true Fe deficiency conditions (Supp. table 1 and 2). These datasets include an extended version of the published *ferrome* for roots (Schmidt and Buckhout, 2011) and a leaf-specific data set that contains genes consistently regulated by Fe availability across several transcriptome data where leaves were analyzed separately from roots (Kumar *et al.*, 2017; Stein and Waters, 2012). In total, the leaf dataset (*leaf ferrome*) included 228 genes (Supp. Table 1, 163 up, 65 down) while the root dataset contains 357 genes (Supp. Table 2, 208 up, 149 down). By using these datasets, we were able to assess the degree of Fe deficiency elicited by Cd. For instance, in wild type leaves we found a significant overlap between Fe deficiency responses and Cd exposure, with 79 induced and 40 repressed genes by both Fe deficiency and Cd in leaves, these numbers represent 52% (induced genes) and 64% (repressed genes) of the true Fe deficiency response from the *leaf ferrome* (**Figure 7A**). Examples of genes deregulated by Cd and Fe in leaves include a short polypeptide known to be involved in Fe deficiency responses IMA3 induced ~5 $\log_2$ fold (Grillet *et al.*, 2018; Hirayama *et al.*, 2018), the jasmonic acid signaling marker PDF1.2 was induced ~9 $\log_2$ fold (Ahmad *et al.*, 2011; Cabot *et al.*, 2013; Zarei *et al.*, 2011) , and FER4, which encodes

a ferritin isoform, was repressed ~2 log_2 fold. Not all Fe related transcripts were found to be deregulated by Cd exposure. For example, Conserved in the Green Lineage and Diatoms 27 (CGLD27) is expected to be induced during Fe deficiency (Urzica *et al.*, 2012), nor did we observe the expected induction of a key regulator of salicylic acid response SARD1 (Wang *et al.*, 2011). Similarly in roots, 144 genes were found to be induced and 54 repressed by both Fe deficiency and Cd exposure, which represent 57% of induced and 43% of repressed genes present in the root *ferrome*, (**Figure 7B**). These results suggest that Cd does induce a Fe deficiency-like response (IDLR, hereafter) in both leaves and shoots.

3.2 Fe overload partially restricts the Cd-induced Fe deficiency response.

The *Arabidopsis* mutant *opt3-2* has previously shown to over accumulate Fe in leaves and roots and while its leaf transcriptome is consistent with an adequate sensing of Fe excess, roots display a constitutive Fe deficiency despite accumulating significant levels of Fe (Khan *et al.*, 2018). Considering that even in the presence of Cd, *opt3-2* still over accumulates Fe (Mendoza-Cózatl *et al.*, 2014), we sought to test whether Cd is still capable of inducing an IDLR even during Fe excess. If so, this would be an indication that Cd interferes with Fe sensing rather than inducing a Fe deficiency by limiting Fe availability in plant tissues. For this analysis, we hierarchically clustered all genes differentially expressed in wild type and *opt3-2* plants exposed or not to 20μM Cd (**Figure 7C**, **D**). To simplify this representation, the clustering scheme is presented as the mean counts per million (CPM) of each sample type, thus allowing a simultaneous inspection across

genotypes and treatments. Using this approach, we were able to identify several distinct patterns (**Figure 7C**). In leaves for instance, some clusters included genes that are Fe responsive and induced by Cd in wild type, but repressed in *opt3-2* due to the Fe excess, yet once again induced in *opt3-2* after Cd exposure (**Figure 7C**). Other leaf clusters followed a similar pattern but the magnitude of induction by Cd varied between wild type and *opt3-2*. Interestingly, we also found clusters of Fe responsive genes induced by Cd but only in wild type and not in *opt3-2* (**Figure 7C**), suggesting that Cd is unable to induce these genes when Fe is in excess. Examples of these representative gene clusters are shown at the right side of the heatmaps as $\log_2$ fold changes within specific contrasts. The leaf Cluster L1 contains genes such as bHLH38/39/100/101, ORG1 and AHP4, which were induced by Cd in wild type and *opt3-2* (see contrasts CT/CN and OT/ON) and the magnitude of changes remained similar (i.e. the contrast OT/CT show minimal or no differences). Leaf Cluster LII follow a similar pattern but the magnitude of the change is different. For instance, ZIF1, BTS and FRO3 are induced by Cd in wild type and *opt3-2* leaves; however, Cd induction in *opt3-2* plants is lower than wild type plants suggesting that these genes are regulated through several inputs, and that Fe excess and Cd provide different cues to the plant, thus resulting in a regulation different from the one observed in wild type plants exposed to Cd alone. In contrast, leaf Cluster LIII includes genes such as AIG2 and AT3G28940, which were first identified as Fe responsive, Cd inducible in wild type plants, but that were not deregulated by Cd in *opt3-2* (i.e. Fe excess). Other genes such as the jasmonic acid inducible TAT protein or the MATE transporter AT3G23550, included in the leaf Cluster LIV, are also induced by Cd in wild type plants but were

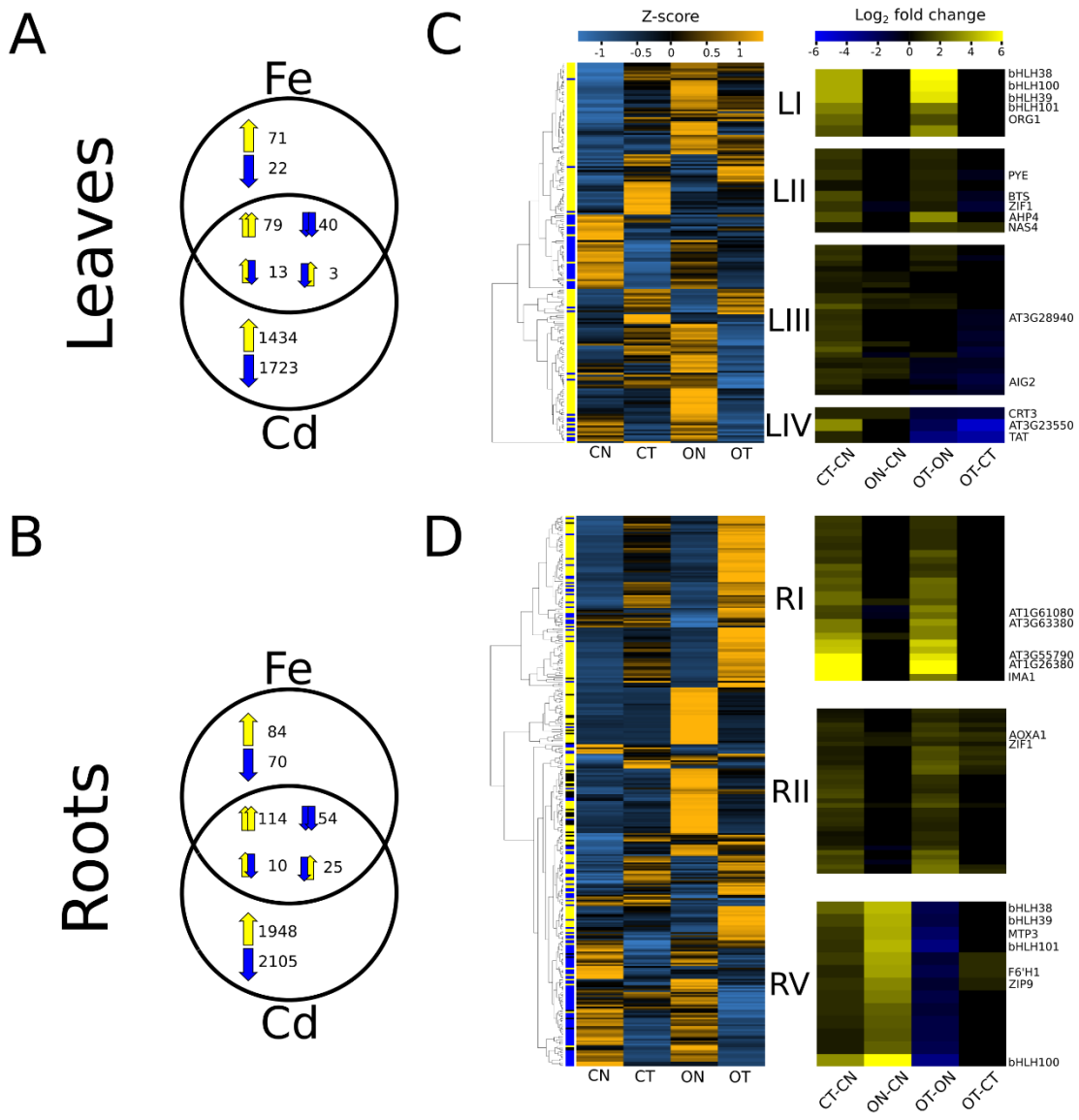

Figure 7 Exposure to Cd differentially regulates genes related to Fe homeostasis, which follow two expression profiles relative to the high Fe concentrations in opt3-2. Overlap between genes consistently induced/repressed under -Fe and those regulated by Cd exposure in Col-0 leaves (A) and roots (B). Mean counts per million for each sample group were hierarchically clustered and colored by their row-wise normalized Z-score, expected induction/repression under -Fe shown to the left side bar, log_2 fold changes of representative clusters displayed the right for (C) leaves and (D) roots

severely repressed by Cd in *opt3-2* plants. These results suggest that Cd triggers an Fe deficiency like response in wild type plants, at mild concentrations; however, when combined with other stresses such as Fe excess, different or even opposite transcriptional programs are activated. Moreover, this staggered regulation seems to be specific to only

certain gene clusters and the combination of Fe and Cd stress was proven useful to separate Fe responsive clusters regulated by few or multiple inputs.

In contrast to *opt3-2* leaves, which are capable of sensing an Fe overload, *opt3-2* roots display a strong and constitutive Fe deficiency response even in the presence of large amounts of Fe being accumulated in root tissues (Mendoza-Cózatl *et al.*, 2014; Zhai *et al.*, 2014; Khan *et al.*, 2018). Consequently, the patterns found in wild type and *opt3-2* roots during Cd exposure were different compared to leaves (**Figure 7D**). Specifically, bHLH38/39/100/101, but not FIT, were significantly induced by Cd in Col plants (Cluster RV), but the magnitude of induction was marginal compared to *opt3-2* roots without Cd (**Figure 7D**, CT/CN and ON/CN). The lack of *FIT* induction by Cd in wild type plants may explain the discreet increase in *IRT1* expression by Cd despite the induction of bHLH38/39/100/101. Moreover, Cd exposure reduced the expression of this group of bHLHs in *opt3-2* plants suggesting that Cd exposure plus Fe excess effectively reduced the Fe deficiency response originally seen in *opt3-2* plants. Interestingly, the largest gene cluster found in roots (Cluster RI) contains genes which were strongly induced by Cd, independently of the Fe status of the plant (*opt3-2)*, such as the small peptide IMA1/FEP3 (Grillet *et al.*, 2018; Hirayama *et al.*, 2018), or the transmembrane protein implicated in ethylene signaling AT3G55790 (Yang *et al.*, 2011), and a Ca^{2+} transporter ACA12 (Limonta *et al.*, 2014). We also identified a cluster similar to cluster RI, RII, but differs in that induction of these genes is less extreme than in RI, and are not independent of the Fe excess condition of *opt3-2*. Although all of these genes have been implicated in Fe homeostasis, few have been fully characterized. Among them, we were able to identify the vacuole NA importer

ZIF1 in this cluster, as well as the mitochondrial alternative oxidase (AOXA1). The alternative oxidase branch of mitochondrial respiration is activated to prevent single electron leakage from the electron transport chain by reducing oxygen to water, thus reducing electron flux through the cytochromes (Saha et al., 2016; Choudnury et al., 2013). AOX expression is correlated with oxidative stress and H_2O_2 concentrations and is expected to be involved in retrograde stress signaling from the mitochondria to the nucleus (Saha et al., 2016). opt3-2 has elevated AOXA1 expression relative to Col-0 in both the presence and absence of Cd, and is further induced by Cd in each genotype, suggesting that *opt3-2* not only suffers from Fe excess, but also oxidative stress which is exacerbated by Cd in an additive manner.

To facilitate comparisons across treatments and genotypes, we have established a stand-alone version of an electronic Fluorescent Pictograph Browser (eFP browser; available at http://gene.rnet.missouri.edu/efp/cgi-bin/public_html/efpWeb.cgi) where all the data reported in this work can be easily visualized in absolute (FPKM) or relative (log_2 fold changes) mode.

3.3 Fe deficiency responses are hierarchically regulated based on the levels of reactive oxygen species.

In the presence of excess Fe, Cd elicits different responses of Fe deficiency markers in leaves and roots (**Figure 7C, D**). While the induction of genes such as *OPT3* and *bHLHs* (subgroup Ib) in leaves indicates that Cd is able to interfere with Fe sensing, the lack of induction of the *FIT network* by Cd in *opt3-2* indicates that the Fe deficiency signals can be overridden by other mechanisms (see Cluster RV in **Figure 7D**). In order to clearly separate Fe and/or Cd responsive genes, we compared

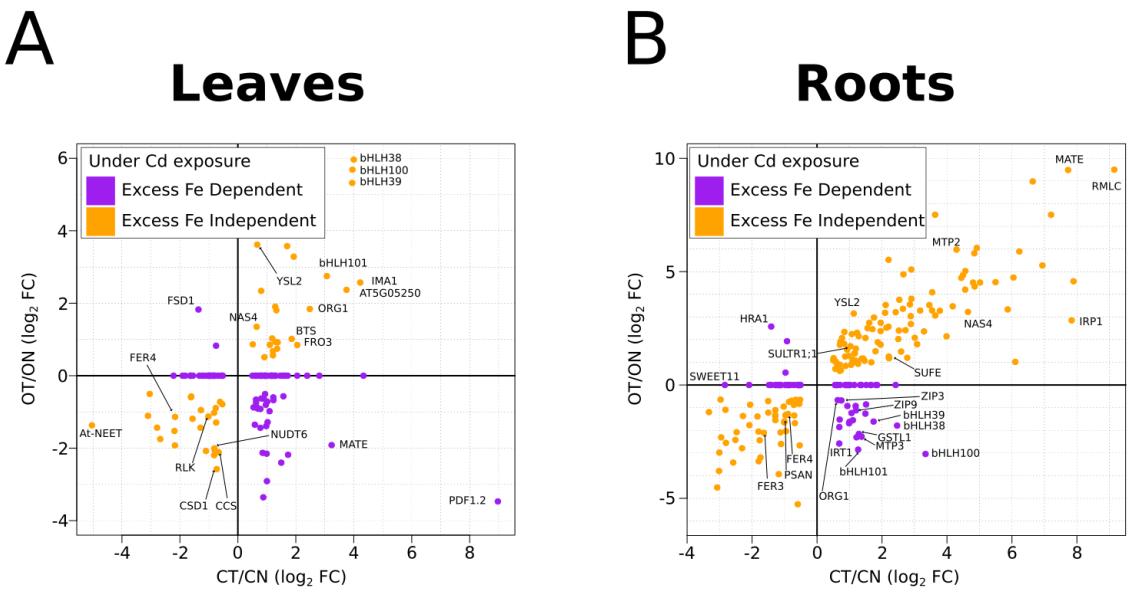

Figure 8 Cd responsive transcripts in leaves and roots were divided into two groups; under Cd exposure Excess Fe Dependent and Independent based on their expression pattern between Cd exposed *opt3-2* and Col-0.

the Fe responsive (*ferrome* datasets) and Cd regulated genes (**Figure 7A-B**) on a genotype-dependent manner (**Figure 8**). This approach resulted in the identification of two distinct groups

of Fe/Cd deregulated genes, one that was induced under Cd exposure, regardless of the Fe status of the plant (**Figure 8A-B**, orange dots) and a different one that was originally induced by Cd in wild type, but repressed when Fe was present in excess (**Figure 8A-B**, purple dots). Interestingly, gene clusters around subgroup Ib of *bHLHs* in leaves were found to be Cd-inducible and Fe excess independent while the same cluster in roots was initially induced by Cd in wild type but ended being repressed when Fe was in excess (i.e. in *opt3-2* + Cd; **Figure 8B**). This trend indicates that the mechanism that represses Fe responsive genes in roots is less prevalent in leaves, and may be a direct function of Cd interfering with Fe sensing in leaves. In roots however, a secondary signaling mechanism may be in place, and in contrast to leaves, it may be sensitive to Cd-induced oxidative damage.

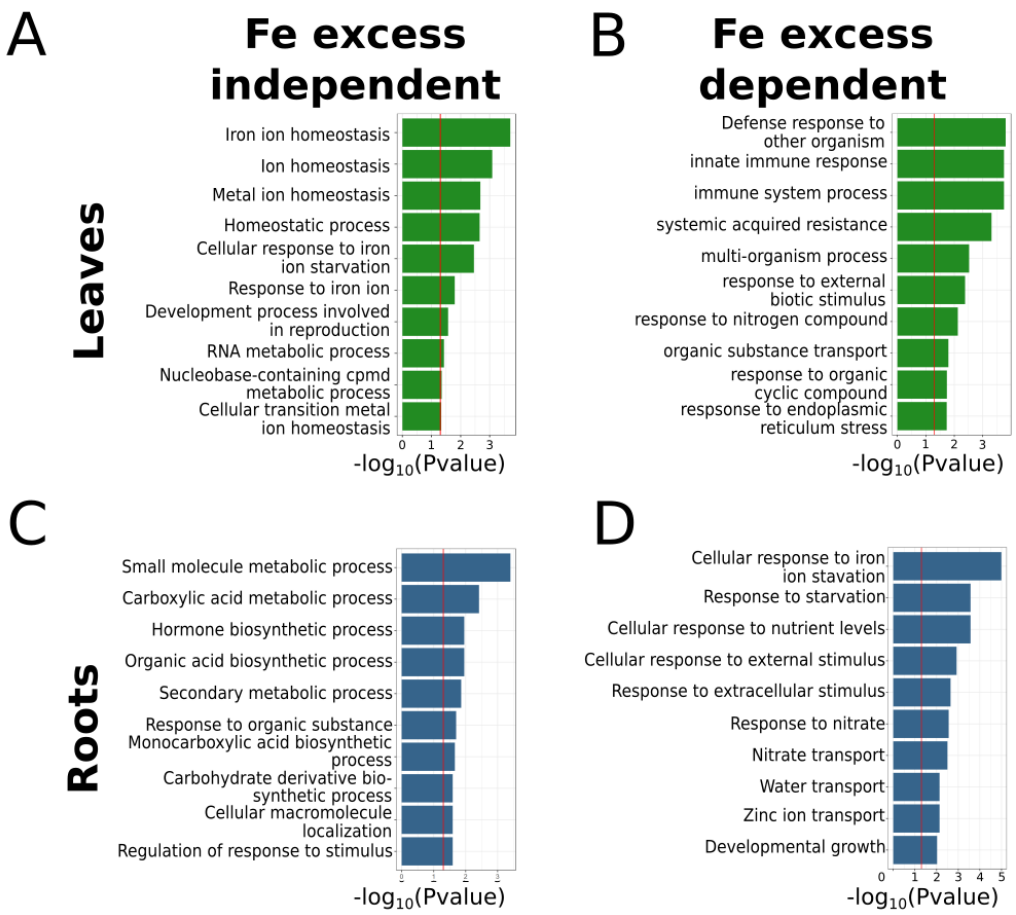

Figure 9 Gene ontology enrichment of the biological process ontology of Excess Fe In/Dependent clusters, comparing each cluster to the union of the clusters for leaves and roots independently.

With the hope of uncovering a signaling mechanism responsible for separating the two independent clusters found in leaves and roots, we used gene ontology (GO) enrichment to identify broad trends associated to the roles of each gene within each cluster (**Figure 9**). In leaves, the Cd-inducible/Fe excess independent cluster contained terms related to Fe or metal ion homeostasis (**Figure 9A**), while the Cd-inducible/Fe excess dependent cluster was particularly enriched in terms related to biotic stress (**Figure 9B**). Genes related to biotic stress have frequently observed in mRNA profiling experiments studying heavy metal homeostasis, but a rationale for this trend has never been identified. Our results however, suggest that the mechanism separating this Fe excess dependent and independent clusters is likely related to biotic stress responses. In roots, the Fe excess independent cluster was enriched in terms related

to secondary metabolism, while the Fe excess dependent cluster in roots was enriched terms relating to heavy metal homeostasis and again biotic stress response terms.

3.4 H_2O_2 over accumulates in leaves and roots of *opt3-2*

Our RNA sequencing data demonstrates that in the context of a high Fe levels, Cd elicits an Fe deficiency like response in a subset of transcripts, while the remainder are strongly repressed, often to wild type levels. These transcripts are disproportionately associated with a biotic stress responses, and likely share a regulatory component. Reactive oxygen species, such as H_2O_2, are generated by Respiratory Burst Oxidase NADPH protein D (RBOHD) during pathogen attack to mediate the defense response (Torres *et al.*, 2013; Maruta *et al.*, 2011; Pogany *et al.*, 2009; Miller *et al.*, 2009). In leaves, RBOHD was induced by Cd in Col-0 and induced in *opt3-2* without Cd exposure to levels similar to Col-0 exposed to Cd (Supplemental Figure 2). Hence, we hypothesized that the repression of Fe deficiency markers in *opt3-2* after Cd exposure may be the result of a H_2O_2 mediated transcriptional reprogramming.

To test this, H_2O_2 levels were measured in leaves and roots of Col-0 and *opt3-2* plants exposed or not to Cd (**Figure 10**). In leaves, we found that *opt3-2* have equivalent levels of H_2O_2 to unexposed Col-0, and both genotypes produced higher H_2O_2 levels after Cd exposure; however, *opt3-2* accumulated significant more H_2O_2 compared to Col-0. The higher levels of ROS in *opt3-2* exposed to Cd, together with the enrichment of ROS-associated genes found through the GO enrichment analysis (**Figure 9A, B**) provides a mechanism to explain why some Fe responsive genes originally induced by Cd in wild type were found to be repressed by Cd in *opt3-2* (i.e. the Cd inducible/Fe excess dependent cluster, **Figure 8A**). Furthermore, it also suggests that when plants experience opposite cues like Fe deficiency-like conditions but high ROS at the same time, there is a

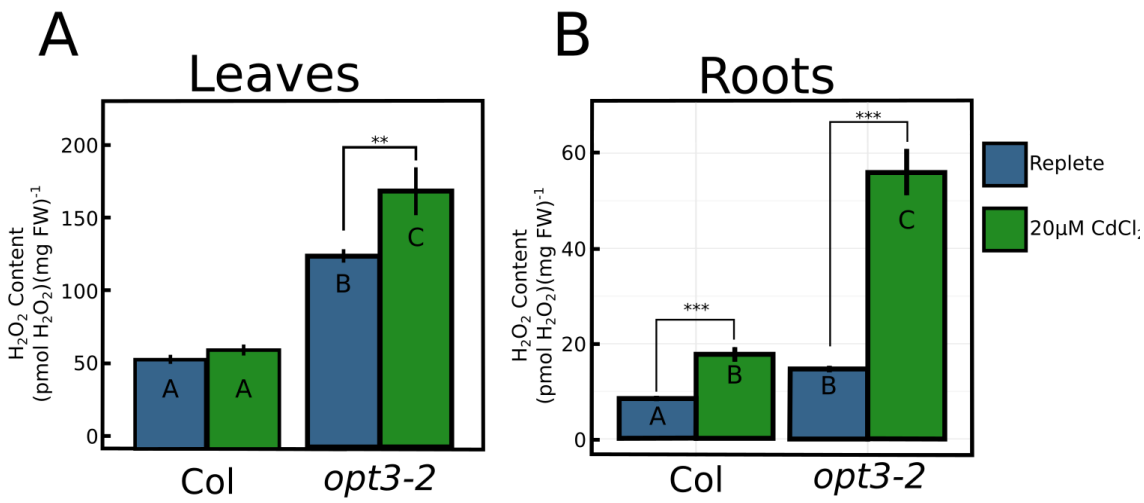

Figure 10 Quantification of H_2O_2 concentration in Col-0 and *opt3-2* roots. *** indicates $p < 0.001$, n = 6-10, representative results of two independent experiments.

hierarchical regulation of Fe deficiency responses where ROS prevent the induction of a now well-defined group of genes that otherwise would have been induced as part of the Fe deficiency response in leaves. Perhaps more interesting is the fact that in leaves, and only in leaves, bHLHs of the subgroup Ib are insensitive to this ROS-mediated hierarchical regulation of Cd-induced Fe deficiency responses. Similarly, we found that in Col-0, Cd exposure increases H_2O_2 to the same concentration as found in unexposed *opt3-2*, while exposed *opt3-2* dramatically increase their H_2O_2 content. This trend also explains part of the transcriptome profiles observed in roots, where Cd exposed Col-0 and unexposed *opt3-2* show similar expression patterns (**Figure 7D**, cluster RV), but the high levels of H_2O_2 in Cd exposed *opt3-2* represses the expression of these transcripts.

3.5 Inhibition of photosynthesis by Cd is a source for the elevated levels of H_2O_2.

Cadmium is not a redox active element and hence is unable to produce ROS by the same chemical process as Fe; however, Cd generates ROS through displacing other ions and altering enzyme activity. In plants, one mechanism in which Cd generates ROS is in the chloroplast, by replacing Ca^{2+} in the Ca-Mn core of the oxygen evolving complex of photosystem II (Sigfridsson *et al.*, 2004).

The Cd-Mn core does not efficiently transfer electrons to water which results in the production of the hydroxyl radical and super oxide anion (Nishiyama *et al.*, 2006). Additionally, this failure to reduce H_2O reduces the photosynthetic efficiency by inhibiting electron flow from the light capturing antennae, whose energy must be dissipated as heat in a process called non-photochemical quenching, which is highly correlated to the production of ROS (Muller *et al.*, 2001). To determine if the increased ROS content of *opt3-2* leaves could be explained by an impaired photosynthetic apparatus, photosynthetic efficiency in Col and *opt3-2*, exposed or not to Cd, was measured using an Imaging PAM system (**Figure 11A**, **B**). While *opt3-2* did not show a decrease in photosynthetic efficiency in the absence of Cd, *opt3-2* did show a ~20% reduction in its photosynthetic efficiency during Cd exposure (**Figure 11C, D**), indicating that the chloroplasts of *opt3-2* generate more H_2O_2 than Col-0 in the presence of Cd. In a different experiment, the F_v/F_m ratios were also measured over a 14 day period where plants were first grown for 14 days in the absence of Cd and then transferred to either fresh media containing 0 or 20µM $CdCl_2$ (**Figure 11E**). Under replete conditions, both *opt3-2* and Col-0 sustained a high photosynthetic efficiency until 14 days after transfer, where a minor decrease was observed, a likely consequence of depletion of nutrients from the media. This is in contrast to plants exposed to 20µM $CdCl_2$, where Col showed a sharp decrease in photosynthetic efficiency after 5 days exposure, and showed no further decrease over the course of the experiment. Similarly, the photosynthetic efficiency of *opt3-2* did not decrease during the first 5 days but continued to decrease over the next 5 days, after which the photosynthetic efficiency stabilized.

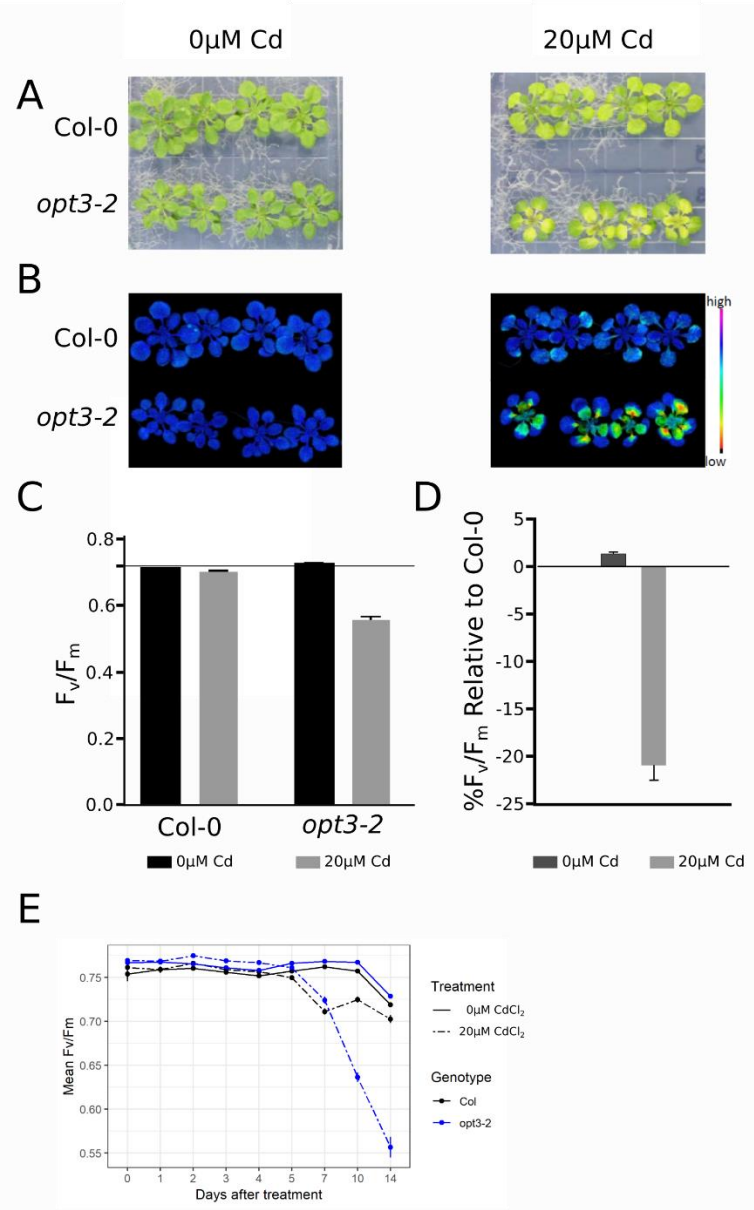

Figure 11 Mild Cd exposure does not dramatically affect photosynthetic capacity of Col-0, in contrast to opt3-2. (A,B) 21 day old plants subjected to 14 days 20µM CdCl2 exposure show a decrease in photosynthetic efficiency, RGB top, false color bottom. (C) Quantification of photosynthetic efficiency. (D) Relative photosynthetic efficiency of opt3-2 compared to Col-0. (E) *opt3-2* and Col-0 show a loss of quantum efficiency after 5 days 20µM $CdCl_2$ exposure, after which does not stabilize in *opt3-2*.

4 Discussion

Fe homeostasis has previously been described as being regulated either systemically by shoot-to-root signaling, or locally, where individual cells decides if it is safe to extract Fe from the soil without promoting an Fe overload. Here we have used Cd to probe the Fe homeostatic network and demonstrate that at low concentration, Cd is capable of inducing an Fe deficiency response. This however, it is not through Fe-Cd competition at the root plasma membrane, but rather by impairing Fe sensing in leaves. Further, we also show part of this leaf-borne Fe deficiency signal can be superseded by a ROS dependent signaling.

4.1 Cd induces Fe deficiency by impairing Fe sensing

Cd has long been known to induce a Fe deficiency like response, and has been attributed to a reduced Fe flux into the plant as Cd and Fe are both substrates of IRT1 in roots. A similar effect is obtained when plants are treated with excess essential heavy metals, but extremely high concentrations are needed to achieve this effect. The quantity of essential heavy metals needed to induce an Fe deficiency-like response (IDLR) complicates the interpretations of this competition-only hypothesis. For example, Lešková *et al.*, 2017 used forty five times as much Zn as Cd to induce similar leaf chlorosis, while yeast uptake assays indicate that IRT1 affinity towards Cd is not sufficient to compensate for the differences in metal concentrations needed to elicit an IDLR (Korshunova *et al.*, 1999). Cd also elicits Fe deficiency responses in leaves (Wu *et al.*, 2012; Herbette *et al.*, 2006; Meda *et al.*, 2007; Solti *et al.*, 2008), which have recently been shown to be the site of systemic Fe status sensing (Khan *et al.*, 2018), hence Cd may produce an IDLR by altering Fe sensing in companion cells.

We used two microarray data sets (Kumar *et al.*, 2017; Stein and Waters, 2012) to compile lists of genes consistently and differentially expressed in response to Fe deficiency for leaves and roots.

A large overlap, ~60% of these Fe deficiency markers, was found to be de-regulated by Cd in wild type plants and in both, leaves and roots (**Figure 6 A**, **B**), suggesting that the Cd induced IDLR is directly affecting Fe homeostasis across the whole plant.

The transcriptional response to Cd is known to be dose dependent (Herbette *et al.*, 2006). In the *Arabidopsis* mutant *opt3-2,* leaves have been shown to accumulate less Cd than wild type plants (Mendoza-Cózatl *et al.*, 2014), which may suggest that *opt3-2* should show a weaker IDLR in leaves. However, here we show that leaves of *opt3-2* display an equivalent response to Cd exposure as Col wild type. This includes the key transcriptional regulators bHLH38/39/100/101, which have been shown to be expressed preferentially in the companion cells (Mustroph *et al.*, 2009). While *opt3-2* leaves are Fe rich, the companion cells contain less Fe than found in wild type plants (Zhai *et al.*, 2014). Under the competition model this smaller Fe pool would favor Cd binding to target proteins, such as the putative Fe sensor, hence inducing an IDLR. However, transcripts which are expressed in the Fe rich leaves of *opt3-2* such as PYE and BTS are similarly induced (**Figure 7C**, cluster II), indicating that the Fe/Cd balance is not significant outside companion cells. Hence, it is most likely that Cd in the companion cell is able to trigger an Fe deficiency response by impairing the Fe sensor through a non-functional replacement of Fe by Cd.

Cd induces the bHLHs in the companion cells in both *opt3-2* and Col, which leads to two distinct regulatory patterns in roots. The first case is shown in **Figure 7D**, clusters RI and RII, where transcripts follow regulatory patterns predicted by the leaf response, i.e. induced/repressed similarly in *opt3-2* and Col (**Figure 8A**). This includes several genes related to phosphate homeostasis, such as the low affinity phosphate transporter *PHT1;2* (repressed), the mitochondrial phosphate transporter *MPT2* (induced), and a regulator of phosphate deficiency responses WRKY75 (induced). *NAS4* is a gene critical for Fe homeostasis and is strongly induced by Cd in each genotype (~3-5 $\log_2$ FC), indicating that this subset of the root response is only

dependent on the leaf-borne signal. The second transcriptional profile elicited by Cd in involves the primary Fe uptake system in roots. The *FIT network*, including bHLH38/39/100/101 and IRT1 are weakly induced by Cd in the Col-0 background, but are highly induced in *opt3-2* in the absence of Cd. Interestingly, these FIT network genes are heavily repressed in *opt3-2* only during Cd exposure (**Figure 7D**, cluster RV). Which is the opposite of the expected regulation from the leaf-borne signal, indicating that a secondary signaling system is able to override the systemic Fe deficiency signal.

Hence, we used the high Fe background of *opt3-2* along with Cd to probe the Fe deficiency network to show that Cd impaired Fe sensing in leaves causes an IDLR response in some root transcripts, while other transcripts show a regulatory pattern indicative of a secondary input overriding the Fe deficiency signal originated in leaves.

4.2 Fe deficiency is hierarchically regulated by competing nutrient acquisition and oxidative stress signals.

Separation of transcripts based on the signs of their fold changes in response to Cd for each genotype (**Figure 8A**, **B**), and subsequent GO enrichment (**Figure 9**) demonstrates that biotic stress responses are dependent on the high Fe status of *opt3-2* (**Figure 9B**, **D**) while canonical Fe deficiency markers (*FIT network*) alternate between in/dependent of the excess Fe status in leaves and roots (**Figure 9C**), respectively. This led us to suspect that altered ROS signaling may explain the differential response of the *FIT network*, as H_2O_2 has been previously been implicated as a repressor of the Fe uptake (Le *et al.*, 2016).

We measured H_2O_2 content in both leaves and roots of Col and *opt3-2* exposed or not to Cd. In roots we found that Cd exposure induces H_2O_2 accumulation in each genotype, although *opt3-2*

has a higher baseline H_2O_2 concentration compared to Col, Cd induces a much larger increase in H_2O_2 (**Figure 10**). We attribute this larger increase in H_2O_2 to the mobilization of stored Fe in response to the Fe deficiency signal generated by the Cd impaired Fe sensor in leaves. Meanwhile the drastically increased H_2O_2 concentration induces an excess Fe status, repressing the Fe uptake system/*FIT network*, without effecting the other Fe deficiency responses. In leaves H_2O_2 concentrations between Col and *opt3-2* were equivalent without Cd exposure, but increased under Cd exposure (**Figure 10A**). Similar to the root response, the increase in H_2O_2 concentration was more pronounced in *opt3-2* compared to Col-0. While it is likely that Fe mobilization from vacuoles contributes to the increased H_2O_2 concentration in *opt3-2* leaves, particularly after relatively short Cd exposures.

While mobilized Fe is likely to play a role in the increased H_2O_2 concentration found in *opt3-2*, the chloroplast redox state is shown to be altered through the 4 fold repression of Fe Superoxide Dismutase 1 (FSD1), a chloroplast localized enzyme which balances the chloroplast redox state by reducing H_2O_2 to H_2O (Kliebenstein *et al.*, 1998; Duy *et al.*, 2011). This is exacerbated by Cd exposure, as photosystem II is drastically effected in *opt3-2* relative to similarly treated Col, which indicates that the *opt3-2* chloroplasts are unable to compensate for alterations in their redox state and consequently suffer reduced photosynthetic efficiency (**Figure 11**), and are likely a significant source of H_2O_2.

5 Conclusion

Here, we have shown that low levels of Cd induce an iron deficiency like response that is not the result of Fe/Cd competition at the root level. Instead we found that Cd impairs Fe sensing, specifically in the leaf vasculature thus affecting the expression in a distinct set of genes. Interestingly, we also found that in roots the *FIT network* and Fe uptake system, among other

genes, are repressed in *opt3-2* after Cd exposure, which is concomitant with a drastic increase in H_2O_2 concentrations. This pattern strongly suggests that high ROS levels can override the induction of some, but not all, of the genes originally induced by Cd in wild type plants. Altogether, our results suggest that Fe deficiency responses in *Arabidopsis* are regulated at multiple levels and by different inputs. Moreover, when plants experience opposite inputs, the level of ROS is critical to define the transcriptional outcome of a large set of Fe responsive genes. Our data also suggest that in leaves, the subgroup Ib bHLH transcription factors are insensitive to this hierarchical regulation and belong to an Fe sensing core, unique to leaves, that is particularly labile and becomes impaired in the presence of cadmium.

6 Materials and Methods

6.1 Plant growth

All plants were germinated on ¼ MS agar plates after two days of stratification at 4°C in the dark. After approximately 10 days plants were transferred to replete hydroponic media containing 1.25 mM KNO_3, 625 µM H_2PO_4, 500 µM $MgSO_4$, 500 µM $CaSO_4$, 50 µM Fe-EDTA, 17.5 µM H_3BO_4, 5.5 µM $MnCl_2$, 0.5 µM $ZnSO_4$, 0.062 µM $NaMoO_4$, 2.5 µM NaCl, and 4 nM $CoCl_2$. At bolting fresh solution was added with indicated concentrations of $CdCl_2$.

6.2 RNA sequencing and data analysis

Leaves and roots were harvested separately, pulverized in a motor and pestle cooled with liquid nitrogen. mRNA was purified using a Qiagen EZ plant RNA kit and contaminant DNA was removed using a TURBO DNase kit. The mRNA was submitted to the University of Missouri Core Facility for 100bp sequencing using a Illumina HiSeq. The resulting reads were trimmed such that all bases were called at a 95% accuracy using ShortRead (Morgan

et al., 2009) and mapped to the TAIR10 genome release using Tophat (Kim Daehwan *et al.*, 2013). The remaining analysis was carried out in R and Bioconductor (R Core Team, 2018; Huber *et al.*, 2015). Feature counting was performed using ShortRead (Morgan *et al.*, 2009) and 92% of raw reads were uniquely mapped. Differential expression was called using edgeR (Robinson *et al.*, 2009), heatmaps and venn diagrams were generated in gplots (Warnes *et al.*, 2016). Ontology enrichment tests were performed using GOstats (Falcon and Gentleman, 2007) using the conditional hypergeometric test with a p-value cutoff of 0.05. The union of the Fe excess dependent and Fe excess independent was used as the gene universe for each test, for leaves and roots independently.

6.3 Hydrogen peroxide quantification

H_2O_2 concentrations in leaves were determined by the method described in (Zhang *et al.*, 2007). Briefly 500mg fresh tissue was homogenized on ice in a solution of 0.1% tri-chloroacetic acid and debris pelleted at 12,000xg. 0.5mL supernatant was added to 0.5mL of 10mM potassium phosphate buffer (pH 7) and 1mL 1M KI. The absorbance at 390nm and compared to a standard curve of H_2O_2. In roots H_2O_2 was quantified using the Amplex Red reagent, according to manufactures instructions.

7 Bibliography

Ahmad, S., Hulten, M. Van, Martin, J., Pieterse, C.M.J., Wees, S.C.M. Van and Ton, J. (2011) Genetic dissection of basal defence responsiveness in accessions of Arabidopsis thaliana. *Plant, Cell Environ.*, **34**, 1191–1206.

Barberon, M., Zelazny, E., Robert, S., Conéjéro, G., Curie, C., Friml, J. and Vert, G. (2011) Monoubiquitin-dependent endocytosis of the iron-regulated transporter 1 (IRT1) transporter controls iron uptake in plants. *Proc. Natl. Acad. Sci.*, **108**, E450--E458.

Cabot, C., Gallego, B., Martos, S., Barceló, J. and Poschenrieder, C. (2013) Signal cross talk in Arabidopsis exposed to cadmium, silicon, and Botrytis cinerea. *Planta*, **237**, 337–349.

Choudnury, S., Panda, P., Sahoo, L. and Panda, S.K. (2013) Reactive oxygen species in abiotic stress signaling. *Plant Signal. Behav.*, **8**, e23681.

Cui, Y., Chen, C.L., Cui, M., Zhou, W.J., Wu, H.L. and Ling, H.Q. (2018) Four IVa bHLH Transcription Factors Are Novel Interactors of FIT and Mediate JA Inhibition of Iron Uptake in Arabidopsis. *Mol. Plant*, **11**, 1166–1183.

Curie, C., Cassin, G., Couch, D., et al. (2009) Metal movement within the plant: Contribution of nicotianamine and yellow stripe 1-like transporters. *Ann. Bot.*, **103**, 1–11.

Curie, C., Panaviene, Z., Loulergue, C., Dellaporta, S.L., Briat, J.-F. and Walker, E.L. (2001) Maize yellow stripe1 encodes a membrane protein directly involved in Fe(III) uptake. *Nature*, **409**, 346.

Duy, D., Stübe, R., Wanner, G. and Philippar, K. (2011) The chloroplast permease PIC1 regulates plant growth and development by directing homeostasis and transport of iron. *Plant Physiol.*, pp--110.

Falcon, S. and Gentleman, R. (2007) Using GOstats to test gene lists for GO term association. *Bioinformatics*, **23**, 257–258.

Grillet, L., Lan, P., Li, W., Mokkapati, G. and Schmidt, W. (2018) IRON MAN, a ubiquitous family of peptides that control iron transport in plants. *Nat. Plants*, 1–26.

Guillaume, D., Neveu, J., Enric, Z. and Vert, G. (2018) Metal Sensing by the IRT1 Transporter-Receptor Orchestrates Its Own Degradation and Plant Metal Nutrition. *Mol. Cell*, **69**, 953–964.

Herbette, S., Taconnat, L., Hugouvieux, V., et al. (2006) Genome-wide transcriptome profiling of the early cadmium response of Arabidopsis roots and shoots. *Biochimie*, **88**, 1751–1765.

Hindt, M.N., Akmakjian, G.Z., Pivarski, K.L., Punshon, T., Baxter, I., Salt, D.E. and Guerinot, M. Lou (2017) BRUTUS and its paralogs, BTS LIKE1 and BTS LIKE2, encode

important negative regulators of the iron deficiency response in Arabidopsis thaliana. *Metallomics*, **9**, 876–890.

Hindt, M.N. and Guerinot, M. Lou (2012) Getting a sense for signals: regulation of the plant iron deficiency response. *Biochim Biophys Acta*, **1823**, 1521–1530.

Hirayama, T., Lei, G.J., Yamaji, N., Nakagawa, N. and Ma, J.F. (2018) The Putative Peptide Gene FEP1 Regulates Iron Deficiency Response in Arabidopsis. *Plant Cell Physiol.*, **59**, 1739–1752.

Huber, W., Carey, V.J., Gentleman, R., et al. (2015) Orchestrating high-throughput genomic analysis with Bioconductor. *Nat. Methods*, **12**, 115–121.

Inoue, H., Kobayashi, T., Nozoye, T., et al. (2009) Rice OsYSL15 is an iron-regulated iron (III)-deoxymugineic acid transporter expressed in the roots and is essential for iron uptake in early growth of the seedlings. *J. Biol. Chem.*, **284**, 3470–3479.

Ivanov, R., Brumbarova, T. and Bauer, P. (2012) Fitting into the harsh reality: Regulation of iron-deficiency responses in dicotyledonous plants. *Mol. Plant*, **5**, 27–42.

Jakoby, M., Wang, H.-Y., Reidt, W., Weisshaar, B. and Bauer, P. (2004) FRU (BHLH029) is required for induction of iron mobilization genes in Arabidopsis thaliana. *FEBS Lett.*, **577**, 528–534.

Khan, M.A., Castro-Guerrero, N.A., McInturf, S.A., et al. (2018) Changes in iron availability in Arabidopsis are rapidly sensed in the leaf vasculature and impaired sensing leads to opposite transcriptional programs in leaves and roots. *Plant. Cell Environ.*, 1–14.

Kim Daehwan, K., Pertea, G., Trapnell, C., Pimentel, H., Kelly, R. and Salzberg, S. (2013) TopHat2 : accurate alignment of transcriptomes in the presence of insertions , deletions and gene fusions. *Genome Biol.*, **14**, 0–9.

Kliebenstein, D.J., Monde, R.-A. and Last, R.L. (1998) Superoxide Dismutase in Arabidopsis: An Eclectic Enzyme Family with Disparate Regulation and Protein Localization. *Plant Physiol.*, **118**, 637–650.

Korshunova, Y.O., Eide, D., Clark, W.G., Guerinot, M. Lou and Pakrasi, H.B. (1999) The IRT1 protein from Arabidopsis thaliana is a metal transporter with a broad substrate range. *Plant Mol. Biol.*, **40**, 37–44.

Kumar, R.K., Chu, H.-H., Abundis, C., Vasques, K., Chan-Rodriguez, D., Chia, J.-C., Huang, R., Vatamaniuk, O.K. and Walker, E.L. (2017) Iron-Nicotianamine Transporters are Required for Proper Long Distance Iron Signaling. *Plant Physiol.*, **175**, pp.00821.2017.

Le, C.T.T., Brumbarova, T., Ivanov, R., Stoof, C., Weber, E., Mohrbacher, J., Fink-Straube, C. and Bauer, P. (2016) ZINC FINGER OF ARABIDOPSIS THALIANA12 (ZAT12) Interacts with FER-LIKE IRON DEFICIENCY-INDUCED TRANSCRIPTION FACTOR (FIT) Linking Iron Deficiency and Oxidative Stress Responses. *Plant Physiol.*, **170**, 540–557.

Lee, S., Chiecko, J.C., Kim, S.A., Walker, E.L., Lee, Y., Guerinot, M.L. and An, G. (2009) Disruption of OsYSL15 Leads to Iron Inefficiency in Rice Plants. *Plant Physiol.*, **150**, 786–800.

Lešková, A., Giehl, R.F.H., Hartmann, A., Fargašová, A. and Wirén, N. von (2017) Heavy Metals Induce Iron Deficiency Responses at Different Hierarchic and Regulatory Levels. *Plant Physiol.*, **174**, 1648–1668.

Liang, G., Zhang, H., Li, X., Ai, Q. and Yu, D. (2017) BHLH transcription factor bHLH115 regulates iron homeostasis in Arabidopsis thaliana. *J. Exp. Bot.*, **68**, 1743–1755.

Limonta, M., Romanowsky, S., Olivari, C., Bonza, M.C., Luoni, L., Rosenberg, A., Harper, J.F. and Michelis, M.I. De (2014) ACA12 Is a Deregulated Isoform of Plasma Membrane Ca2+-ATPase of Arabidopsis thaliana. , **84**, 387–397.

Long, T.A., Tsukagoshi, H., Busch, W., Lahner, B., Salt, D.E. and Benfey, P.N. (2010) The bHLH transcription factor POPEYE regulates response to iron deficiency in Arabidopsis roots. *Plant Cell*, **22**, 2219–2236.

Maruta, T., Inoue, T., Tamoi, M., Yabuta, Y., Yoshimura, K., Ishikawa, T. and Shigeoka, S. (2011) Arabidopsis NADPH oxidases, AtrbohD and AtrbohF, are essential for jasmonic acid-induced expression of genes regulated by MYC2 transcription factor. *Plant Sci.*, **180**, 655–660.

Meda, A.R., Scheuermann, E.B., Prechsl, U.E., Erenoglu, B., Schaaf, G., Hayen, H., Weber, G. and Wiren, N. von (2007) Iron Acquisition by Phytosiderophores Contributes to Cadmium Tolerance. *Plant Physiol.*, **143**, 1761–1773.

Meiser, J., Lingam, S. and Bauer, P. (2011) Posttranslational Regulation of the Iron Deficiency Basic Helix-Loop-Helix Transcription Factor FIT Is Affected by Iron and Nitric Oxide. *Plant Physiol.*, **157**, 2154–2166.

Mendoza-Cózatl, D.G., Xie, Q., Akmakjian, G.Z., et al. (2014) OPT3 is a component of the iron-signaling network between leaves and roots and misregulation of OPT3 leads to an over-accumulation of cadmium in seeds. *Mol. Plant*, **7**, 1455–1469.

Miller, G., Schlauch, K., Tam, R., Cortes, D., Torres, M.A., Shulaev, V., Dangl, J.L. and Mittler, R. (2009) The plant NADPH oxidase RBOHD mediates rapid systemic signaling in response to diverse stimuli. *Sci. Signal.*, **2**.

Morgan, M., Anders, S., Lawrence, M., Aboyoun, P., Pagès, H. and Gentleman, R. (2009) ShortRead: A bioconductor package for input, quality assessment and exploration of high-throughput sequence data. *Bioinformatics*, **25**, 2607–2608.

Muller, P., Li, X.P. and Niyogi, K.K. (2001) Non-Photochemical Quenching. A Response to Excess Light Energy. *Plant Physiol.*, **125**, 1558–1566.

Mustroph, A., Zanetti, M.E., Jang, C.J.H., Holtan, H.E., Repetti, P.P., Galbraith, D.W., Girke, T. and Bailey-Serres, J. (2009) Profiling translatomes of discrete cell

populations resolves altered cellular priorities during hypoxia in Arabidopsis. *Proc. Natl. Acad. Sci.*, **106**, 18843–18848.

Nishiyama, Y., Allakhverdiev, S.I. and Murata, N. (2006) A new paradigm for the action of reactive oxygen species in the photoinhibition of photosystem II. *Biochim. Biophys. Acta - Bioenerg.*, **1757**, 742–749.

Pogany, M., Rad, U. von, Grun, S., et al. (2009) Dual Roles of Reactive Oxygen Species and NADPH Oxidase RBOHD in an Arabidopsis-Alternaria Pathosystem. *Plant Physiol.*, **151**, 1459–1475.

R Core Team (2018) R: A Language and Environment for Statistical Computing.

Robinson, M.D., McCarthy, D.J. and Smyth, G.K. (2009) edgeR: A Bioconductor package for differential expression analysis of digital gene expression data. *Bioinformatics*, **26**, 139–140.

Römheld, V. and Marschner, H. (1986) Mobilization of iron in the rhizosphere of different plant species. *Adv. Plant Nutr.*, **2**, 155--204.

Rout, G.R. and Sahoo, S. (2015) Role of Iron in Plant Growth and Metabolism. *Rev. Agric. Sci.*, **3**, 1–24.

Saha, B., Borovskii, G. and Panda, S.K. (2016) Alternative oxidase and plant stress tolerance. *Plant Signal. Behav.*, **11**, e1256530.

Santi, S. and Schmidt, W. (2009) Dissecting iron deficiency-induced proton extrusion in Arabidopsis roots. *New Phytol.*, **183**, 1072–1084.

Schmidt, W. and Buckhout, T.J. (2011) A hitchhiker's guide to the Arabidopsis ferrome. *Plant Physiol. Biochem.*, **49**, 462–470.

Sigfridsson, K.G.V., Bernát, G., Mamedov, F. and Styring, S. (2004) Molecular interference of Cd2+with Photosystem II. *Biochim. Biophys. Acta - Bioenerg.*, **1659**, 19–31.

Sivitz, A., Grinvalds, C., Barberon, M., Curie, C. and Vert, G. (2011) Proteasome-mediated turnover of the transcriptional activator FIT is required for plant iron-deficiency responses. *Plant J.*, **66**, 1044–1052.

Sivitz, A.B., Hermand, V., Curie, C. and Vert, G. (2012) Arabidopsis bHLH100 and bHLH101 control iron homeostasis via a FIT-independent pathway. *PLoS One*, **7**, e44843.

Solti, Á., Gáspár, L., Mészáros, I., Szigeti, Z., Lévai, L. and Sárvári, É. (2008) Impact of iron supply on the kinetics of recovery of photosynthesis in Cd-stressed poplar (Populus glauca). *Ann. Bot.*, **102**, 771–782.

Stacey, M.G., Koh, S., Becker, J. and Stacey, G. (2002) AtOPT3, a member of the oligopeptide transporter family, is essential for embryo development in Arabidopsis. *Plant Cell*, **14**, 2799–2811.

Stacey, M.G., Patel, A., McClain, W.E., Mathieu, M., Remley, M., Rogers, E.E., Gassmann, W., Blevins, D.G. and Stacey, G. (2008) The Arabidopsis AtOPT3 protein functions in metal homeostasis and movement of iron to developing seeds. *Plant Physiol.*, **146**, 589–601.

Stein, R.J. and Waters, B.M. (2012) Use of natural variation reveals core genes in the transcriptome of iron-deficient Arabidopsis thaliana roots. *J. Exp. Bot.*, **63**, 1039–1055.

Torres, M.A., Morales, J., Sanchex-Rodgriguez, C., Molina, A. and L, D.J. (2013) Functional Interplay Between Arabidopsis NADPH Oxidases and Heterotrimeric G Protein. *Mol. plant-microbe Interact.*, **26**, 686–694.

Urzica, E.I., Casero, D., Yamasaki, H., et al. (2012) Systems and *Trans* -System Level Analysis Identifies Conserved Iron Deficiency Responses in the Plant Lineage. *Plant Cell*, **24**, 3921–3948.

Vert, G. a, Briat, J.F. and Curie, C. (2003) Dual regulation of the Arabidopsis high-affinity root iron uptake system by local and long-distance signals. *Plant Physiol.*, **132**, 796–804.

Wang, L., Tsuda, K., Truman, W., Sato, M., Nguyen, L. V., Katagiri, F. and Glazebrook, J. (2011) CBP60g and SARD1 play partially redundant critical roles in salicylic acid signaling. *Plant J.*, **67**, 1029–1041.

Wang, N., Cui, Y., Liu, Y., Fan, H., Du, J., Huang, Z., Yuan, Y., Wu, H. and Ling, H.Q. (2013) Requirement and functional redundancy of Ib subgroup bHLH proteins for iron deficiency responses and uptake in Arabidopsis thaliana. *Mol. Plant*, **6**, 503–513.

Warnes, G.R., Bolker, B., Bonebakker, L., et al. (2016) *gplots: Various R Programming Tools for Plotting Data*,.

Wu, H., Chen, C., Du, J., et al. (2012) Co-Overexpression FIT with AtbHLH38 or AtbHLH39 in Arabidopsis-Enhanced Cadmium Tolerance via Increased Cadmium Sequestration in Roots and Improved Iron Homeostasis of Shoots. *Plant Physiol.*, **158**, 790–800.

Yang, C.-Y., Hsu, F.-C., Li, J., Wang, N.-N. and Shih, M.-C. (2011) The AP2/ERF Transcription Factor AtERF73/HRE1 Modulates Ethylene Responses during Hypoxia in Arabidopsis. *Plant Physiol.*, **156**, 202–212.

Yang, Y., Ou, B., Zhang, J., Si, W., Gu, H., Qin, G. and Qu, L.J. (2014) The Arabidopsis Mediator subunit MED16 regulates iron homeostasis by associating with EIN3/EIL1 through subunit MED25. *Plant J.*, **77**, 838–851.

Yuan, Y., Wu, H., Wang, N., Li, J., Zhao, W., Du, J., Wang, D. and Ling, H.-Q. (2008) FIT interacts with AtbHLH38 and AtbHLH39 in regulating iron uptake gene expression for iron homeostasis in Arabidopsis. *Cell Res.*, **18**, 385–397.

Zarei, A., Korbes, A.P., Younessi, P., Ontiel, G., Champion, A. and Memelink, J. (2011)

Two GCC boxes and AP2/ERF-domain transcription factor ORA59 in jasmonate/ethylene-mediated activation of the PDF1.2 promoter in Arabidopsis. *Plant Mol. Biol.*, **75**, 321--331.

Zhai, Z., Gayomba, S.R., Jung, H., et al. (2014) OPT3 Is a Phloem-Specific Iron Transporter That Is Essential for Systemic Iron Signaling and Redistribution of Iron and Cadmium in Arabidopsis. , 1–17.

Zhang, F., Wang, Y. and Lou, Z. (2007) Effect of heavy metal stress on antioxidative enzymes and lipid peroxidation in leaves and roots of two mangrove plant seedlings (Kandelia candel and Bruguiera gymnorrhiza). , **67**, 44–50.

Chapter 3
bZIP23 as a putative link between zinc and iron homeostasis

Highlights

bZIP23 is a transcription factor involved in Zn homeostasis, but interestingly suppresses *opt3* phenotypes such as Fe over accumulation and Cd hypersensitivity by inducing *OPT3* expression in the *bzip23-1/opt3-2* double mutant; however, this suppression was only partially reproduced using independent alleles. Using additional approaches such as protein-DNA binding assays (Y1H), we also found that bZIP23 may control Fe homeostasis through the direct regulation members of the *FIT network*. Protein-protein screens also help us determine that bZIP23 interacts with a putative ubiquitin E3 ligase, DAFL1, and we hypothesize that this interaction may control bZIP23 protein abundance.

1 Abstract

Iron (Fe) and Zinc (Zn) are vital nutrients for all forms of life and exhibit homeostatic cross talk to balance intracellular concentrations of each metal. In this work, we focused on the characterization of bZIP23, a protein previously characterized in Zn homeostasis; our data however, suggests that bZIP23 may coordinate the Fe/Zn cross talk by suppressing Fe related phenotypes of *opt3.* This mutant has been described previously as a plant with a constitutive Fe deficiency response. Our original genetic suppression approach found that *bzip23-1/opt3-2* results in the loss of Fe deficiency responses in *opt3*. These phenotypes however, were not fully

reproduced in a second independent double mutant, *bzip23-2/opt3-3*, and a F1 cross of the double mutants root length displayed heterosis when exposed to Cd. Independently, we also determined that bZIP23 does not regulate *OPT3* directly, but instead binds to the promoters of several FIT network members (*FIT1, bHLH38, IRT1*, and *FRO2*), which control the expression of the Fe machinery in roots. Overexpression of YFP:bZIP23 results in variable YFP signal within organs, indicating that bZIP23 is likely subject to protein degradation to control its activity. Along this line, we have also identified DAFL1 as an ubiquitin E3 ligase that may target bZIP23 for degradation. Altogether, our data offer a rare glimpse of the intricate crosstalk between Fe and Zn homeostasis and suggests that bZIP23 may regulate Fe homeostasis to ultimately prevent Zn toxicity.

2 Introduction

Zinc (Zn), like iron (Fe), is an essential micronutrient for all forms of life. Similar to Fe, Zn serves as a cofactor in proteins involved in diverse biological processes. However, the relatively low redox potential of Zn compared to Fe makes it far less reactive, thus it frequently serves as a cofactor in different reactions with a strong presence in the nucleus (i.e. as co-factors for transcription factors). Zn storage and mobilization is mediated by several families of transport proteins such as heavy metal transporting ATPase (HMA), plant cadmium resistance (PCR), and ZRT/IRT-like protein (ZIP) families, which have been shown to directly import Zn from the rhizosphere. Notably, the high affinity Fe transporter IRT1, located at the root epidermis, is a member of the ZIP family and is able to transport several transition elements such as Zn, Fe, Mn and the non-essential element cadmium (Cd). The uptake and allocation of essential transition elements such as Fe and Zn are known to undergo cross talk, where the status of individual metals can affect the homeostasis of the other heavy metals (Eroglu *et al.*, 2017; Wu *et al.*, 2012; Arrivault

et al., 2006). For instance, Zn excess is able to induce an artificial Fe deficiency through competitive binding of target proteins, and similarly Zn toxicity can occur during Fe deficiency through Zn uptake by IRT1 (Grotz and Guerinot, 2006). Hence a Fe/Zn crosstalk system is thought to exist to co-regulate the uptake, transport, sequestration of these elements (Zargar, Kurata, *et al.*, 2015; Zargar, Fujiwara, *et al.*, 2015). While many transcription factors regulating Fe homeostasis have been identified, very few regulators of Zn have been described.

The best characterized transcription factors for Zn homeostasis are a pair of basic leucine zipper (bZIP) proteins, bZIP19 and bZIP23 (Assuncao *et al.*, 2010). bZIP proteins are thought to function exclusively as dimers, and are composed of a basic DNA binding domain, which binds A, G, and C-box motifs (Izawa *et al.*, 1993), and a leucine zipper, which is responsible for dimerization specificity (Deppmann *et al.*, 2006). The leucine zipper is an alpha helix in which every seventh residue is a leucine (Hurst, 1995), this spacing forces the leucine residues and their hydrophobic side chains to align on one side of the alpha helix, allowing non-polar interactions to facilitate dimerization. bZIP family proteins share this leucine zipper domain, but ubiquitously have other substantial N and/or C terminal domains relative to the bZIP domain (Jakoby, 2002). bZIP subfamilies often contain subsequences which are conserved within the subfamily, but have no known functions (Jakoby, 2002).

bZIP19 and bZIP23 contain one such unknown yet conserved sequence, which is rich in histidine and cysteine residues known to bind divalent cations such as Zn and Fe in other proteins (Jakoby, 2002; Assuncao *et al.*, 2010). The architecture of bZIP19 and bZIP23 is loosely divided into three 100 amino acid sections, with the bZIP domain centrally located and the conserved Cys/His sequence within the N terminus and no annotated domains in either the N or C terminal domains. The proximity of the Cys/His rich region to the DNA binding domain immediately suggest a role for heavy metals to induce conformational changes that may alter the capacity their DNA binding

domain to interact with its target DNA (e.g. the presence of excess heavy metals causes a dimerization of the N-terminal domains, sterically inhibiting DNA binding of the DNA binding domain).

bZIP19 and bZIP23 were first identified as regulators of Zn deficiency when Assuncao *et al.*, 2010 reported that they found bZIP19 and bZIP23 in a Y1H screen against the known Zn deficiency responsive transporter, ZIP4 (Grotz *et al.*, 1998). These authors also observed that single knock out mutants of bZIP19 or bZIP23 exhibit no visible phenotype on Zn deficient plates, while the double mutant *bzip19-1/bzip23-1* shows extremely stunted growth. Further, overexpression of bZIP19 or bZIP23 in the *bzip19-1/bzip23-1* mutant restored growth on Zn deficient plates. Indeed, gel shift mobility assays demonstrate that both bZIP19 and bZIP23 are able to bind a palindromic motif, named the Zinc Deficiency Response Element (ZDRE), found in the multiple copies in several putative Zn transporters (ZIPs) which are induced under Zn deficiency (Assuncao *et al.*, 2010). Although this work indicates the bZIP19 and bZIP23 are redundant, Assuncao *et al.*, 2010 also observed that when grown in soil, mature *bzip19-1* plants are slightly stunted and show the same under accumulation of Zn as *bzip19-1/bzip23-1*, while *bzip23-1* resembles a wild type plant in these respects.

Zn deficiency is technically difficult to achieve, owing to the plant's capacity to scavenge even trace amounts of Zn included in agar recipes often used in plant laboratories (Inaba *et al.*, 2015). Perhaps unsurprisingly, Inaba *et al.* found *bzip23* to display a minor reduction in root growth under Zn limiting conditions, as well as a far more drastic Zn deficiency phenotype of *bzip19* than the observed in Assuncao *et al.*, 2010. bZIP19 was further implicated as the primary inducer of Zn deficiency responses, as ZIP3 and ZIP9 transcript and protein abundance and was dramatically reduced in the *bzip19* mutant (Inaba *et al.*, 2015), while *bzip23* showed a relatively modest, but significant, transcriptional repression of these transporters, indicating that bZIP19 and bZIP23

each serve to induce ZIP3 and ZIP9, but bZIP19 is the primary regulator of each ZIP transporter. However, and in contrast to the apparent dominance of bZIP19, the putative Zn transporter ZIP12 is repressed in *bzip23*, but not *bzip19* (Inaba *et al.*, 2015). Little is known to the function of ZIP12, although it is expressed in both leaves and roots and is induced during both Zn deficiency (Inaba *et al.*, 2015) and hypoxia (Mustroph *et al.*, 2009).

To date, bZIP19 and bZIP23 are implicated as functionally redundant transcription factors based on the following 5 observations: (1) they shared binding properties to the ZDRE motif, (2) both are induced under Zn deficiency, (3) short root phenotypes of single mutants on Zn deficiency plates, (4) the dramatic phenotype of the *bzip19/bzip23* mutant on Zn deficiency plates, and (5) repression of Zn-related transporters. Of the two bZIP putative homologues, bZIP19 is implicated as the dominant one based on the stronger short root phenotype in *bzip19* mutants and the stronger repression of ZIP3 and ZIP9 in the *bzip19-1* mutant, relative to *bzip23-1*. Therefore, bZIP19 and bZIP23 are not fully redundant, as bZIP23 seems to regulates the transition metal transporter ZIP12 independently of the presence of bZIP19 (Assuncao *et al.*, 2010; Inaba *et al.*, 2015).

The homeostasis of Zn and Fe networks are thought to be interdependent owing both similar mechanisms for uptake and interaction with Fe and/or Zn binding proteins. For instance, the Oligopeptide Transporter 3 (OPT3) is a transporter which mediates the Fe deficiency signal from leaves to roots (Khan *et al.*, 2018; Zhai *et al.*, 2014); the knock-down mutant *opt3-2* displays a constitutive Fe deficiency response in roots, and consequently over-accumulate heavy metals such as Fe, Zn, and Mn (Stacey *et al.*, 2008; Mendoza-Cózatl *et al.*, 2014). Further details of the *opt3-2* mutant and its role in Fe homeostasis can be found in Chapters 1 and 2. But for the purpose of this chapter, *opt3* mutants have a deregulation of Fe and Zn homeostasis networks (Khan *et al.*, 2018).

In this work, and in an effort to study Fe homeostasis without impacting the Zn homeostasis network, we introgressed the *bzip19-1/bzip23-1* mutations into *opt3-2*. Surprisingly, rather than finding that the crosstalk between Zn and Fe homeostasis had been eliminated, we found that the *opt3-2* phenotype (i.e Fe over accumulation) had been suppressed. We later determined that only *bzip23-1* was needed to recapitulate this suppression. Interestingly, while YFP:bZIP23 overexpression lines were able to partially complement the suppression of *opt3* in the *bzip23-1/opt3-2* mutant, the particular expression pattern of YFP suggested that rapid protein turnover through degradation may be important for proper bZIP23 function. Further, we identified an E3 ligase which interacts with bZIP23 in a yeast 2-hybrid system, and this ligase may be part of the bZIP23 degradation mechanism. We also found that independent alleles of *opt3* and *bzip23*, do not fully recapitulate the suppression of *opt3-3*, a different allele of *opt3*. At the end of this chapter we explore different alternatives and hypothesis to explain these unexpected results.

3 Results

The results section below describes our current understanding of bZIP23 and how it may relate to Fe/Zn crosstalk. While the body of work centered on the bzip23-1/opt3-2 double mutant clearly show a pivotal role for bZIP23 attenuating the OPT3 dependent Fe deficiency response, the inability of our second double mutant (bzip23-2/opt3-3) to reproduce the suppression of opt3 suggest that additional loci may be needed for this suppression. However, additional and independent approaches, particularly the interaction between bZIP23 and Fe-related promoter sequences further support the role of bZIP23 in the crosstalk between Fe and Zn homeostasis.

3.1 *bzip23-1/opt3-2*, but not *bzip23-2/opt3-3*, is able to completely suppress *opt3-2* phenotypes

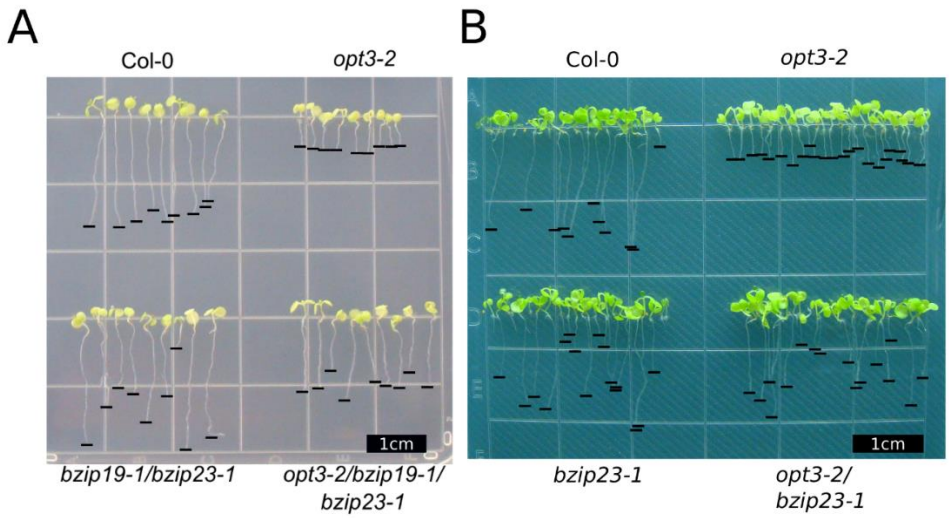

Figure 12 The loss of bZIP23 suppresses the phenotypes of *opt3-2*. (A) Attempts to eliminate Fe/Zn cross talk through by crossing *opt3-2* and *bzip19/bzip23* resulted in suppression of *opt3-2* phenotypes. Plants grown on 20μM $CdCl_2$ show a hypersensitive response due increased IRT1 activity. (B) The suppression of *opt3-2* phenotypes is specific to *bzip23-1*.

The Arabidopsis *opt3-2* mutant has been shown to have constitutive Fe deficiency responses but also shows deregulation of Zn homeostasis (Khan *et al.*, 2018). In an effort to separate these two homeostatic networks, and with the aim of better studying Fe homeostasis isolated from the Fe/Zn cross talk, we crossed *opt3-2* and *bzip19-1 bzip23-1* (*b19b23)* to create the triple mutant *opt3-2 bzip19-1 bzip23-1* (*o3b19b23)*. First, we tested to see if the *o3b19b23* showed the same Cd hypersensitivity as *opt3-2*. Surprisingly, we found that while *b19b23* had no discernable Cd phenotype of its own, *o3b19b23* showed a partial restoration of root growth relative to Col-0, implying that the *opt3-2* dependent induction of *IRT1* had been suppressed (**Figure 12**). If the suppression of *opt3-2* phenotypes in *o3b19b23* were truly a product of altered Zn homeostasis, then introgression of either bZIP19 or bZIP23 should reverse the suppression of *opt3* phenotypes. Hence, *bzip19-1* and *bzip23-1* were each crossed into the *opt3-2* background to produce the

double mutants o_2b19_1 and o_2b23_1, which were again grown on 20µM $CdCl_2$. Interestingly, we found that only *bzip23-1*, but not *bzip19-1*, was sufficient to suppress the short root phenotype seen in *opt3-2*. This suggests that in some cases bZIP19 and bZIP23 may function as dual regulators, working together to regulate Zn homeostasis; however, they also have independent roles in other homeostatic networks, which seems to be the case for bZIP23 and Fe homeostasis.

To further validate that this cross talk was reproducible, as second *opt3/bzip23* mutant was made using a pair of independent alleles, *opt3-3* and *bzip23-2* (**Figure 13 A**, **B**). The *opt3-2* and *opt3-3* mutants are very similar, as each have a T-DNA insertion in the promoter near the start codon, resulting in a knocked-down expression of *OPT3*. Unlike the *opt3* mutants, *bzip23-1* and *bzip23-2* mutants are both knock out mutants, but the T-DNA insertion in *bzip23-1* is located in the 5' UTR, while the *bzip23-2* T-DNA is located in the first exon (**Figure 13**). Hence, an independent double mutant o_3b_2 was produced by crossing *bzip23-2* and *opt3-3* (o_3b23_2).

To determine the similarity of o_2b_1 and o_3b_2 each were grown in hydroponic media to bolting stage (~4 weeks) and visually inspected for *opt3* suppression (**Figure 14**). In addition to the Fe deficiency phenotypes, *opt3-2* also demonstrates a reduced rosette diameter and darker green leaves, which was fully suppressed in o_2b23_1, but an intermediate rosette diameter was observed in o_3b23_2. More concretely, we found that the o_3b23_2 mutant accrued necrotic lesions, an *opt3-2* phenotype

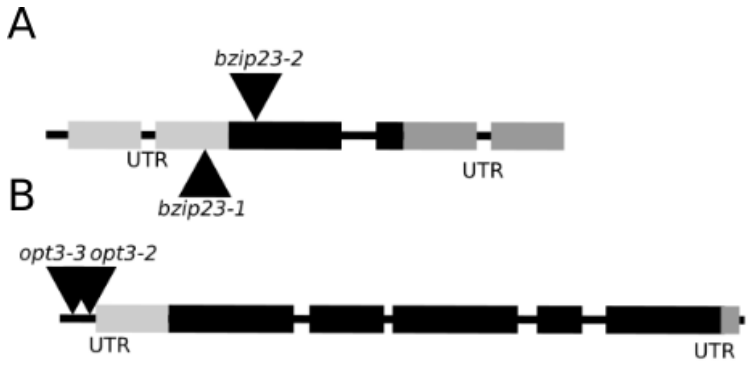

Figure 13 Schematic representation of the *opt3* and *bzip23* mutants.

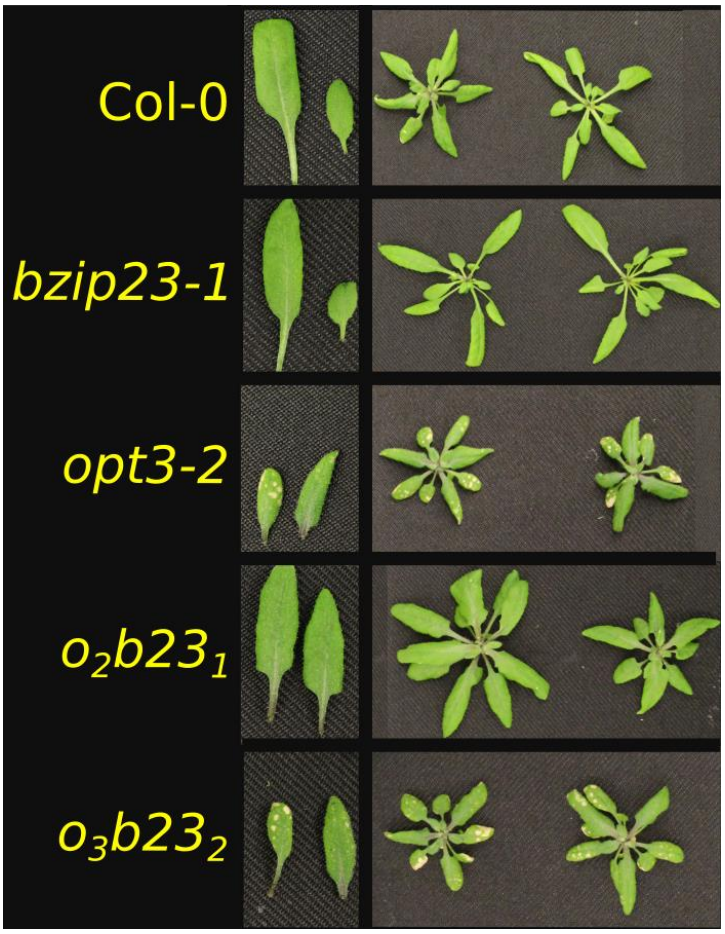

Figure 14 The *o₃b23₂* mutant does not reproduce the suppression of *opt3* phenotypes in leaves, most clearly shown in the development of necrotic lesions in *opt3-2* and *o₃b23₂* leaves.

resulting from Fe over accumulation, a clear sign of *opt3*-dependent *IRT1* induction.

Next, we compared *o₂b23₁* and *o₃b23₂* against Col-0 and the *o3b19b23* mutant on Cd plates to determine if the root growth had been similarly inhibited. As expected from the phenotypes observed when hydroponically grown, plate grown *o₃b23₂* seedlings showed shorter roots than Col-0 and the *opt3* suppressing mutants (**Figure 15A**). Next, we directly compared *o₂b23₁* and *o₃b23₂* against *opt3-2* and Col-0 at vegetative stage and found similar results (**Figure 15B**, **C**). While the difference in root lengths is visible in seedlings, when grown to the vegetative stage it became apparent that the shoots of o_3b23_2 did not show the same Cd phenotype as *opt3-2* leaves (**Figure 15D**). Like the observed root lengths, the fresh weight of o_2b23_1 was never fully restored

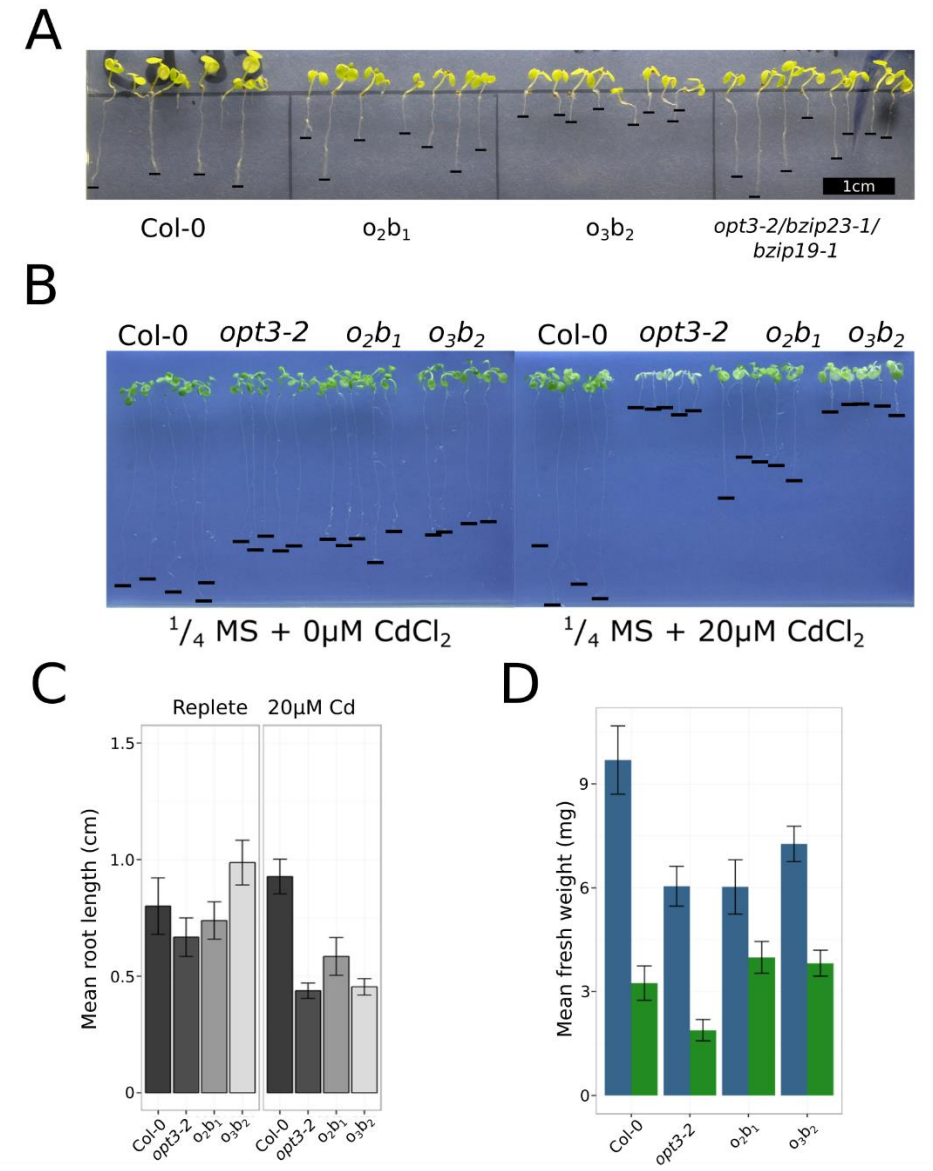

Figure 15 Further characterization of the o_3b23_2 mutant on 20μM $CdCl_2$ plates. (A) The o_3b23_2 mutant is Cd hypersensitive at the young seedling stage, at the emergence of true leaves. (B) Extended exposure to Cd does not alter the Cd hypersensitivity phenotype. (C) Quantification of root length of (B). (C) Fresh weight of plants in (B) demonstrate that despite the short root phenotype, o_3b23_2 plants have a similar shoot mass as o_2b23_1

to Col levels, which was similarly reflected in the o_3b23_2 mutant. This indicates that while *o_3b23_2* does

not fully suppress *opt3* phenotypes as seen in *o_2b23_1*, the *bzip23-2* mutation does affect *opt3-3* dependent Fe homeostasis.

It is possible for SALK lines, like bzip23-1 and opt3-2, to carry additional unannotated T-DNA insertions. Whole genome RNA sequencing was used to show that no genes near the bZIP23 locus were strongly affected, suggesting that the loss of bZIP23 is primarily responsible for the opt3-2 suppression (Supplemental figure 1).

These results suggest that the specific mutant backgrounds may have an effect in the resulting phenotypes. To further determine if a dominance exists between the alleles, a F1 heterozygous mutant, which has no wild type loci and two independent T-DNA insertions at each locus, was produced by crossing o_2b23_1 and o_3b23_2 to produce the F1 $o_{2/3}b23_{1/2}$ mutant. Again, plants were grown on 20µM $CdCl_2$ to assay for the short root phenotype. Unexpectedly, $o_{2/3}b23_{1/2}$ showed neither o_2b23_1 nor o_3b23_2 like root growth, instead $o_{2/3}b23_{1/2}$ exhibited a slight increase in root length relative to o_2b23_1, but still smaller than Col-0 (**Figure 16**). This dominant (or semi-dominant) phenotype currently prevents us from clearly defining the contribution of each allele to the final phenotype. However, other crosses are being generated (o_2b23_2, o_3b23_1), which we hope may help us determining the dominance relationship between alleles.

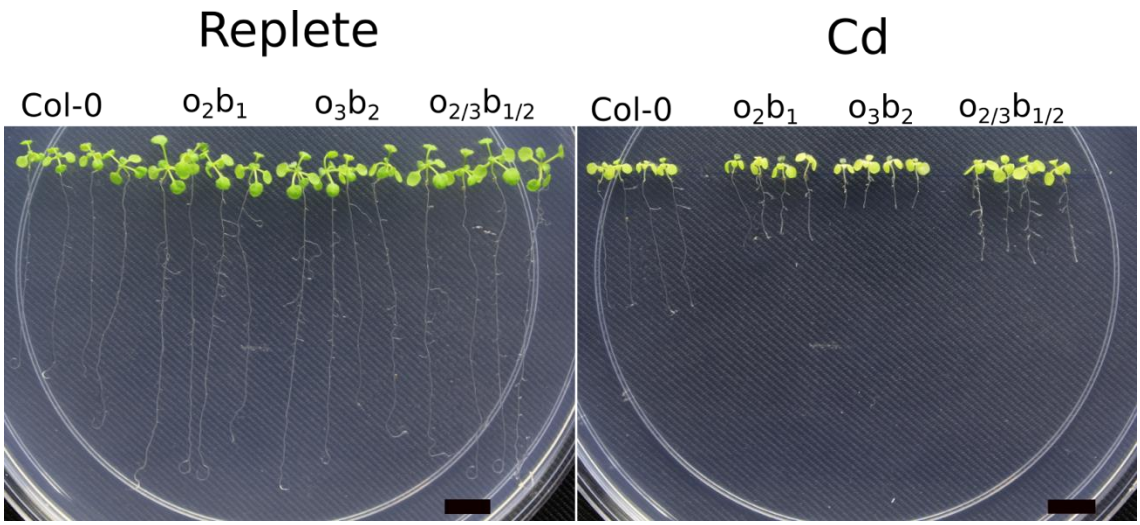

Figure 16 The heterozygous mutant $o_{2/3}b23_{1/2}$ display heterosis, where the $o_{2/3}b23_{1/2}$ mutant suppresses the short root phenotype of *opt3-2* better than either parent line, indicating that the allelic effects are non-additive.

In summary, we found the *o₂b23₁* mutant to fully suppress *opt3-2* phenotypes, while the *o₃b23₂* mutant failed to fully suppress these phenotypes. In addition, the heterozygous F1 *o₂/₃b23₁/₂* was able to suppress the *opt3* phenotypes, suggesting a dominant or semi-dominant behavior for one of the *b23* alleles. Further work is needed to determine the cause of *bzip23*-mediated suppression of *opt3* phenotypes.

3.2 The *o₂b23₁* mutant contains wild type levels of heavy metals

To determine if *o₂b23₁* suppressed the short root phenotype through reduced metal uptake, or by some other mechanism, plants were grown in replete hydroponic media for 4 weeks and were harvested for quantification of trace metals. We found that in agreement with our initial hypothesis the heavy metals Zn, Mn, and Fe were all found to be in equal abundance in Col-0, *bzip23-1*, and *o₂b23₁,* while *opt3-2* over accumulated each metal. Additional genotypes were also assayed and can be found in Supplemental Figure 2. These results led us to suggest a working model where bZIP23 may interact with the OPT3 signaling pathway that controls Fe and Zn uptake and in the absence of bZIP23, *IRT1* expression is reduced to prevent Zn toxicity.

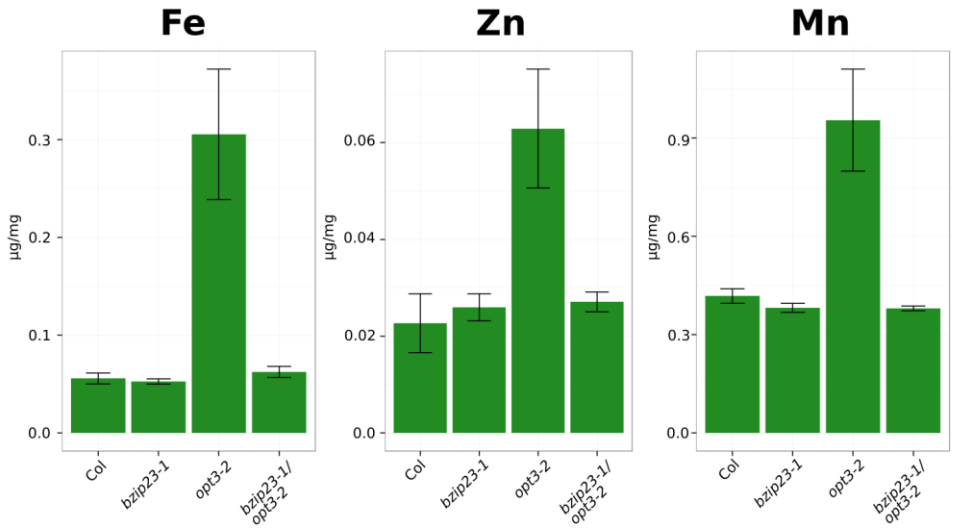

Figure 17 Suppression of the *opt3-2* short root phenotype in *o₂b23₁* is concomitant with reduced heavy metal accumulation associated with the constitutive Fe deficiency phenotype of *opt3-2*.

3.3 mRNA profiling demonstrates the extent of *opt3* suppression in o_2b23_1

The loss of heavy metal accumulation in o_2b23_1 compared to *opt3*, indicate that the source of o_2b23_1 suppression may be an altered regulation of the *FIT network*, which is up regulated in *opt3* mutants thus leading to a constitutively high expression of IRT1 that ultimately overloads the

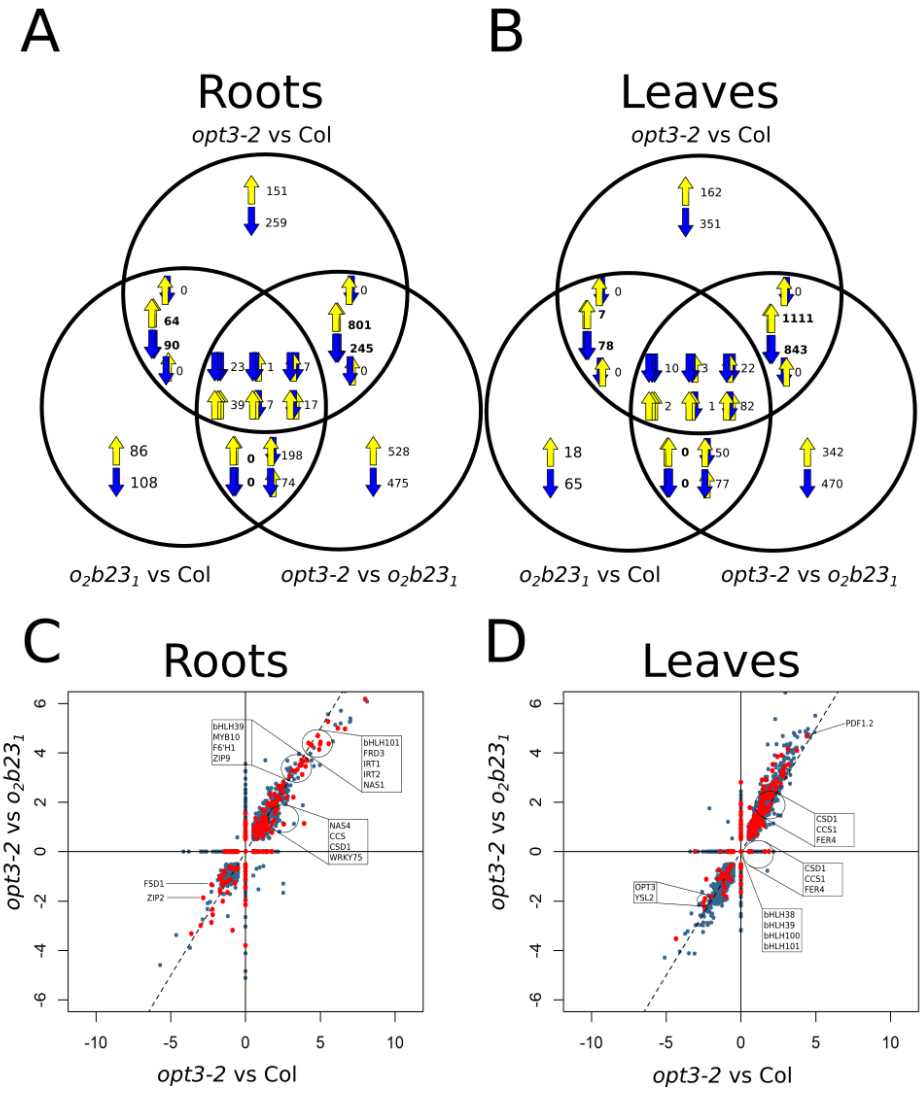

Figure 18 RNA sequencing of Col, *opt3-2,* and o_2b_1 demonstrate the extent of *opt3-2* suppression in o_2b_1. (A-B) Venn diagram of fold change signs in leaves and roots, respectively. Arrows indicate fold change sign, tiled arrows are in the order <opt3 v Col, o_2b_1 v Col, opt3 v o_2b_1>, arrows for contrasts outside of a given intersection are omitted, but follow the given order from left to right. (C-D) Scatter plot of $\log_2$ fold changes. Genes known to be consistently responsive to Fe deficiency are highlighted in red.

plant with heavy metals. To gain more insight into the molecular mechanisms behind the suppression of *opt3* phenotypes by the loss of bZIP23, we pursued whole genome transcriptome in Col, opt3, and o_2b23_1.

Leaves and roots of Col-0, *opt3-2*, and o_2b23_1 were harvested separately after being grown to bolting stage in hydroponic media. mRNA isolated as described in Materials and Methods and submitted for library preparation and single end 100bp sequencing using an Illumina HiSeq at the MU DNA core. Cleaned reads were mapped to the TAIR10 genome release using Tophat2 (Kim Daehwan *et al.*, 2013) with a mapping efficiency of ~95%. All differential expression calls which were not supported by at least 50 uniquely mapped reads in the lower of the two conditions, as well as not significant changes, were set to have a fold change of zero.

Tabulating the sign of the fold changes in each contrast (**Figure 18A**, **B**) demonstrates several key points: First, the majority of the differentially expressed genes (DEGs) are shared, with the same sign, between comparisons of *opt3* v Col and *opt3* v o_2b23_1 in leaves as well as roots. Explicitly, the choice of reference (Col or o_2b23_1) makes little difference in the resulting $\log_2$ ratio, suggesting that o_2b23_1 and Col share similar expression profiles. This is further supported by the contrast

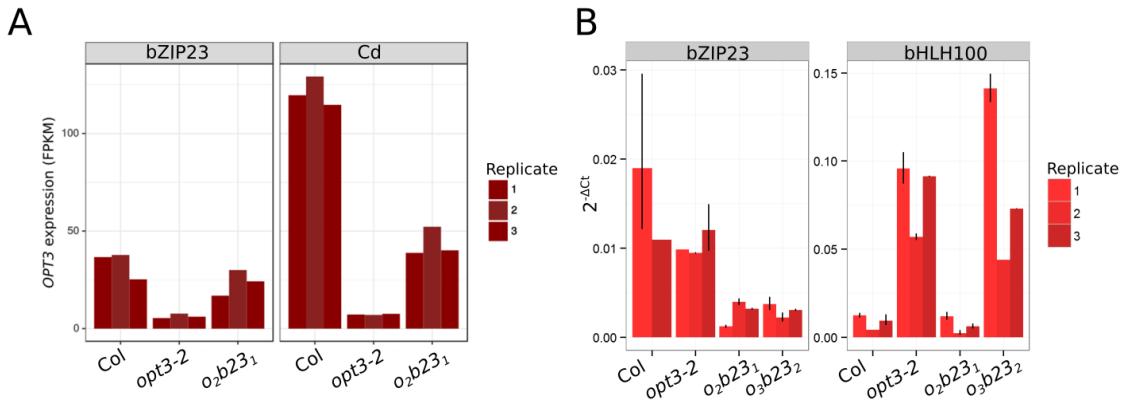

Figure 19 The o_2b23_1 phenotype can be explained by the induction of OPT3, which is not reproduced in the o_3b23_2 mutant. (A) OPT3 expression is induced in o_2b23_1 relative to *opt3-2*, and OPT3 in *opt3-2* is transcriptionally regulated during Cd stress. (B) OPT3 is induced in the o_3b23_3 relative to o_2b23_1 (C) o_2b23_1 and o_3b23_2 show similar expression of bZIP23. bHLH100 is similarly induced in o_3b23_2 as *opt3-2*, indicating that the o_3b23_2 phenotype directly results from a failure to repress *opt3-2* dependent transcripts

o_2b23_1 vs Col, which shows fewer unique DEGs relative to the unique DEGs in *opt3-2* against any reference, and most remarkably have no shared DEGs with opposing signs.

Secondly, the magnitude of the differential expression is similar between the contrasts *opt3* vs Col and *opt3* vs o_2b23_1 (**Figure 18C**, **D**), where the majority of DEGs lie near the identity line (dotted line). Further, many of these DEGs along the identity are consistently differentially expressed during Fe deficiency (gene set developed in Chapter 2).

Importantly, we found that in the *o_2b23_1* mutant, *OPT3* expression is moderately induced, indicating that the suppression of *opt3* may be related to the baseline expression of *OPT3* (**Figure 19A**). Using the Cd data set discussed in Chapter 2, we determined that not only is *OPT3* expression higher in *o_2b23_1* than *opt3-2*, but *OPT3* expression can respond to Cd exposure (**Figure 19A**). Having made these discoveries, and knowing that the *opt3* phenotypes are not suppressed in the independent cross *o_3b23_2,* we first asked if bZIP23 regulation was differed between the two lines and found that the expression levels were equivalent. Next we asked if the failure to induce *OPT3* in *o_3b23_2* was the reason for the lack of suppression. Although we were unable to satisfactorily measure *OPT3* expression to draw any conclusions, we did find that bHLH100, a gene which is dependent on *OPT3* expression, and induced in the *opt3-2* mutant, was induced to *opt3-2* like levels in *o_3b23_2,* suggesting that OPT3 expression is at *opt3-2* levels.

Next we asked if any discontinuity between *o_2b23_1* and Col-0 exists within the major regulatory networks (MYB10/72, *FIT network*, *PYE network*) which might explain why *OPT3* is induced in *o_2b23_1*. We found no discrepancies in these regulatory networks, finding all deregulation caused by *opt3-2* to be repressed in *o_2b23_1* (**Figure 20**). As expected we found the *FIT network* to be strongly induced in *opt3-2* and subsequently repressed in *o_2b23_1,* the same pattern was observed for MYB10 and MYB72, indicating that the biosynthesis of chelating agents such as nicotianamine,

the Fe uptake mechanism, and regulation of the reduction strategy had been induced and subsequently suppressed. The PYE network was not fully induced as observed in a true Fe deficiency response, but no deviations from the suppression profile were found. Hence, we found a nearly complete suppression of *opt3-2* dependent differential expression, but at this point we were unable to identify the underlying mechanism for the induction of *OPT3* in o_2b23_1.

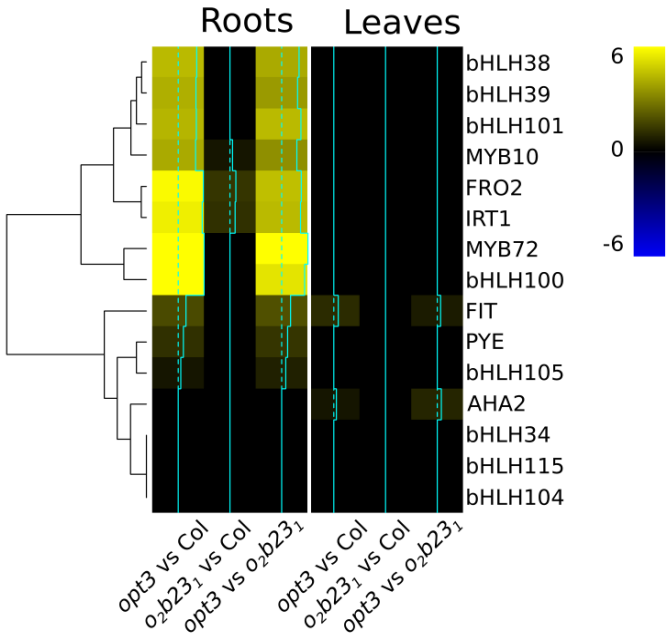

Figure 20 Heatmap of the $\log_2$ fold changes for the members of the Fe uptake pathway, FIT and PYE networks show that the suppression of *opt3-2* Fe deficiency induction independently of these networks.

3.4 bZIP23 overexpression complements the o_2b23_1 phenotype and suggests post-translational regulation of bZIP23.

To demonstrate that *bZIP23* is the causal agent suppressing the *opt3-2* phenotypes, an N-terminal YFP bZIP23$_{cds}$ fusion protein was driven by the strong UBQ10 promoter in the o_2b23_1 background. Growth on Cd plates showed a partial complementation, with UBIQ10$_{pro}$:bZIP23 lines displaying shorter roots than Col, but longer than *opt3-2* (**Figure 21A-B**).

In roots, YFP was found to localize to the nucleus throughout the root body, as expected from the $UBQ10_{pro}$. However, and unexpectedly, this was not uniform, with roots of the same plants showing dramatically different YFP signal in both primary roots and emergent lateral roots (**Figure 21B-E**). In contrast to roots, leaves of YFP:$bZIP23_{cds}$ plants showed extremely weak YFP signal which was limited to single nuclei or small fields of nuclei, but were most often completely absent (**Figure 21F-G**). The variability in YFP signal driven by a strong promoter is often indicative of silencing of the transgene, cleavage and subsequent degradation of YFP, or degradation of the YFP:bZIP23 fusion protein.

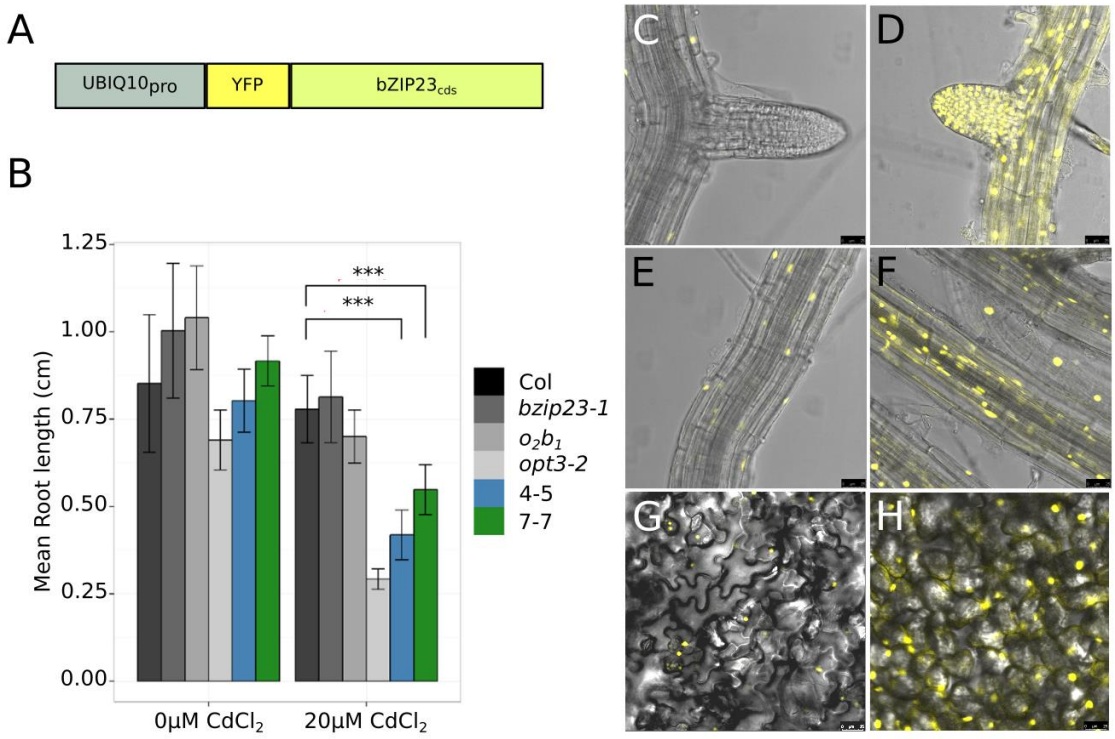

Figure 21 Complementation of o_2b_1 through overexpression of YFP:bZIP23cds suggests post translational regulation of bZIP23. (A) Schematic of the over expression construct. (B) Exposure to 0 or 20µM CdCl2 demonstrates the partial alleviation of the suppressed short root phenotype of *opt3-2*. Ectopic expression of YFP:bZIP23cds results in variable bZIP23 abundance in emergent lateral roots (C-D) mature roots (E-F), and mature leaves (G-H). *** indicates $p < 0.01$ from a two tailed Student's t-test.

To rule out the hypothesis that the transgene was silenced, YFP expression was measured via qRT-PCR and normalized against *UBQ10*; all tested lines showed UBQ10 like expression (Supplemental Figure 3A), suggesting that the loss of YFP signal is not related to transcriptional regulation. To further determine if the variability in YFP signal was due to protein degradation, plants were exposed to the protease inhibitor MG132, but no differences in YFP signal were found (Supplemental Figure 3B). At this point however, we have not determined if the YFP has being cleaved in leaves or roots. Notably, and in contrast to the complementation of o_2b23_1 other attempts to complement the o_2b23_1 mutant were unsuccessful. This includes a second over expression line using the 35S promoter, a native promoter driving a genomic copy of bZIP23 with a 3xFLAG 6xHIS C-terminal tag, and a complete reintroduction of the bZIP23 locus (3kb promoter, 5' UTR, $bZIP23_g$, 3' UTR) (Supplemental Figures 4, 5, and 6) and the reason for this lack of complementation has not been fully elucidated. However, we were able to demonstrate that despite the disagreement between the o_3b23_2 and o_2b23_1 mutants, the loss of *opt3-2* phenotypes can be partially complemented through over expression of bZIP23. The lack of complementation using alternative strategies suggests that there is an additional levels of regulation that need to be identified and may be related to the spatial variance in YFP:bZIP23, which suggests that bZIP23 is regulated by a highly active turnover and protein degradation.

3.5 bZIP23 localizes to the vasculature of leaves and roots

bZIP23 is not included on commercially available microarrays, hence little is known about where bZIP23 is expressed. To determine the tissue level localization of bZIP23 we used a 3kb of the 5' regulatory region of bZIP23 to drive β-glucuronidase (GUS) which catalyzes conversion of the colorless and water soluble to X-gluc to the blue and insoluble indigo.

The promoter region used was selected because 3kb 5' of bZIP23 is the next locus, and this region is transcriptionally available, as it is not bound by histones (Liu *et al.*, 2018) (Supplemental Figure 7). GUS staining revealed bZIP23 expression in the leaf, root, and floral organs (**Figure 22**, Supplemental Figure 8). 10 µm cross sections of leaves showed bZIP23 expression was strongest in the vascular parenchyma (**Figure 22A**, **D**). While in roots expression was localized to the stele and emergent lateral roots (**Figure 22E-G**). Similar to the YFP results, within one plant, roots showed GUS staining on a root-to-root basis (**Figure 22E, G**). Finally bZIP23 expression was detected in immature florets and peduncle, but was not observed in siliques (supplemental figure 8). Based on the spatial distribution of bZIP23, which resembles the spatial distribution of OPT3, it is tempting to suggest that both participate in a common signaling pathway. If bZIP23 is acting

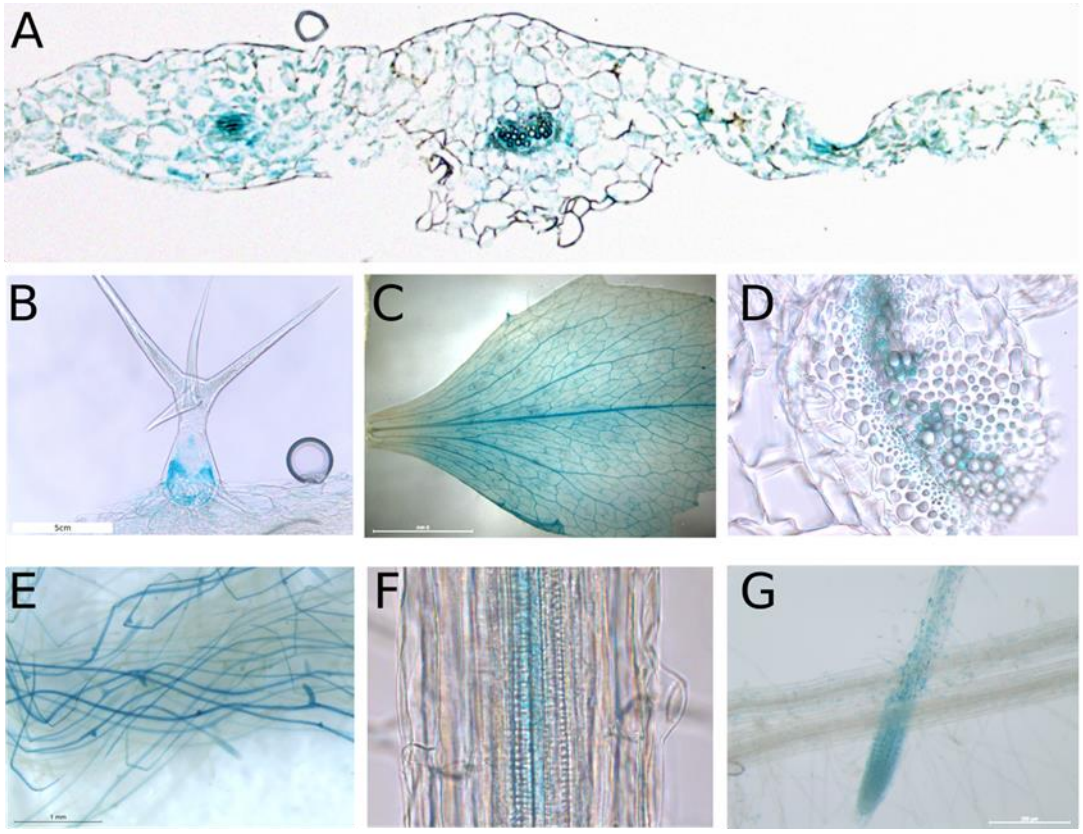

Figure 22 GUS staining reveals tissue level localization of bZIP23. bZIP23 expression was detected throughout the plant body; (A) vasculature of mature leaf (10µm cross section), (B) trichome, (C) cauline leaf, (D) vascular parenchyma (10µm cross section), (E) root system, (F) longitudinal view of the root stele, and (G) root tip

as a transcriptional repressor of OPT3, then the absence of bZIP23 may allow OPT3 expression to reach levels sufficient to repress the *opt3-2* phenotypes described before.

3.6 bZIP23 binds to the promoters of the Fe uptake pathway in a protein-DNA binding screens (Y1H)

Given the induction of *OPT3* in o_2b23_1, we hypothesized that bZIP23 may be acting as a transcriptional repressor of *OPT3*. Hence, we began screening three 300bp fragments of $OPT3_{pro}$ against bZIP23 in a Y1H assay. We found no evidence that bZIP23 was able to bind any section of the $OPT3_{pro}$, which indicates that, at least based on Y1H technologies, bZIP23 is unlikely to directly regulate *OPT3* expression.

More recently we began using a library of 1,957 transcription factors to screen for regulators of target promoters (see Chapter 5 for further description). Dr. Mather Khan screened the FIT network members $bHLH38_{pro}$, $FIT1_{pro}$, $IRT1_{pro}$, and $FRO2_{pro}$ by first cloning three or four ~300bp fragments of each promoter, and screened each against the complete library. Dr. Khan found that bZIP23 binds to $bHLH38_{pro}$ fragment 1, $FIT1_{pro}$ fragment 4, $IRT1_{pro}$ fragment 3, and $FRO2_{pro}$ fragments 2 and 3, while bZIP19 was not observed to bind any of these promoters despite being present in the library.

To verify this interaction each of these colonies were grown to saturation and diluted to 0.5 OD^{600}, ten-fold serially diluted, and stamped in quadruplicate using different stringencies for growth by increasing the concentration of 3-AT to determine the relative binding affinity of bZIP23 against each promoter fragment (**Figure 23A**). The interaction between bZIP23 and the promoters of the transcriptional regulators bHLH38 and FIT1 was found to be strongest, growing in concentrations upwards of 60 mM 3-AT. These results once more suggest an interaction between Fe and Zn

homeostasis through bZIP23 but not bZIP19. While direct regulation of gene expression by transcription factors is a critical component of gene regulation, the availability of chromatin to receive TFs is equally important. Moreover, the most significant transcription factors for gene regulation are not necessarily those which bind closest to the transcription start site (Sijacic *et al.*,

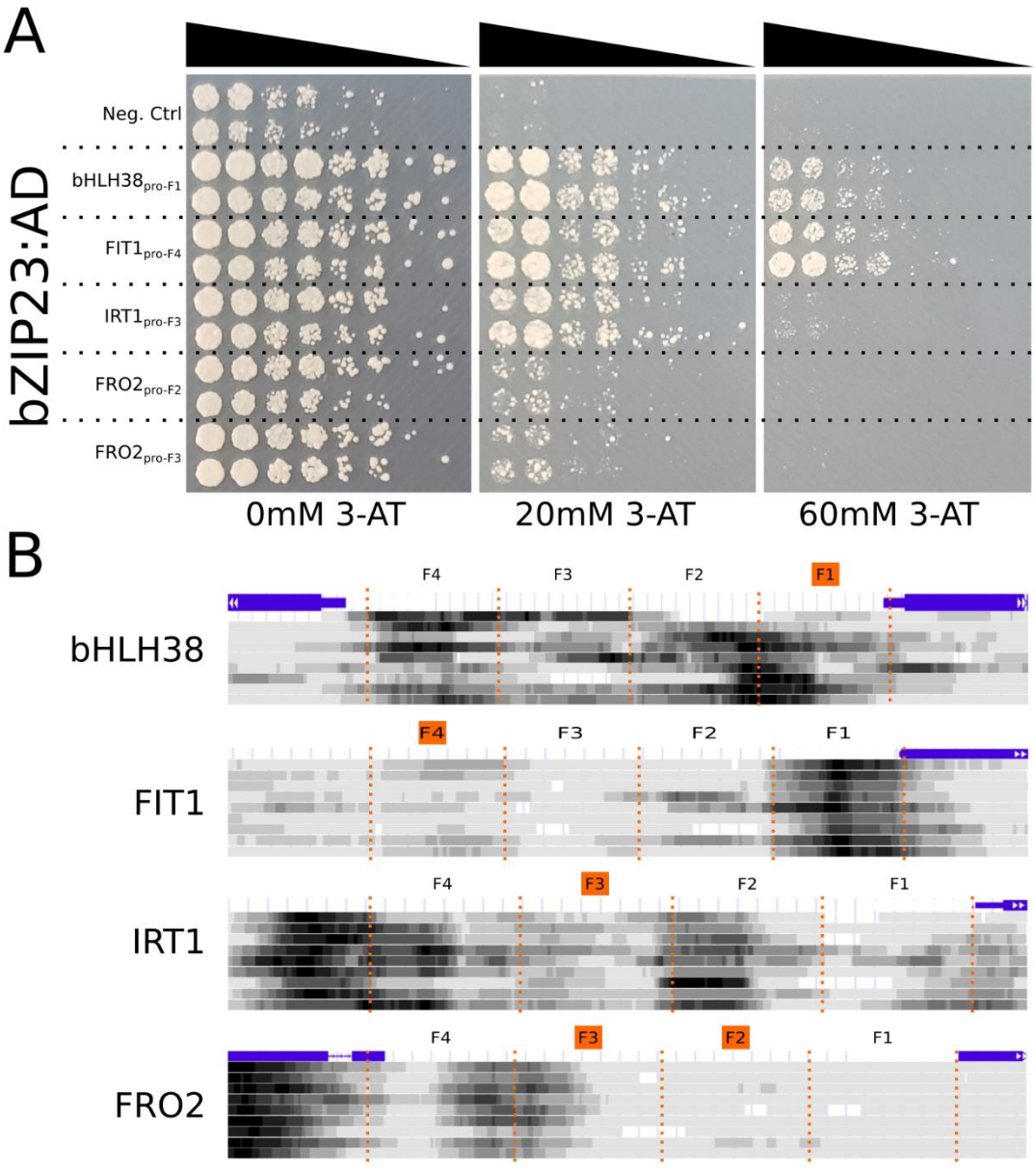

Figure 23 bZIP23 likely regulates Fe homeostasis through the direct regulation of bHLH38, FIT1, and FRO2. (A) Ten-fold serial dilution of bZIP23:AD and indicated promoter fragments under increasing stringency. (B) Promoter availability, as monitored by histone occupancy of promoters which bZIP23 bind in a Y1H. Dark shading indicates regions which are not bound by histones, orange lines indicate the fragment divisions, fragments highlighted in orange show where bZIP23 was shown to bind.

2018). Using publically available data sets of seedlings, 7 day old plants, and seedling roots (Liu *et al.*, 2018; Lu *et al.*, 2016) we identified histone depleted regions of these promoters and found that bZIP23 binds the most histone depleted region of bHLH38, with other promoters showing less obvious patterns of histone depletion near bZIP23 binding regions (**Figure 23B**). The consensus sequence of bZIP23 and bZIP19 in Zn deficiency responses is defined as the ZDRE, but the absence of bZIP19 binding to any promoter suggest that bZIP23 has a unique DNA binding sequence independent of bZIP19, supporting the hypothesis that bZIP19 and bZIP23 work redundantly to regulate Zn homeostasis while bZIP23 may participate independently in a Fe-Zn crosstalk.

3.7 DAFL1 as a putative regulator of bZIP23.

Given the phenotype of o_2b23_1 and the potential regulation of FIT members by bZIP23, we have incorporated bZIP23 into the current negative feedback model of Fe homeostasis where a Fe-related signaling molecule is transported from the leaf vasculature to the root to signal the Fe status of the plant. This signal is then relayed to the root epidermis to regulate the *FIT network*. We hypothesize that bZIP23 acts in a protein complex which requires bZIP23 to induce the *FIT network*. With the aim of identifying bZIP23 binding partners, we pursued a whole-genome yeast 2-hybrid (Y2H) screen.

Y2H screens require that the bait transcription factor does not induce transcription of the reporter genes by the action of its own activation domain. To determine if bZIP23 exhibited auto-activation, DB:bZIP23$_{cds}$ was co-expressed with AD:empty vector into the Yeast2Gold yeast strain (**Figure 24A**). We found bZIP23 to auto-activate the Y2H reporter system. Hence, the N-terminal truncations of 72, 34, and 18 residues were produced, which showed no auto-activation of the

reporter system, indicating that the N terminal domain contains a promiscuous activation domain.

Hence, we used the Δ18 residue truncation (bZIP23$_{\Delta 18}$), which contains the His/Cys rich sequence,

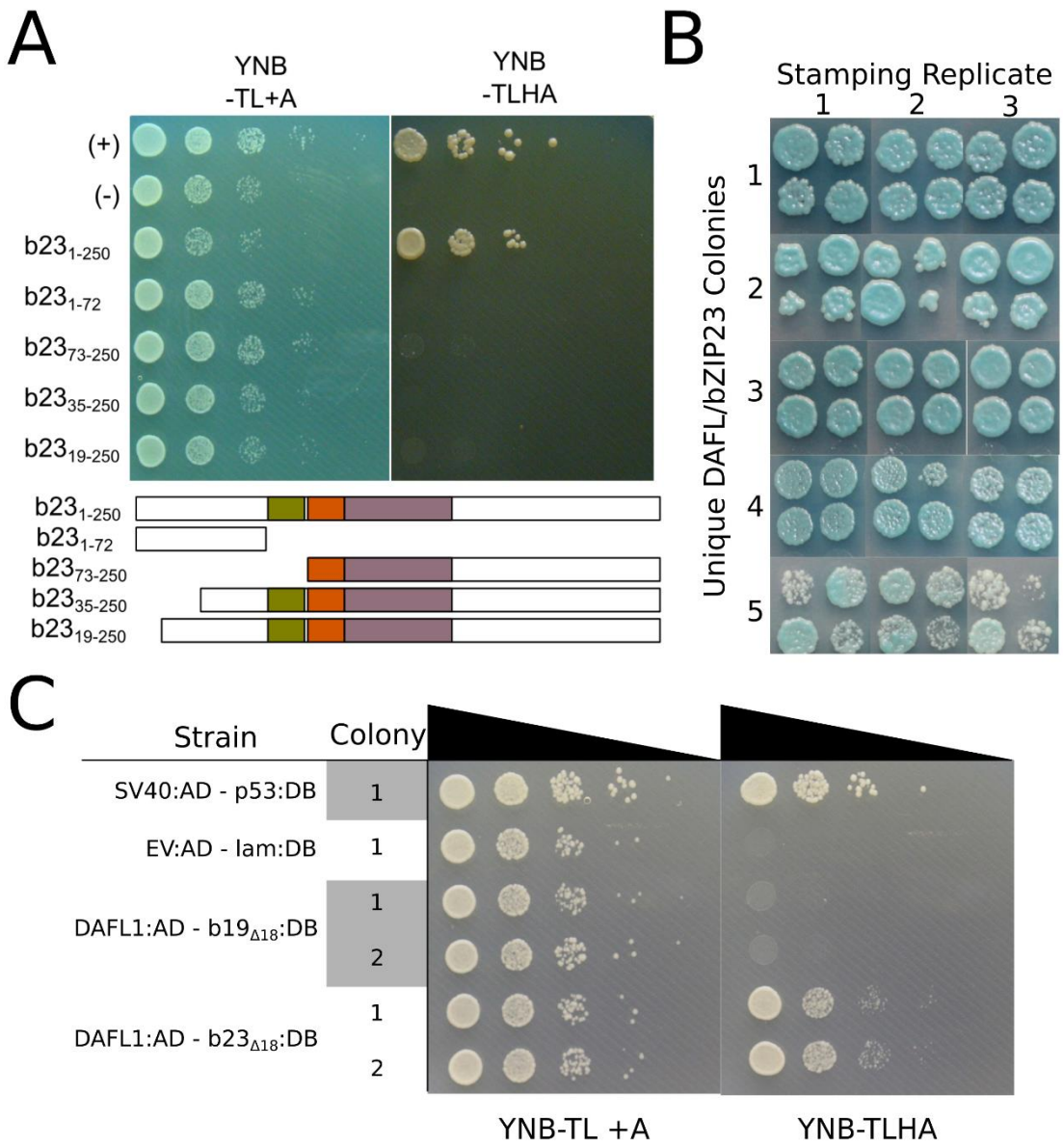

Figure 24 bZIP23, and not bZIP19, interacts with DAFL1 in a Y2H assay. (A) Truncation series of the bZIP23 protein demonstrate that the first 19AA of bZIP23 are needed to induce auto-activation of the Y2H reporter system, the resulting 19AA truncation line denoted as bZIP23$_{F11}$. Schematic shows the architectures of the truncations; zipper domain (purple), DNA binding domain (orange), his/cys rich region (green). (B) cDNA library screening of bZIP23$_{F11}$ identified DAFL1, a E3 ubiquitin ligase, as a interactor of bZIP23, five positive colonies grown on YNB-TLHA+X-gal shown in three separate assays. (C) Serial dilution stamping of AD:DAFL1 with DB:bZIP19$_{F11}$ or DB:bZIP23$_{F11}$ show bZIP23, and not bZIP19, interact with DAFL1.

to screen a commercially available abundance-normalized cDNA library and identified 12 proteins in three or more independent colonies. Most notably, eight independent colonies resulted in the identification of a putative E3 RING ligase, Defective in Anther Dehiscence-like 1 (DAFL1). This interaction was verified through replicate quadruplicate stamping on stringent selective media (**Figure 24B**). DAF-like 1 (DAFL1) is a member of a small clade of three E3 ligases named after DAD1 Factor (DAF) which is expected to ubiquitinate Defective in Anther Dehiscence (DAD1) to regulate jasmonic acid signaling in the stamen (Peng *et al.*, 2013) (DAF was shown to be ubiquitinated by an E2 ligase, but ubiquitination of its substrate has not been reported). DAFL1 and DAFL2 were are not expected to be redundant to DAF, as they are not expressed in stamens (Peng *et al.*, 2013).

To determine if the DAFL1 interaction was unique to bZIP23, we asked if bZIP19 interacted with DAFL1. This was done by cloning a similar bZIP19 truncation ($bZIP19_{\Delta 18}$), as well as DAFL1 without the large 5' UTRs found in the Y2H clone, and co-transforming each $DB:bZIP_{\Delta 18}$ construct with $AD:DAFL1_{cds}$. The resulting strains were grown to 1.0 OD before being serial diluted and stamped on drop out media (**Figure 24C**). In addition to verifying that the 5' UTR did not have an effect on protein-protein interaction, it demonstrated that bZIP19 does not interact with DAFL1 in yeast.

Given that bZIP23 is possibly mediating some of the Fe-Zn crosstalk, the degradation of bZIP23 through poly-ubiquitination by DAFL1 would provide a mechanism for the suppression of *opt3-2* phenotypes in o_2b23_1. Specifically, under zinc excess the degradation of bZIP23 could serve as a mechanism that prevents the induction of the Fe uptake pathway under Zn excess conditions.

4 Discussion

4.1 The *o₂b23₁* mutant implicates bZIP23 in Fe homeostasis.

The *o₂b23₁* mutant strongly indicates that bZIP23 is able to influence Fe homeostasis. The absence of a strong Fe-related phenotype in the single *bzip23-1* mutant suggests that the action of bZIP23 is not incorporated into the standard Fe deficiency response, instead it suggests that the action of bZIP23 is only able to affect the Fe deficiency response in the absence of a functional OPT3 signaling pathway. While the majority of phenotypes were not fully reproduced in the *o₃b23₂* mutant (long root phenotype, loss of necrotic lesions, bHLH100 induction) (**Figure 14**, **Figure 15A**, **Figure 15B**, **Figure 19**) the small shoot mass phenotype was suppressed in both double mutants suggesting a still unknown mechanism behind the *opt3* suppression phenotype (**Figure 15D**).

We may gain insight into the discrepancy between *o₂b23₁* and *o₃b23₂* in the truncation series developed for bZIP23 (**Figure 24A**). Here it was shown that the N terminus of bZIP23 is important for the activation of RNA polymerase, as deletion of the first 18 residues abolish auto-activation of the Y2H reporter system. While expression of bZIP23 is equally abolished in both *bzip23-1* and *bzip23-2* (**Figure 19B**), these measurements were made in the second exon, after the T-DNA insertion found in *bzip23-2.* Hence it is possible for a portion of the bZIP23 N-terminus to be translated and still be functional enough to maintain the *opt3-3* phenotype.

Clearly the suppression of *opt3* phenotypes in the *o₂b23₁* mutant is a direct result of the induction of *OPT3* (**Figure 19A**), and the failure to suppress *opt3* phenotypes in *o₃b23₂* can be attributed to the continued low expression of *OPT3*, as inferred by the induction of bHLH100 (**Figure 19B**). It is unclear if the failure to suppress *opt3* phenotypes arises in the differences in T-DNA lines between *opt3-2* and *opt3-3*, or *bzip23-1* and *bzip23-2*. In the former case it is possible for a regulatory element to bind the narrow promoter section unimpeded by a T-DNA insert in the *opt3-3* line and

keep *OPT3* expression low. Alternatively the N-terminus of *bZIP23* could be functional and induce *OPT3* expression. The allelic contributions in heterozygous mutant line $o_{2/3}b_{1/2}$ are non-additive, and does not show phenotypes corresponding to a stronger induction of *OPT3*, suggesting that there may be in an interactive effect within these mutant lines. Clearly the ongoing production of the o_2b23_2 and o_3b23_1 lines will shed needed light on to the nature of these mutants.

4.2 Regulation of Fe homeostasis by bZIP23

Although the specific role of bZIP23 is not fully resolved using *ob23* mutant lines, our Y1H assays suggest an additional and direct role for bZIP23 in Fe homeostasis. We found bZIP23 to bind transcriptionally active regions of the promoters of bHLH38, FIT1, IRT1, and FRO2 (**Figure 23**). The GUS localization to the root tip (**Figure 22G**), as well as bZIP23's role in inducing target genes in Zn homeostasis (Assuncao *et al.*, 2010; Inaba *et al.*, 2015) suggest that bZIP23 may also participate in the regulation of the FIT network. Although the behavior in Y2H and in Zn homeostasis can only provide conjecture to bZIP23s role in Fe homeostasis. Fe deficiency experiments have not shown bZIP23 to be transcriptionally responsive to Fe deficiency, indicating that bZIP23 is not involved in a Fe deficiency response in the conditions tested. Hence it is likely that bZIP23 plays a role in mediating Fe-Zn cross talk only during specific environmental conditions by actively promoting novel interactions or the formation of different transcriptional complexes. The latter case better agrees with the suspected interaction between Fe and Zn homeostasis, where Fe deficiency can cause a Zn excess, repressing bZIP23 expression and inhibiting activation of Fe uptake. Although this root-centric model does little to explain the suppression of Fe deficiency responses outside of the FIT network or Fe uptake pathway.

Two other models for bZIP23 function rely on the vascular GUS staining (**Figure 22**). The most obvious mechanism would be bZIP23 binding $OPT3_{pro}$ as a repressor, although screening the first 900bp of the $OPT3_{pro}$ showed no interaction of bZIP23 or bZIP19. It is yet possible for bZIP23 to directly regulate $OPT3_{pro}$ under specific conditions, likely as a function of the N-terminal putative metal binding domain. Similarly, bZIP23 may regulate the direct regulator of *OPT3,* but no candidates for this mechanism have been identified. Alternatively if bZIP23 is responsible for regulating the sequestration of Zn in companion cells, then the o_2b23_1 mutant could be explained as having a higher effective Fe deficiency status due to excess Zn, resulting in OPT3 protein accumulation sufficient to restore the *opt3* phenotype.

While localizing bZIP23 expression we found that bZIP23 is expressed in leaves and roots (**Figure 21**) but in each case the staining was inconsistent between and within plants. Similarly, overexpression of YFP:bZIP23 showed inconsistent YFP signal, and was rarely observed in leaves (**Figure 22**). These results were reproduced using plants at multiple developmental stages (seedling, vegetative, and reproductive), indicating that the variance in bZIP23 expression is not dependent on the developmental stage. Although the signals which mediate bZIP23 expression remain unknown, the identification of DAFL1 as an interacting E3 ligase provides a possible mechanism for bZIP23 degradation, which is supported by the absence of a reliable YFP signal in overexpression lines.

5 Conclusion

Here we have explored the role of bZIP23 in Fe-Zn cross talk. Initially using bZIP23 in the strict context of Fe homeostasis, the failure to fully reproduce the suppression of *opt3* phenotypes using independent alleles indicates that the bZIP23 is more likely involved in Fe-Zn cross talk, rather than serving independent roles in each homeostatic network. Hence it may be necessary to impose multiple treatments (high zinc, low Fe) to elicit a phenotype. The additional proposed allele combinations should provide insight into the role of bZIP23 as it pertains to the *opt3* mutants.

Identification of bZIP23 as the substrate of DAFL1 is an appealing avenue to explain the variant YFP abundance in the UBQ10 lines, although as seen in IDF1 (Barberon *et al.*, 2011), not all ubiquitination events lead to 26S proteasome degradation. Regardless, it will be important to purify sufficient soluble protein to asses DAFL1 ubiquitination activity *in vitro*. Purification of functional bZIP23 will also allow facilitate determination of the metal binding capacity of the conserved His/Cys domain, which is also outstanding question to explain bZIP19/23 function in Zn homeostasis

6 Materials and methods

Plants, and growth conditions

The *opt3-2* (SALK_021168C), *bzip19-1* (SALK_005336C), *bzip23-1* (SALK_045200C), and *bzip23-2* (SALK_018248C) mutants were obtained from the SALK institute, while *opt3-3* (SALK_058794C) was provided by Dr. Olena Vatamaniuk (Cornell University).

Hydroponically grown plants were plated on ¼ MS (1/4 dilution of standard Murashige and Skoog salts plus vitamins (Sigma-Aldrich, MO), 1mM MES pH 5.7, and 1% Phytoagar (Duchefa Biochemie, NL)) media and vernalized at 4°C in the dark for 48hr. After 10 days of growth plants were transferred to hydroponic media containing 1.25 mM KNO_3, 625 µM H_2PO_4, 500 µM $MgSO_4$, 500 µM $CaSO_4$, 50 µM Fe-EDTA, 17.5 µM H_3BO_4, 5.5 µM $MnCl_2$, 0.5 µM $ZnSO_4$, 0.062 µM $NaMoO_4$, 2.5 µM NaCl, and 4 nM $CoCl_2$. The hydroponic solution was aereated through commercially available fish tank bubble stones. Plants were grown to bolting stage (appx. 4 weeks) unless otherwise specified.

Quantification of trace metals

After harvesting, residual nutrient solution was removed by two washes in wash buffer (10mM Tris-HCl and 5mM EDTA, pH 8) and one rinse with DI H_2O. Harvested material was dried in a 60°C oven, and homogenized using a glass rod. Dry tissue was digested in concentrated HNO_3 overnight and subsequently incubated in recently boiled water for 15 minutes, three times. Debris was pelleted in a benchtop centrifuge, and 600µL of supernatant was diluted into 9.4mL MilliQ H_2O for quantification using a Perkin Elmer inductively coupled plasma-optical emission spectrometer.

GUS staining

3kb of the bZIP23 promoter was cloned into pENTR, and transferred to a gateway-compatible pBGGUS vector. Col-0 was transformed using the floral dip method (Clough and Bent, 1998) and T1 seedling were screened on 50µg/mL hygromycin B (Invitrogen, CA), T2 and T3 generations were similarly screened to produce stabile transgenic plants with a single transgenic locus. GUS staining was carried out by vacuum infiltrating fresh material in ~20mL GUS staining buffer (100 mM $NaHPO_4$, 50 mM EDTA, 10% methanol (v/v), 0.1% Triton X-100, and 10 µM 5-bromo-4-chloro-indolyl-β-D-glucopyranosiduronic acid (X-gluc)). Stained material was cleared using 70%

EtOH. For thick sections (50µm) plants were embedded in 2% agarose (Fisher Scientific, MA), and sectioned on a Vibratome 3000 Plus. Thin sections (15 µm) were embedded in paraffin and sectioned on using a microtome (IDEXX BioAnalytics, MO). All light microscopy and thick sectioning was carried out at the University of Missouri Molecular Cytology Core.

RNA sequencing

Plant material was immediately flash frozen and stored in liquid N_2 prior to pulverization. mRNA was isolated using a Qiagen RNeasy Plant Mini Kit, according to the manufacturer's protocol. Contaminant genomic DNA was removed using am Invitrogen TURBO DNase kit prior to submission for library preparation and 100bp Illumina sequencing at the University of Missouri DNA Core Facility. Raw reads were trimmed to remove all bases with a confidence less than 95%, and reads shorter than 25bp were discarded using ShortRead (Morgan *et al.*, 2009). Reads were mapped to the TAIR10 genome release using Tophat2 (Kim Daehwan *et al.*, 2013), and uniquely mapping reads were subsequently used to obtain per-locus counts using ShortRead. Differentially expressed transcripts were identified with edgeR (Robinson *et al.*, 2009), using the tagwise dispersion estimate, and holding the false discovery rate to 0.05 using Benjamani and Hochberg correction (Benjamini and Hochberg, 1995).

Yeast 1-hybrid

The OPT3, FIT1, IRT1, FRO2, and bHLH38 promoters were cloned as ~300bp fragments into pENTR using the USER cloning system (Lund *et al.*, 2014). Fragments were transferred to gateway compatible pHIS and pLACZ vectors, which were integrated into Y1H-aS2 strain (Reece-Hoyes *et al.*, 2012). The library containing 1957 *Arabidopsis* transcription factors (TFs) was originally obtained from TAIR from Pruneda-paz *et al.*, 2015 in the low copy number pDEST22 vector and transformed into the Y1867α yeast strain (Reece-Hoyes *et al.*, 2012). The Y1H-aS2 strain carrying the promoter fragments and the Y1867α strain carrying the TFs were mated using

a RoToR (Singer Instruments, UK) pinning robot on YPDA media. Mated colonies were selected for on YNB -His -Trp -Ura (Sunrise Scientific, CA). The concentration of 3-aminotrizol (Sigma-Aldrich, MO) for optimal screening was determined empirically for each promoter.

Yeast 2-hybrid

$bZIP23_{cds}$, $bZIP19_{cds}$, and subsequent truncations were cloned into pENTR using the Gateway system and transferred to the GAL4 DNA binding vector PGBKT7 (Clontech), and expressed in the yeast strain Y2G (Clontech). DAFL1 (AT3G10910) was similarly cloned in the GAL4 activation domain vector pGADT7, and transformed in to the Y187α yeast strain (Clontech). A whole-genome Y2H screening was performed using Clonetech Mate & Plate Library, an abundance normalized cDNA library prepared from multiple *Arabidopsis* tissue types. Screening was performed using the following reporters: histidine synthase, adenosine synthase, aureobasidin resistance, and β-galactosidase.

Confocal microscopy

Full length $bZIP23_{cds}$ was cloned into pENTR and transferred to a gateway compatible pUBQ10 vector, which contains the $UBQ10_{pro}$ and an N-terminal YFP. This vector was integrated into the Col-0 and the *opt3-2 bzip23-1* double mutant, and stable transgenic lines were developed as described for GUS lines. Plants were grown hydroponically prior to imaging freshly harvested tissue on a Leica TCP SP8 MP at the University of Missouri Molecular Cytology Core facility. For MG132 experiments YFP:$bZIP23_{cds}$ in the Col-0 background was used, and exposed to 50µg/mL MG132 or the carrier DMSO.

7 Bibliography

Arrivault, S., Senger, T. and Krämer, U. (2006) The Arabidopsis metal tolerance protein AtMTP3 maintains metal homeostasis by mediating Zn exclusion from the shoot under Fe deficiency and Zn oversupply. *Plant J.*, **46**, 861–879.

Assuncao, A.G.L., Herrero, E., Lin, Y.-F., et al. (2010) Arabidopsis thaliana transcription factors bZIP19 and bZIP23 regulate the adaptation to zinc deficiency. *Proc. Natl. Acad. Sci.*, **107**, 10296–10301.

Barberon, M., Zelazny, E., Robert, S., Conéjéro, G., Curie, C., Friml, J. and Vert, G. (2011) Monoubiquitin-dependent endocytosis of the transporter controls iron uptake in plants. *Proc. Natl. Acad. Sci. U. S. A.*, **108**, e450–e458.

Benjamini, Y. and Hochberg, Y. (1995) Controlling the false discovery rate: a practical and powerful approach to multiple testing. *J. R. Stat. Soc. Ser. B*, 289–300.

Clough, S.J. and Bent, A.F. (1998) Floral dip: a simplified method forAgrobacterium-mediated transformation ofArabidopsis thaliana. *plant J.*, **16**, 735–743.

Deppmann, C.D., Alvania, R.S. and Taparowsky, E.J. (2006) Cross-species annotation of basic leucine zipper factor interactions: Insight into the evolution of closed interaction networks. *Mol. Biol. Evol.*, **23**, 1480–1492.

Eroglu, S., Giehl, R.F.H., Meier, B., et al. (2017) Metal Tolerance Protein 8 Mediates Manganese Homeostasis and Iron Reallocation during Seed Development and Germination. *Plant Physiol.*, **174**, 1633–1647.

Grotz, N., Fox, T., Connolly, E., Park, W., Guerinot, M. Lou and Eide, D. (1998) Identification of a family of zinc transporter genes from Arabidopsis that respond to zinc deficiency. , **95**, 7220–7224.

Grotz, N. and Guerinot, M. Lou (2006) Molecular aspects of Cu, Fe and Zn homeostasis in plants. *Biochim. Biophys. Acta - Mol. Cell Res.*, **1763**, 595–608.

Hurst, H.C. (1995) Transcription factors 1: bZIP proteins. *Protein Profile*, **2**, 101—168.

Inaba, S., Kurata, R., Kobayashi, M., Yamagishi, Y., Mori, I., Ogata, Y. and Fukao, Y. (2015) Identification of putative target genes of bZIP19, a transcription factor essential for Arabidopsis adaptation to Zn deficiency in roots. *Plant J.*, **84**, 323–334.

Izawa, T., Foster, R. and Chua, N.-H. (1993) Plant bZIP Protein DNA Binding Specificity. *J. Mol. Biol.*, **230**, 1131–1144.

Jakoby, M. (2002) bZIP transcription factors in Arabidopsis. , **7**, 106–111.

Khan, M.A., Castro-Guerrero, N.A., McInturf, S.A., et al. (2018) Changes in iron availability in Arabidopsis are rapidly sensed in the leaf vasculature and impaired sensing leads to opposite transcriptional programs in leaves and roots. *Plant. Cell Environ.*, 1–14.

Kim Daehwan, K., Pertea, G., Trapnell, C., Pimentel, H., Kelly, R. and Salzberg, S. (2013) TopHat2 : accurate alignment of transcriptomes in the presence of insertions , deletions and gene fusions. *Genome Biol.*, **14**, 0–9.

Liu, Y., Tian, T., Zhang, K., You, Q., Yan, H., Zhao, N., Yi, X., Xu, W. and Su, Z. (2018) PCSD: A plant chromatin state database. *Nucleic Acids Res.*, **46**, D1157–D1167.

Lu, Z., Hofmeister, B.T., Vollmers, C., DuBois, R.M. and Schmitz, R.J. (2016) Combining ATAC-seq with nuclei sorting for discovery of cis-regulatory regions in plant genomes. *Nucleic Acids Res.*, **45**, 1–13.

Lund, A.M., Kildegaard, H.F., Petersen, M.B.K., Rank, J., Hansen, B.G., Andersen, M.R. and Mortensen, U.H. (2014) A versatile system for USER cloning-based assembly of expression vectors for mammalian cell engineering. *PLoS One*, **9**.

Mendoza-Cózatl, D.G., Xie, Q., Akmakjian, G.Z., et al. (2014) OPT3 is a component of the iron-signaling network between leaves and roots and misregulation of OPT3 leads to an over-accumulation of cadmium in seeds. *Mol. Plant*, **7**, 1455–1469.

Morgan, M., Anders, S., Lawrence, M., Aboyoun, P., Pagès, H. and Gentleman, R. (2009) ShortRead: A bioconductor package for input, quality assessment and exploration of high-throughput sequence data. *Bioinformatics*, **25**, 2607–2608.

Mustroph, A., Zanetti, M.E., Jang, C.J.H., Holtan, H.E., Repetti, P.P., Galbraith, D.W., Girke, T. and Bailey-Serres, J. (2009) Profiling translatomes of discrete cell populations resolves altered cellular priorities during hypoxia in Arabidopsis. *Proc. Natl. Acad. Sci.*, **106**, 18843–18848.

Peng, Y.J., Shih, C.F., Yang, J.Y., Tan, C.M., Hsu, W.H., Huang, Y.P., Liao, P.C. and Yang, C.H. (2013) A RING-type E3 ligase controls anther dehiscence by activating the jasmonate biosynthetic pathway gene DEFECTIVE in ANTHER DEHISCENCE1 in Arabidopsis. *Plant J.*, **74**, 310–327.

Pruneda-paz, J.L., Breton, G., Nagel, D.H., Kang, S.E., Doherty, C.J., Ravelo, S., Galli, M., Ecker, J.R. and Kay, S.A. (2015) Arabidopsis transcription factors. , **8**, 622–632.

Reece-Hoyes, J.S., Diallo, A., Lajoie, B., Kent, A., Kadreppa, S., Pesyna, C., Dekker, J., Myers, C.L. and Walhout, A.J.M. (2012) Enhanced yeast one-hybrid (eY1H) assays for high-throughput gene-centered regulatory network mapping. *Nat. Methods*, **8**, 1059–1064.

Robinson, M.D., McCarthy, D.J. and Smyth, G.K. (2009) edgeR: A Bioconductor package for differential expression analysis of digital gene expression data. *Bioinformatics*, **26**, 139–140.

Sijacic, P., Bajic, M., McKinney, E.C., Meagher, R.B. and Deal, R.B. (2018) Changes in chromatin accessibility between Arabidopsis stem cells and mesophyll cells illuminate cell type-specific transcription factor networks. *Plant J.*, **94**, 215–231.

Stacey, M.G., Patel, A., McClain, W.E., Mathieu, M., Remley, M., Rogers, E.E., Gassmann, W., Blevins, D.G. and Stacey, G. (2008) The Arabidopsis AtOPT3 protein functions in metal homeostasis and movement of iron to developing seeds. *Plant Physiol.*, **146**, 589–601.

Wu, H., Chen, C., Du, J., et al. (2012) Co-Overexpression FIT with AtbHLH38 or AtbHLH39 in Arabidopsis-Enhanced Cadmium Tolerance via Increased Cadmium Sequestration in Roots and Improved Iron Homeostasis of Shoots. *Plant Physiol.*, **158**, 790–800.

Zargar, S.M., Fujiwara, M., Inaba, S., Kobayashi, M., Kurata, R., Ogata, Y. and Fukao, Y. (2015) Correlation analysis of proteins responsive to Zn, Mn, or Fe deficiency in Arabidopsis roots based on iTRAQ analysis. *Plant Cell Rep.*, **34**, 157–166.

Zargar, S.M., Kurata, R., Inaba, S., Oikawa, A., Fukui, R., Ogata, Y., Agrawal, G.K., Rakwal, R. and Fukao, Y. (2015) Quantitative proteomics of Arabidopsis shoot microsomal proteins reveals a cross-talk between excess zinc and iron deficiency. *Proteomics*, **15**, 1196–1201.

Zhai, Z., Gayomba, S.R., Jung, H., et al. (2014) OPT3 is a phloem-specific iron transporter that is essential for systemic iron signaling and redistribution of iron and cadmium in Arabidopsis. *Plant Cell*, **26**, 2249–2264.

Chapter4
SPIP: A Small Plant Imaging Platform

Highlights

We developed a fully automated system capable of acquiring high quality images of agar-grown *Arabidopsis* seedlings for automated root identification and growth measurements. The system was designed to be user-friendly, easy to assemble and affordable so it can be widely distributed. The project was collaborative in nature, drawing from three unique disciplines: computer science, bioengineering, and plant science. The data presented show how the platform can be utilized to quantify root growth under different iron availability conditions.

1 Abstract

Plants are sessile organisms, which rely on their root structures to acquire water and some nutrients. Hence the root structure is extremely plastic and responds to environmental changes in a dynamic fashion. Standard laboratory methods for assessing phenotypes, such as primary root length in response to different environmental stimuli are frequently carried out by growing plants on vertical agar plates or by scanning mature root systems on a flatbed scanner. However, these methods are time-consuming and fail to capture dynamic root growth; on the other hand, more precise methods, such as X-ray microtomography (µCT) systems, are not cost-effective. To this end, we decided to develop an affordable solution for users to capture dynamic root growth through a robotics platform called the Small Plant Imaging Platform (SPIP, model *Sunbear*) and a

root tracing algorithm that we have called *iRoot*. *Sunbear* images up to six plates in a pre-determined time course at a predetermined or custom intervals via a simple interface that minimizes user interaction. Although *Sunbear* minimizes/eliminates most image artifacts, automated background correction further refines the images. Data analysis is integrated in the software and currently reports primary root length, while other growth parameters are still in development.

Sunbear is highly modular for accessibility by multiple audiences, with application variants easily developed through 3D printed parts. Sunbear is also cost-effective; cost projections for a new platform fall below $3,000 USD (as fall 2018).

To demonstrate *Sunbears* performance, iron (Fe) availability in the growth media was modified and root growth dynamics was investigated. Fe is an essential nutrient for plants and has a strong impact on root growth (Lešková *et al.*, 2017). Sunbear was capable of capturing differential rates of root growth during both germination and active growth in the presence and absence of Fe.

In summary *Sunbear* is an easy-to-use, cost-effective platform that captures dynamic root growth to be made available for the plant science community.

2 Introduction

Roots are a vital plant organ that allow anchoring of the aerial tissues and are the primary site of water and nutrient acquisition (Wraith and Wright, 1998). To provide optimal growth, roots must compensate for adverse environments and heterogeneous nutrient distributions across the rhizosphere. Both, the branching structure and manner in which roots grow and proliferate in soil as a response to genetic and environmental factors is collectively called Root System Architecture

(RSA). RSA is an extremely plastic trait, owing to the variety of soil environments which a plant may experience (Postma *et al.*, 2014; Paez-Garcia *et al.*, 2015). Alterations in RSA have been shown to be linked to phosphorus availability (Hufnagel *et al.*, 2014), water stress (Tuberosa *et al.*, 2002), soil exploration for water acquisition (Johnson *et al.*, 2000), and heavy metal stress (Lešková *et al.*, 2017).

RSA is inherently a 3+1 dimensional trait, but proper measurement of RSA in three spatial dimensions is wrought with technical challenges. First and foremost, removal of root systems from the soil is a destructive process and notoriously difficult, which prohibits time-course measurements (Ryan *et al.*, 2016). To overcome this, great strides have been made to image roots non-destructively (Metzner *et al.*, 2015; Iyer-Pascuzzi *et al.*, 2010). One common method involves growing plants in large containers of gellan gum media and reconstructing 3D architectures from 2D photographs (Topp *et al.*, 2013; Clark *et al.*, 2011). This is an effective method for studying crop plants with comparatively large roots, as they provide suitable contrast for detection. However, detection of fine roots structures, such as those of the model species *Arabidopsis thaliana*, require more precise measurements usually made through X-ray computed microtomography (μCt) or nuclear magnetic resonance imaging (MRI) platforms (Morris *et al.*, 2017; Rellán-Álvarez *et al.*, 2015; Jahnke *et al.*, 2009). These methods are able to make submicron measurements of live tissue (Landis and Keane, 2010; Rogers *et al.*, 2016) and have been applied in QTL mapping of rice and *maize* root architectures (Bray and Topp, 2018; Topp *et al.*, 2013). Unfortunately, these methods are prohibitively expensive, preventing broad adoption by the plant science community.

With such advanced methods out of reach for most laboratories, a simple but effective method is typically employed. That is: plants are grown on vertical agar plates such that the roots grow over the agar surface. While unrepresentative of real world soil conditions, this method still holds

tremendous value as it has been used to identify important regulatory systems through the distinct root phenotypes of mutant plants such as SCARECROW and SHORT ROOT, which coordinate the differentiation of the endodermis and cortex, and T-DNA insertion mutants show distinct short root phenotypes (Cui *et al.*, 2012; Koizumi and Gallagher, 2013). Also, mutants lacking functional regulators of Fe homeostasis such as bHLH115, and FIT also show stunted roots under Fe deficiency (Liang *et al.*, 2017; Jakoby *et al.*, 2004). Similarly, the transcription factor PYE shows both stunted primary root growth and impaired lateral root formation (Long *et al.*, 2010) under iron deficiency. JAR1, a regulator of methyl jasmonate production, was similarly identified through root phenotypes observed on agar plates (Staswick *et al.*, 1992). A final example of agar based root phenotypes elucidating molecular mechanisms in plants is in the identification a vitamin B_6 deficient mutant PDX1 (Chen and Xiong, 2005), which shows recovery of an extremely stunted root/shoot growth with application of pyridoxine.

These typically short root phenotypes are easily identified due to their dramatic nature. Unfortunately all genes involved in a given biological system are unlikely to deliver such dramatic phenotypes, as has been demonstrated in the study of the phytohormone auxin (Ljung *et al.*, 2005). Time course experiments have the capacity to identify phenotypes which do not easily manifest or are not fully described in end point observations. Time course data of roots is typically acquired by photographing or scoring the plate, and measured *post hoc*. Each method introduces its own errors; measurements of scored plates produce straight line drop measurements, which do not accounting for root curvature, while both photographed and scored plates are subject to human inaccuracy. Most importantly these methods, are prohibitively time consuming and are difficult to execute for more than a handful of plants.

To mitigate the issues involved in collecting root measurements, several programs have been developed, each providing different functionalities. *RootRTFlow* was developed with the aim of

capturing detailed information of sections of individual roots imaged under a compound microscope, and is able to identify changes in root length on the order of microns (van der Weele, 2003). *RootScape* diverges from classical interpretations of measuring RSA. Under this frame work 20 points are manually placed at defined positions on the root structure and are analyzed under an allometric model, summarizing the RSA as variations between each landmark. This produces data in a 40 dimensional space which is subsequently analyzed using principal component analysis to compare treatments (Ristova *et al.*, 2013). *RootTrace* provides the most intuitive description of a root structure. Rather than develop root boundaries, a model predicts the probability of each pixel being within the root, and takes a random subset of these pixels to serve as graph nodes, and edge weights are determined by a predictive model. This graph is then pruned to yield an unbroken series of nodes which is used to define the centerline of each root. Unlike *RootSpace*, *RootTrace* outputs easily interpreted metrics such as root length, number and length of lateral roots and their entry angles (Naeem *et al.*, 2011; French *et al.*, 2009). Like *RootRTFlow*, *TipTracker* (Wells *et al.*, 2012) was developed to track root tips but is also able to trace unbranched roots. *TipTracker* is unique in that an imaging platform was also described for its implementation, featuring two IR cameras and IR pass filters over the plates which allow the roots to grow in darkness. Unfortunately no plans were distributed or discussion of the construction were released for this platform.

This considered, no imaging platform exists that is readily available for the plant science community to reliably capture time course images suitable for automated image analysis. To this end we have developed a Small Plant Imaging Platform (SPIP) under the model name *Sunbear*.

Sunbear uses two operational modes, single pass image collection and automated time course. A single pass simply involves imaging all the designated plates (up to 6 plates) one time, while the time course mode will trigger a single pass at user defined intervals. These two modes of

operation are not exclusive, allowing users to exchange plates and perform single pass operations without disturbing the time course experiment. Operation of the machine is handled through a simple GUI called *SPIPware*. Personalized experimental profiles within *SPIPware* allow for simple recall of user settings and allow images to be saved with a pre-fixed identification number, a time stamp and custom suffix for simple file management. While images produced by *Sunbear* are usable in the previously discussed software programs, we have begun developing a custom root tracing algorithm (*iRoot*), which will be optimized for use with the *Sunbear* platform. Finally *Sunbear* is easily assembled and material costs are kept below $3,000 USD. Thus *Sunbear* is an easily accessible and affordable device to effectively quantify dynamic root growth data.

3 *Sunbear*

Interested readers can find a complete detailing of the design process, student management, and schematics in Chapter 4 Appendix: Design Overview.

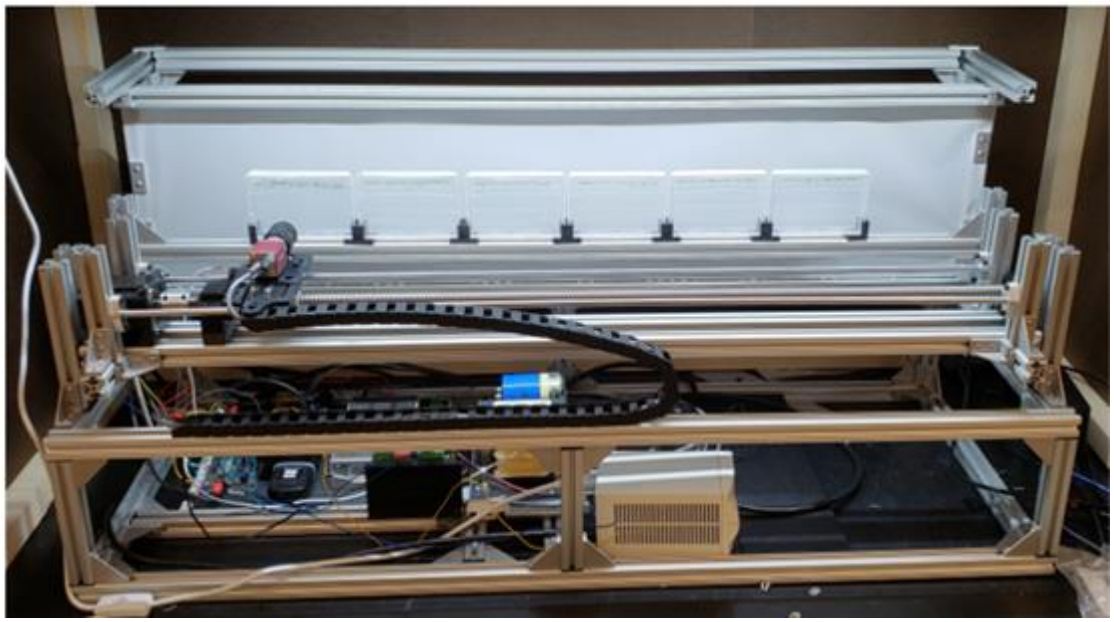

Figure 25 Front view of Sunbear

3.1 *Sunbear* mechanics

Sunbear (**Figure 25**) is largely constructed from T-slotted extruded aluminum, making it light weight, easily modified, and easily assembled, as all of the brackets are attached using a hex key and machine screws. The 5 megapixel RGB camera moves across the plate array by means a of a ball screw driven by a 5.6 amp stepper motor (**Figure 27A**). A ball screw is simply a leadscrew with a housing 'nut', filled with ball bearings on a helical raceway, which translates along the ball screw, similar to a nut on a standard screw. The ball screw differs from a regular screw as it features wide trapezoidal threads whose top surface is beveled, which interface with the ball bearings to provide smooth motion. The camera attaches directly to the housing through a 3D printed camera sled which is outfitted with linear bearings and accompanying guide rails, which force the camera to translate instead of rotate as the stepper motor turns, while also preventing binding between the sled and guide rails (**Figure 27A**).

A stepper motor is a type of electrical motor which turns in discrete steps, rather than simply turning while current is applied, which is the mechanism found in most fans. Consequently each 'step' of the motor corresponds to a constant translational distance (in this case roughly 1mm/step). Although these motors are more difficult to control, they allow for accurate and reproducible movement needed to consistently position the camera in front of each plate.

While Sunbear can be quickly modified to hold any type of plate, the standard case uses plain rectangular plates which are held in place by 3D printed brackets. The dimensions of these brackets were refined to provide adequate holding force, while not holding the plate so tightly as to be difficult to remove (and disturb the delicate plants). If alternative plates are required, the user must simply place the new brackets on the plate array, and adjust the steps/plate parameter to reflect the new distance between plates.

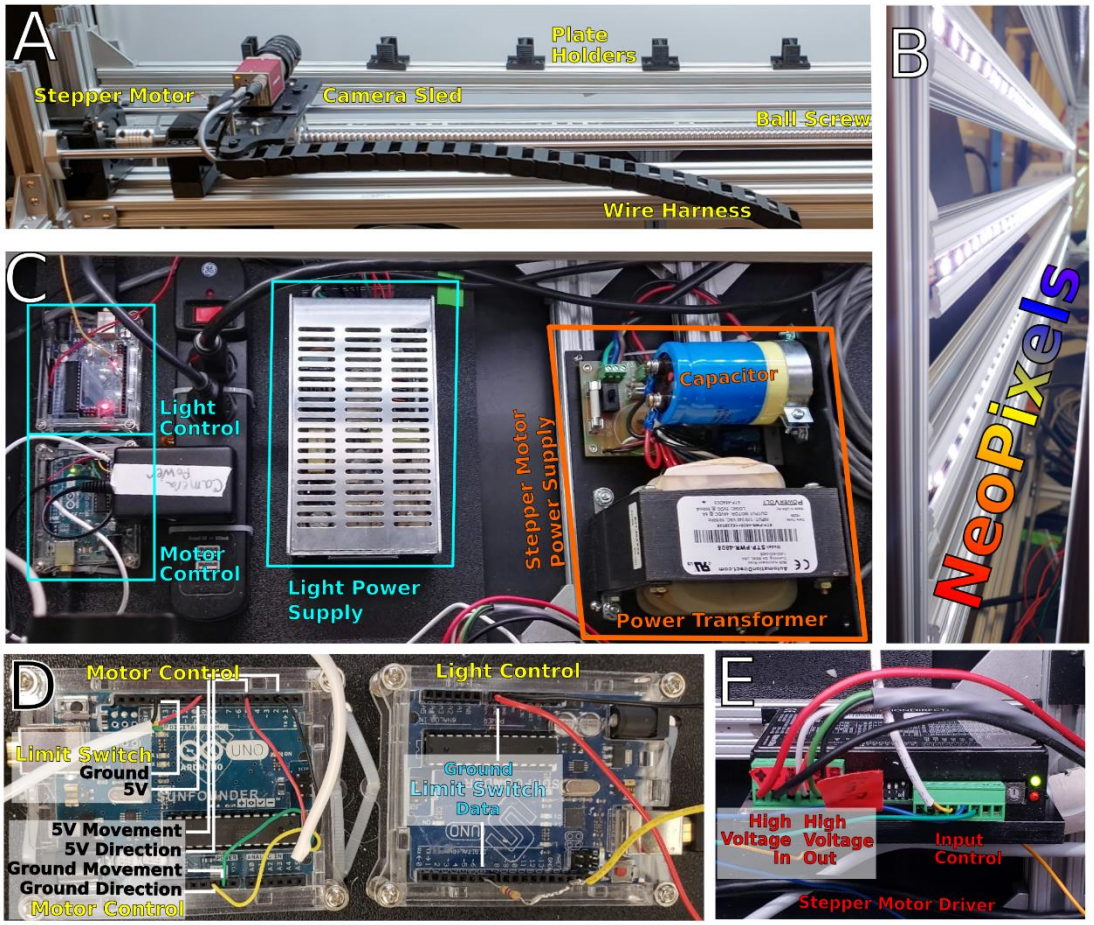

Figure 26 Mechanical and electrical components of *Sunbear*. (A) Images are acquired through a camera mounted to a ball screw which is driven by a large stepper motor. (D) The LED backlights are mounted within T-slotted aluminum rods. (C) Layout of the microcontrollers and power supplies which power and control the backlights and motor. (D) Wiring of the motor and lighting microcontrollers. (E) The voltages needed to drive the stepper motor require a stepper motor driver, which is physically divided into a high and low voltage circuits.

These plates sit in front of a diffusing film, backlit by an array of ~300 RGB LEDs (**Figure 27B**). The LEDs, NeoPixels, were chosen because they are readily available, require minimal wiring, are easily controlled, and produce 255 intensities of 'white' light (~16.5 million RGB colors) so the light intensity can be optimized for the roots being imaged. The LED strips are arrayed in four horizontal lines, housed inside the T-slot of an aluminum rod, preventing the strip from sagging or otherwise changing position.

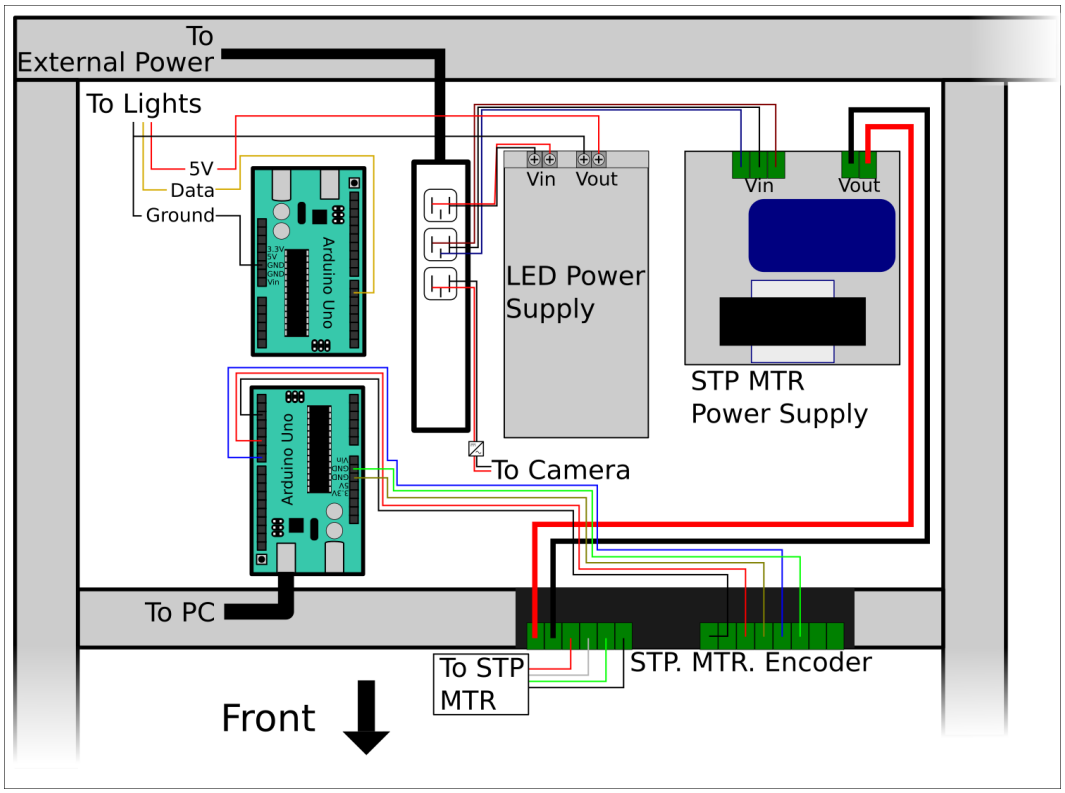

Figure 27 Primary wiring of *Sunbears* motors and back lighting. Two Arduino Unos are used to control the LED back lighting (top) and the stepper motor (bottom). The LED array and stepper motor are each powered by dedicated power supplies, which are connected to a power strip, powered by a 120V AC source (wall power). The LED power supply takes a 120V AC input (red) and ground (black) to output 5V DC (red) and ground (black), which powers the LED array: data (yellow), ground (black) and 5V DC (red). The LEDs and Arduino share a common ground, which ensures the LED timing is maintained. The stepper motor (STP MTR) takes similar inputs with an additional earth ground (blue), and outputs 120/240 V AC (thick, red). The 120/240 V AC powers the high voltage output of the stepper motor driver. *SPIPware* controls the stepper motor through a USB2.0 cable, and interfaces with the driver through six wires, have a high voltage counterparts which control the rotation of the stepper motor. The driver dip switch configuration and wiring for the grow light, camera sled home sensor, and redundant LED wiring are omitted.

Sunbear contains two major electrical systems to manage the backlight and the motor. The backlights are controlled by a single microcontroller (Arduino Uno) (**Figure 27C**) which cannot provide enough current to power the large LED array. Hence, a 21W 5VDC power supply provides current for both the LEDs and the Arduino. NeoPixels are individually addressable, that is, they only require one wire to individually control each pixel. This requires the Arduino and the LEDs to share a common ground (**Figure 27D**, right).

Small stepper motors can be directly controlled by an Arduino, but cannot power the a large stepper motor needed to drive the ball screw, which introduces several additional components.

First, SPIPware connects to the motor control Arduino (**Figure 27D**) to relay two signals, one for direction and one for the distance (movement) (**Figure 27E**), to a stepper motor driver. The driver is needed due the high voltages required power the stepper motor, which is provided by a 120/240VAC power supply (**Figure 27C**). Although, the high voltage power line and low voltage signal line must be electrically isolated to prevent the microcontroller from igniting. Hence, the driver is physically divided in to a high and low voltage circuit, bridged by an IR emitter/detector. A wiring schematic is shown in (**Figure 27**). All these processes are hidden from the user, and are handled internally through SPIPware.

3.2 *SPIPware v1.5*

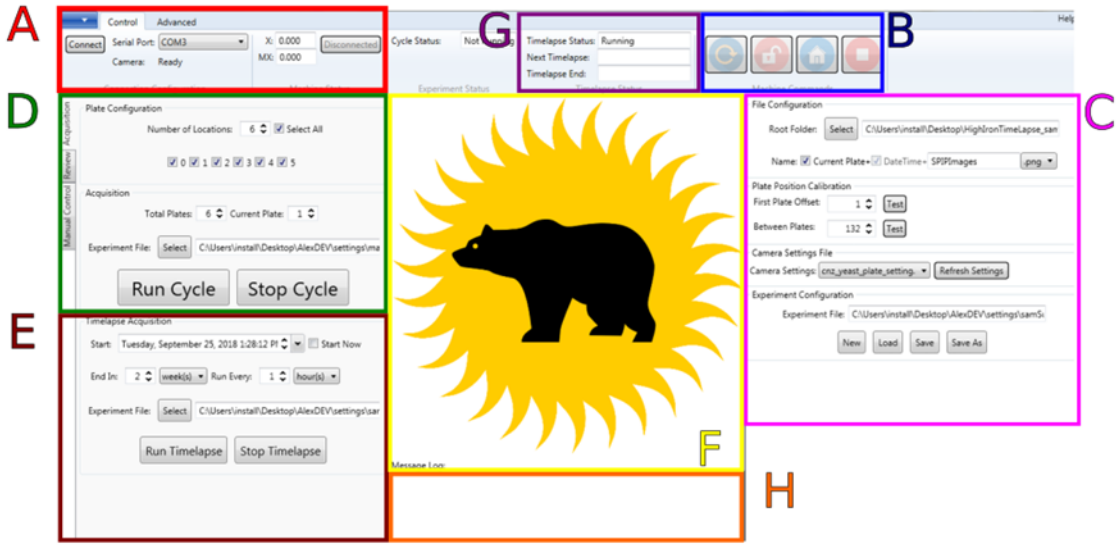

Figure 28 *SPIPware* 1.5 interface. *SPIPware* is divided into seven parts (A) Initiation and disconnection controls. (B) Homing and emergency controls. (C) Experiment profile parameters including the directory to save files, file name prefix and suffix options, motor steps between plates, camera settings file, and profile save/load options. (D) Single pass imaging controls including options to change which plates are imaged in a non-propagative manner. (E) Time course imaging controls, including setting start/stop dates and imaging frequency. (F) Display of last image taken. (G) Time till next time course pass to allow users to know how long they have to make a concurrent single pass. (F) G-code logger for debugging

SPIPware is the only interface needed to operate *Sunbear*, and the complete interface of *SPIPware* v1.5 is shown in **Figure 28**. The interface is broken into seven sections. On start up the user

connects *SPIPware* to *Sunbear* in the connection panel (**Figure 28A**). The system must first be homed to register the location of the camera (**Figure 28B**). Emergency controls to lock and halt the motor can also be found here (i.e. emergency stop). A new user uses the experiment profile creation panel (**Figure 28C**) to establish the parameters used in their subsequent image acquisitions such as the folder where images will be saved, prefix and suffix information for the saved file, and the camera settings to be used. Although *SPIPware* does not have many settings, users are unlikely to notice small changes in the settings, or forget which of the camera settings they liked best. Hence, the purpose of the experiment profile is to remove this trouble from the user and store it internally. A user who desires to image a handful of plates loads their experiment profile in the single acquisition panel (**Figure 28D**) and indicates which positions along the track have plates to image, as well as the prefixed numbering scheme desired. Time lapse experiments are established in the time lapse panel (**Figure 28E**), where users can load an experiment profile to establish base parameters, as well as options such as start date, acquisitions per day, and experiment length. Because the parameters used in single acquisition and time lapse are loaded as global variables prior to running, as long as the experiment profiles are not altered, parameter fidelity is guaranteed. The remaining panels are rarely used, but important in specific cases. The last acquired image is displayed after capture (**Figure 28F**), a countdown until the next time lapse instance is displayed **Figure 28G**), and the instructions sent to the motor are displayed too (**Figure 28H**).

4 Automated image analysis

Sunbear is capable of acquiring high quality images suitable for image analysis, but presents a unique opportunity to develop an image processing suite designed for images acquired on the platform. Problems in image processing such as color balancing, contrast, and image stabilization

are difficult to account for when attempting to provide a solution for photographs from different cameras, under different lighting, and in the case of time course images from a moving platform, slight deviations in the field of view within different photographs. Given that the images are acquired on *Sunbear*, many of these problems can be avoided and more precisely tuned algorithms can be implemented for subsequent analysis.

The development of the root tracing algorithm (*iRoot*), is the result of an ongoing collaboration with Dr. Bunyak and Ph.D candidate Ke Gao. Although the algorithm is in its early stages, a functioning algorithm has already been developed. Under the current implementation, a unique mark is placed on two corners of the plate which are used to place roots in the same positions

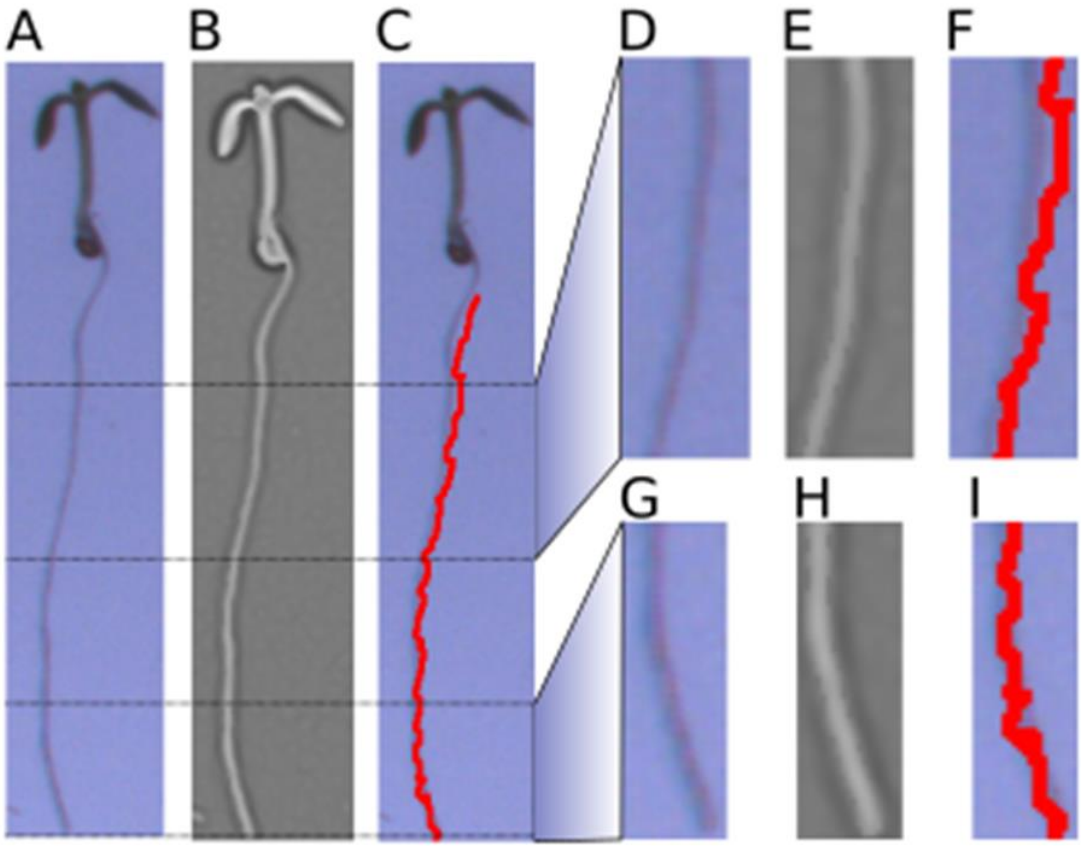

Figure 29 Sample images acquired from Sunbear. Roots of Col-0 grown on replete media measure 12-16 pixels in width allowing for normalization and root tracing. (A) Raw image (B) Hessian transformation, (C) Root trace overlay. (D, G) (E,H) (F, I) Close up of mid and root tip of (A) (B) and (C) respectively.

across all images by computing the normalized cross correlation of the reference image against the image to be centered. The optimal fit is then found, and the image is centered between the two reference marks. This operation requires a single reference mark and corrects for vertical

and horizontal translations. The second mark is used in conjunction with the first to account for rotations of the plate which may occur if the plate is removed and not re-seated correctly.

Gaussian blurring is applied to the image to remove punctate perturbations in the background. The final stage of image preprocessing utilizes the Hessian Affine Region Detection algorithm to highlight the edges of the plant roots. This operation identifies regions whose RGB values rapidly change, such as the edges of the plates, leaves, and roots. Roots are then traced by first manually identifying the seed, and applying an energy maximization algorithm on the Hessian transformed images. The results of these operations are shown in **Figure 29**. Although the algorithm does function, some of the traces fail to stay on the root and draw a true centerline (**Figure 29F, I**) and will be addressed in the coming months.

5 Case studies

5.1 Effect of iron nutrition on root growth

Figure 30 Time course imaging of Col-0 under multiple Fe treatments demonstrates how increasing Fe availability promotes root growth. Measurements were made manually, sampling 2 time-points per day over 9 days. Each root trace is displayed with a LOESS regression overlaid (black).

Iron (Fe) is an essential element for all life; serving as a cofactor in many metaloproteins and an electron carrier in both the mitochondrial and chloroplastic electron transport chains, among other roles. Although Fe is essential for life, over accumulation of Fe is toxic due to the production of reactive oxygen species. We sought to determine how increasing Fe exposure will effect root growth by monitoring plants grown in 0, 50, and 350µM Fe-EDTA over 12 days growth. To completely remove trace Fe from the 0µM Fe plate, 100µM of the Fe chelator ferrozine (FRZ) was added, and are hence labeled FRZ. At the time of these experiments, *iRoot* was not operational; hence measurements were done manually at two time points per day using imageJ (0, 50, 350 µM Fe-EDTA) (Rueden *et al.*, 2017) and are shown in **Figure 30**.

Plants with no supplemental Fe halt growth 4 days after the initiation of germination, while increased Fe availability increases the rate of root growth. It is clear that the Fe starved plants have consumed their Fe reserves in the endosperm prior to halting root growth, prompting the question how Fe availability affects root growth during germination while seed storage is available, and then during active growth after these reserves have been consumed. Growth rates were calculated for each plate during the first four days and the latter five using ordinary least squares regression (**Figure 31**). We observed that the growth rate is affected by Fe availability regardless of the phase, but is far more pronounced during active growth. This demonstrates that, for *Arabidopsis*, standard plate preparations (50 µM Fe-EDTA) do not contain enough Fe to reach maximal root growth during the first ten days of growth.

These manually acquired measurements can be compared to the automated root length determinations for FRZ and 50µM Fe-EDTA plates using *iRoot* (Figure 32). Interestingly, the

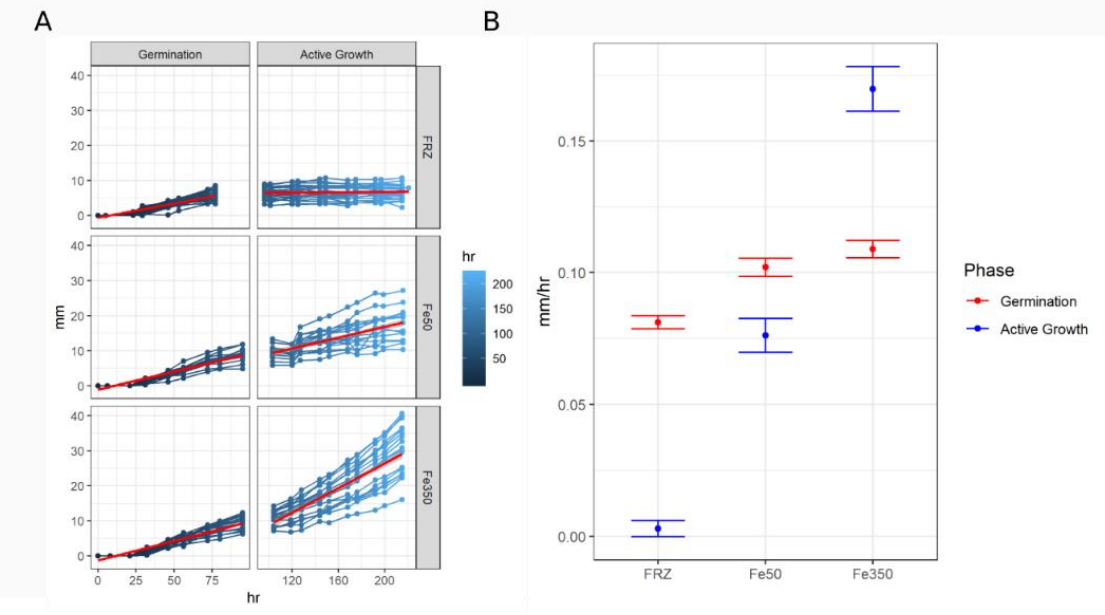

Figure 31 Root growth during germination and active growth is promoted by Fe availability. (A) Col-0 was germinated on media containing 0µM + FRZ, 50µM, and 350µM Fe-EDTA and imaged for 9 days, two time points per day were selected for manual measurement. (B) Linear regression of root length on time shows two distinct phases of growth. (C) Average growth rates of each phase and treatment. Error bars show standard error calculated by OLS, N = 23.

automated determinations suggest that Fe starved roots are able to continue growing but at a severely reduced rate. These data are far more reproducible than the manual measurements as shown through their monotonicity. Unfortunately, the root tracing failed on multiple plants and condensation produced rapid jumps in height for some measurements. While these matters will come to resolution they still represent a major area for future improvement.

This analysis also demonstrates the type of information which can be extracted from time course root growth data. Agar plates are typically made with Murashige and Skoog media which contains 100µM $FeSO_4$, which as demonstrated may be Fe limiting for longer periods of plant growth. Further we show that seedlings undergo two distinct phases of root growth which are environmentally dependent.

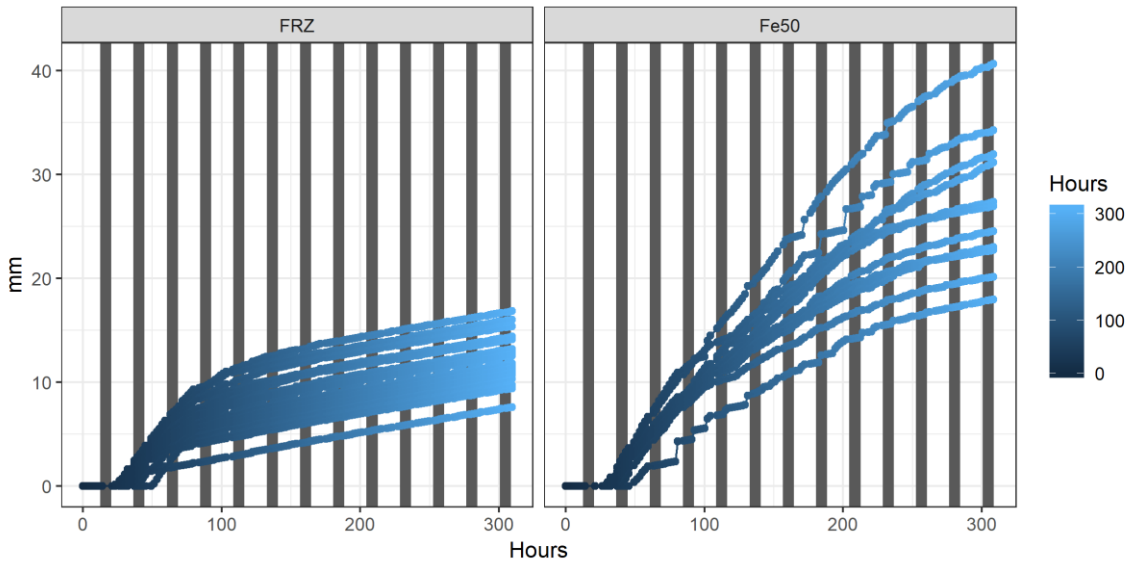

Figure 32 Automated root length determination for 50µM Fe-EDTA and FRZ. 133 images were processed to yield far less noisy growth curves than can be achieved manually.

5.2 Imaging Y1H growth

Although the SPIP was designed expressly for imaging plant roots, additional uses were found. The Mendoza-Cózatl lab began screening promoter fragments in a Yeast 1 Hybrid (Y1H) against a

library of 1,956 transcription factors (see Chapter 5 for additional technical information). Y1H is used to detect interactions between transcription factors and promoter fragment and the result of a positive interaction is increased growth on histidine deficient media. Further selection of these positive and negative interactions is aided by a titration with 3-amino-1,2,4-triazole (3AT), which inhibits histidine synthase allowing for better discrimination of putative positive colonies.

The initial and primary screen is carried out on 31 plates each of which are photographed multiple times per day over a three day interval. The quantity of images needed to document these assays is further increased by subdividing the target promoter into smaller fragments, resulting in ~100 plates per promoter and represents a significant work load to acquire high quality images. Adapting Sunbear to accommodate this assay was done without modification as Sunbear and the Y1H assay use the same plates, hence no hardware modifications were need. Images of these screens are shown **Figure 33**.

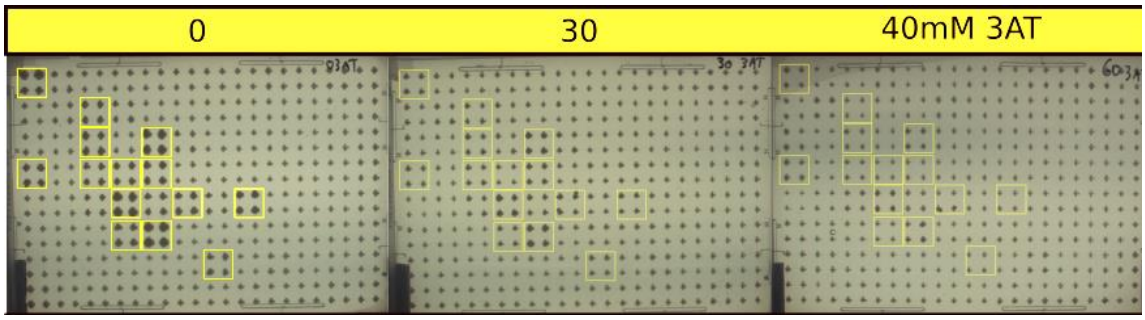

Figure 33 Example *Sunbear's* versatility by imaging Y1H primary 3AT screens. Shown is a screen of the first three hundred base pairs of OLIGOPEPTIDE3 promoter against three concentrations of 3AT to assess non-specific growth for this fragment.

6 Conclusion

The development of high throughput technologies is vital for continued plant biology research. While extraordinary µCt and X-ray systems provide the cutting edge of technological development

there is a necessity to bring inexpensive and modular platforms to laboratories with diverse research interests. Here we have developed a strong prototype to automate the acquisition of computer vision quality images during time course experiments. Our platform features a complete GUI software which allows for multiple experiments be run concurrently. The entire system is affordable to nearly any laboratory and is designed for simple assembly which can be performed with a minimal set of technical skills.

7 Bibliography

Bray, A.L. and Topp, C.N. (2018) The Quantitative Genetic Control of Root Architecture in Maize. *Plant Cell Physiol.*, **10**, 1–12.

Chen, H. and Xiong, L. (2005) Pyridoxine is required for post-embryonic root development and tolerance to osmotic and oxidative stresses. *Plant J.*, **44**, 396–408.

Clark, R.T., MacCurdy, R.B., Jung, J.K., Shaff, J.E., McCouch, S.R., Aneshansley, D.J. and Kochian, L. V. (2011) Three-Dimensional Root Phenotyping with a Novel Imaging and Software Platform. *Plant Physiol.*, **156**, 455–465.

Cui, H., Hao, Y. and Kong, D. (2012) SCARECROW Has a SHORT-ROOT-Independent Role in Modulating the Sugar Response1. *Plant Physiol.*, **158**, 1769–1778.

French, A., Ubeda-Tomas, S., Holman, T.J., Bennett, M.J. and Pridmore, T. (2009) High-Throughput Quantification of Root Growth Using a Novel Image-Analysis Tool. *Plant Physiol.*, **150**, 1784–1795.

Hufnagel, B., Sousa, S.M. de, Assis, L., et al. (2014) Duplicate and Conquer: Multiple Homologs of PHOSPHORUS-STARVATION TOLERANCE1 Enhance Phosphorus Acquisition and Sorghum Performance on Low-Phosphorus Soils. *Plant Physiol.*, **166**, 659–677.

Iyer-Pascuzzi, A.S., Symonova, O., Mileyko, Y., Hao, Y., Belcher, H., Harer, J., Weitz, J.S. and Benfey, P.N. (2010) Imaging and Analysis Platform for Automatic Phenotyping and Trait Ranking of Plant Root Systems. *Plant Physiol.*, **152**, 1148–1157.

Jahnke, S., Menzel, M.I., Dusschoten, D. Van, et al. (2009) Combined MRI-PET dissects dynamic changes in plant structures and functions. *Plant J.*, **59**, 634–644.

Jakoby, M., Wang, H.-Y., Reidt, W., Weisshaar, B. and Bauer, P. (2004) FRU (BHLH029) is required for induction of iron mobilization genes in Arabidopsis thaliana. *FEBS Lett.*, **577**, 528–534.

Johnson, W.C., Jackson, L.E., Ochoa, O., Wijk, R. Van, Peleman, J., Clair, D.A.S. and Michelmore, R.W. (2000) Lettuce, a shallow-rooted crop, and Lactuca serriola, its wild progenitor, differ at QTL determining root architecture and deep soil water exploitation. *Theor. Appl. Genet.*, **101**, 1066–1073.

Koizumi, K. and Gallagher, K.L. (2013) Identification of SHRUBBY, a SHORT-ROOT and SCARECROW interacting protein that controls root growth and radial patterning. *Development*, **140**, 1292–1300.

Landis, E.N. and Keane, D.T. (2010) X-ray microtomography. *Mater. Charact.*, **61**, 1305–1316.

Lešková, A., Giehl, R.F.H., Hartmann, A., Fargašová, A. and Wirén, N. von (2017) Heavy Metals Induce Iron Deficiency Responses at Different Hierarchic and Regulatory Levels. *Plant Physiol.*, **174**, 1648–1668.

Liang, G., Zhang, H., Li, X., Ai, Q. and Yu, D. (2017) BHLH transcription factor bHLH115 regulates iron homeostasis in Arabidopsis thaliana. *J. Exp. Bot.*, **68**, 1743–1755.

Ljung, K., Hull, A.K., Celenza, J., Yamada, M., Estelle, M., Normanly, J. and Sandberg, G. (2005) Sites and Regulation of Auxin Biosynthesis in Arabidopsis Roots. *The Plant Cell2*, **17**, 1090–

1104.

Long, T.A., Tsukagoshi, H., Busch, W., Lahner, B., Salt, D.E. and Benfey, P.N. (2010) The bHLH transcription factor POPEYE regulates response to iron deficiency in Arabidopsis roots. *Plant Cell*, **22**, 2219–2236.

Metzner, R., Eggert, A., Dusschoten, D. van, Pflugfelder, D., Gerth, S., Schurr, U., Uhlmann, N. and Jahnke, S. (2015) Direct comparison of MRI and X-ray CT technologies for 3D imaging of root systems in soil: Potential and challenges for root trait quantification. *Plant Methods*, **11**, 1–11.

Morris, E.C., Griffiths, M., Golebiowska, A., et al. (2017) Shaping 3D Root System Architecture. *Curr. Biol.*, **27**, R919–R930.

Naeem, A., French, A.P., Wells, D.M. and Pridmore, T.P. (2011) High-throughput feature counting and measurement of roots. *Bioinformatics*, **27**, 1337–1338.

Paez-Garcia, A., Motes, C., Scheible, W.-R., Chen, R., Blancaflor, E. and Monteros, M. (2015) Root Traits and Phenotyping Strategies for Plant Improvement. *Plants*, **4**, 334–355.

Postma, J.A., Schurr, U. and Fiorani, F. (2014) Dynamic root growth and architecture responses to limiting nutrient availability: Linking physiological models and experimentation. *Biotechnol. Adv.*, **32**, 53–65.

Rellán-Álvarez, R., Lobet, G., Lindner, H., et al. (2015) GLO-Roots: An imaging platform enabling multidimensional characterization of soil-grown root systems. *Elife*, **4**, 1–26.

Ristova, D., Rosas, U., Krouk, G., Ruffel, S., Birnbaum, K.D. and Coruzzi, G.M. (2013) RootScape: A Landmark-Based System for Rapid Screening of Root Architecture in Arabidopsis. *Plant Physiol.*, **161**, 1086–1096.

Rogers, E.D., Monaenkova, D., Mijar, M., Nori, A., Goldman, D.I. and Benfey, P.N. (2016) X-Ray Computed Tomography Reveals the Response of Root System Architecture to Soil Texture. *Plant Physiol.*, **171**, 2028–2040.

Rueden, C.T., Schindelin, J., Hiner, M.C., DeZonia, B.E., Walter, A.E., Arena, E.T. and Eliceiri, K.W. (2017) ImageJ2: ImageJ for the next generation of scientific image data. *BMC Bioinformatics*, **18**, 1–26.

Ryan, P.R., Delhaize, E., Watt, M. and Richardson, A.E. (2016) Plant roots: Understanding structure and function in an ocean of complexity. *Ann. Bot.*, **118**, 555–559.

Staswick, P.E., Su, W. and Howell, S.H. (1992) Methyl jasmonate inhibition of root growth and induction of a leaf protein are decreased in an Arabidopsis thaliana mutant. *Proc. Natl. Acad. Sci.*, **89**, 6837–6840.

Topp, C.N., Iyer-Pascuzzi, A.S., Anderson, J.T., et al. (2013) 3D phenotyping and quantitative trait locus mapping identify core regions of the rice genome controlling root architecture. *Proc. Natl. Acad. Sci.*, **110**, E1695–E1704.

Tuberosa, R., Sanguineti, M.C., Landi, P., Giuliani, M.M., Salvi, S. and Conti, S. (2002) Identification of QTLs for root characteristics in maize grown in hydroponics and analysis of their overlap with QTLs for grain yield in the field at two water regimes. *Plant Mol. Biol.*, **48**,

697–712.

Weele, C.M. van der (2003) A New Algorithm for Computational Image Analysis of Deformable Motion at High Spatial and Temporal Resolution Applied to Root Growth. Roughly Uniform Elongation in the Meristem and Also, after an Abrupt Acceleration, in the Elongation Zone. *Plant Physiol.*, **132**, 1138–1148.

Wells, D.M., French, A.P., Naeem, A., Ishaq, O., Traini, R., Hijazi, H., Bennett, M.J. and Pridmore, T.P. (2012) Recovering the dynamics of root growth and development using novel image acquisition and analysis methods. *Philos. Trans. R. Soc. B Biol. Sci.*, **367**, 1517–1524.

Wraith, J.M. and Wright, C.K. (1998) Soil water and root growth. *HortScience a Publ. Am. Soc. Hortic. Sci.*

Chapter 5
Insights into the transcriptional and translational regulation of companion cells during Fe deficiency

1 Abstract

Phloem-loading cells, also known as companion cells, have been strongly implicated in housing the systemic Fe sensor which mediates the transduction of a leaf-to-root iron (Fe) deficiency signal. To gain insight into the rapid response to Fe deficiency observed in leaf companion cells, we implemented two complementary approaches: (I) we measured the transcript abundance in translating ribosomes within companion cells over a 12 hour period of Fe deficiency, and (II) we identified transcriptional regulators of *OPT3* through a targeted high throughput yeast 1-hybrid screening system. Our results suggest that the transcriptional regulator PYE is a likely candidate for mediating rapid responses to Fe deficiency in companion cells, and also suggest that additional PYE network members may participate in the transcriptional regulation of *OPT3*. Correlation analysis further indicates that the cell wall of companion cells is likely to be modified during Fe deficiency, presumably to release Fe from the cell wall for mobilization to Fe demanding tissues. This work represents a data source to direct further experiments, which has begun through select candidates which regulate OPT3.

2 Introduction

Iron (Fe) is a vital nutrient for plant health, facilitating enzymatic reactions as a cofactor in diverse biological processes. As has been discussed throughout this thesis (Chapters 1 and 2), companion cells play a key role in sensing the Fe status of the plant and during Fe deficiency, transmitting a mobile Fe deficiency signal to the roots to induce the corresponding Fe deficiency responses (i.e. the *FIT network*). The role of leaves however, and more specifically companion cells, in Fe sensing is very recent and therefore only a handful of publications have described detailed Fe deficiency responses in leaves (Stein and Waters, 2012; Rodríguez-Celma *et al.*, 2013; Kumar *et al.*, 2017; Khan *et al.*, 2018). One of the most prominent gene in the leaf Fe deficiency response is the Oligopeptide Transporter 3 (OPT3), which has been shown to be critical for the systemic transduction of the Fe status at the whole plant level. Consequently, the knock down mutants *opt3-2* and *opt3-3* show a constitutive Fe deficiency response in roots that results in an over accumulation of heavy metals such as Fe, Mn, and Zn (Stacey *et al.*, 2008; Mendoza-Cózatl *et al.*, 2014; Zhai *et al.*, 2014; Khan *et al.*, 2018), and this over accumulation is thought to be a consequence of the induction of the high affinity Fe transporter Iron Regulated Transporter 1 (IRT1) (Korshunova *et al.*, 1999; Guillaume *et al.*, 2018). Although, both roots and leaves of *opt3-2* over accumulate Fe, only leaves are able to properly sense their Fe status and show a transcriptional profile in line with a Fe excess response (Khan *et al.*, 2018). OPT3 is preferentially expressed in the companion cells of the phloem (Mendoza-Cózatl *et al.*, 2014; Zhai *et al.*, 2014), and is expected to load an Fe containing ligand from the vascular apoplast into the companion cell, hence the phloem sap of *opt3* mutants contains approximately half of the Fe found wild type plants (Zhai *et al.*, 2014). It further determined, using early time points and wild type plants, that changes in gene expression during Fe deficiency occur in companion cells faster than either

mesophyll cells or roots. Of particularly note are *OPT3* and *bHLH100* (Khan *et al.*, 2018). bHLH100 is a transcription factor which performs multiple roles in regulating Fe homeostasis. bHLH100 is capable of inducing *IRT1* to extract Fe from the rhizosphere, but has a broader spatial expression pattern than *IRT1* (Sivitz *et al.*, 2012; Wang *et al.*, 2013). Indeed, bHLH100 is directly regulated by members of the *PYE network* (bHLH115, bHLH104, ILR3 (Liang *et al.*, 2017; Zhang *et al.*, 2015)), which regulate Fe homeostasis in both leaves and roots. Unlike these *PYE network* members which are expressed throughout the leaf, bHLH100 has been shown to be preferentially expressed in companion cells (Mustroph *et al.*, 2009). Their companion cell localization and rapid induction in leaves after exposure to Fe deficiency suggests that bHLH100 and OPT3 share transcriptional regulators. Hence, it is tempting to suggest that the PYE network members regulate the companion cell Fe deficiency response.

At a different level, phytohormones have also been implicated in the regulation of Fe deficiency. Auxin is one of such hormones, and has been implicated in nearly all aspects of plant physiology including development, stress responses, and light avoidance (Tao *et al.*, 2008; Keuskamp *et al.*, 2010; Keuskamp *et al.*, 2011; Morelli *et al.*, 2000; Giehl *et al.*, 2012). One well described family of transcription factors which control auxin dependent gene regulation are the aptly named Auxin Response Factors (ARFs) (Guilfoyle and Hagen, 2007), whose activity is inhibited after heterodimerization with Aux/IAA proteins (IAA). The ARF and IAA gene families are relatively large, containing 22 and 29 members, respectively, and have unique spatial/temporal expression patterns to form an expansive regulatory network (Guilfoyle and Hagen, 2007). Increased Fe supply induces the formation of lateral roots (Lešková *et al.*, 2017), which has been shown to be an auxin-dependent process (Giehl *et al.*, 2012). Auxin has also been shown to mediate Fe uptake. This was demonstrated using *Cucumis melo* (cucumber) treated with exogenous foliar auxin,

which resulted in Fe accumulation through the induction of *csFRO2* and *csIRT1* (Bacaicoa *et al.*, 2011).

Hormones such as ethylene (ET) and nitric oxide (NO) have generally been described as mediating stress responses, and have also been shown to partially mediate Fe deficiency responses by inducing the expression *IRT1* and *FRO2* (García *et al.*, 2010; Lucena *et al.*, 2006). Ethylene is able to induce Fe deficiency responses through the induction of EIN3/EIL1 which are able to dimerize with FIT1, MYB10, and MYB72 as part of the larger Mediator transcriptional complex (Palmer *et al.*, 2013; Yang *et al.*, 2014; Lingam *et al.*, 2011). While the related stress hormone nitric oxide has been shown to inhibit FIT1 degradation by the 26S proteasome (Chen *et al.*, 2010), facilitate remobilization of Fe from the cell wall (Zhu *et al.*, 2016), and induce FRO2 activity (Chen *et al.*, 2010).

While auxin, ET, and NO have been shown to induce Fe deficiency responses, jasmonic acid (JA) and cytokinin (CK) have been shown to repress Fe deficiency responses. In the absence of JA, the transcriptional co-repressor complex consisting of MYC2 or MYC3 and JAZ proteins, bind to target promoters to inhibit transcription (Goossens *et al.*, 2015; Cheng *et al.*, 2011; Pauwels *et al.*, 2010). When exposed to JA, the JAZ/MYC complex dissociates and is targeted for degradation via the COI1 complex (Devoto *et al.*, 2002), thereby allowing for transcription of the MYC target. Exogenous JA has been shown to inhibit *IRT1* induction, while split root experiments using the JA response inhibitor ibuprofen demonstrated that JA is able to regulate IRT1 activity locally (Maurer *et al.*, 2011).

Interestingly, NO and ET are known to inhibit JA dependent stress responses (Mur *et al.*, 2013; Clarke *et al.*, 2000) which is congruent with their observed roles in Fe homeostasis (Hindt and Guerinot, 2012; Maurer *et al.*, 2011). Similarly, cytokinins (CK) have been shown to inhibit the

expression of *IRT1*, *FIT1*, and *FRO2* (Séguéla *et al.*, 2008). Séguéla *et al.*, 2008 demonstrated that this regulation is likely a mechanism to limit Fe uptake during low demand, as plants subjected osmotic stress show a CK dependent repression of *IRT1* in the presence of sufficient Fe. Thus, JA, CK, ET, and NO have been reported to regulate Fe uptake at the site of Fe uptake, and perhaps are involved in local Fe sensing (see Chapter 1 Section 5), while auxin has been reported to regulate Fe deficiency responses systemically. NO, ET, and JA drive a complex series of competing regulatory pathways (Ku *et al.*, 2018), which has been described in the context of root responses, but is likely to play also a significant role in the leaf response to Fe deficiency.

OPT3 and *bHLH100* are expected to operate up-stream of the systemic Fe sensor, but the transcriptional regulators of OPT3 have not been identified, nor have the transcriptional programs which mediate the induction of Fe deficiency responses in the companion cell been elucidated. Unfortunately, the companion cell, and other low abundance/difficult to access cell types cannot be isolated by conventional methods. Several novel methods have been utilized to obtain biological material from these sample types, such as laser capture microdissection (Ithal *et al.*, 2007; Casson *et al.*, 2005) and translating ribosome affinity purification sequencing (TRAPseq) (Mustroph *et al.*, 2009; Heiman *et al.*, 2014). The advent of amplification of picogram levels of RNA have allowed these methods to be used with next generation sequencing to obtain cell type specific RNA profiles.

Here we describe our ongoing efforts to identify transcriptional regulators of Fe deficiency in companion cells using two complementary methods. First, TRAPseq was used to immunoprecipitate actively translated RNA from companion cells for RNA sequencing during a 12 hour Fe deficiency time course and next, we identified transcriptional regulators of OPT3 by screening a library of 1,957 *Arabidopsis* transcription factors in a yeast 1 hybrid (Y1H) screen against the first kilobase of the *OPT3* promoter.

3 Results

3.1 Isolation of companion cell specific mRNA by TRAPseq

TRAPseq allows for the purification of cell type specific transcripts by utilizing a tissue specific promoter to express an epitope-tagged version of the large ribosome subunit (RPL18). This epitope (FLAG tag) is used to selectively immunopurify ribosomal complexes in their native state allowing the purification of mRNA being translated at the moment of purification. This mRNA is subsequently used for whole-genome sequencing. To purify translating ribosomes from companion cells, we used the companion cell specific promoter SUC2 (Mustroph *et al.*, 2009; Deeken *et al.*, 2008).

To verify that our immunoprecipitation protocol was effective in enriching companion cell transcripts, we first tested the abundance of the *SUC2* mRNA from immunopurified and total RNA fractions and found a substantial enrichment of the *SUC2* transcript (**Figure 34A**). Next we grew *SUC2*$_{pro}$*:RPL18* plants to maturity (~5 weeks) in replete hydroponic media and transferred half of the plants to Fe deficient media, after removing residual Fe in roots and hydroponic containers, while the other half was placed in replete media. We collected leaf tissue at 0, 3, 6, 9, and 12 hours after treatment, beginning at 10am. Total RNA from Fe sufficient and deficient plants was sampled at each time point. Companion cell RNA was immumopurified from Fe sufficient plants at time 0, and from Fe deficient plants at each subsequent time point in triplicate. Companion cells are a low abundance cell type and even when enriched yield low total masses of RNA. Consequently this experiment was conducted using approximately 1,400 plants, grown in 26 5L tanks holding 50 plants each and required a massive effort to properly conduct this experiment. We must thank the following individuals for their help in the execution of this experiment:

Benjamin Spears, Patrick Nittler, Katlynn Koskie, David Porciani, Janlo Robil, Norman Best, as well as the full repertoire of Mendoza-Cózatl lab members.

RNA was submitted for sequencing at the MU DNA core facility for Illumina sequencing, resulting in 500 million reads. To increase the detection of low abundance transcripts each library was re-sequenced to yield a total of 834 million reads, or 20 million reads per library. Data processing, including differential expression analysis, was carried out as described in Chapters 2 and 3. To verify that companion cell RNA had been enriched, we compared the mean counts per million (CPM) of *SUC2* in companion cell and total RNA fractions (**Figure 34B**). Indeed, we found that SUC2 transcripts were enriched in all immunoprecipitated samples. Previous experiments in our lab have shown that during Fe deficiency, OPT3 expression rapidly increases to its maximum expression and then is slightly repressed (Khan *et al.*, 2018). While we did observed *OPT3* to be induced in both the companion cell and Fe deficient fractions, we did not observe a decrease in

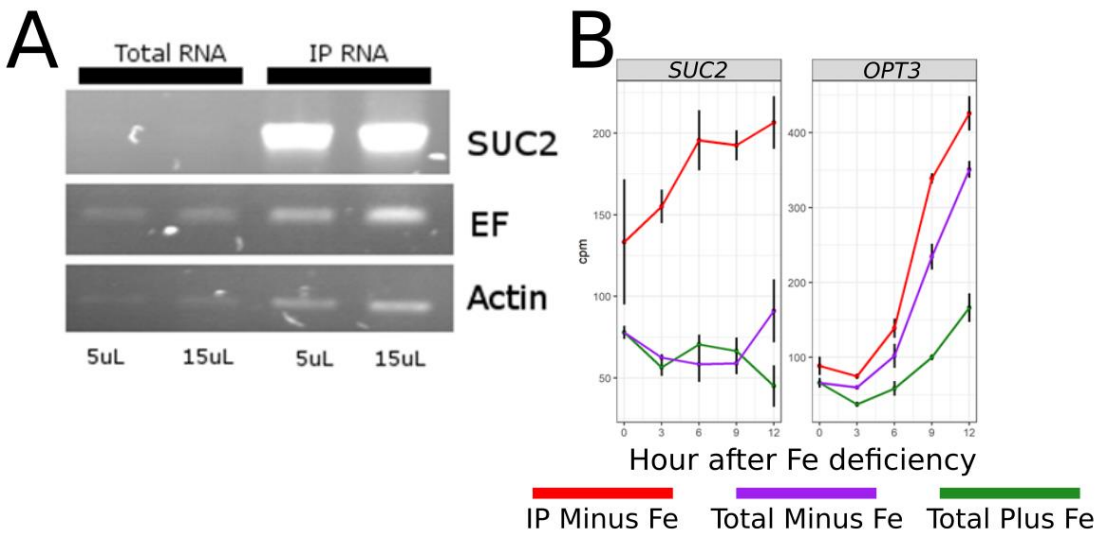

Figure 34 Immunopurification of ribosomes from *SUC2*$_{pro}$*:RPL18* enriches for companion cell transcripts. (A) RT-PCR shows that SUC2 transcript is enriched in the IP fraction, the housekeeping genes elongation factor (EF) are used as loading controls. (B) SUC2 and OPT3, transcripts known to be enriched in the companion cell, show higher enrichment in the RNA sequencing data. Mean CPM and SEM shown.

OPT3 abundance suggesting that that we had captured the earliest phase of Fe deficiency (**Figure 34B**).

We then used edgeR's group-mean approach to test for differential expression between Fe deficient and Fe sufficient total RNA fractions, and observed very few differentially expressed genes before the 12 hr time point. Manual inspection of the expression of Fe markers however, shows a clear trend of induction (**Figure 35**). This indicates that the model employed is insufficient to properly account for the time dependent nature of this dataset. Application of a linear model which properly accounts for correlation between time points is a critical aspect of our ongoing research. Consequently, and throughout this Chapter, mean CPM and standard error used to infer induction/repression.

3.1.1 Fe deficiency responses in leaves are rapidly induced

We began our analysis by determining which canonical Fe deficiency markers quickly responded to Fe deficiency in the total RNA fractions. The *FIT network* bHLH100 is known to quickly respond to Fe deficiency, but the behavior of the other *FIT network* members has not been reported. We found that bHLH38/39 to be clearly induced after 12 hr of deficiency, with clear signs of induction after 6 hrs. While bHLH101 showed a more erratic behavior, being slightly repressed after 3 hours and induced thereafter. OBP3 responsive protein 1 (ORG1), a putative protein kinase (Kang *et al.*, 2003), and FRO3, a vascular-localized metaloreductase, were found to be induced after 6 hours of deficiency, while the E3 ligase BTS and OPT3 each show weak induction after 3 hours, which became pronounced thereafter. The vacuolar transporter ZIF1 (Haydon *et al.*, 2012) and the putative Mn transporter ZIP9 (Milner *et al.*, 2013) respond much later than OPT3 and are clearly induced after 9 hours. A recently described short peptide, IRONMAN1 (IMA1, also as FEP3) (Grillet *et al.*, 2018; Hirayama *et al.*, 2018), was found to be strongly induced after 6 hours. Interestingly,

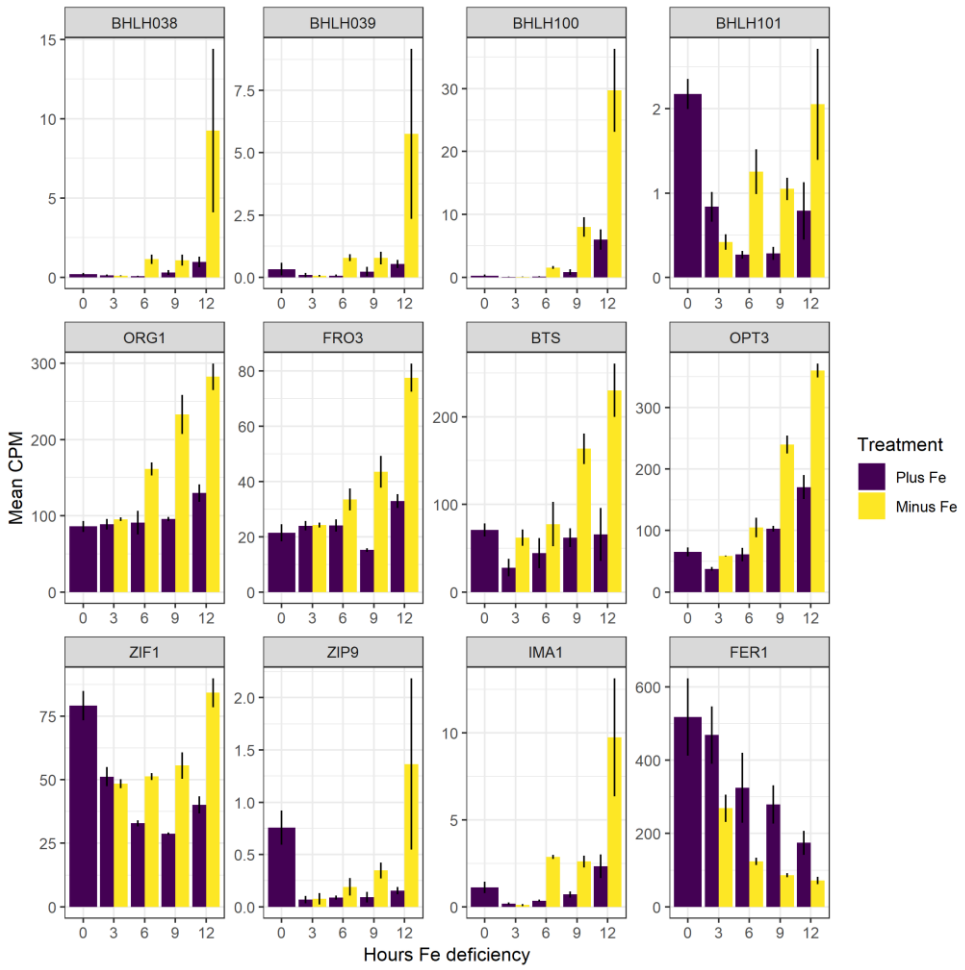

Figure 35 Many leaf Fe deficiency markers are able to rapidly respond to Fe deficiency in the total RNA fraction. Shown are mean counts per million, error bars show standard error, n=3.

Ferritin 1 (FER1) shows clear repression in response to Fe starvation after only three hours of Fe deficiency. Taken together we find that most markers are weakly induced after six hours and show strong induction after 12 hour of Fe deficiency, while OPT3 and BTS appear to react within the same time scale, and demonstrate that changes in Fe deficiency markers are evident. This trend again reinforces the need for a more appropriate statistical model to properly process TRAPseq data during a time-series experiment.

While the interpretation of the CPM of total RNA samples is straight forward (the proportion of a given transcript abundance against all the sum of all other transcript abundances), the CPM for the companion cell fraction must be interpreted with care. For instance, CPM in the companion

cell fraction measure the proportion of RNAs actively being translated, rather than the relative size of the transcript pool. Additionally, the regulation of almost 50% of Arabidopsis genes is known to be subject to circadian regulation, whose sinusoidal oscillations differ in their magnitudes and periods and as of today, the degree of circadian regulation control on the translation processes is uncertain. Therefore, to move forward, we assume that the circadian rhythm of companion cells and total RNA is identical, which is reasonable considering that our analysis was focused at companion-cell specific transcripts. Also, and because the companion cell constitutes an extremely small portion of total RNA, we will hereafter refer to expression observed in the total RNA fractions, but not in companion cell TRAP fractions, as 'mesophyll genes' and similarly genes in the TRAP-fractions will be referred to as 'companion cell genes'.

3.1.2 Role of PYE in the regulation of a discrete group of transcription factors in leaves.

bHLH100 has been shown to be regulated by members of the *PYE network*, which are expressed in leaves and roots (Liang *et al.*, 2017; Zhang *et al.*, 2015; Li *et al.*, 2016; Long *et al.*, 2010). Unlike bHLH100, bHLH38/39/101 have not been implicated in the rapid Fe deficiency response in companion cells. Hence, we first asked if we were able to detect changes in the Ib bHLHs translation in companion cells (**Figure 36**). As expected we found bHLH100 to be induced and more associated to ribosomes in companion cells after 3 hours (3 vs 6 hours in companion cells, $p = 0.0015$), as well as bHLH101. FIT1, bHLH38, and bHLH39 however, were not found to be responsive to Fe deficiency in companion cells (**Figure 36**). Next, we examined the induction patterns of the *PYE network* to determine if they respond to short term Fe deficiency (at the translation level) in either mesophyll or companion cell. Of the five PYE network members only PYE was found to be responsive to Fe deficiency after 6 hours (**Figure 36**), although bHLH105 does show an increase in mean expression increase in companion cells between 9 and 12 hr, it is insignificant under any model. Finally, we asked if the induction of PYE at the translational level

could explain the induction of bHLH100/101. All three genes show induction after 3 hours of Fe deficiency, bHLH100 is less highly induced than PYE, while bHLH101 is more highly induced than PYE. Hence it is unlikely for PYE to be the sole driver of bHLH101, but may be related to the induction of bHLH100.

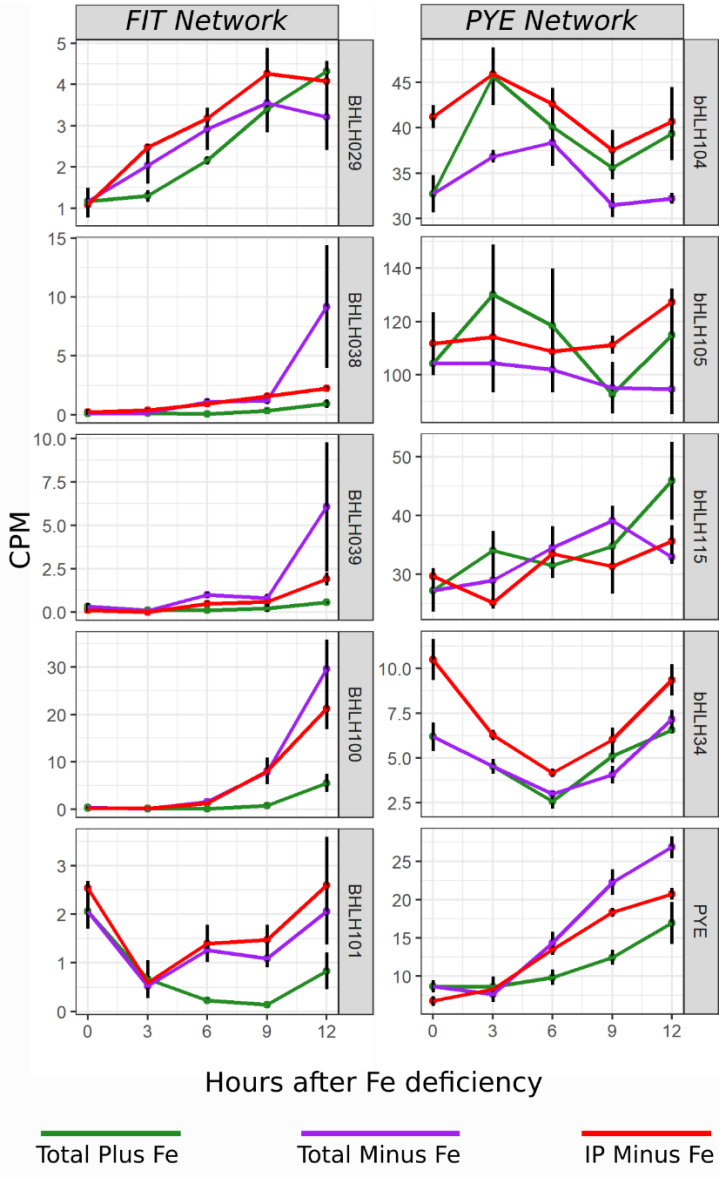

Figure 36 Only PYE is able to repond to Fe deficiency on a time scale appropriate to induce its target Ib bHLHs. Similarly bHLH100 and bHLH101 are the only Ib bHLHs which rapidly respond to Fe deficiency. Mean and standard error shown

Correlation analysis implicates the phenylpropanoid pathway in Fe deficiency responses

We are interested in identifying genes which correlated with OPT3 expression/translation, as those genes are likely to mediate processes within the Fe homeostatic network. In order to reduce the computational overhead, we reduced the number of candidate genes by first selecting genes whose abundance changed over time in companion cells ($|\log_2 FC| > 1$ for T_n/T_0 in companion cells, T_n is any time point). Next, the CPM values for those induced/repressed genes were rescaled to have a mean of zero with unit variance, and we computed Pearson's correlation coefficient for all genes against *OPT3*, and further selected only those genes with an absolute $r > 0.8$. From this list we then computed all pairwise Pearson correlation coefficients. This resulted in the identification of 103 genes, 10 of which are negatively correlated, and 93 of which are positively correlated (**Figure 37A**).

Gene ontology analysis of this gene set against the complete genome revealed an enrichment of the terms 'phenylpropanoid metabolic process', 'cinnamic acid ester metabolic process', and 'lignin biosynthesis'. We cross referenced the enriched terms to the genes correlated with OPT3 and identified six genes which regulate, or have enzymatic activity against metabolites in the phenylpropanoid pathway (**Figure 37C**). We identified AT2G23910, a putative cinnamaldehyde CoA reductase, CAD4, a cinnamyl alcohol dehydrogenase, TT4, Chalcone and stilbene synthase family protein, MYB4, a transcription factor which targets a cinnamate 4-hydroxylase, BRT1, an enzyme with sinapic acid:UDP-glucose glucosyltransferase activity, and a P450 enzyme of unknown function, CYP711A1. CAD4, MYB4, and CYP711A1 showed the most dramatic departure from their circadian rhythm, and were not induced in the Fe deficient mesophyll datasets. BRT1 and TT4 showed similar Fe deficient companion cell and mesophyll profiles, while AT2G23910 only seems to be induced in companion cells after 9 hours Fe deficiency. Genes related to phenylpropanoid metabolism are interesting in the context of Fe homeostasis because the Fe

chelators scopoletin and its derivatives are synthesized from the phenylpropanoid pathway (Kai *et al.*, 2008), Although CAD4, MYB4, and BRT1 have been shown to operate on lignin monomers (cinnamic acids and sinapic acid) (Anderson *et al.*, 2015; Jin *et al.*, 2000; Ruegger and Chapple, 2001), suggesting a role for cell wall modification in response to Fe deficiency.

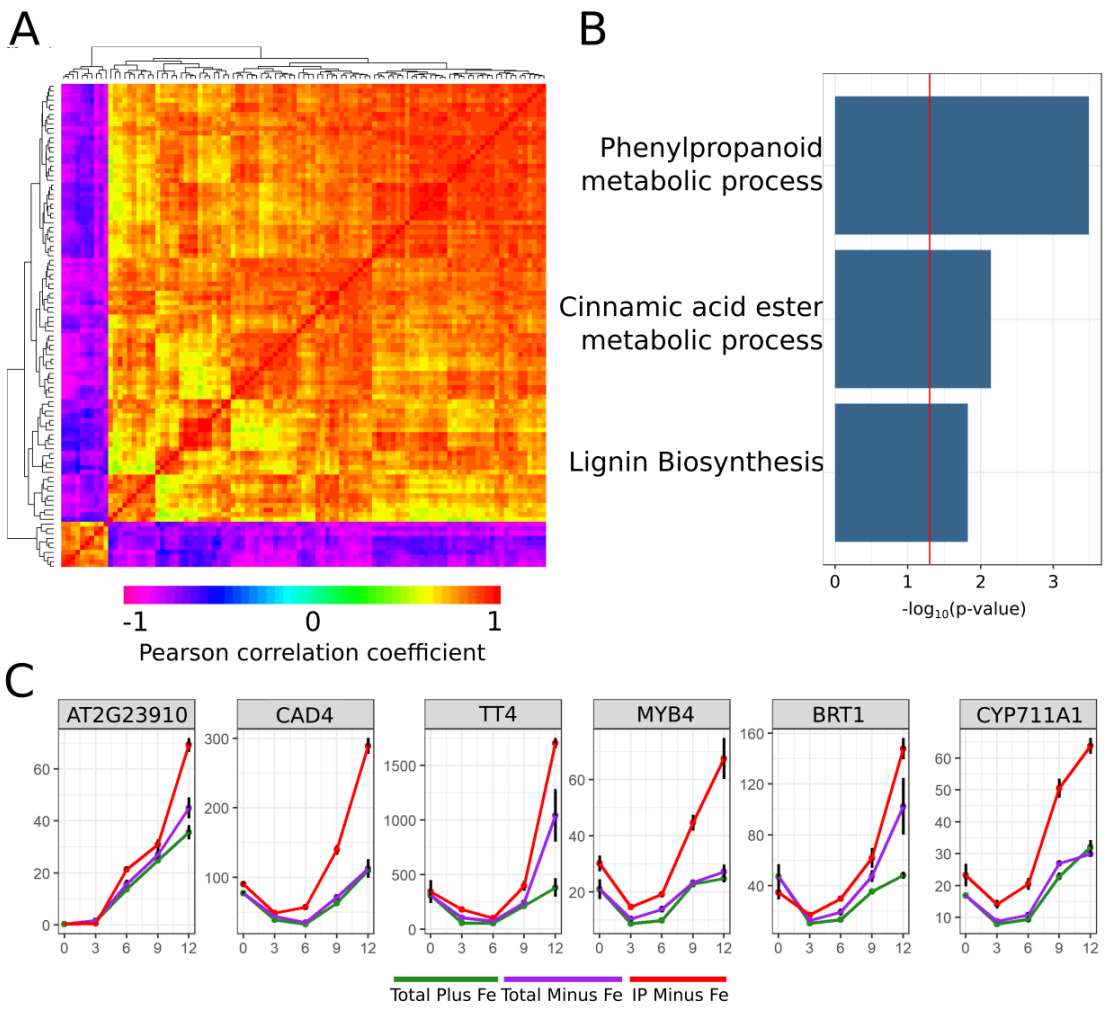

Figure 37 Genes involved in the phenylpropanoid pathway and lignin biosynthesis are enriched in a cluster of genes highly correlated with OPT3. (A) 103 genes were found to be both induced in the companion cell over 12 hours of Fe deficiency are correlated with OPT3 ($|r|$ >0.8). (B) Ontology enrichment of the OPT3 correlated genes against all genes in the *Arabidopsis* genome. (C) phenylpropanoid and lignin biosynthetic genes which were enriched in the correlated gene cluster.

As we have just begun analyzing this data set, in the near future we will implement differential expression model which properly accounts for the data structure, and begin mutant analysis as we learn more about the transcriptional and translational regulation of the companion cells.

3.2 Yeast 1 hybrid screening implicates *PYE network* members, auxin, JA, and ET to regulate OPT3

Our second approach to elucidating the transcriptional regulation of companion cell response to Fe deficiency focused on the identification of transcriptional regulators of OPT3. Typically, Y1H screens are performed using cDNA libraries generated from whole RNA, this approach is limiting in that it is difficult to detect low abundance transcription factors. Alternatively, individual bait-prey combinations can be individually cloned and tested for interaction, which is labor intensive. Hence, we employed a preassembled library of 1,957 transcription factors from *Arabidopsis* (Pruneda-paz *et al.*, 2015) in combination with a high throughput yeast pinning machine. Each transcription factor was cloned in the low expression vector pDEST22, and transformed into the yeast strain Y1867α.

In yeast, the promoter region is typically less than 300bp (Chen *et al.*, 2011), thus, we divided the first kilobase of the *OPT3* promoter into three overlapping fragments. Regulatory elements are known to bind the 5' UTR, so we labeled the first fragment F1' which consists of 320 basepairs of the promoter up to the start codon; the remaining fragments are F2 (300bp) and F3 (372bp). These fragments were first cloned into pHIS and pLACZ which provide histidine synthase (HIS) and lacZ reporters, respectively, and integrated into the genome of Y1H-aS2.

The strains containing the bait promoter fragment and prey transcription factors were subsequently mated on rich media and propagated on YNB -Trp -His -Ura. The HIS reporter system

functions as both a reporter and a selectable marker through a minimal promoter, hence all colonies grow on restrictive media in the absence of the HIS inhibitor 3-amino-1,2,4-trizole (3AT). For each fragment one array of 96 colonies was used to determine the background induction of HIS by pinning the plate onto a range of 3AT concentrations. Coincidently, all three fragments showed the best inhibition of growth for negative colonies using 60mM 3AT.

3.2.1 High throughput Y1H screens implicate PYE network members in regulation of OPT3

Across the three promoters, we identified 69, 76, and 148 transcription factors which interact with the OPT3 promoter. We found no transcription factors which bind all three fragments, 2 factors which bind both F1' and F2, 5 factors which bind F1' and F3, and seven factors which bind F2 and F3 (**Figure 38A**). We calculated the abundance of each transcription factor family on each promoter fragment and found and abundance of Ethylene Response Factors (ERF), basic Helix loop Helix (bHLH), and the related TCPs, Zinc Fingers (ZF), MYB, and WRKY members (**Figure 38B**). This analysis was then repeated for the individual fragments (**Figure 39**). F1' contains mostly ERF,

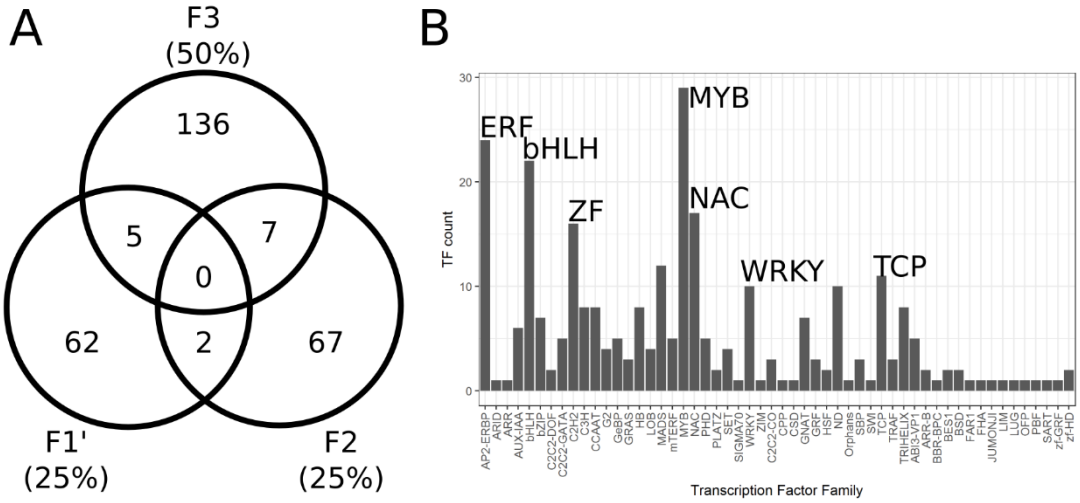

Figure 38 Summary of transcription factors identified to bind the *OPT3* promoter through a high throughput directed Y1H. (A) The most distal section of the OPT3 promoter contains is bound by the largest variety of transcription factors. (B) The entire OPT3 promoter is enriched for the ERF, bHLH, ZF, MYB, WRKY, and TCP transcription factor families.

MYB, and WRKY family transcription factors, while the second fragment contains bHLH, TCP, and MYB family transcription factors. The third fragment, which is apparently subject to many transcriptional inputs, is primarily enriched in ERF, bHLH, and MYB families.

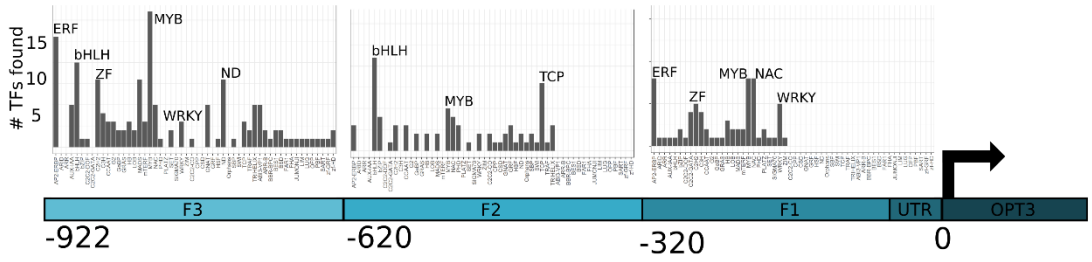

Figure 39 Schematic of the OPT3 promoter fragments and the distribution of transcription factor families along the promoter.

We have used this data to begin screening T-DNA mutants (**Figure 40**). Although the majority of the transcription factors which bound the OPT3 promoter have not been functionally characterized, several significant transcription factors were identified. Most importantly, we identified the *PYE network* members bHLH34, bHLH104, bHLH115, as well as MYC3 were all found to bind F2 (**Figure 41**), although bHLH115 and to a lesser extent bHLH104 showed extremely mild growth on restrictive media which must be further validated. While bHLH34 and MYC3 showed much stronger induction of the HIS reporter. None of these genes showed deregulation during Fe deficiency which deviated from their circadian rhythms. This is unsurprising for the transcriptional co-repressor MYC3, but indicates that the *PYE network* members either are functional on a different time scale, or are active after a post translational modification/activation (i.e. there is no need for them to be translated but they are as part of transcriptionally inactive complexes under Fe sufficient conditions).

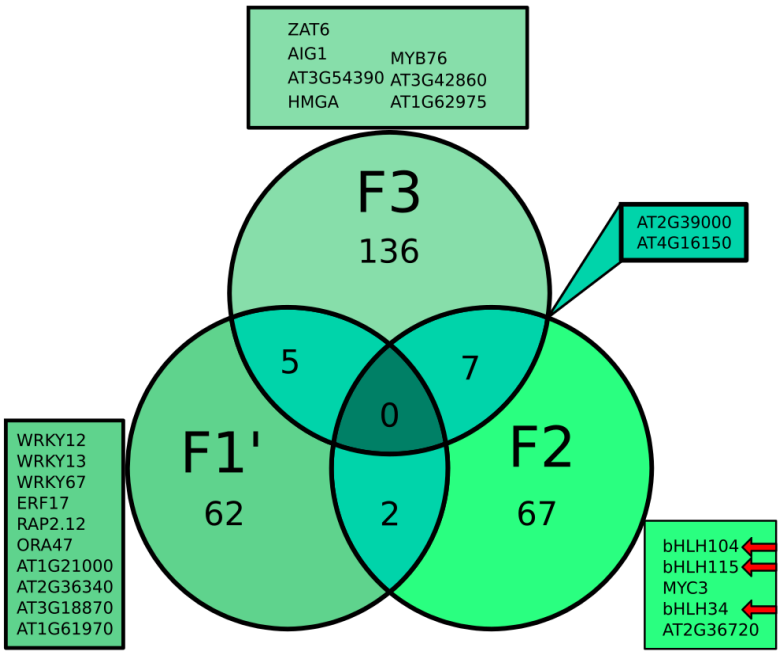

Figure 40 Candidate genes which are being pursued for a role in the regulation of OPT3. *PYE network* members bHLH104, bHLH115, and bHLH34 are of high interest.

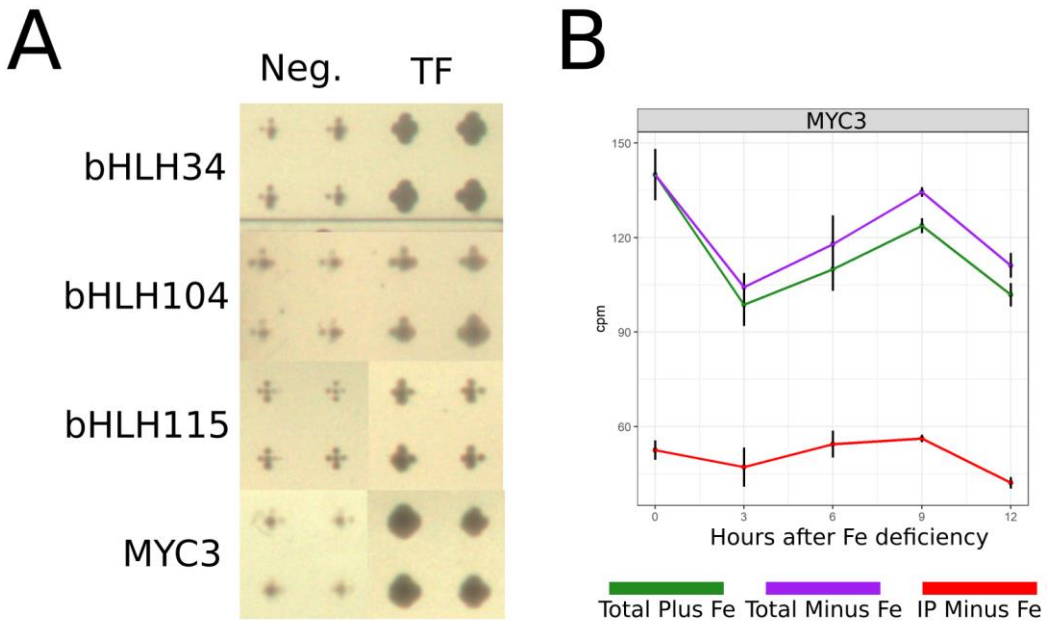

Figure 41 bHLH34, bHLH104, bHLH115, and MYC3 bind the OPT3 promoter. (A) Yeast carrying OPT3 promoter fragment 2 and bHLH34/104/115 or MYC2 are able to grow in the absence of histidine supplemented with 60mM 3AT. (B) Expression profile of MYC3

3.2.2 OPT3 expression may be regulated by auxin, JA, and ET.

Additionally, we identified genes which regulate JA, auxin, and ET signaling (**Figure 42**). Three TCPs which are annotated as members of JA signaling (TCP3, TCP5, TCP10) were found to bind F2, F3, and F2 respectively (**Figure 42A**). Similar to MYC3, we did not observe any clear patterns of induction or repression in the TCPs which differed from their circadian rhythms. Although between 3 and 9 hours after Fe deficiency TCP5 undergoes a circadian induction which peaks at 9 hours, after which it is repressed, this is not maintained in Fe deficient mesophyll, where TCP5 expression is held constant after 9 hours of Fe deficiency, possibly initiating the repression of OPT3 expression after its expression has reach its local maxima.

Three IAA proteins were identified which bind F3 (IAA10, IAA19, IAA32) (**Figure 42B**). IAAs inhibit ARF dependent induction, suggesting a role in repressing OPT3 expression. Although no ARFs were found, we found MBY12 to bind F3, which has been shown to promote auxin dependent gene expression. MYB12 was shown to respond to UV induced stress (Stracke, Favory, *et al.*, 2010), and directly regulate chalcone synthase in the phenylpropanoid pathway (Stracke *et al.*, 2007; Stracke, Jahns, *et al.*, 2010), but rather than leading to the formation of coumaric acid derivatives or lignin, chalcone is a flavonoid precursor, which has been shown to chelate heavy metals such as Fe (Leopoldini *et al.*, 2006), and application of the flavonoids naringenin and quercetin were shown to rescue Cd and Zn induced root growth inhibition (Kelig and Ludwig-Muller, 2009).

Lastly we identified three ethylene responsive genes (ERF17, ORA47, and RAP2.12). Again similar to the JA dependent TCPs, none of these ethylene responsive genes show any indication of Fe dependent regulation at the transcription/translational level. Taken together, we have identified several transcription factors which have been implicated in JA, ET, and auxin signaling to directly

bind the promoter of OPT3 in a Y1H screen. Further, we found the *PYE network* members bHLH34, bHLH104, and bHLH115 to bind the same fragment of OPT3's promoter, linking co-expression of bHLH100 and OPT3 with common transcriptional regulators

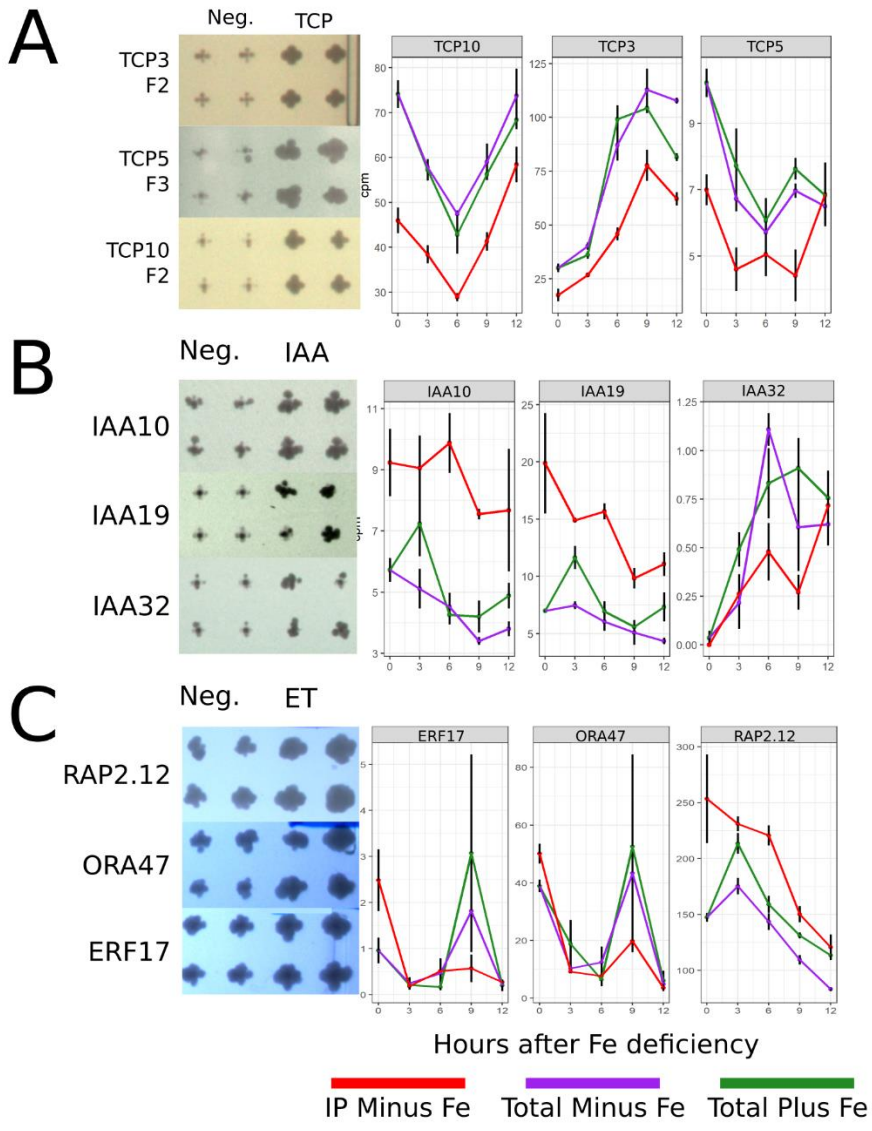

Figure 42 Transcription factors which mediate hormone dependent regulation bind the OPT3 promoter. (A) TCPs which are annotated as being involved in JA signaling. (B) Transcriptional repressors of auxin. (C) Ethylene response factors.

4 Discussion

In this work we have begun to unravel the transcriptional networks which mediate Fe deficiency responses in companion cells using two complementary approaches by directly measuring gene translation in companion cells in response to short term Fe deficiency, and by identifying transcriptional regulators of *OPT3*.

bHLH100 has previously been shown to be rapidly induced by Fe deficiency, although slightly lagged relative to *OPT3*, and directly regulated by bHLH34, bHLH104, and bHLH115 (Liang *et al.*, 2017; Zhang *et al.*, 2015). *bHLH34*, *bHLH104*, and *bHLH115* were found to not be transcriptionally/translationally responsive during the first 12 hr of Fe deficiency in mesophyll or companion cells (**Figure 36**), but were able to bind the *OPT3* promoter (**Figure 41**). This suggests that if bHLH34/104/115 are responsible for the rapid induction of *OPT3* and *bHLH100*, then it must occur through a post translational mechanism. Alternatively, bHLH34/104/115 induction of *OPT3* and *bHLH100* may be dependent on dimerization with PYE, which is responsive to Fe deficiency in both mesophyll and companion cells (**Figure 36**)

Using standard statistical methodologies used in RNA sequencing to identify differentially expressed genes was shown to be inadequate (**Figure 35**), directing our future work to implement an appropriate model. However, our gene ontology enrichment analysis identified five enzymes and one transcription factor which are predicted, or shown, to be involved in the phenylpropanoid pathway, flavonoid biosynthesis, and lignin biosynthesis. Each of these genes shows a strong induction only in companion cells (CAD4, MYB4, and CYP711A1) or a strong induction in both Fe deficient mesophyll cells and companion cells (TT4 and BRT1) (**Figure 37C**). These proteins suggest two non-competing models. If these enzymes are incorrectly annotated, or are able to

catalyze multiple reactions, then they may be involved in the synthesis of a novel Fe chelator in companion cells. Although not beyond question, Fe sensing is likely to be a function of the ratio of free chelator and chelated-Fe in a protein complex. This unknown chelator may be synthesized from these enzymes, although the rapid induction suggests that the chelator complex undergoes rapid turnover. Alternatively, the annotations relating to cinnamic acids and sinapic acids suggest that they may be modifying the cell wall. In roots, Fe is bound by the carboxylic acid and alcohol moieties found in the lignin monomers and serves as a Fe reservoir (Jin *et al.*, 2007). In leaves, mutants impaired in Fe transport often show increased Fe In the vasculature (e.g. *opt3*, *frd3, ysl1/ysl3*) (Zhai *et al.*, 2014; Green, 2004; Kumar *et al.*, 2017). Further, OPT3 is induced upon Fe deficiency, suggesting an attempt to load Fe from the vascular apoplast into the companion cell. CAD4 (also as CADC) has been shown to have atypical incorporation of hydroxycinnamaldehydes in the cell wall (Anderson *et al.*, 2015) which may result in an altered Fe binding capacity. Hence the apoplastic Fe reserve may be mobilized through modifications to the cell wall to mobilize Fe to Fe deficient cells.

Finally, we combined the RNA sequencing and Y1H data in an attempt to identify possible hormonal signals that may induce *OPT3.* We were able to identify ten transcription factors which are able to bind the *OPT3* promoter (**Figure 41**, **Figure 42**), although none of these genes showed a clear transcription/translation pattern, indicating that their activity is either post translationally controlled, a likely mechanism of rapid responses, or non-physiological in the conditions tested (i.e. related to development or circadian rhythm). We also identified three ethylene response factors (ER17, ORA47, and RAP2.12) which are expected to induce OPT3 expression and their mutants are currently being screened for Fe deficiency phenotypes. Auxin is able to induce Fe deficiency responses in roots, so the presence of multiple IAA proteins on the *OPT3* promoter is suggestive of a repressive mechanism after Fe sufficiency has been restored, and/or to repress

OPT3 after it has reached its maximum induction, neither of which were reached during this experiment. Four proteins related to JA signaling were also identified (TCP2/5/10, MYC3). Although, transcriptional repression of MYC3 is alleviated in the presence of JA, indicating that JA is an inducer of OPT3 in leaves, while in roots JA acts as a repressor (Maurer *et al.*, 2011), or is a involved in cross talk between multiple hormones.

5 Conclusion

Leaves have recently become an active area of research in the Fe sensing field. Although studies in *opt3* mutants have provided many key insights into the role of companion cells, the transcriptional control of OPT3, and in turn the Fe deficiency response of the companion cell, is still unknown. Our translatome approach describing the earliest responses to Fe deficiency in companion cells suggest the presence of a novel mechanism for the release of Fe from the cell wall during Fe deficiency. Further, our high throughput yeast 1-hybrid screening led us to the identification of novel regulators of OPT3, which show that the PYE network mediates, at least in part, the expression of OPT3, although we are unable to ascertain if PYE network members are responsible for the rapid induction of *OPT3* during Fe deficiency. However, the integration of our large datasets are being proven useful to guide the direction of our immediate future studies.

6 Bibliography

Anderson, N.A., Tobimatsu, Y., Ciesielski, P.N., Ximenes, E., Ralph, J., Donohoe, B.S., Ladisch, M. and Chapple, C. (2015) Manipulation of Guaiacyl and Syringyl Monomer Biosynthesis in an Arabidopsis Cinnamyl Alcohol Dehydrogenase Mutant Results in Atypical Lignin Biosynthesis and Modified Cell Wall Structure. *Plant Cell*, **27**, 2195–2209.

Bacaicoa, E., Mora, V., Zamarreño, Á.M., Fuentes, M., Casanova, E. and García-Mina, J.M. (2011) Auxin: A major player in the shoot-to-root regulation of root Fe-stress physiological responses to Fe deficiency in cucumber plants. *Plant Physiol. Biochem.*, **49**, 545–556.

Casson, S., Spencer, M., Walker, K. and Lindsey, K. (2005) Laser capture microdissection for the analysis of gene expression during embryogenesis of Arabidopsis. *Plant J.*, **42**, 111–123.

Chen, W.H., Wei, W. and Lercher, M.J. (2011) Minimal regulatory spaces in yeast genomes. *BMC Genomics*, **12**, 320.

Chen, W.W., Yang, J.L., Qin, C., Jin, C.W., Mo, J.H., Ye, T. and Zheng, S.J. (2010) Nitric Oxide Acts Downstream of Auxin to Trigger Root Ferric-Chelate Reductase Activity in Response to Iron Deficiency in Arabidopsis. *Plant Physiol.*, **154**, 810–819.

Cheng, Z., Sun, L., Qi, T., Zhang, B., Peng, W., Liu, Y. and Xie, D. (2011) The bHLH transcription factor MYC3 interacts with the jasmonate ZIM-domain proteins to mediate jasmonate response in arabidopsis. *Mol. Plant*, **4**, 279–288.

Clarke, J.D., Volko, S.M., Ausubel, F.M. and Dong, X. (2000) Roles of salicylic acid, jasmonic acid, and ethylene in cpr-induced resistance in arabidopsis. *Plant Cell*, **12**, 2175–90.

Deeken, R., Ache, P., Kajahn, I., Klinkenberg, J., Bringmann, G. and Hedrich, R. (2008) Identification of Arabidopsis thaliana phloem RNAs provides a search criterion for phloem-based transcripts hidden in complex datasets of microarray experiments. *Plant J.*, **55**, 746–759.

Devoto, A., Nieto-Rostro, M., Xie, D., et al. (2002) COI1 links jasmonate signalling and fertility to the SCF ubiquitin-ligase complex in Arabidopsis. *Plant J.*, **32**, 457–466.

García, M.J., Lucena, C., Romera, F.J., Alcántara, E. and Pérez-Vicente, R. (2010) Ethylene and nitric oxide involvement in the up-regulation of key genes related to iron acquisition and homeostasis in Arabidopsis. *J. Exp. Bot.*, **61**, 3885–3899.

Giehl, R.F.H., Lima, J.E. and Wiren, N. von (2012) Localized Iron Supply Triggers Lateral Root Elongation in Arabidopsis by Altering the AUX1-Mediated Auxin Distribution. *Plant Cell*, **24**, 33–49.

Goossens, J., Swinnen, G., Bossche, R. Vanden, Pauwels, L. and Goosens, A. (2015) Change of a conserved amino acid in the MYC2 and MYC3 transcription factors leads to release of JAZ repression and increased activity. *New Phytol.*, **206**, 1229–1237.

Green, L.S. (2004) FRD3 Controls Iron Localization in Arabidopsis. *Plant Physiol.*, **136**, 2523–2531.

Grillet, L., Lan, P., Li, W., Mokkapati, G. and Schmidt, W. (2018) IRON MAN, a ubiquitous family of peptides that control iron transport in plants. *Nat. Plants*, 1–26.

Guilfoyle, T.J. and Hagen, G. (2007) Auxin response factors. *Curr. Opin. Plant Biol.*, **10**, 453–460.

Guillaume, D., Neveu, J., Enric, Z. and Vert, G. (2018) Metal Sensing by the IRT1 Transporter-Receptor Orchestrates Its Own Degradation and Plant Metal Nutrition. *Mol. Cell*, **69**, 953–964.

Haydon, M.J., Kawachi, M., Wirtz, M., Hillmer, S., Hell, R. and Kramer, U. (2012) Vacuolar Nicotianamine Has Critical and Distinct Roles under Iron Deficiency and for Zinc Sequestration in Arabidopsis. *Plant Cell Online*, **24**, 724–737.

Heiman, M., Kulicke, R., Fenster, R.J., Greengard, P. and Heintz, N. (2014) Cell type–specific mRNA purification by translating ribosome affinity purification (TRAP). *Nat. Protoc.*, **9**, 1282.

Hindt, M.N. and Guerinot, M. Lou (2012) Getting a sense for signals: regulation of the plant iron deficiency response. *Biochim Biophys Acta*, **1823**, 1521–1530.

Hirayama, T., Lei, G.J., Yamaji, N., Nakagawa, N. and Ma, J.F. (2018) The Putative Peptide Gene FEP1 Regulates Iron Deficiency Response in Arabidopsis. *Plant Cell Physiol.*, **59**, 1739–1752.

Ithal, N., Recknor, J., Nettleton, D., Maier, T., Baum, T.J. and Mitchum, M.G. (2007) Developmental Transcript Profiling of Cyst Nematode Feeding Cells in Soybean Roots. *Mol. Plant-Microbe Interact.*, **20**, 510–525.

Jin, C.W., You, G.Y., He, Y.F., Tang, C., Wu, P. and Zheng, S.J. (2007) Iron Deficiency-Induced Secretion of Phenolics Facilitates the Reutilization of Root Apoplastic Iron in Red Clover. *Plant Physiol.*, **144**, 278–285.

Jin, H., Cominelli, E., Bailey, P., Parr, A., Mehrtens, F., Jones, J., Tonelli, C., Weisshaar, B. and Martin, C. (2000) Transcriptional repression by AtMYB4 controls production of UV-protecting sunscreens in Arabidopsis. *EMBO J.*, **19**, 6150–6161.

Kai, K., Mizutani, M., Kawamura, N., Yamamoto, R., Tamai, M., Yamaguchi, H., Sakata, K. and Shimizu, B.I. (2008) Scopoletin is biosynthesized via ortho-hydroxylation of feruloyl CoA by a 2-oxoglutarate-dependent dioxygenase in Arabidopsis thaliana. *Plant J.*, **55**, 989–999.

Kang, H.G., Foley, R.C., Oñate-Sánchez, L., Lin, C. and Singh, K.B. (2003) Target genes for OBP3, a Dof transcription factor, include novel basic helix-loop-helix domain proteins inducible by salicylic acid. *Plant J.*, **35**, 362–372.

Kelig, K. and Ludwig-Muller, J. (2009) Effect of flavonoids on heavy metal tolerance in Arabidopsis thaliana seedlings. *Bot. Stud.*, **50**, 311–318.

Keuskamp, D.H., Pollmann, S., Voesenek, L. a C.J., Peeters, A.J.M. and Pierik, R. (2010) Controls Shade Avoidance and Fitness During Competition. *Pnas*, **3**, 22740–22744.

Keuskamp, D.H., Sasidharan, R., Vos, I., Peeters, A.J.M., Voesenek, L.A.C.J. and Pierik, R. (2011) Blue-light-mediated shade avoidance requires combined auxin and brassinosteroid action in Arabidopsis seedlings. *Plant J.*, **67**, 208–217.

Khan, M.A., Castro-Guerrero, N.A., McInturf, S.A., et al. (2018) Changes in iron availability in Arabidopsis are rapidly sensed in the leaf vasculature and impaired sensing leads to opposite transcriptional programs in leaves and roots. *Plant. Cell Environ.*, 1–14.

Korshunova, Y.O., Eide, D., Clark, W.G., Guerinot, M. Lou and Pakrasi, H.B. (1999) The IRT1

protein from Arabidopsis thaliana is a metal transporter with a broad substrate range. *Plant Mol. Biol.*, **40**, 37–44.

Ku, Y.-S., Sintaha, M., Cheung, M.-Y. and Lam, H.-M. (2018) *Plant Hormone Signaling Crosstalks between Biotic and Abiotic Stress Responses*,.

Kumar, R.K., Chu, H.-H., Abundis, C., Vasques, K., Chan-Rodriguez, D., Chia, J.-C., Huang, R., Vatamaniuk, O.K. and Walker, E.L. (2017) Iron-Nicotianamine Transporters are Required for Proper Long Distance Iron Signaling. *Plant Physiol.*, **175**, pp.00821.2017.

Leopoldini, M., Russo, N., Chiodo, S. and Toscano, M. (2006) Iron Chelation by the Powerful Antioxidant Flavonoid Quercetin. *J. Agric. Food Chem.*, **54**, 6343–6351.

Lešková, A., Giehl, R.F.H., Hartmann, A., Fargašová, A. and Wirén, N. von (2017) Heavy Metals Induce Iron Deficiency Responses at Different Hierarchic and Regulatory Levels. *Plant Physiol.*, **174**, 1648–1668.

Li, X., Zhang, H., Ai, Q., Liang, G. and Yu, D. (2016) Two bHLH Transcription Factors, bHLH34 and bHLH104, Regulate Iron Homeostasis in *Arabidopsis thaliana*. *Plant Physiol.*, **170**, 2478–2493.

Liang, G., Zhang, H., Li, X., Ai, Q. and Yu, D. (2017) BHLH transcription factor bHLH115 regulates iron homeostasis in Arabidopsis thaliana. *J. Exp. Bot.*, **68**, 1743–1755.

Lingam, S., Mohrbacher, J., Brumbarova, T., Potuschak, T., Fink-Straube, C., Blondet, E., Genschik, P. and Bauer, P. (2011) Interaction between the bHLH Transcription Factor FIT and ETHYLENE INSENSITIVE3/ETHYLENE INSENSITIVE3-LIKE1 Reveals Molecular Linkage between the Regulation of Iron Acquisition and Ethylene Signaling in *Arabidopsis*. *Plant Cell*, **23**, 1815–1829.

Long, T.A., Tsukagoshi, H., Busch, W., Lahner, B., Salt, D.E. and Benfey, P.N. (2010) The bHLH transcription factor POPEYE regulates response to iron deficiency in Arabidopsis roots. *Plant Cell*, **22**, 2219–2236.

Lucena, C., Waters, B.M., Romera, F.J., García, M.J., Morales, M., Alcántara, E. and Pérez-Vicente, R. (2006) Ethylene could influence ferric reductase, iron transporter, and H+-ATPase gene expression by affecting FER (or FER-like) gene activity. *J. Exp. Bot.*, **57**, 4145–4154.

Maurer, F., Müller, S. and Bauer, P. (2011) Suppression of Fe deficiency gene expression by jasmonate. *Plant Physiol. Biochem.*, **49**, 530–536.

Mendoza-Cózatl, D.G., Xie, Q., Akmakjian, G.Z., et al. (2014) OPT3 is a component of the iron-signaling network between leaves and roots and misregulation of OPT3 leads to an over-accumulation of cadmium in seeds. *Mol. Plant*, **7**, 1455–1469.

Milner, M.J., Seamon, J., Craft, E. and Kochian, L. V (2013) Transport properties of members of the ZIP family in plants and their role in Zn and Mn homeostasis. *J. Exp. Bot.*, **64**, 369–381.

Morelli, G., Ruberti, I., Molecolare, B., Sapienza, L. and Moro, P.A. (2000) Update on Light Signaling Shade Avoidance Responses . Driving Auxin along Lateral Routes. *Plant Physiol.*, **122**, 621–626.

Mur, L.A.J., Prats, E., Pierre, S., Hall, M.A. and Hebelstrup, K.H. (2013) Integrating nitric oxide into salicylic acid and jasmonic acid/ ethylene plant defense pathways. *Front. Plant Sci.*, **4**, 1–7.

Mustroph, A., Zanetti, M.E., Jang, C.J.H., Holtan, H.E., Repetti, P.P., Galbraith, D.W., Girke, T. and Bailey-Serres, J. (2009) Profiling translatomes of discrete cell populations resolves altered cellular priorities during hypoxia in Arabidopsis. *Proc. Natl. Acad. Sci.*, **106**, 18843–18848.

Palmer, C.M., Hindt, M.N., Schmidt, H., Clemens, S. and Guerinot, M. Lou (2013) MYB10 and MYB72 are required for growth under iron-limiting conditions. *PLoS Genet*, **9**, e1003953.

Pauwels, L., Barberdo, G.F., Geerinck, J., et al. (2010) NINJA connects the co-repressor TOPLESS to jasmonate signalling. , **464**, 788–791.

Pruneda-paz, J.L., Breton, G., Nagel, D.H., Kang, S.E., Doherty, C.J., Ravelo, S., Galli, M., Ecker, J.R. and Kay, S.A. (2015) Arabidopsis transcription factors. , **8**, 622–632.

Rodríguez-Celma, J., Pan, I.C., Li, W., Lan, P., Buckhout, T.J. and Schmidt, W. (2013) The transcriptional response of Arabidopsis leaves to Fe deficiency. *Front. Plant Sci.*, **4**, 1–10.

Ruegger, M. and Chapple, C. (2001) Mutations that reduce sinapoylmalate accumulation in Arabidopsis thaliana define loci with diverse roles in phenylpropanoid metabolism. *Genetics*, **159**, 1741–1749.

Séguéla, M., Briat, J.F., Vert, G. and Curie, C. (2008) Cytokinins negatively regulate the root iron uptake machinery in Arabidopsis through a growth-dependent pathway. *Plant J.*, **55**, 289–300.

Sivitz, A.B., Hermand, V., Curie, C. and Vert, G. (2012) Arabidopsis bHLH100 and bHLH101 control iron homeostasis via a FIT-independent pathway. *PLoS One*, **7**, e44843.

Stacey, M.G., Patel, A., McClain, W.E., Mathieu, M., Remley, M., Rogers, E.E., Gassmann, W., Blevins, D.G. and Stacey, G. (2008) The Arabidopsis AtOPT3 protein functions in metal homeostasis and movement of iron to developing seeds. *Plant Physiol.*, **146**, 589–601.

Stein, R.J. and Waters, B.M. (2012) Use of natural variation reveals core genes in the transcriptome of iron-deficient Arabidopsis thaliana roots. *J. Exp. Bot.*, **63**, 1039–1055.

Stracke, R., Favory, J.J., Gruber, H., Bartelniewoehner, L., Bartels, S., Binkert, M., Funk, M., Weisshaar, B. and Ulm, R. (2010) The Arabidopsis bZIP transcription factor HY5 regulates expression of the PFG1/MYB12 gene in response to light and ultraviolet-B radiation. *Plant, Cell Environ.*, **33**, 88–103.

Stracke, R., Ishihara, H., Huep, G., Barsch, A., Mehrtens, F., Niehaus, K. and Weisshaar, B. (2007) Differential regulation of closely related R2R3-MYB transcription factors controls flavonol accumulation in different parts of the Arabidopsis thaliana seedling. *Plant J.*, **50**, 660–677.

Stracke, R., Jahns, O., Keck, M., Tohge, T., Niehaus, K., Fernie, A.R. and Weisshaar, B. (2010) Analysis of PRODUCTION OF FLAVONOL GLYCOSIDES-dependent flavonol glycoside accumulation in Arabidopsis thaliana plants reveals MYB11-, MYB12- and MYB111-independent flavonol glycoside accumulation. , 985–1000.

Tao, Y., Ferrer, J.L., Ljung, K., et al. (2008) Rapid Synthesis of Auxin via a New Tryptophan-Dependent Pathway Is Required for Shade Avoidance in Plants. *Cell*, **133**, 164–176.

Wang, N., Cui, Y., Liu, Y., Fan, H., Du, J., Huang, Z., Yuan, Y., Wu, H. and Ling, H.Q. (2013) Requirement and functional redundancy of Ib subgroup bHLH proteins for iron deficiency responses and uptake in Arabidopsis thaliana. *Mol. Plant*, **6**, 503–513.

Yang, Y., Ou, B., Zhang, J., Si, W., Gu, H., Qin, G. and Qu, L.J. (2014) The Arabidopsis Mediator subunit MED16 regulates iron homeostasis by associating with EIN3/EIL1 through subunit MED25. *Plant J.*, **77**, 838–851.

Zhai, Z., Gayomba, S.R., Jung, H., et al. (2014) asdfa iron transporter that is essential for systemic iron signaling and redistribution of iron and cadmium in Arabidopsis. *Plant Cell*, **26**, 2249–2264.

Zhang, J., Liu, B., Li, M., et al. (2015) The bHLH Transcription Factor bHLH104 Interacts with IAA-LEUCINE RESISTANT3 and Modulates Iron Homeostasis in Arabidopsis. *Plant Cell*, **27**, 787–805.

Zhu, X.F., Wang, B., Song, W.F., Zheng, S.J. and Shen, R.F. (2016) Putrescine Alleviates Iron Deficiency via NO-Dependent Reutilization of Root Cell-Wall Fe in Arabidopsis. *Plant Physiol.*, **170**, 558–567.

7 Chapter 2
Supplemental data

7.1 Comparison of *opt3-2* and Col-0's response to Cd in leaves and roots

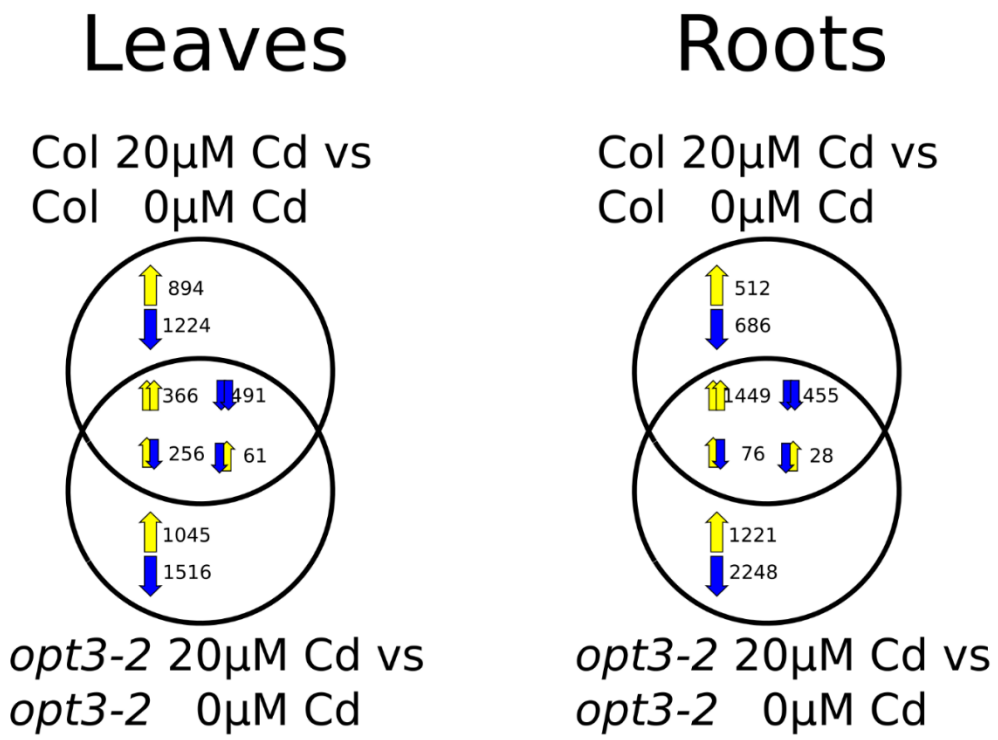

Supp. Fig. 1 Fold change induced or repressed in the contrasts CT - CN and OT - ON (Cd responsive per genotype). Within the intersection the first arrow indicates the sign taken by Col-0, and the second arrow the sign taken by opt3-2.

7.2 RBOHD expression visualized in our eFP browser

At5g47910 At5g47910 *ATRBOHD*

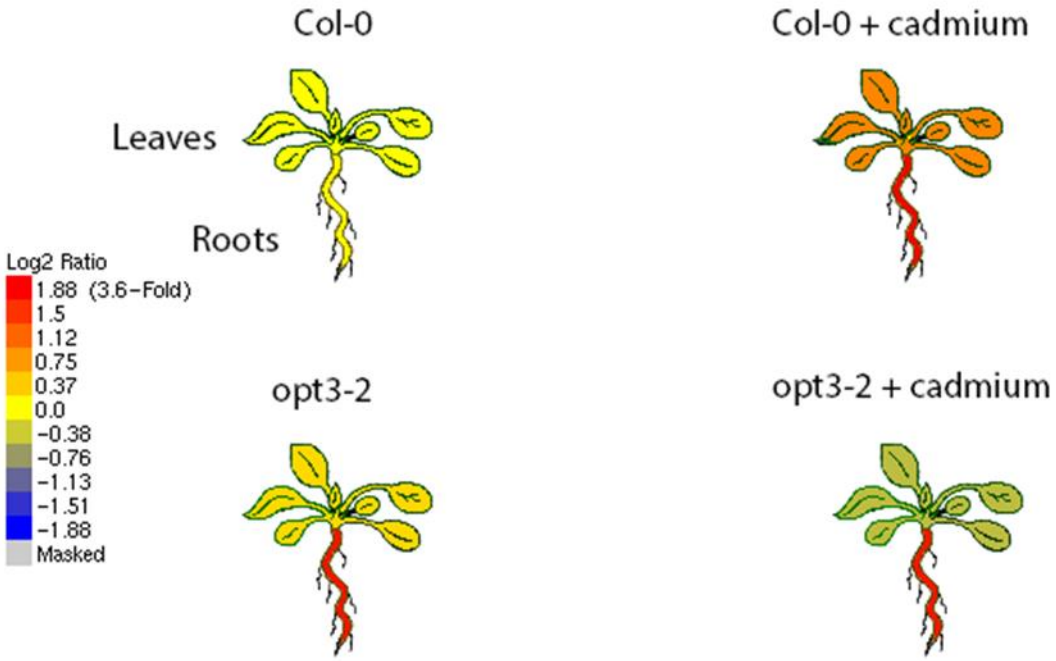

Supp. Fig. 2 RBOHD in the eFP browser, relative mode

7.3 Determination of consistently Fe regulated genes in leaves and roots

DThe first gene set, obtained from (Stein and Waters, 2012), contains genes differentially expressed in the Tsu and Kas ecotypes exposed to 24 and 48hr –Fe. These were compared against Col-0 subjected to 72hr –Fe published by (Kumar *et al.*, 2017). Genes were filtered in the following manner. An expected sign was determined for each ecotype separately. For Kas and Tsu, the sign of the latest time point was used for later comparisons, unless it is zero, in which case the earlier

time point is used. The expected sign for the Col-0 data, with only one time point, was simply the observed sign of the fold change. This produced a set of genes with three expected iron signs, and the majority direction was taken as the overall expected sign. Several genes, namely bHLH38 and bHLH100, were added to these lists as they are not present on the microarrays used but are well established regulators of Fe homeostasis. The *ferrome* effectively describes Fe deficiency responses in roots, so was appended to the root list. The same procedure was used in leaves and roots.This code runs in R version 3.5.1 (2018-07-02). Written without packages so should remain stable.

```
consensusGroup = function(MM){
# consensusGroup applies the function getExpectedSign to a matrix with columns
# containing tsu/kas/col
# getExpectedSign outputs numeric vectors, so we are applying a function to the rows
# to a matrix which we are building on the fly, which simply pastes the outputs of
# getExpectedSign together separated by a '/'.
       blerp = apply(cbind("tsu" = getExpectedSign(M = MM, group = "tsu"),
                           "kas" = getExpectedSign(M = MM, group = "kas"),
                           "col" = sign(MM[,grep('Fe[R|L]', colnames(MM))])),
                     1, function(x) paste0(x, collapse = "/"))
       return(blerp)
}



getExpectedSign = function(M, group){
# getExpectedSign takes a matrix 'M', and an atomic character vector 'group'
# 'M' must have two column names in 'group' (partial string match)
# getExpectedSign will pull any number of columns matching 'group', but only will
# use the first two.
# First the sign of all values is calculated ('used' refers to the sign, -1/0/1).
# The second time point is checked to see if it is zero
# if so, the first time is used.  Else the second time point is used
# Because this is only done for Kas and Tsu, we presume that the biologically
significant
# sign is the one closer to the 72hr deficiency, while allowing for the 24hr deficiency
# to remain relevant in the calculations.
       # M is a matix, group is some character string which identifies the groups
       # M = swRootFC ; group = "tsu"
       myGenes = sign(M[,grep(group, colnames(M))])              # find signs
       res = vector(mode = "numeric", length = nrow(myGenes))    # prepare a output
vector
       for(i in 1:nrow(myGenes)){
              # If not DE at T2, then use T1, else use T2
              T1 = myGenes[i,1] ; T2 = myGenes[i,2]              # Define the vectors
       of times
              if(T2 == 0){                                       # begin comparisons
                     res[i] = T1
              }else{
                     res[i] = T2
```

```
                }
        }
        TMP = myGenes[apply(myGenes, 1, function(x) !any(x == 0)),]
        cat(paste0("How many genes did NOT change sign between 24 and 48hr? (",
group,")"))
        print(table(TMP[1] == TMP[2]))
        return(res)
}



signSorter = function(va){
# signSorter takes the output of consensusGroup and performs comparisons on the
expected
# signs generated therein
# the input vector is split into its component parts, and the number of zeros is
counted.
# if only one zero, remove it and compare the two remaining. If they differ, then
return
# “NC”, else return the sign of the first (which is the same as the second)
# If there two zeros return “NC”
# If there are no zeros, check to see if they are all the same as the first (all the
same)
# and return the sign of the first if true.
# else take the sum of all signs and return that value (MUST be -1 or 1, zero and
higher
# values are impossible, given no zeros.
        # signSorter takes a character vector with three ‘/’ deliminated values
        # of -1, 0, or 1.
        #va = "1/1/-1"
        va = unlist(strsplit(va, split = "/"))
        # if there is one zero do this:
        if(sum(va == 0) == 1){
                va = va[va != 0]                    # remove the zero
                if(va[1] == va[2]){                         # if they are the same,
        return TRUE
                        return(va[1])
                }else{
                        return("NC")
        }
        }
        # if there are two zeros do this:
        if(sum(va == 0) >= 2){
                return("NC")
        }
        # If there are no zeros do this:
        # If all the same, just return the sign (duh)
        # if there is no zeros and they arent the same, then it has to be
        # something like 1/1/-1.  So sum them and return "1" if over 1, -1 else.
        # (1) + (1) + (-1) = 1 <up>, (-1) + (-1) + 1 = -1 <down>
        if(sum(va == 0) == 0){
        if(all(va == va[1])){
                return(va[1])
        }else{
                return(ifelse(sum(as.numeric(va)) >= 1, "1","-1"))
        }
        }
}

addConsensus = function(M){
# addConsensus is a utility function to apply signSorter and integrate it into the
```

```
# matrix, placing it in a nice position (instead of just at the end).
       #M = swmLeafFC
       m = M
       myCols = colnames(M)
       patterns = M$Pattern
       # I need all groups to have fewer than 2 zeros and the remaining signs to be the
same
       ironSign = sapply(patterns, function(x) signSorter(va = x))
       m$ironSign = ironSign
       pos = grep("Fe",myCols)
       m = m[,c(myCols[1:pos], "ironSign", myCols[(pos+1):length(myCols)])]
       return(m)
}
```

8 Chapter 3
Supplemental data

8.1 Differentially expressed genes near the bZIP23 locus

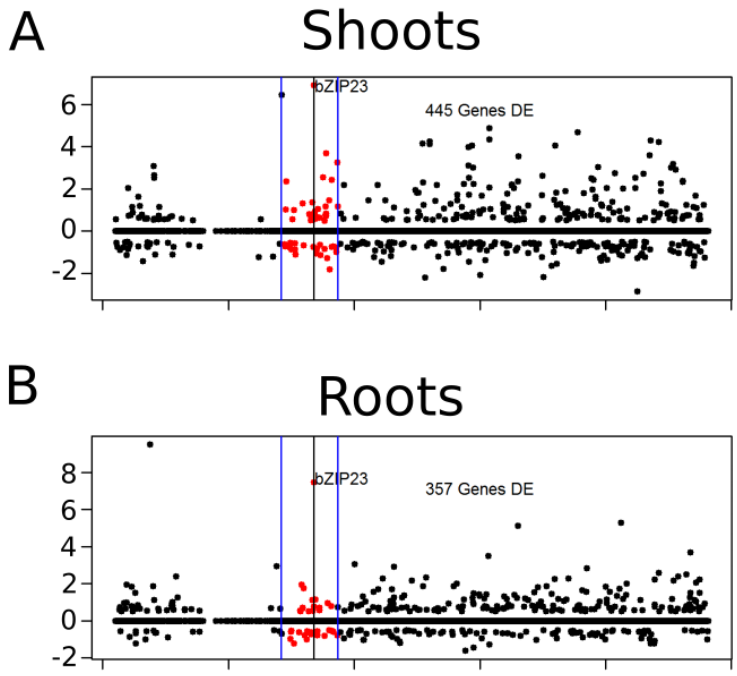

Supp. Fig. 3 No genes which co-segregate with bZIP23 provide a clear explanation for the differential suppression of *opt3-2* phenotypes in o_2b23_1 and o_3b23_2. (A) Differential expression of genes on chromosome 2 in the *opt3-2/bzip23-1* vs Col-0 shoots contrast, blue vertical lines denote a 1,900kb window around bZIP23, differentially expressed genes within this boundary marked in red. (B) As in (A) showing the root contrast. Vertical axis is the $\log_2$FC of *opt3-2 vs* o_2b23_2, horizontal axis is chromosome 2.

8.2 ICP data for *bzip23* related mutants

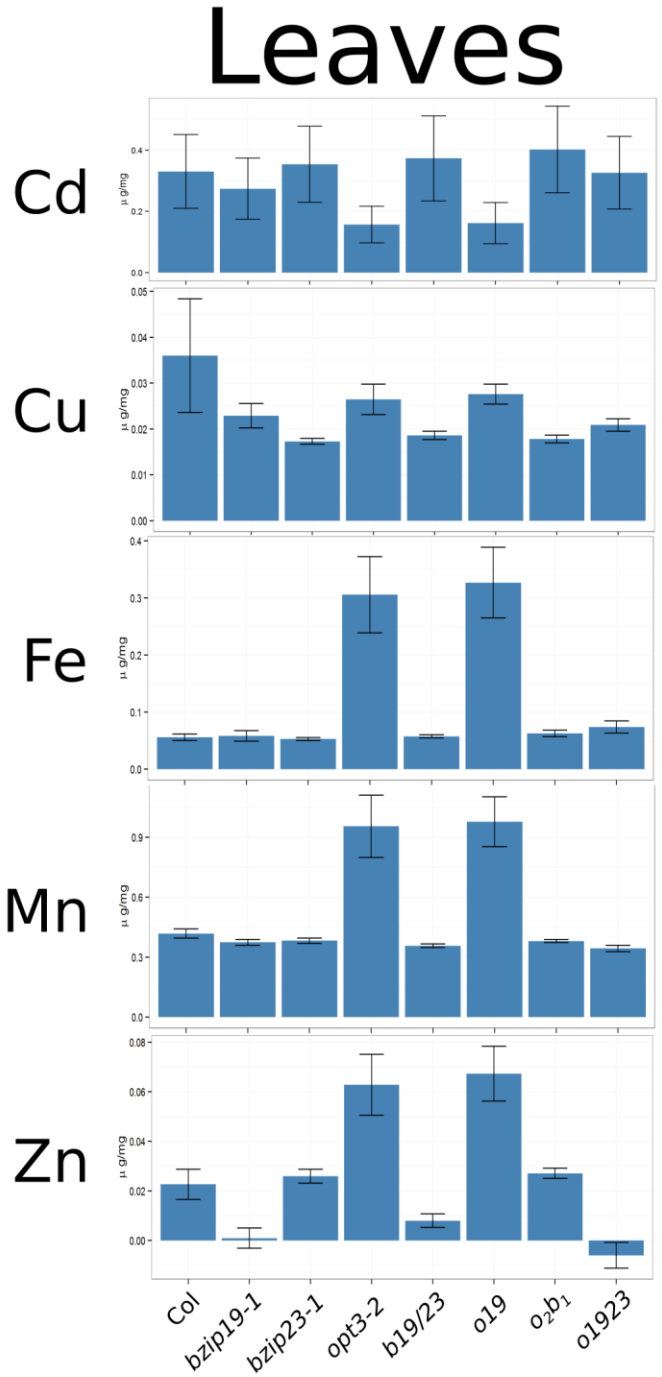

Supp. Fig. 4 ICP profile of heavy metals in bzip related mutants exposed to 72hr 20µM CdCl2. We observe that the low zinc phenotype of *bzip19/23* is reproduced and maintained in o_2b23_1. While Cd, Cu, Fe, and Mn all show suppression profiles

8.3 Expression of YFP:bZIP23 under MG132 exposure

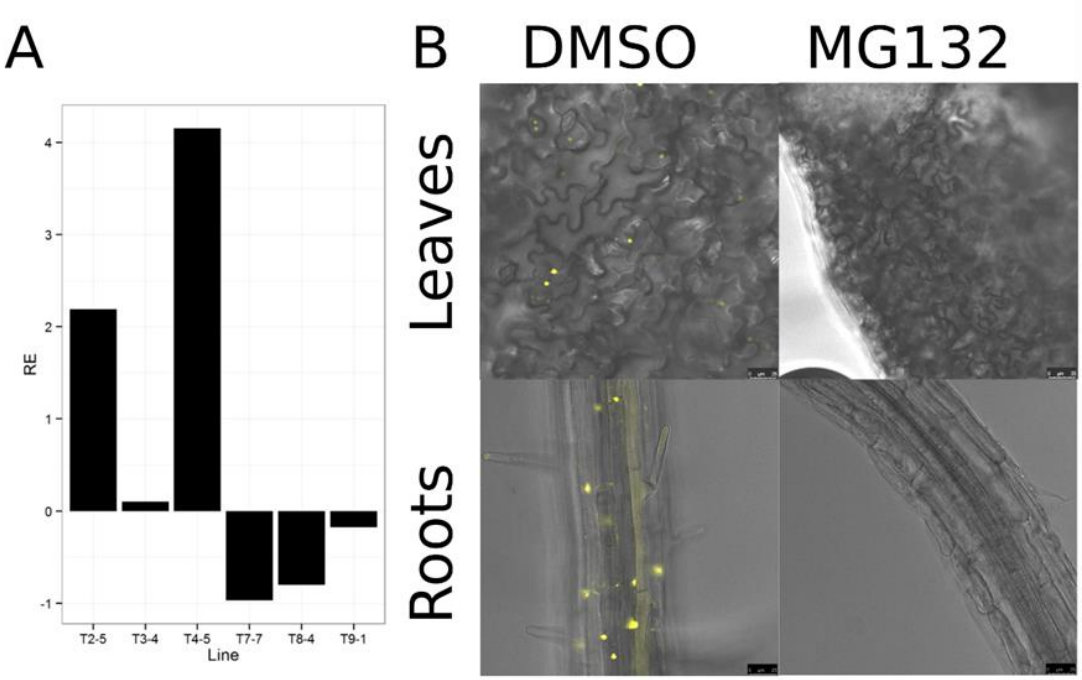

Supp. Fig. 5 (A) Expression of YFP in the $UBIQ10_{pro}$:YFP:$bZIP23_{cds}$ lines. (B) o_2b_1/$UBIQ10_{pro}$:YFP:$bZIP23_{cds}$ plants exposed to the protease inhibitor MG132 did not promote YFP abundance

8.4 35Spro:bZIP23 does not complement *opt3-2/bzip23-1*

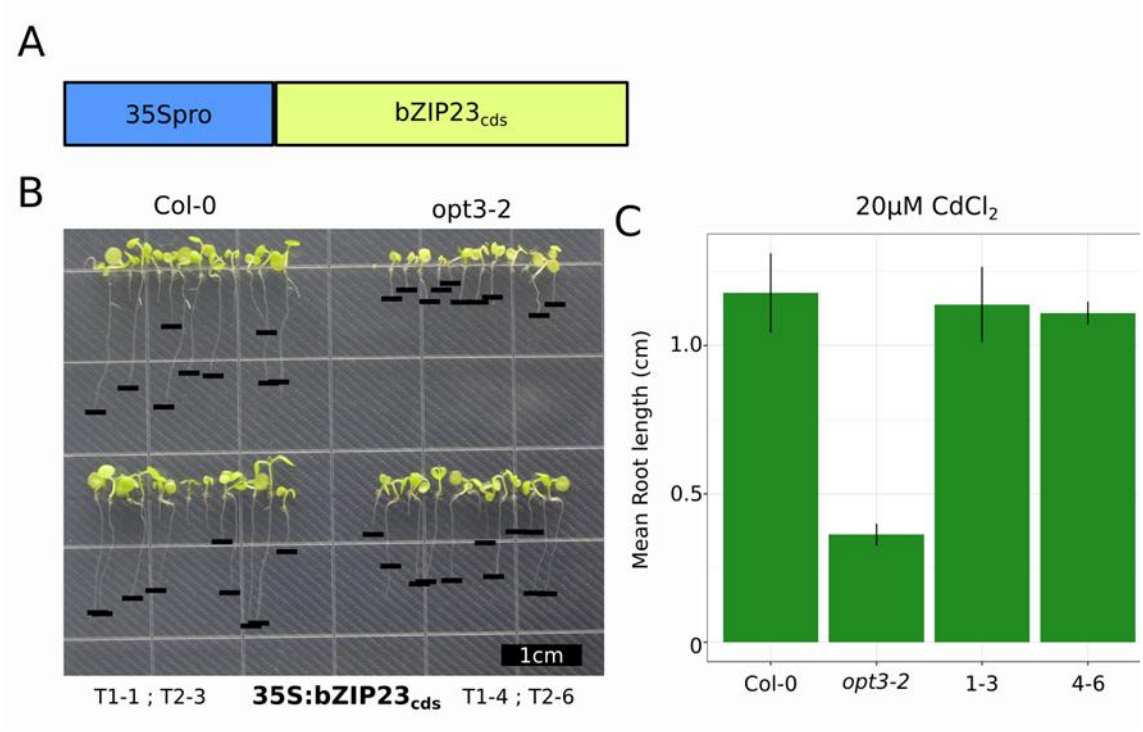

Supp. Fig. 6 35Spro:bZIP23 does not restore the short root phenotype of *opt3-2* in o_2b_1

8.5 Reintroductionof the bZIP23 locus does not complement *opt3-2/bzip23-1*

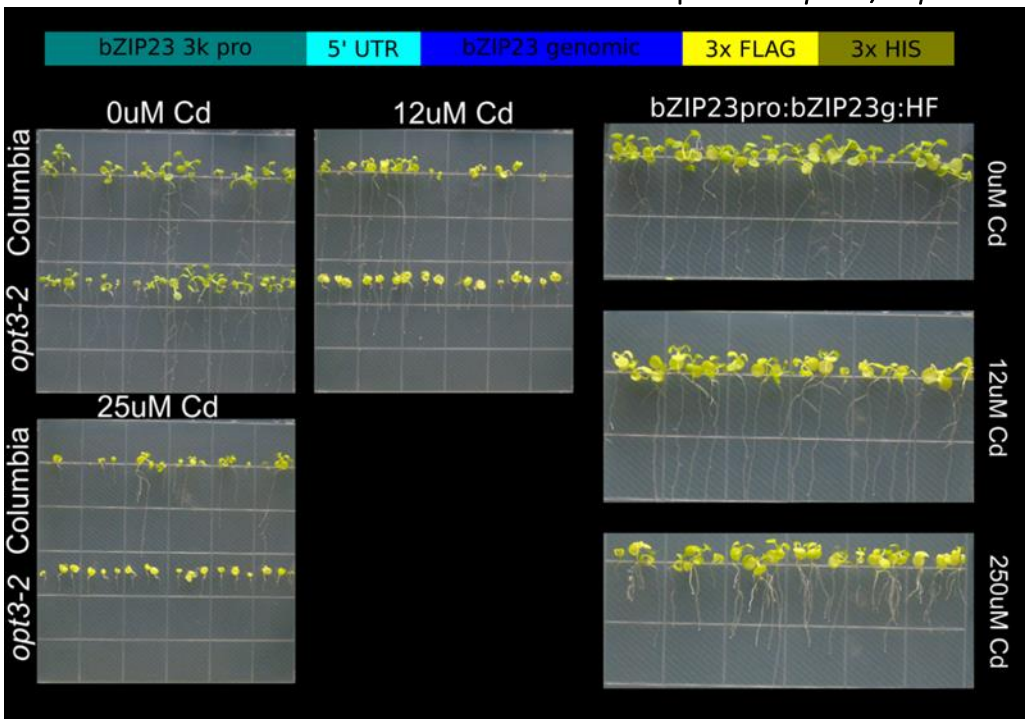

Supp. Fig. 7 bZIP23 expression driven by the native promoter with a C terminal FLAS HIS tag does not complement the o_2b_1 mutant

8.6 Reintroduction of the bZIP23 does not complement the Cd phenotype of *opt3-2*

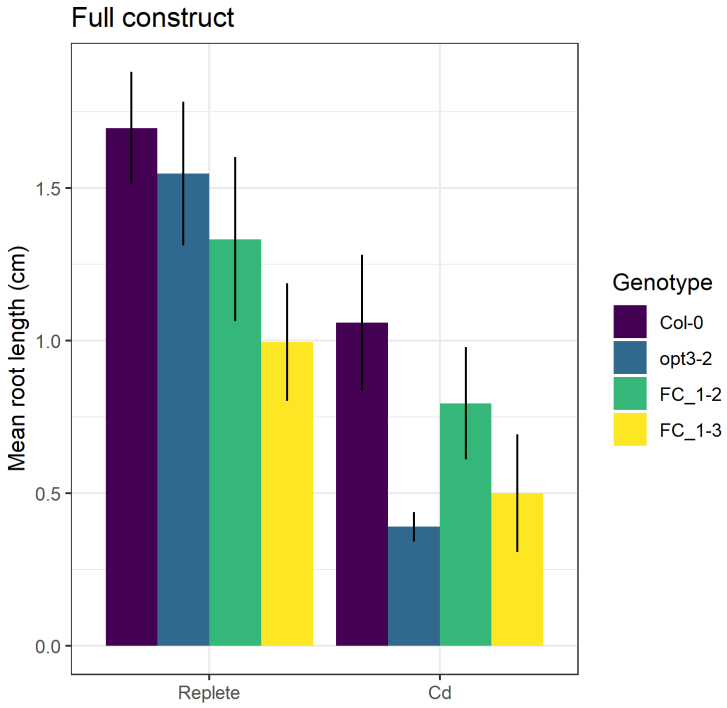

Supp. Fig. 8 Reintroduction of the complete bZIP23 locus (3kb bZIP23 promoter, 5' UTR, bZIP23 genomic, 3' UTR) did not complement the o_2b_1 phenotype. Although FC_1-3 is not significantly different than Col-0 during Cd exposure, it is also much smaller than Col-0, suggesting an issue related to seed health.

8.7 The bZIP23 locus is transcriptionally available 3kb 5' of the start codon

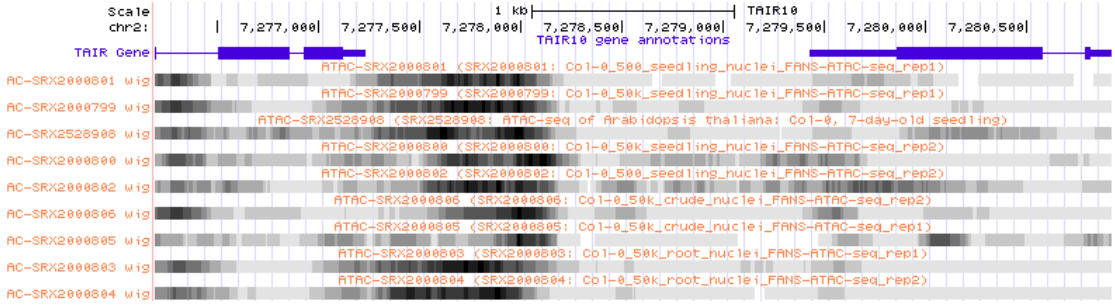

Supp. Fig. 9 bZIP23 promoter is not bound by histones in the kb region used for GUS assay.

8.8 GUS staining detected in floral organs, as well as leaves and roots

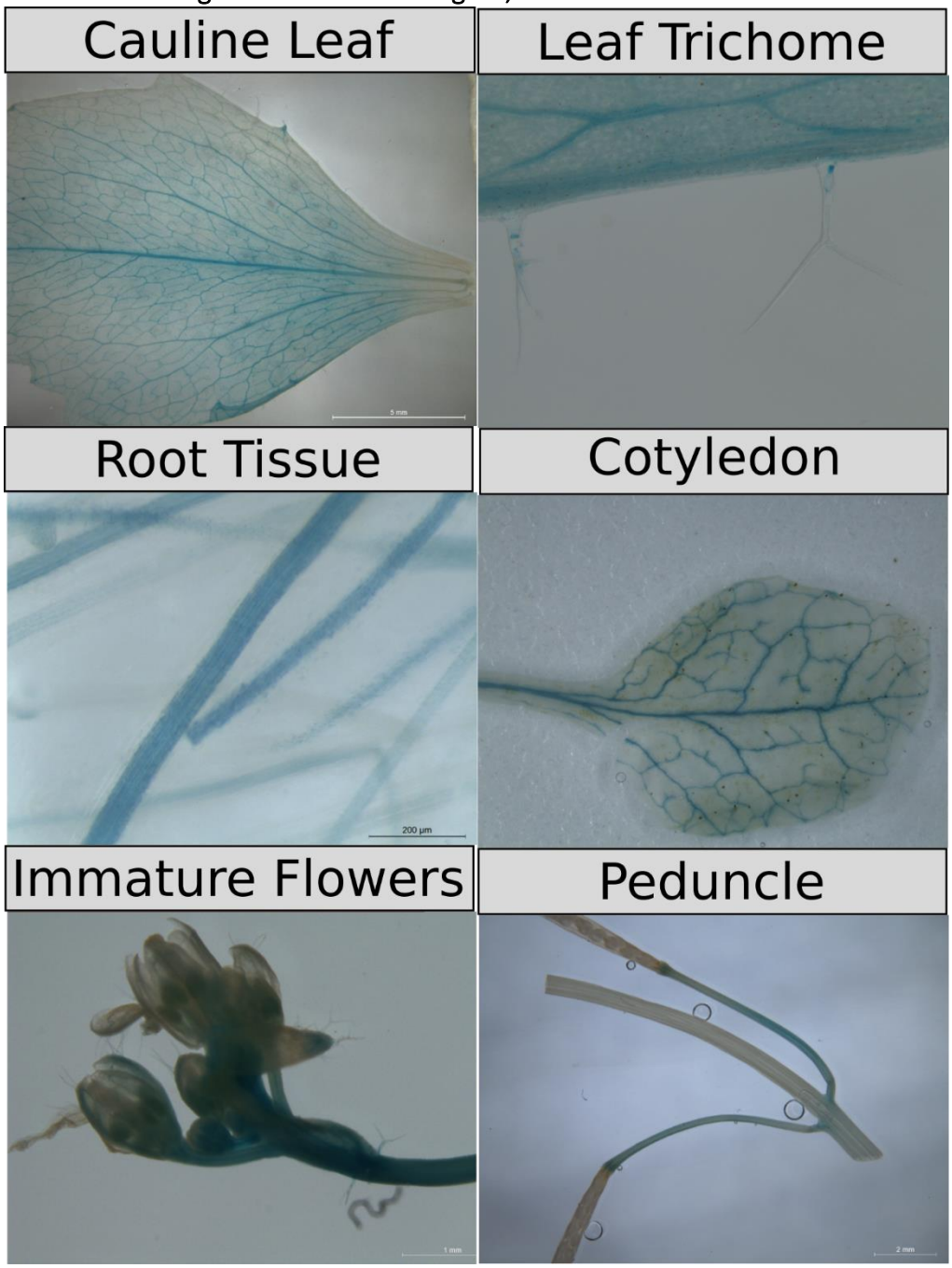

Supp. Fig. 10 Additional images of bZIP23$_{pro}$:GUS staining

9 Chapter 4 Supplemental Data - Design Process

The aim of the primary text is to describe the production of the model *Sunbear*. *Sunbear* was the product of a larger body of work, involving team management and the design process. As this information is not pertinent to the final product, it is included in this appendix.

9.1 Project overview and team management

The entirety of this project is a product of collaboration of which I served as the project manager. Presented here is a brief discussion of the progression of student cohorts which worked on the project, and a commentary on the three most significant developments as well as my capacity to manage these teams.

9.2 Group origins and development over time

High throughput technologies are difficult to manufacture, requiring a variety of skill sets mandating teamwork across disciplines. In order to facilitate this collaborative work, in Fall 2016 several teams of undergraduate bioengineers were formed, each led by two graduate students, and managed by an overall project manager (McInturf). The goal was for the biology-oriented graduate students to guide the engineering-oriented undergraduates through the development of a functional machine, while promoting competition between teams. These teams of students were recruited from the bioengineering senior design course (BE4980) and those who were interested were invited to continue on a semester to semester basis for further credit.

Two cohorts of students were recruited in this fashion for a total of three semesters. In the first semester four students worked through several design considerations and developed a minimally

functional prototype. In the following term two more students joined this group and brought the prototype to a new level of functionality, although that prototype still lacked a user interface and suffered from motor related issues. In the final term a new group of four students was recruited, to finish refinement and develop a graphic user interface (GUI). At this time the second graduate mentor departed to focus on their biologically oriented research. The second cohort lasted one semester, and recruitment from bioengineering was halted, favoring students with a stronger computer science background and one exemplary student was ultimately recruited and retained.

9.3 Progression of individual students

Each student recruited possessed unique skill sets, which were not immediately apparent and evolved over the course of the project. This presented a challenge in determining the proper role to assign each student while maintaining enough flexibility for each student to evolve. This is exemplified in Student A, who started the project with ample enthusiasm, a poor capacity to work within the team, and showed hostility towards criticism of their work, despite having admittedly poor technical skills. Student A is notable as they were given a series of smaller tasks by the project manager on which they were able to hone their technical skills, and was eventually developed respect within the group for their work and capacities. With this group acceptance Student A softened their temperament and learned to work effectively within the group, ultimately being a primary contributor to the semester's progress. In contrast, Student B initially showed ample modeling skills and tremendous charisma, which was used to rally the team and float between individuals to transfer information and ideas. Student B's capacity as a leader quickly waned in their second term as they showed indifference towards the project goals, believing that they would receive a good grade regardless of their output. This was extremely problematic as Student B had established themselves as a center of morale within the group.

Although efforts were made to retain their good workmanship it became apparent that they were unwilling, and the group suffered as a result of their reluctance to do any meaningful work.

When the cohorts shifted and a new group was brought in to finish the work done in the first year Student C joined and wished to expressly serve as a leader within the group. Student C started with an extremely heavy hand, showing little compassion for errors of their peers, seemingly intent on enforcing some level of superiority, which could not be demonstrated in their technical capacities, as these were not significantly above the other students. After a student lied about finishing a model, and further lied about being capable of using the software to design such a part, Student C proceeded into an outburst. To resolve this matter each student was taken aside and talked down to a level tone, addressing each ones issues. Student C was left in his leadership role for approximately one month after this as he slowly transitioned into a more standard role. This slow transition prevented Student C from suffering humiliation or losing face to the group and allowed for a smooth continuation of progress.

9.4 Origins and management of group conflicts

Team efficiency is held by group cohesion and attitude, which is subject to the personalities of those involved. Each person brought their own perspectives and behaviors, for better and for worse, which are difficult to control as it pertains to keeping a group together, as a heavy hand can sever the group connection and inter-reliance of the members. Engineering in particular is a male dominated field and 'boys clubs' are easily founded as an emergent property of the group. The development of such a culture only occurred once during the project, when Student D and Student E joined the initial team. Student D and E had been long time friends were each technically capable, with the foresight to understand the project's past and future progression. Their skills put them at the forefront of group, providing innovative solutions to problems which had been plaguing the group thus far. Once challenged beyond their immediate capacity and

after feeling let down by their peers, Students D and E began instigating encounters which saw condescension, down talking, and blaming the largely female students for their troubles. Due to the genders and capacities of the group, these out bursts became focused on the women within the group and fostered a 'men out rank women' mentality. Students D and E are not persons who would be outright labeled sexists or bigots, but none the less brought expectation of 'second rank' to life. Despite addressing this issue as it became manifest, the damage to the group mentality had been done and the group suffered flairs of temper, long running fights, and the development of factions within the team. These issues were never fully resolved, but were tempered by separating Students C and D and pairing them with the students which they had most offended, forcing them to continually be exposed to the product of their outbursts. Although initially turbulent, this did have a cooling effect within the group, and the students were able to end the semester on far better terms that would otherwise be expected.

9.5 Morale and the late nights

Finally, the need for the project manager to hold the group together and keep spirits high during long stressful nights in the 11th hour showed its importance nearly immediately. Before presentations and other deadlines, each team would spend long hours finishing assemblies, printing parts, and debugging code in order to meet their deadlines. Under these and other stressful times, personalities can flair, fights and long running confrontations can surface, and frustration can lead to despair. During these times, the project manager's role was to manage each person's temperament on an individual basis, or take over projects to facilitate teamwork and keep spirits up. One example of this type of management tactic occurred near the end of the second term, where one student had struggled with developing the appropriate program to allow one microcontroller to send motor control signals to a pair of microcontrollers. This caused consternation within the group, due to the vital importance of this program and the short

timeline. To prevent a loss of morale the project manager took control of this aspect and adjusted parts of the program while the student helped another subgroup to connect the back lighting system. This allowed the student to take back their program and adjust the appropriate lines of code to complete their program in a manner which was consistent with the previously outlined structure. On several occasions quint essential walks around the building or grounds were taken to relieve the individual demeanors, with other less subtle persuasions taken in the form of pizza and ice cream to keep long early morning hours from impeding progress.

Although I personally learned a tremendous amount about engineering, construction, and design during this project I believe that the lessons of managing groups of students with wildly differing personalities, and often conflicting personalities, has been the most significant personal aspect of this project.

9.6 Design overview

Presented here is a breakdown of the progression of each model, focusing on changes between each design element as the models evolved. Several design choices were maintained from outset to completion, while others were pursued for short periods and rapidly dropped. A complete annotation of the design progression can be seen in **Supp. Fig. 11**. On the outset our design parameters were as follows. **(I)** The machine must be able to capture images of plant roots with enough fidelity for subsequent processing. **(II)** The machine must be able to process multiple plates without user intervention, the exact number required is unspecified. **(III)** The machine must progress through the plates in under three minutes before returning to home. **(IV)** The machine costs must be minimized and kept below $5,000.

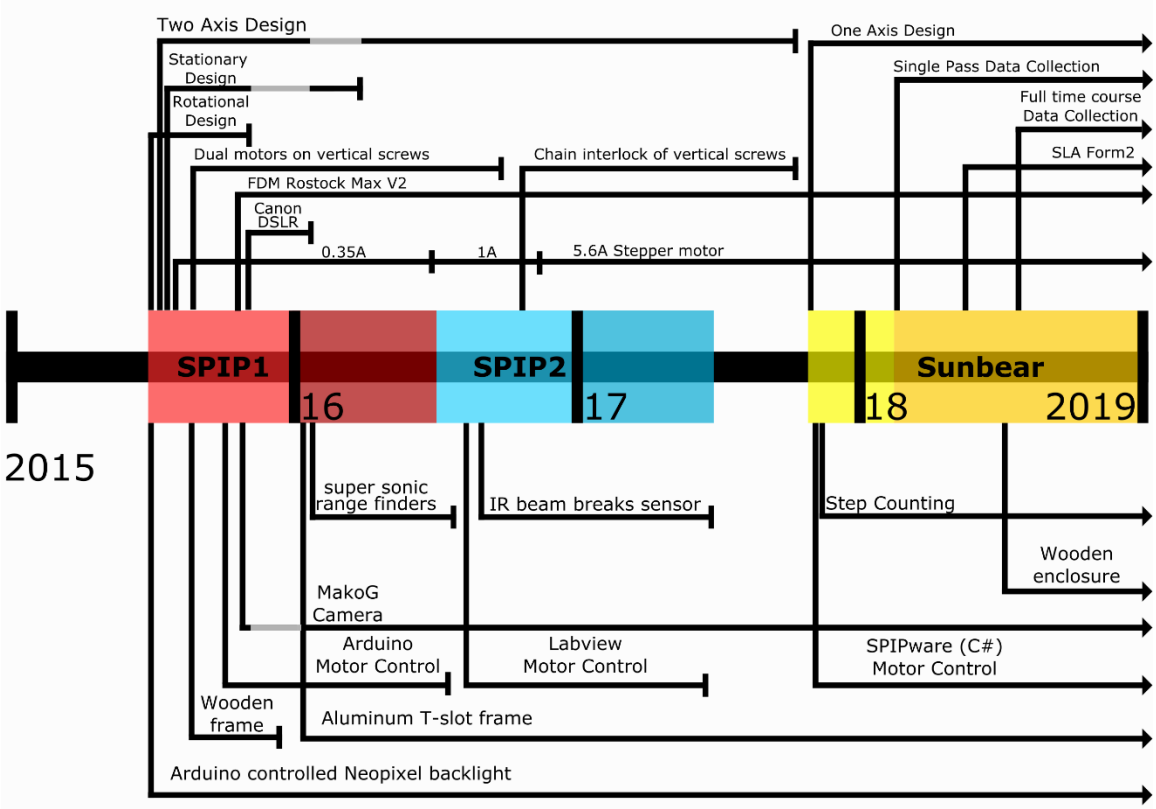

Supp. Fig. 11 The progression of SPIP models are marked by multiple phases to reach the current design. Shown are the three models produced and the major changes in construction are noted. Of particular note are the progression in the size of stepper motors and alterations in the control system.

9.7 SPIP 0.5

SPIP 0.5 was developed during the first semester and served as a demonstration of the direction of the project.

Several designs were initially considered, falling into two broad groups; those where the plates moved about the camera, and those where the camera moved around the plates. The latter was chosen to move forward under the assumption that it would be easier to consistently locate a small lightweight camera relative to a large assembly of plates. This considered, the plate field must form an upright grid forcing the camera to move along two axes. Although this initial decision, to immediately move forward with a two-axis design, was the most consequential

mistake made throughout the project. Although moving two motors is no more complicated than moving one, the number of related issues grows substantially. Although this simple fact was known from the outset, the project manager underestimated their significance and further underestimated the difficulty of overcoming them, causing these related issues to become perennial problems.

9.7.1 Drive system - horizontal and vertical translation

The first consideration was in how the camera sled was to move about the plate field. Although several formats were put forward the use of a ball screw was quickly taken. A ball screw is a simple and widely used device which resembles a long screw with beveled crests. A ball screw nut attaches to the screw and provides smooth motion along the screw though small ball bearings held in place on the interior of the nut. When the screw turns, the rotation of the nut is halted by a pair of rails, forcing the nut to translate along the long axis of the screw, providing a simple mechanism for movement along each axis. A second advent of the ball screw is that they are relatively stable under malfunction. A broken ball screw cannot rapidly fail and drop the camera sled, as may happen if a belt snaps. Three ball screws were implemented in the design, one for the horizontal axis and two for the vertical axes with a single stepper motor driving each ball screw.

9.7.2 Drive system – motors

A ball screw must be rotated to induce translation. Of the variety of motors possible, stepper motors were the only seriously considered option. Stepper motors are composed of two concentric rings with small teeth which face one another. The outer ring is fixed in place and the interior ring is connected to the drive shaft. The inner ring of teeth is polarized by a strong permanent magnet, while the outer ring is physically divided into six subunits which are further

divided into electrically connected pairs. These electrically polarized teeth on the outer ring are called stators. There are two fewer teeth on the outer ring of stators to allow for the teeth to be offset from one another. Each stator pair is positioned on opposing sides of the drive shaft and positioned such that the teeth of one stator pair is always aligned with the teeth of the inner ring, one always out of alignment, and one partially in alignment. The inner rings permanent magnet creates a magnetic field, and the stators only carry magnetic fields when polarized. As the stators are polarized in sequence the drive shaft rotates to minimize the free energy contained in these fields. Consequently the angular rotation in a stepper motor is discrete (proportionate to the number of teeth, typically 1.8°/step), and provides highly accurate movement which can be controlled using off the shelf microcontrollers. These motors also produce more torque per volt than comparable motors. The combination of precision, high torque, and relatively simple implementation made stepper motors the obvious choice.

SPIP0.5 used a NEMA17 350mA 12V motor (**Supp. Fig. 12**), as it could be powered and controlled directly by an Arduino, a routinely used microcontroller. NEMA17 is a form factor, describing the dimensions of the housing and several other parameters. This 350mA motor was far too small for this application and was plagued by missed steps, as the magnetic field rotated faster than the drive shaft would spin, resulting in inconsistent and slow rotation. The amperage describes the amount of work which can be done by the motor and function of the supplied voltage. In principal supplying a higher voltage to the motor would increase amperage, but in practice the motors malfunction, preventing us from simply increasing the input voltage.

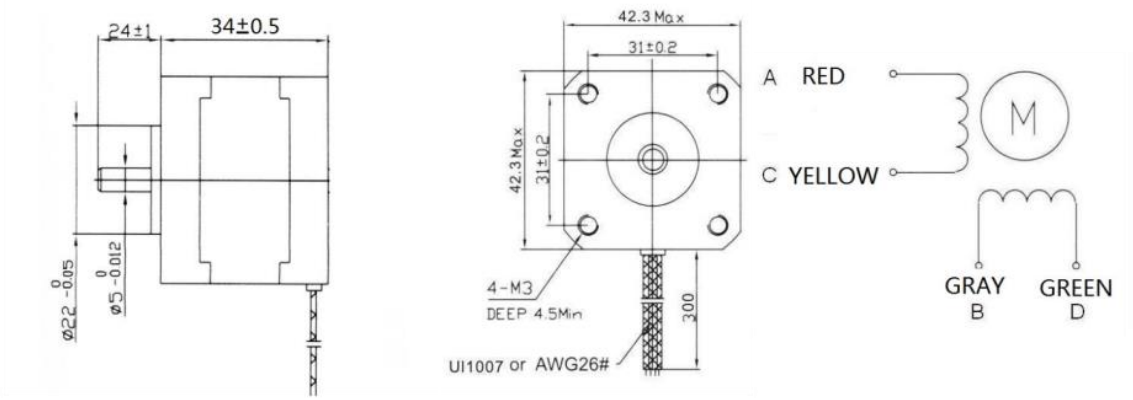

Supp. Fig. 12 Schematic diagram of the 350mA NEMA17 motor dimensions and wiring. Schematics downloaded from Adafruit (https://www.adafruit.com/product/324

9.7.3 Drive system - motor control

Stepper motors come in several varieties, but are always controlled by passing a pulsing current to each stator. This action can be easily controlled with Arduino with a stepper motor shield, a breakout board which attaches to the top of the Arduino. This shield serves three functions. First it boosts the 5V output voltage of the Arduino to 12V, allowing it to power small stepper motors. Second, stepper motor libraries provide functions to control the stepper motor without dictating the exact series of stator activations. Finally it allows for more complex procedures such as signal input/output, timing, and flow control to be directly integrated. Two Arduinos were used to control SPIP0.5, one for the horizontal ball screw, and one for both vertical ball screws. The motors were controlled by the user via push buttons on the surface of the frame, with vertical inputs and horizontal inputs being received by separate microcontrollers.

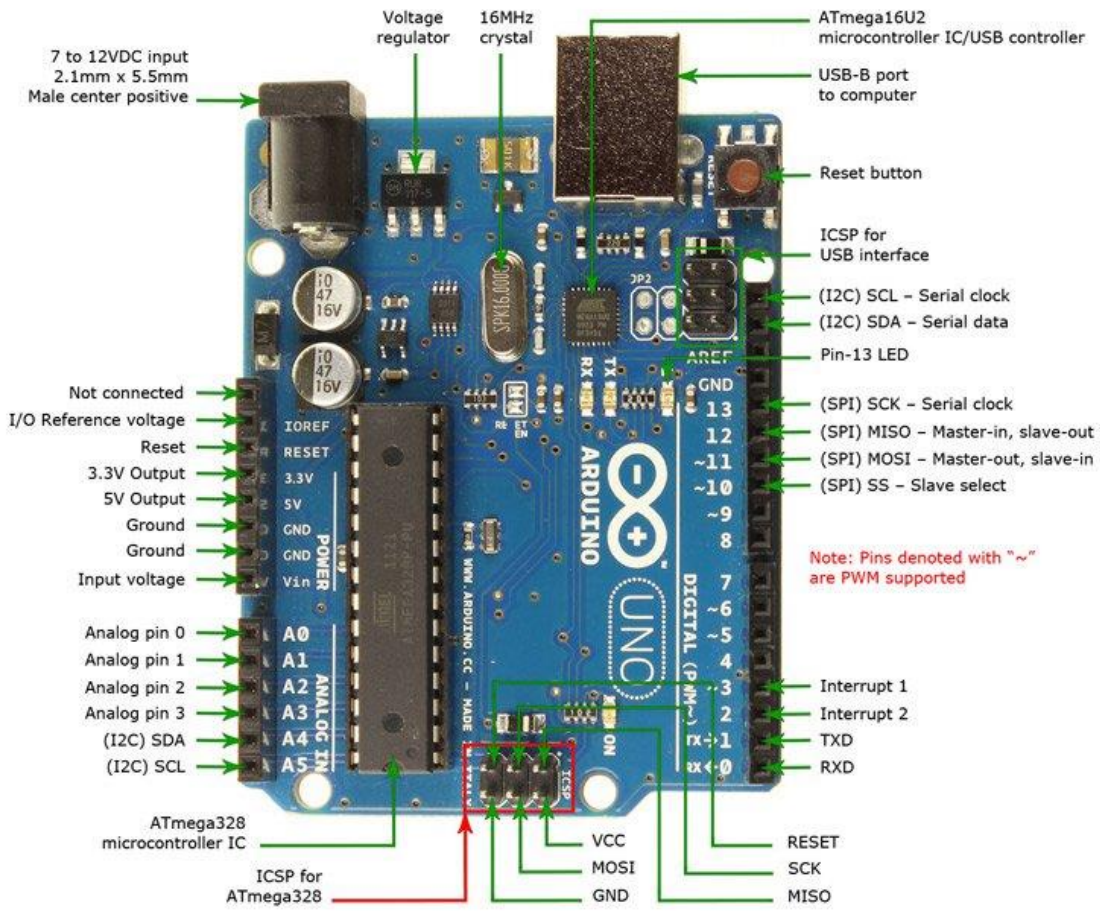

Supp. Fig. 13 Annotation of an Arduino Uno microcontroller. Several important features on this board are the 5V output), analog and digital pins to provide I/O, and as 12V DC input jack to the current needed. Image provided from Jamco Electronics (https://www.jameco.com/jameco/workshop/circuitnotes/cn-arduino-uno.html)

9.7.4 Image capture with a MakoG-503C

Several camera solutions were considered and implemented in SPIP0.5 which ultimately resulted in the use of a MakoG-503C from Allied Vision (**Supp. Fig. 14**). This camera takes 5MP RGB images with a manually adjustable focus, eclipsing the issue of finding a secondary lens and physically moving the camera into focus. Although higher resolution images could be desired, such devices are relatively costly, and the benefits of a higher pixel count do not guarantee better performance

by the root tracing algorithms. This model transfers data via Gigabit Ethernet (GigE) which allows easy communication with MatLab and LabViews (discussed in 9.8.6 and 9.9.3, respectively).

Supp. Fig. 14 Render and implemented view of the MakoG-503C camera used in all SPIP models. Producing 5MP RGB images, the 503C has provided ample resolution and color balancing capacities to produce high quality images for downstream processing. Render provided by Allied Vision

.

9.7.5 Backlighting

In order to acquire suitable images a strong light source must be evenly diffused across the plate. To accomplish this, a photography grade diffusing film was attached to the frame using binder clips and NeoPixel LEDs used as the light source. NeoPixels are individually controllable RGB LEDs sold in four meter long strips. NeoPixels are popular among hobbyist and are priced accordingly. Despite this increased cost, NeoPixels were selected to ensure that anyone unfamiliar with soldering small LED pins could easily manage their installation. Keeping the soldering operations to a minimum is a central design consideration, as one bad solder could short the entire grid or series of LEDs. Poor connections can also introduce hard to diagnose problems such as flickering and random outages. Additionally, this arrangement reduces the number of wires to be managed

by 25%. Standard RGB LEDs have four pins (ground, red, green, and blue), while NeoPixels use three pins (hot, ground, and data) where the data line is a pulse width modulated signal which carries the voltage of each color to each LED in series, allowing for control of individual LEDs without the need to implement a shift register. This configuration does have one drawback, in that all LEDs must share a common ground with the microcontroller to ensure proper timing, although this is only a concern when wired incorrectly.

9.7.6 Framing and plate holders

SPIP0.5 was a basic construction, largely composed of wooden rectangles, measuring 1.75x3.5 inches with all components attached with finishing nails or machine screws. A simple yet effective plate holder was developed (**Supp. Fig. 21**), designed for common square plates and 3D printed, the plate simply slides into the holder and held in place by short side walls. The bottom of the plate holder has one circular hole and one half circular hole below the first. Each of these holes allow for an 8mm steel rod to hold the plate in place. These steel rods were mounted by passing them through the wooden frame. Despite the imprecise construction, this arrangement was stable to translation and pitching of the plates.

9.7.7 Camera sled

The camera was mounted to the ball screw nut (Section 9.7.2) through a ball screw nut bracket fitted with 8mm steel bars. The ball screw nut bracket was designed in Blender, and exported as an STL file for 3D printing. It was then attached directly to the nut via machine screws. The 8mm bars extended away from the screw where they passed through the sled bracket. In this way horizontal and vertical movement of the ball screw nut would push the sled in the proper direction. This design was found to have flaws based on the following reasons: (I) while the horizontal rods (connecting to the vertical ball screws) were secured at both ends, the top of the

vertical bars (attaching to the horizontal balls screw) were not properly secured and excess play induced binding/jerking of camera sled. (II) Alterations to the sled, bars, or ball screw nut brackets required the disassembly of a large portion of the machine frame, making all modifications and work extremely time consuming. (III) Linear bearings were not installed in the sled, preventing smooth movement. (IV) After printing, the bars securely fit into the bracket holes, but rapidly widened, exacerbating other areas where excess play existed. (V) If the two vertical motors were not coordinated in their movement, undue stress would be placed on the ball screw nut, brackets, and sled.

9.8 SPIP1

SPIP1 (**Supp. Fig. 15**) expanded upon the rough design of SPIP0.5 largely refining the materials used, motor controls, and user s

Supp. Fig. 15 SPIP 1 featured two axis movement, IR range finders, and manual control through push button controls. Image taken at Life Sciences Week, 2016

9.8.1 interface.Drive system – motor

The 350mA motors had proven insufficient to reliably rotate the ball screw. A new trio of NEMA17 1A motors were installed and largely overcame the power issues. Dimensions and wiring are identical to those in**Supp. Fig. 12** Although largely reliable, infrequent missed steps were still observed. This motor was not immediately replaced for two reasons. First increasing the motor amperage would mandate a dedicated power supply and a method to interface the Arduino with the motor/power

supply. Second, the project manager believed that adjustments elsewhere would alleviate the missed steps.

9.8.2 Drive system – motor control

SPIP0.5 used two independent Arduinos to control each motor. This was changed in SPIP1 where three Arduinos were implemented. In this configuration one Arduino served as a master with two slaves. The master controller handled all processes related to determining when to move each motor by taking user inputs from an array of push buttons. These signals were encoded in the master as HIGH/LOW voltages and passed to the slave via I/O pins, where they were converted to stepper motor instructions. This system could be arranged execute predefined movement schemes, although time constraints limited it to only accepting direct user commands.

9.8.3 Materials

SPIP1 was the first machine to implement the now ubiquitous 80/20 aluminum T-slot extrusion and ABS paneling. Aluminum T-slot extrusions are square aluminum beams with a center bore and trapezoidal void insets on each face of the square bar (the T-slot) (**Supp. Fig. 16**). This allows for parts to be attached to the bar via a nut and machine with ease, while providing a more polished aesthetic. The wooden base of SPIP0.5 rebuilt as a wooden frame covered in black plastic panels with the ball screws recessed into the base.

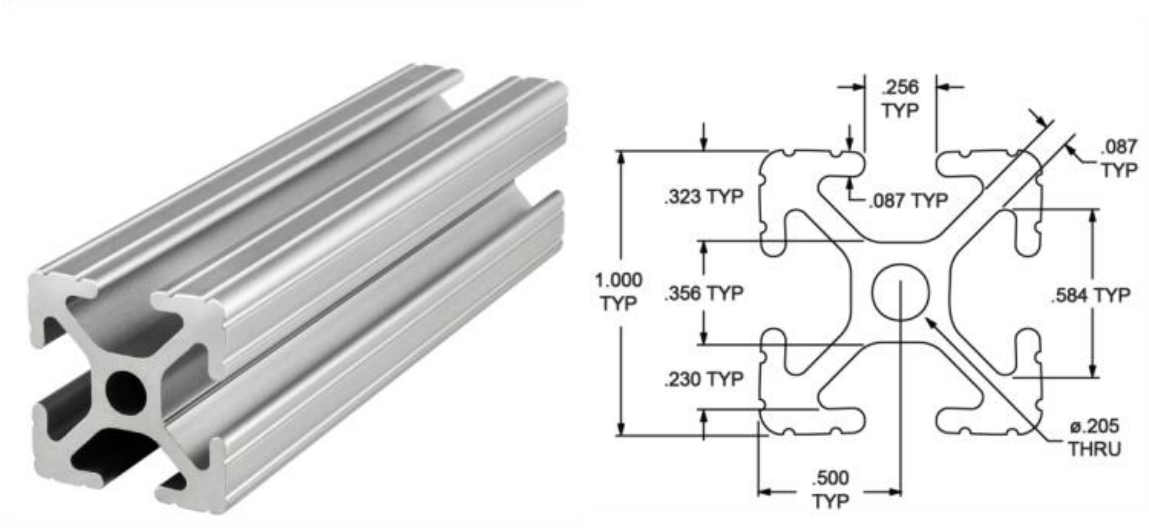

Supp. Fig. 16 T-slotted aluminum extrusions from 80/20 INC were used extensively in the framing of all SPIP models. These bars are light-weight and T-slots on each face make them versatile, as they are easily connected to one another or to axillary parts. Image and schematic provided by 80/20 INC (https://8020.net/1010.html)

9.8.4 IR range finders

The combination of excess play in the camera sled, missed steps, and several close calls, where the motor did not halt when the ball screw nut reached the end of the ball screw, called for the integration of a failsafe. SPIP1 used IR range finders for this task. These range finders have a maximum and minimum measureable distance based on distance between the two emitters/detectors (the higher the maximum range the larger the dead zones near the detector). Consequently no single range finder could both detect both the maximum and minimum distances needed to keep the sled within its boundaries. To overcome this constraint a short and long range device were implemented for each axis of movement, with a and a large flat target was placed that the end of the horizontal/vertical bars which carried the sled. At a defined threshold the distance measured would alternate between the long and short range devices, allowing for an effective failsafe. This came at the cost of a redesigned sled on which to mount the IR range finders, which often failed to be successfully printed, and a large wire loom extending from the camera sled which required several additional parts to prevent wire strain.

9.8.5 Camera sled

The camera sled was redesigned to minimize contact on the steel bars to help remove some of the binding experienced in SPIP0.5, as well as mount the aforementioned range finders. When considering a round bar passing through a round hole on the sled, it is more stable to have a large contact area, but comes at the price of increased friction/binding. Stability was sacrificed for less binding and a narrow profile was used to mount the sled to the support bars..

9.8.6 Image management

MatLab is a common programing environment, extremely similar to R in function and syntax, but features better image handling capacities with libraries for image input from GigE. Hence a script was made to read in and display the live feed from the camera as well as capture frames and write them to file. This implementation was passable, particularly because MatLab is a commons scripting language among engineers, but could not be used to develop a GUI, preventing long term adoption of MatLab.

9.9 SPIP2

SPIP2 (**Supp. Fig. 17**) was constructed by the second cohort of bioengineering students with two major goals: finalizing each component for a fully functional machine, and migrate the user control to LabView.

9.9.1 Drive system – motors

Once again the motor upgrade had been found to be insufficient so an overkill option was taken by implementing a NEMA23 5.6A 120/240V motor. This motor requires two additional parts, a large power supply and a driver (akin to the Arduino's shield) to mediate the high voltage signals to the motor. The high voltages required to drive the motor are not compatible with the low

voltage logic signals from an Arduino or computer. Hence the motor is controlled by the driver which is physically divided into two circuits, one low and one high voltage, and are bridged by an IR relay to transmit information between the controller and motor. The driver demands that the controller (LabView or Arduino) outputs two 5V signals, one for direction and one for movement, to the driver which then relays them to the high voltage circuit and encodes them into appropriate stator induction patterns. The driver is connected to a large power supply to power these heavy duty motors. This arrangement, while more complex and expensive, has proven to be both an effective and reliable solution which can accommodate a much heavier load for modular upgrades.

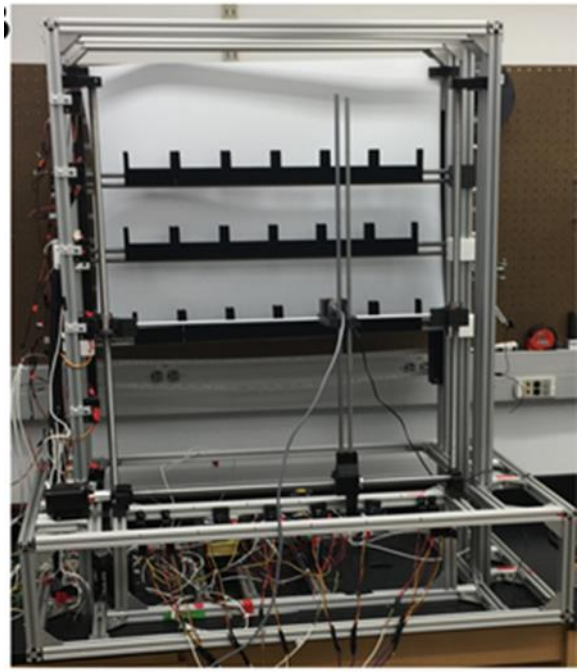

Supp. Fig. 17 SPIP2 was largely similar to SPIP1, featuring the same two axis movement, but replaced the IR range finders for IR beam breaks. Manual and automated control was moved away from the platform and onto a LabView interface. This image was taken shortly after presentation at the BE4890 poster session

9.9.2 Drive system – interlocking the vertical bars

SPIP1 used the same three motor design as SPIP0.5. Under this design three drivers and three motors would be needed which was seen as an undue expense. To reduce the number of motors the two vertical ball screws were interlocked by a cog and chain design. This was effective in reducing the cost while also reducing the possibility the two ball screws falling out of synch.

9.9.3 GUI and control through LabView

The MatLab interface had proven to be untenable, so a new control system was developed in LabView. LabView is a programming environment which uses a graphical interface to arrange components akin to a circuit diagram to control input/output from a desktop computer; an environment quite different than compiled code like C/#/++, or the linear flow of scripting languages like R or MatLab. It has the advent of being compatible with a large range of I/O devices (sensors, cameras, and motors) and has the capacity allow a user to interact with all of these parts through a custom built GUIs. In the second cohort, one student had previous experience using LabView and was able to implement a user interface which allowed for manual control, and a partially complete an automated movement function.

9.9.4 Beam breaks

Prior efforts to prevent the ball screw nut from reaching either terminus of the ball screw utilized IR range finders. Although they were successfully implemented the range finders showed far too much signal variance to precisely locate the camera sled along either axis. The range finders were removed as the larger motor eclipsed concerns of missed steps and imprecise movement. Still an issue came in controlling the movement of the sled and its capacity to follow an arbitrary path. To develop a grid which the camera could follow, and easily be encoded in LabView, IR beam breaks were installed long the T-slots of the support beams, and each ball screw nut mounting

bracket was outfitted with a fin to block the beam. Although this introduced a massive wire management burden, with forty new wires to be strung along the T-slot, it was an effective solution to providing LabView simple inputs to determine where the camera needed to move.

9.10 SPIP3 - Sunbear

After the second cohort of students departed it became clear that there were too many unfinished parts which needed to be addressed individually before building up to 2D movement. Hence the development of Sunbear (**Supp. Fig. 18**) is largely characterized by polishing existing components, removing non-essential parts, and most importantly developing an effective GUI. Additional schematics of the Sunbear frame can be found in **Supp. Fig. 23**, **Supp. Fig. 24**, and **Supp. Fig. 25**. Although our initial intention was to quickly solve issues related to 1D movement before moving back to 2D movement, we transitioned to solve issues related to user interface and full implementation, hence Sunbear never progressed to 2D movement.

9.10.1 Development of SPIPware

While the progression from simple microcontrollers to LabView integration had been largely successful, student turn over, along with an inability to find a student worker experienced in LabView, became a serious problem. The solution to developing a GUI was found in the GNU software LASERGRBL (http://lasergrbl.com/en/). LASERGRBL is a program designed for DIY laser engravers who encounter the problem converting their designs into GCODE, and then streaming

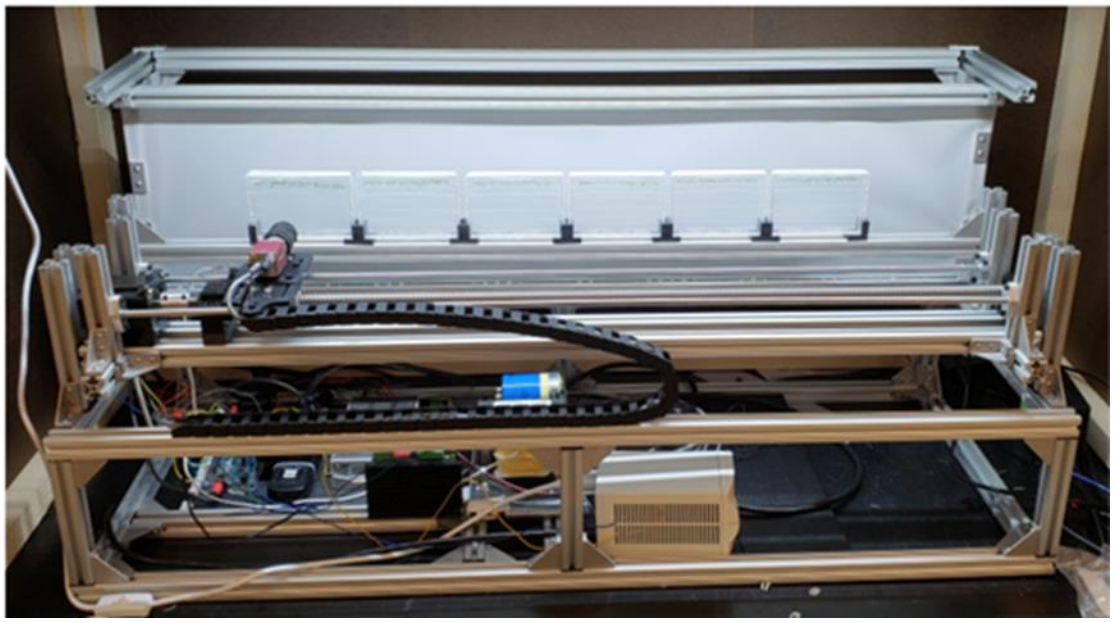

Supp. Fig. 18 SPIP3 Sunbear deviated from the design of SPIP1 and 2 by striping down non-essential parts and focusing on refining the simplified design. The two axis design was reduced to a single axis of motion, and emphasis was put into developing *SPIPware* to control Sunbear, rather than expanding on the design. Consequently Sunbear does not have the intended throughput, but is fully functional and the Mendoza-Cózatl laboratory has adopted its regular use.

The GCODE to Arduinos. GCODE is language developed exclusively for controlling Computer Numeric Control (CNC) machines such as mills, lathes, and routers which all rely on stepper motors to position their tools. With the built in GUI, converting LASERGRBL to *SPIPware* largely entailed changing the graphics in the UI to reflect the needs and application of Sunbear. Additionally *SPIPware* integrated limit switches, lighting operations, and most significantly interfacing with the Allied Vision Vimba SDK to activate, trigger, load camera settings, and finally write captured images to file. The complete interface of *SPIPware* v1.5 is described in the primary text

9.10.2 Camera sled

The removal of the second axis of movement allowed for a simple low profile sled to be directly mounted to the ball screw nut, and the wire loom to be replaced with a segmented cable carrier mounted directly to a T-slot. Outriggers with linear bearings ridding on chrome plated 8mm steel

bars replaced the prior fin and wall mechanism. Although this solution is far more effective than prior implementations, the current steel grade is far too flexible and must be replaced with larger and more rigid bars.

9.10.3 Back lighting

While the use of NeoPixels has been a consistent feature of SPIP models, SunBear resolved a long standing issue of mounting them. The strip in which each LED is embedded is not electrically insulated, and is covered in a silicone sheath. Prior models clamped the sheath and strip to the frame and over time the lights would sag. Although this did not affect the picture quality, owing to the diffusing film, it was not aesthetically pleasing. Removal of this sheath allows the strip to be placed within a T-slot for a clean appearance with evenly spaced lights. Without the sheath, the bare electric contacts on the strip are able to short against the metal frame. This was resolved by applying a thin coat of electrical insulation film, which is applied in the exact manner as nail polish, keeping user assembly easy.

9.11 3D modeling and printing

Designing small parts such as brackets and mounts is important in any design process. Several software packages exist to design and export models suitable for 3D printing such as Solid Works, SketchUp, Blender, and Autodesk Inventor. In effort to utilize open source software Blender was initially chosen to design the 3D printed parts. This was ultimately a poor choice; as Blender is tailored towards animations rather than designing components. Ultimately Autodesk Inventor was chosen, which fortunately is available to students for free, keeping modifications in the hands of downstream users.

While most of the connecting brackets of SPIP2 and Sunbear were prefabricated, owing to the use of T-slotted aluminum, 3D printing played a major role in development. The camera carriage,

plate holders, and motor bracket have always been printed. This is significant because they are by far the most complex of all the parts and underwent the most modification, which would have incurred untold cost in aluminum and manufacturing time.

9.12 FDM printing – Rostock Max V2

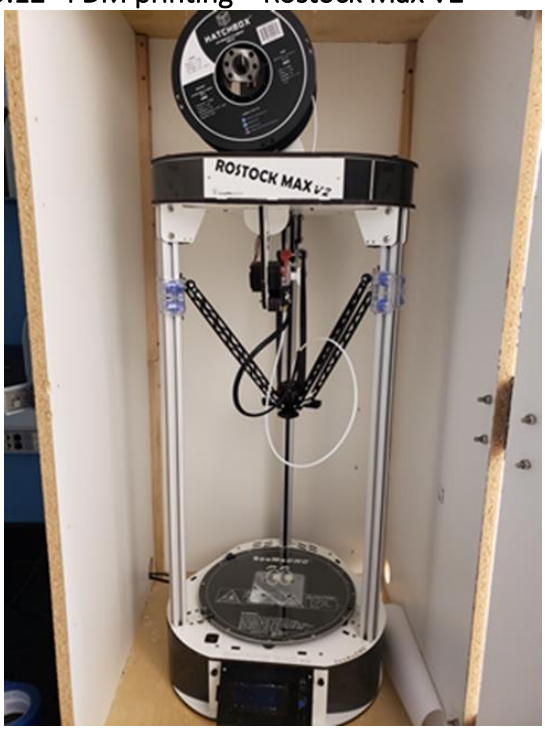

Supp. Fig. 19 Rostock Max V2 FDM printer loaded with white ABS filament. This printer features an extremely large build area. The entire printer was encased in a wooden housing to prevent uneven cooling, and subsequent warping, of the printed parts

The first printer used in this project was a Rostock Max V2 Fused Deposition Modeling (FDM) printer**(Supp. Fig. 19**). FDM is a technology where a thin plastic filament made of acrylonitrile butadiene styrene (ABS) or polylactic acid (PLA) is passed from a large spool through a drawing gear to push the filament through a narrow nozzle, heated to ~200°F. The nozzle passes above a heated glass plate and deposits the filament onto the bed and builds upon each successive layer to create the part. This technology is the most accessible printing technology due to the low cost of the filament, which is available from manufacturers and third parties. Due to the constraints

of the nozzle size FDM printing is not as precise as other methods and, like many printers, tend tobe in need of constant maintenance and recalibration, as well as employing trial and error tricks to get successful prints. Specifically the Rostock Max in our lab needs an ample layer of Aquanet hairspray or Elmers white stick glue to be applied immediately before printing to properly adhere ABS filament. This in in contrast to PLA, which requires an even layer of blue painters tape (any brand) for adherence. The glass plate is attached to the heating bed via three binder clips which make the glass plate slightly convex. This curvature changes whenever the clips are adjusted or the glass plate moved, demanding constant recalibration. This is particularly problematic when removing completed parts which sometimes take notable force to remove the bed causing the glass plate to slip, or when removing excess glue/hairspray from the bed with a razor. Additionally the printer can jam, requiring the complete disassembly of the nozzle assembly, blown ceramic fuses, in addition to any number of misprints and step errors plagued the Rostock Max.

9.13 SLA printing - Form Labs Form2

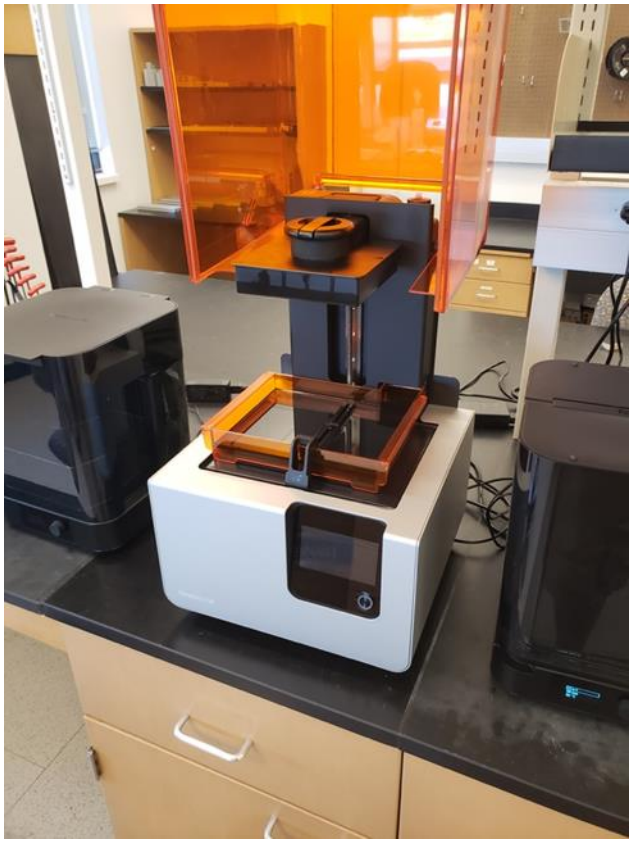

Supp. Fig. 20 Form Labs Form2 SLA printer and isopropyl alcohol wash and UV curing stations (left and right, respectively).

Recently, we purchased a Form Labs Form2 (**Supp. Fig. 20**), an industrial grade stereolithography (SLA) printer, which has proven to be a valuable asset and will be an important tool during full production. SLA is a method where a basin is filled with a viscous resin, and a UV laser passes through the basins base, tracing the shape of the part. This induces a polymerization of the resin, and successive layers are built upon one another as the part is pulled from the resin. SLA printing is far more accurate than FDM printing, as the layer height is determined by the height of the printing surface above the basin base, while the minimum feature width is the laser diameter. The Form2 is capable of printing at 25µm resolution along each axis, compared to the 500µm resolution of the Rostock. Resins used in the Form2 are also far more useful than ABS/PLA. ABS and PLA are hard plastics which largely differ in their handling during printing, not in their finished

properties. The Form2 features a diverse line up of resins with a variety of physical and chemical properties. Shortly after assembly Sunbear began to rattle itself apart during operation. To circumvent this small ABS inserts were added at each junction, but had a tendency to fall out as they were only secured by pressure between the adjoining faces. The flexible rubber like resin was used to create inserts which are secured to the beam such that they would not fall out and effectively dampen machine vibration.

10 Future directions

While the progress presented here represents a completely functional machine, modifications and tweaks are yet to come. Several are detailed here.

10.1 A better cabinet

The development of SPIP 1.5 and the associated hardware has been a recent development. Consequently the immediate need for a cabinet to hold Sunbear was relegated to an effective but unsightly wooden case. Designs for a proper case with associated doors and panels have been completed and a portion of the parts have been sourced but remain to be assembled. Encasement in the cabinet allows for a side door to be opened and the simple removal of plant rods. In the case where maneuvering plant rods to the right of Sunbear is not permissible, and for servicing needs, a pair of forward swinging doors will be implemented. The two door panels will seal via a spring loaded deadbolt with light occlusion along the door joint covered by a 3D printed screen which bolts to the interior T-slot.

10.2 Air handling and electrical connections

After Sunbear and *SPIPware* 1.0 were fully functional, the decision to implement full automation was made, mandating the installation of growth lights. While LEDs produce nominal heat, the

ballast can become quite warm and over the course of an experiment the chamber becomes hotter than desired. Hence computer case style fans will be attached to the cabinet to keep warm air from accumulating.

Sunbears' electronics are all mounted onto a lower shelf but in a poorly ergonomic or otherwise convenient manner. A set of standard connectors will be attached to the cabinet so Sunbear can be directly wired to the cabinet. This prevents users from having to reach into the machine to make any wiring adjustments. Furthermore, a set of push buttons will be installed to provide manual control over the head and back lights. This is currently implemented on a breadboard, but a more permanent solution is needed.

10.3 Plates

During image processing, it is important to have a clean background, devoid of obscuring features. For this reason standard square plates could not be used, due to the presence of grid lines, which would obscure actual root growth. Several plates were tried, but ultimately ~5"x3" plates from VWR were selected (Cat # 75780-348) and can be used effectively with 40mL of media. Additionally the single body plate holders were replaced with smaller parts which mount directly to a T-slot and are shown in **Supp. Fig. 22**.

11 Additional schematics

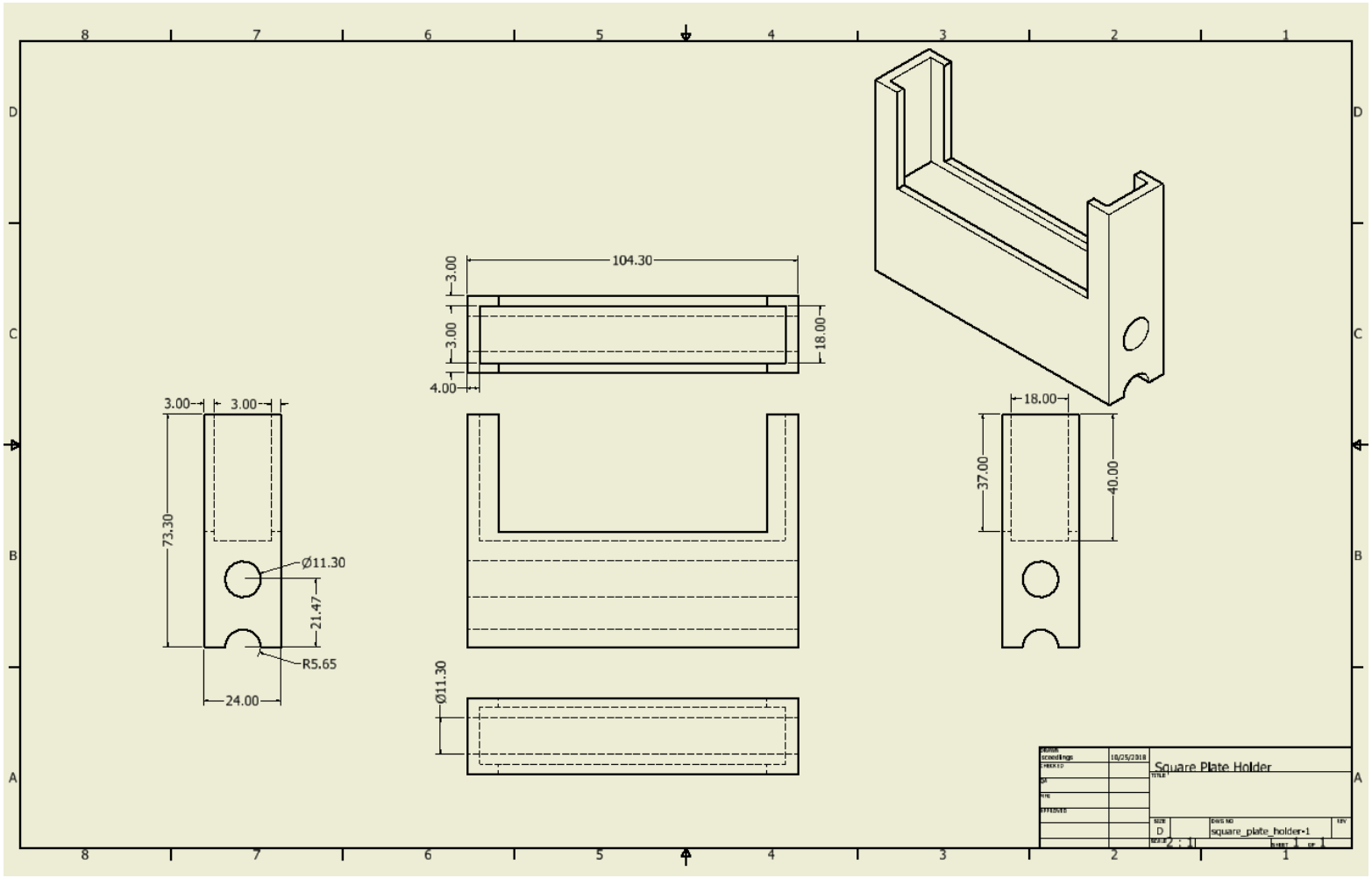

Supp. Fig. 21 orthographic views of single body plate holders

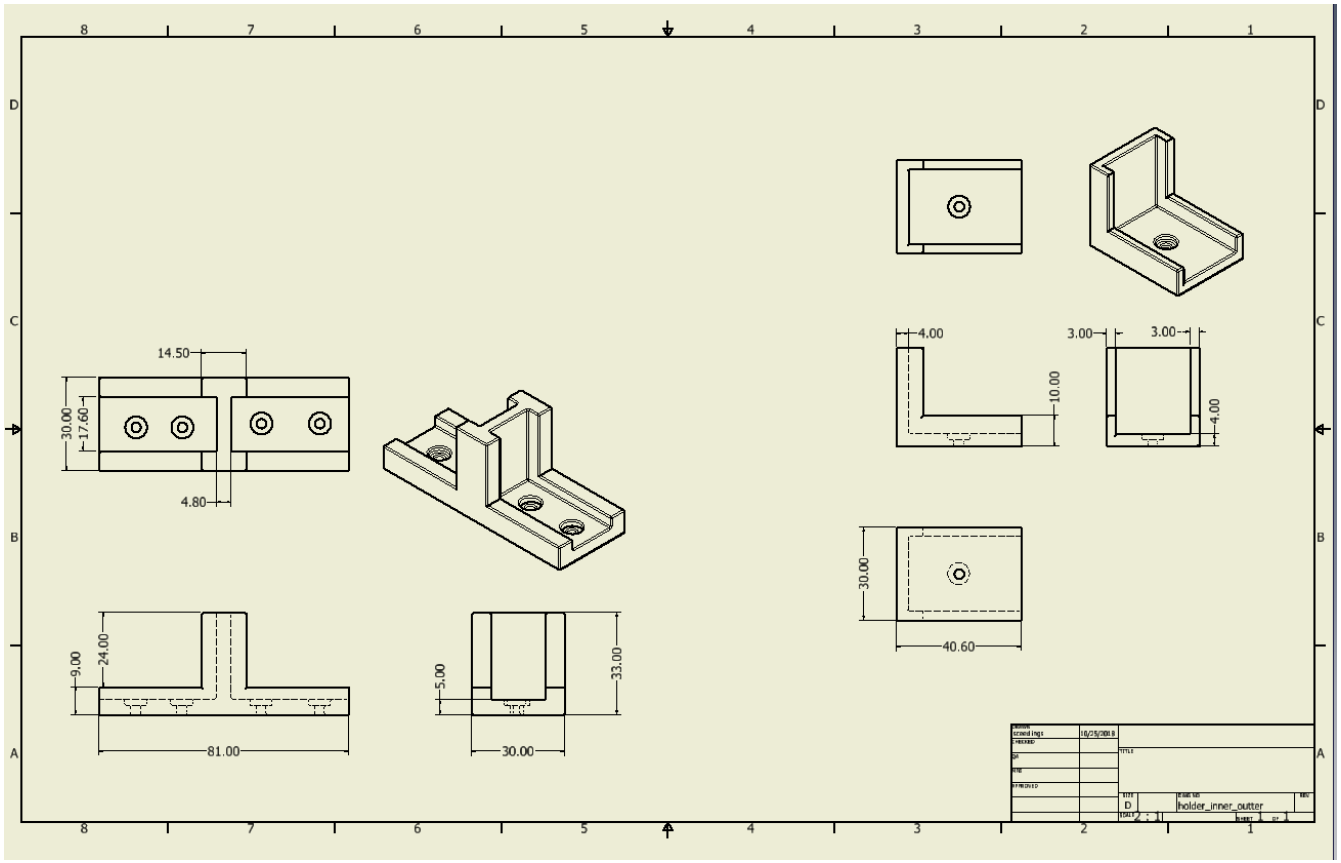

Supp. Fig. 22 orthographic views of inner and outer plate holders

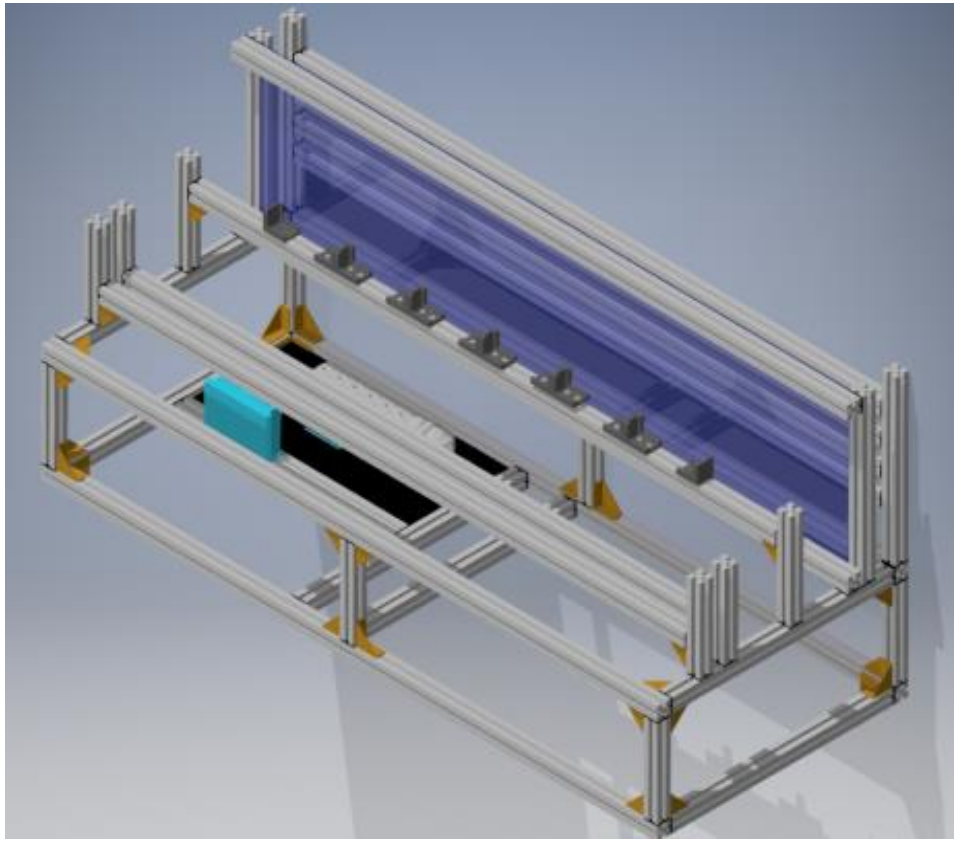

Supp. Fig. 23 Render of Sunbear 3D model

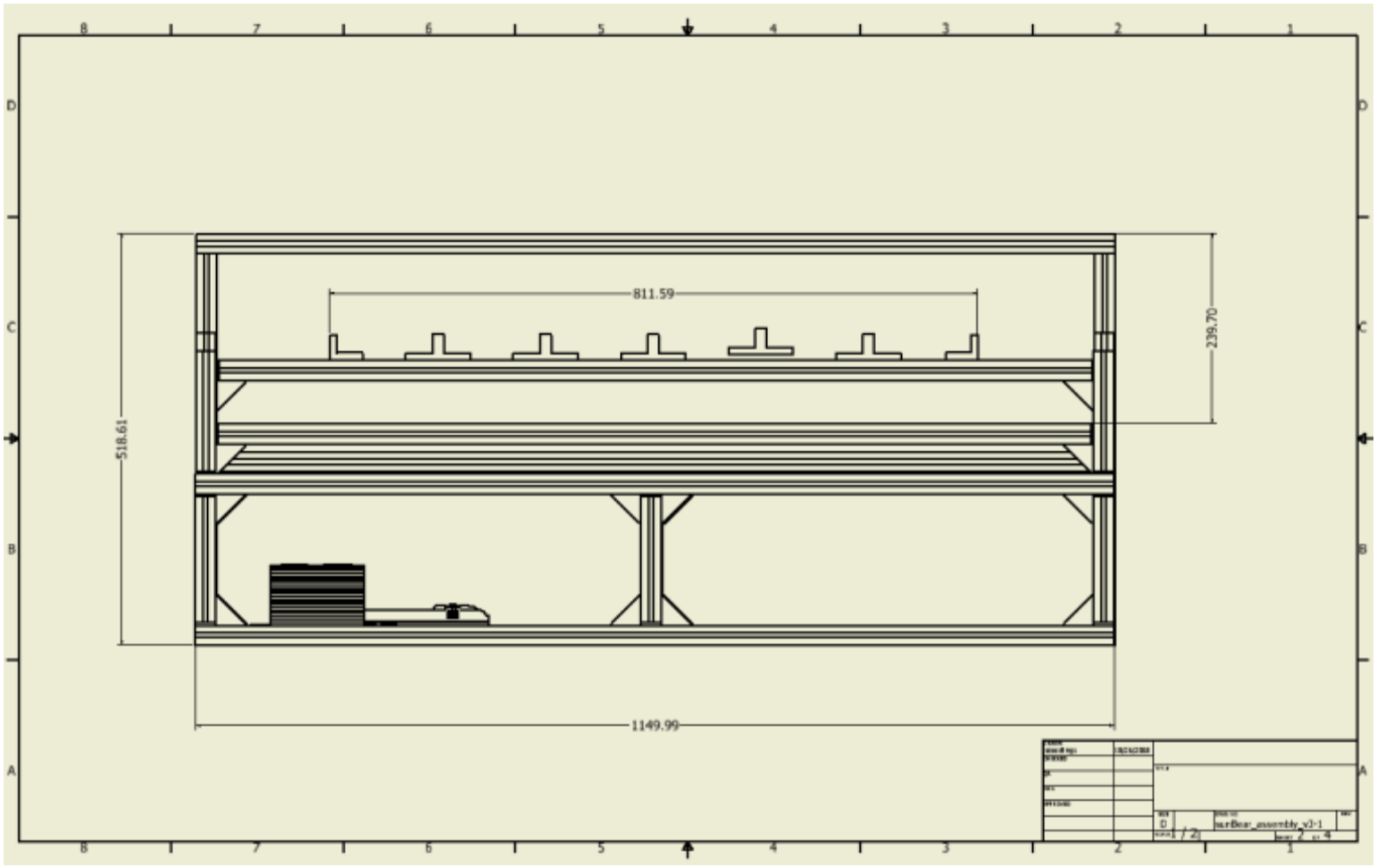

Supp. Fig. 24 Detailed forward view of the Sunbear frame

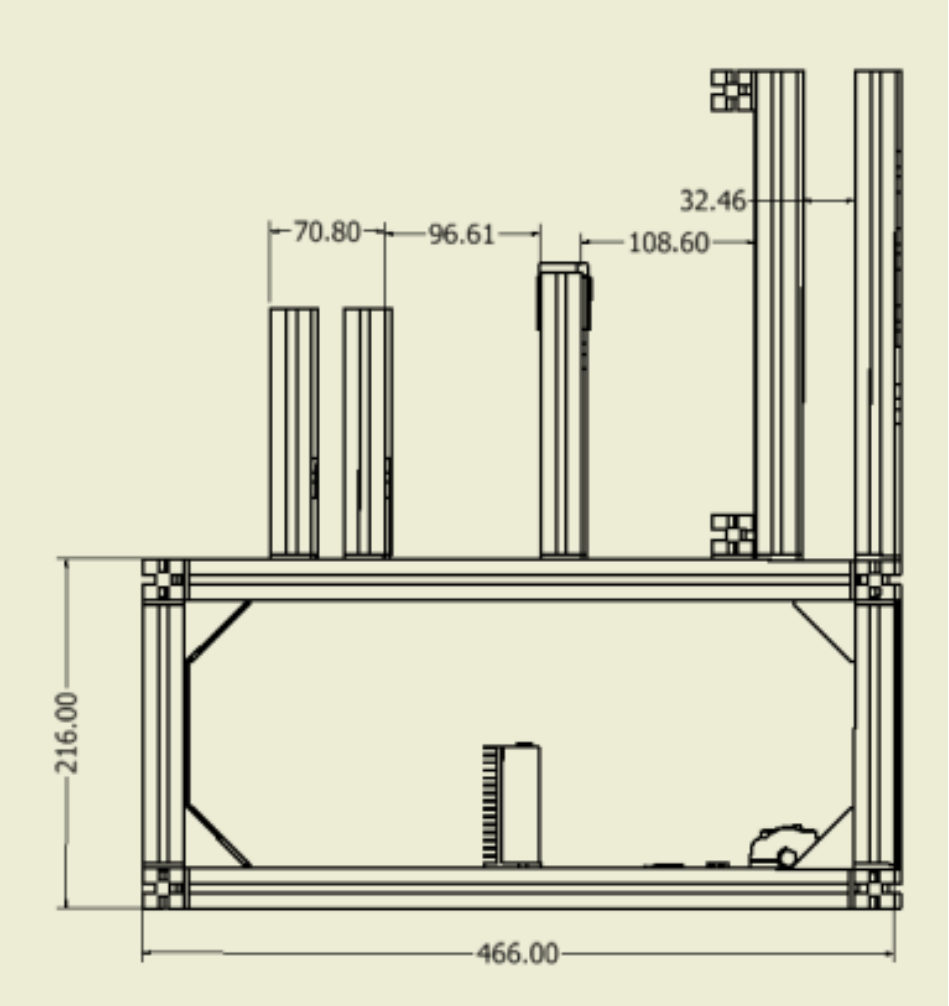

Supp. Fig. 25 Detailed side view of Sunbear Frame

VITA

Samuel Alonzo McInturf was born to William and Lanelle McInturf of Stamford and Stromsberg, Nebraska. He was raised in Omaha Nebraska, and showed a strong interest in physical sciences from an early age which has clearly continued to adulthood. Through the high school years, Samuel nearly dropped out at multiple times, a product of misplaced angst and a desire to join the work force. Consequently, his studies failed as he spent more time working than focusing on school work. A happenchance suggestion to seek employment at a local nursery provided the keystone experiences which produced a love and fascination with plants in all their myriad forms. Finding that the life of a laborer is a hard life indeed, Samuel went to college, with some reluctance, to study engineering. These efforts ultimately failed due to a lack of interest, until Biology 101 connected the interest in plant life and molecular systems. This began an onslaught of working in multiple laboratories, vacillating between mathematical and biochemical approaches, ultimately finding work in the laboratories of Dr. Istvan Ladunga creating co-expression networks in *Chlamydomonas* and characterizing ZIP transporters under the supervision of Dr. Brian Waters. Clearly, the result has been a hybrid body of work integrating engineering, biochemical studies, and computational approaches to study heavy metal homeostasis.

These motifs have persist outside of the laboratory, as he become a full-fledged DIY craftsman, scavenging parts from microwaves to provide enough electricity to place Lichtenberg figures on hand crafted furniture, and maintaining a substantial colony of orchids and bonsai trees. Socially he develops few, but strong, friendships which culminate in gaming sessions which draw friends from no fewer than six states to spend the evening playing make believe.

Ph'nglui mglw'nafh Cthulhu R'lyeh wgah'nagl fhtagn!